

# Ideal magnetohydrodynamic theory of magnetic fusion systems

J. P. Freidberg

Department of Nuclear Engineering and Plasma Fusion Center,  
Massachusetts Institute of Technology, Cambridge, Massachusetts 02139

Ideal magnetohydrodynamic theory and its application to magnetic fusion systems are reviewed. The review begins with a description and derivation of the model as well as a discussion of the region of validity. Next, the general properties are derived which are valid for arbitrary geometry and demonstrate the inherently sound physical foundation of the model. The equilibrium behavior of the currently most promising toroidal magnetic fusion concepts are then discussed in detail. Finally, the stability of such equilibria is investigated. Included are discussions of the general stability properties of arbitrary magnetic geometries and of detailed applications to those concepts of current fusion interest.

## CONTENTS

I. Introduction	802	6. The flux-conserving tokamak	838
A. The role of ideal MHD in magnetic fusion	802	D. Three-dimensional configurations	841
B. Outline of Section II (the MHD model)	803	1. Flux function in a closed-line system	842
C. Outline of Section III (general properties of ideal MHD)	803	2. The Elmo bumpy torus (EBT)	843
D. Outline of Section IV (equilibrium)	803	3. The high- $\beta$ stellarator (HBS)	845
E. Outline of Section V (stability)	804	4. Stellarators, heliotrons, and torsatrons	848
F. Units	805	5. The parallel current constraint	851
II. The MHD Model	805	E. Summary	852
A. Introduction	805	V. Stability	852
B. Ideal MHD equations	805	A. Introduction	852
C. Starting equations	806	B. Basic theoretical concepts	853
D. Two-fluid equations	807	1. Exponential stability: the homogeneous plasma	853
E. Asymptotic approximations	807	2. General linearized stability equations	854
F. Single-fluid equations	808	3. Properties of the force operator $F$	855
G. The ideal MHD limit	809	a. Self-adjointness of $F$	855
H. Region of validity	811	b. Real $\omega^2$	856
I. Perpendicular MHD	812	c. Spectrum of $F$	856
1. General discussion	812	4. The Energy Principle	857
2. Derivation from the Boltzmann equation	813	a. Variational formulation	857
3. Derivation from single-particle orbit theory	814	b. Statement and proof of the Energy Principle	857
III. General Properties of Ideal MHD	815	c. The extended Energy Principle	858
A. Introduction	815	d. Forms of $\delta W_F$	859
B. Boundary conditions	815	e. $\sigma$ stability	860
1. Perfectly conducting wall	816	5. Incompressibility	861
2. Insulating vacuum region	816	6. Vacuum versus force-free plasma	862
3. Plasma surrounded by external coils	816	7. Classification of MHD instabilities	863
C. Local conservation relations	817	a. Current-driven modes	863
D. Global conservation laws	818	b. Pressure-driven modes	863
1. Perfectly conducting wall	818	c. Internal/fixed-boundary modes	863
2. Insulating vacuum region	818	d. External/free-boundary modes	863
3. Plasma surrounded by external coils	819	e. Kink modes	863
E. Conservation of flux	819	f. Interchange instabilities	864
IV. Equilibrium	820	g. Ballooning modes	865
A. General properties	820	8. Summary	865
1. Basic equations	820	C. Application to 1D configurations	865
2. Virial theorem	820	1. The $\theta$ pinch	866
3. Toroidal geometry	821	2. The $Z$ pinch	866
4. Magnetic flux surfaces	822	3. The general screw pinch	868
5. Freedom to specify an equilibrium	822	a. Evaluation of $\delta W$	868
6. The basic problem of toroidal equilibrium	823	b. Suydam's criterion	869
B. One-dimensional configurations	825	c. Newcomb's analysis	870
1. $\theta$ pinch	825	d. Oscillation theorem	872
2. $Z$ pinch	825	4. The reversed field pinch (RFP)	874
3. General screw pinch	826	a. Introduction	874
C. Two-dimensional configurations	827	b. Pressure-driven modes	874
1. The Grad-Shafranov equation	827	c. Current-driven modes	876
2. The reversed field pinch	829	d. Summary and numerical results	877
3. The conventional tokamak	830	e. Taylor's theory	877
4. The high- $\beta$ tokamak	833	f. Overview of the RFP	879
5. Noncircular tokamaks	837	5. The "straight" tokamak	879
		a. Introduction	879
		b. Internal modes (localized)	880
		c. Internal modes (general)	880

d. External modes ( $m=1$ Kruskal-Shafranov limit)	881
e. External modes ( $m \geq 2$ kinks)	882
f. Summary	883
D. Application to 2D configurations	884
1. Tokamak	884
a. Introduction	884
b. Internal modes (localized: Mercier criterion)	885
c. Internal modes (localized: ballooning modes)	887
d. Internal modes (general)	889
e. External modes	890
f. Axisymmetric modes	892
g. Overview of the tokamak	893
2. Closed-line configurations	894
a. Interchanges, ballooning modes, and the "magnetic well"	894
b. Application to the Elmo bumpy torus	896
VI. Conclusions	899
Acknowledgments	899
References	899

## I. INTRODUCTION

### A. The role of ideal MHD in magnetic fusion

In order to develop a viable fusion reactor there are three basic physics requirements which must be satisfied. (1) A sufficient density of plasma must be: (2) confined for a sufficiently long time at: (3) a sufficiently high temperature to produce net thermonuclear power [see Ribe (1975) for a review of fusion reactor systems]. In its most elementary form the net power balance for a magnetic fusion system is described in terms of the Lawson parameter  $n\tau_E$ , with  $n$  the plasma number density and  $\tau_E$  the energy confinement time (Lawson, 1957). At break-even conditions  $n\tau_E \geq f(T)$ , where typically  $f(T) \approx 10^{14} \text{ cm}^{-3} \text{ sec}$  for the optimized temperature  $T \approx 15 \text{ keV}$ .

From an admittedly oversimplified view of the physics, the problem of maximizing  $n\tau_E$  separates into two relatively independent parts. First, the maximum energy confinement time  $\tau_E$  is determined by the microscopic behavior of the plasma. This behavior ultimately leads to macroscopic transport, which can be either classical or anomalous depending on the processes involved. Since these phenomena require a knowledge of individual particle motion on short length and time scales, they are usually treated by kinetic models, but including only limited geometry [see, for instance, Montgomery and Tidman (1964), Krall and Trivelpiece (1973), and Hinton and Hazeltine (1976)]. Such models are also used to determine the energy disposition and plasma temperature  $T$  associated with various methods of heating.

Second, the maximum density  $n$  is almost always determined, not by microscopic kinetic processes, but rather by macroscopic equilibrium and stability limits set by the magnetic geometry. Actually, at a given  $T$ , the critical figure of merit is  $\beta \equiv 2\mu_0 nT/B^2$ , the ratio of plasma energy to magnetic energy. Because of the relatively slow time and large length scales involved, these phenomena are best described by fluid models.

Ideal magnetohydrodynamics (MHD) is the most basic single-fluid model for determining the macroscopic equilibrium and stability properties of a plasma. The model essentially describes how magnetic, inertial, and pressure forces interact within an ideal (i.e., perfectly conducting) plasma in an arbitrary magnetic geometry. [Other reviews of ideal MHD equilibrium and stability theory have been given by Shafranov (1966), Kadomtsev (1966), Wesson (1978), Bateman (1978), and Goedbloed (1979).] There is general consensus that any magnetic geometry meriting consideration as a fusion reactor must satisfy the equilibrium and stability limits set by ideal MHD. If not, violent termination of the plasma on a very short time scale (i.e., typically less than 100  $\mu\text{sec}$ ) is often the consequence.

Thus the role of ideal MHD in magnetic fusion is the discovery and analysis of different magnetic geometries, with the aim of distinguishing those which are particularly attractive for use in fusion reactors.

One should keep in mind, however, that while favorable ideal MHD properties are necessary in a reactor, they may not, even in the restrictive context of low-frequency macroscopic behavior, be sufficient. It is sometimes possible for nonideal effects such as electrical resistivity to allow the development of slower, weaker instabilities, which nevertheless may still lead to enhanced transport or even, in certain circumstances, violent termination of the plasma. Clearly a complete evaluation of any given concept requires a knowledge of both the strong, ideal MHD behavior and the weaker, but still potentially dangerous, nonideal effects. In the present review consideration is given only to the ideal MHD model. The effects of resistivity on macroscopic equilibrium and stability have been reviewed by Greene (1976).

Another point to note is that the separation of the two basic physics questions (i.e.,  $n \rightarrow$  ideal MHD and  $\tau_E \rightarrow$  kinetic) is only approximately correct, and often there is significant overlap. For instance, ideal MHD often sets limits on the current that can flow as well as on  $\beta$ . Clearly a current limit will have a direct effect on the maximum possible ohmic heating. Another example is associated with the fact that pressure and current profiles are usually determined by transport. In certain magnetic configurations the pressure and current limits are strong functions of the profiles, again indicating overlap in the physics. It should be kept in mind that by studying only ideal MHD behavior one does not treat such interactions self-consistently.

With these considerations as background, it is the goal of this article to review the ideal MHD equilibrium and stability theory of magnetic fusion configurations and to develop an understanding as to why certain geometries are preferable to others. Since a main virtue of ideal MHD is its ability to distinguish different magnetic geometries, a number of specific examples are discussed. These are chosen from the currently most promising concepts in the international magnetic fusion program and include the tokamak, stellarator, Elmo bumpy torus (EBT), and reversed field pinch (RFP). Each of these is

a toroidal configuration. For reasons discussed later, ideal MHD provides a very poor description of the behavior of open-ended devices. Thus there is no discussion of the important mirror concept. The topic of mirror physics has been reviewed by Baldwin (1977), and the recent tandem mirror concept has been discussed by Dimov *et al.* (1976), Fowler and Logan (1977), and Baldwin and Logan (1979).

The approach that has been adopted in the presentation of this review is one which relies heavily on analytic theory. In particular, once the general properties of the model are established, each magnetic configuration is distinguished by its own characteristic asymptotic expansion (where the expansion parameters are usually geometric or field amplitude ratios). Although such expansions are sometimes only marginally valid in actual experiments, they are extremely useful in delineating the basic physics issues of a given concept. Extensive numerical computations have been carried out for many ideal MHD problems, and these results are summarized in the context of the analytic theory.

The review is organized as follows.

## B. Outline of Section II (the MHD model)

The main purpose of Sec. II is to provide a physical understanding of the ideal MHD model. This is accomplished by deriving the model from a more basic kinetic description and then discussing its regions of validity. The starting point of the derivation is a kinetic model described by the Boltzmann-Maxwell system of equations. After taking moments, a set of two-fluid equations is obtained, and the ideal MHD model represents a low-frequency, long-wavelength limit of these equations.

It is shown that ideal MHD accurately describes phenomena involving the macroscopic length scale  $a$ , the ion thermal velocity scale  $V_{Ti}$ , and the corresponding time scale  $\tau = a/V_{Ti}$  if the following three conditions are satisfied: (1) the gyroradius of an average ion must be much less than the macroscopic scale length; (2) the plasma must be sufficiently large and collision free so that resistive diffusion is negligible; and (3) the plasma must be sufficiently collision dominated so that the pressure is isotropic, the heat conduction parallel to the field is small, and the electron and ion temperatures are equilibrated.

Although there is always a region of parameter space where these three conditions are simultaneously satisfied, plasmas of fusion interest usually lie outside this region. Specifically, the condition of collision dominance is violated. Despite its apparent lack of validity it is pointed out that in practice MHD has had wide success in predicting the macroscopic behavior of experiments. The difficulty is resolved by noting that the errors resulting from violation of collision dominance involve phenomena with gradients parallel to the magnetic field. However, in the analysis of most MHD equilibrium and stability problems, the parallel gradients are either zero or small; that is, the model is incorrect only when it is

not important. The situation is further simplified by the introduction of the "perpendicular MHD model," which is valid over a wider range of parameters, including low collisionality, but which is more restrictive in the class of allowable motions. This model makes predictions very similar to those of ideal MHD.

## C. Outline of Section III (general properties of ideal MHD)

Section III discusses some of the general properties of ideal MHD, with the aim of demonstrating that the model does indeed possess a firm physical foundation for investigating the macroscopic behavior of fusion plasmas. The first topic considered is that of boundary conditions, that is, conditions that must be satisfied at the plasma surface when connecting the plasma to its external environment under a variety of situations. The simplest case corresponds to a boundary which is a rigid, perfectly conducting wall. A more realistic situation allows the plasma to be isolated from the wall by a vacuum region. The most realistic case has the plasma surrounded by vacuum, without a conducting wall, but with fixed external current-carrying conductors.

The second topic discussed concerns conservation laws. It is shown that despite the significant number of assumptions made in the derivation, the model exactly, nonlinearly conserves the mass, momentum, and the energy of the system.

The final topic involves the conservation of flux. Because of the assumption of perfect conductivity associated with the ideal model, it is possible to interpret the plasma motion as one in which both the plasma and magnetic flux move together. This has important implications for plasma stability, in that the magnetic field line topology is constrained to remain unchanged during any plasma motion occurring on the MHD time scale.

## D. Outline of Section IV (equilibrium)

The aims of Sec. IV are to investigate the properties of static ideal MHD equilibria and to develop a physical understanding of how the various forces are developed which hold a plasma in macroscopic force balance. To begin, the general properties of such equilibria are discussed. It is pointed out that, in order to avoid the potentially large end losses implied by the enormous ratio of the thermal conductivities parallel and perpendicular to the magnetic field, most magnetic fusion configurations are toroidal.

It is then shown that two basic problems must be solved in order to produce toroidal equilibria. The first is that of radial pressure balance, which requires "cylindrical" plasma confinement within the minor cross section. The second problem concerns toroidal force balance, which requires the development of a restoring force to compensate for the outward force inherent in any toroidal configuration. If uncompensated, this force

causes a uniform expansion of the major radius of the plasma.

By considering large-aspect-ratio tori, one can achieve asymptotic separation of these two problems; radial pressure balance corresponding to zeroth order and toroidal force balance to first order.

In this expansion radial pressure balance reduces to that in a one-dimensional, infinitely long, straight cylinder. It is demonstrated that two fundamental configurations can produce radial pressure balance: (1) the  $Z$  pinch (i.e., toroidal current); and (2) the  $\theta$  pinch (i.e., poloidal current). Attempts to "bend" these configurations into a torus by accounting for toroidal force balance show that (1) the  $Z$  pinch has satisfactory toroidal equilibria, but that (2) no such equilibria exist for the  $\theta$  pinch. It is pointed out, however, that stability analysis predicts strong instabilities for the  $Z$  pinch, but either positive or neutral stability for the  $\theta$  pinch.

This, then, is the basic dilemma of macroscopic toroidal confinement. Its solution lies in the discovery of optimal combinations of  $Z$  pinch,  $\theta$  pinch, and perhaps other small auxiliary fields which maximize the density and  $\beta$  that can be held in stable toroidal equilibrium.

Such equilibria have been found in two- and three-dimensional geometries. They each make use of one of three different mechanisms which generate a toroidal restoring force. The two-dimensional configurations discussed are axisymmetric tori and include the reversed field pinch (RFP), the conventional tokamak, the high- $\beta$  tokamak, the noncircular tokamak, and the flux-conserving tokamak. In these configurations, toroidal force balance is similar to that in a  $Z$  pinch; that is, it occurs by the interaction of a net toroidal plasma current with either an externally applied vertical field or the image currents induced by a perfectly conducting shell surrounding the plasma.

The most successful axisymmetric toroidal configuration at present is clearly the tokamak. Despite its many virtues it does have the disadvantage as a reactor of being an inherently pulsed device, since the toroidal current required for equilibrium usually corresponds to the secondary of a transformer. [One recent idea to avoid this problem makes use of a radio-frequency current drive (Fisch and Bers, 1978; Fisch, 1978)].

In fact it is the desire to have configurations with zero net toroidal current that is perhaps the prime motivation for studying the very much more complicated three-dimensional geometries, in particular the Elmo bumpy torus (EBT), the high- $\beta$  stellarator, and the conventional stellarator. Each of these concepts has auxiliary helical or bumpy fields superimposed on a basic  $\theta$ -pinch field, but zero net toroidal current. These configurations make use of the two other, somewhat subtle, mechanisms of generating toroidal force balance. These restoring forces result from the interaction of the applied helical (or bumpy) field with induced helical sideband currents and/or induced toroidal dipole currents.

In summary, Sec. IV demonstrates how the ideal

MHD model can be used to calculate a variety of different equilibria of interest to the magnetic fusion program. These equilibria serve two valuable purposes. First, they represent the basis for stability analysis which can then distinguish which configurations are most attractive in terms of  $\beta$  and current limits. Second, numerically computed ideal MHD equilibria are very useful in the practical design and operation of experiments—for example, in choosing the location and current distribution of external conductors, in determining the shape of the plasma, in the investigation of single-particle confinement, and in the interpretation of many diagnostics.

### E. Outline of Section V (stability)

Section V contains a discussion of the linear stability properties of static ideal MHD equilibria. The goal is to distinguish those configurations which are potentially attractive for use in fusion reactors with respect to  $\beta$  and current limits, and to develop an understanding of the basic features of magnetic geometries which are favorable for macroscopic stability.

The first part of the discussion concerns the basic theoretical concepts of ideal MHD stability. It is shown that a current-free, infinite, homogeneous system is exponentially stable; that is, the natural waves which propagate are purely oscillatory. In order to investigate more interesting, inhomogeneous equilibria, a general formulation of the linearized stability equations is presented. These equations, valid for arbitrary geometry, are ultimately cast in the form of an eigenvalue problem. The resulting system is shown to be self-adjoint, implying that the eigenfrequencies are either purely real or purely growing and that stability transitions occur when the eigenfrequency crosses zero.

The linearized eigenvalue equations are then cast into a variational form from which it is possible, because of the conservation of energy, to derive an Energy Principle. This principle determines whether or not a system is stable by examining the sign of a single potential energy integral for all allowable plasma motions. It is the simplest and most convenient procedure for testing stability and is used in all the later applications. The simplicity follows because the Energy Principle, which gives exact information about instability thresholds, only estimates the eigenfrequencies (i.e., growth rates). This lack of information is usually not important because ideal MHD growth times are much shorter than experimental times. Hence a knowledge of the threshold conditions to avoid such instabilities is far more important.

Proceeding with the general formulation of ideal MHD stability, it is demonstrated that, except for certain special configurations, the eigenfunction at a stability threshold corresponds to an incompressible motion of the plasma. A subtle point is then discussed to illustrate the difference in stability between a plasma surrounded by a vacuum region and an ideal force-free plasma carrying zero current in the equilibrium. Because of the topo-

logical constraints associated with perfect conductivity, the vacuum case is often far less stable. In reality the colder, low-density, current-free plasma surrounding the plasma core is usually a good, but not perfect, conductor. However, the small resistivity of the outer plasma causes the thresholds to be identical to those of the vacuum case but with much smaller growth rates.

The final point concerning the general formulation is the classification of ideal MHD instabilities. While the current-free, infinite homogeneous plasma is stable, systems with current flowing either parallel or perpendicular to the magnetic field can drive instabilities. These are referred to as current-driven modes or pressure-driven modes, respectively. Both classes of modes have relatively small parallel wave numbers. The least stable pressure-driven modes have large perpendicular wave numbers and occur when: (1) the average curvature of the magnetic field lines is convex to the plasma (interchange perturbations), or (2) the local curvature is convex (ballooning modes). Current-driven modes, however, have small to moderate perpendicular wave numbers and occur when the parallel current gradient and/or the total parallel current is too large (kink modes).

With this as background, a number of applications are considered. These are restricted to one- and two-dimensional equilibria, since the stability theory for three-dimensional systems is rather incomplete. For the one-dimensional case the first stability analyses presented correspond to the pure  $\theta$  and  $Z$  pinches. The results demonstrate the stability properties stated in connection with the problem of toroidal equilibrium. A formulation is then given of the energy principle for an arbitrary hybrid  $\theta$ - $Z$  pinch, known as the general screw pinch. The reversed field pinch (RFP) is accurately described by this one-dimensional model, and its stability properties are discussed in detail. It is also possible to make a one-dimensional model of a "straight" tokamak. The corresponding stability analysis is reasonably reliable with respect to current-driven modes, but makes optimistic predictions for pressure-driven modes. A more exact treatment of tokamak stability, including pressure-driven modes, is the main topic of the two-dimensional applications. Finally, the stability properties of an infinitely long, two-dimensional model of the Elmo bumpy torus (EBT) are summarized.

This chapter thus demonstrates how the ideal MHD model can be used to test the macroscopic stability of realistic magnetic geometries and indicates why the specific concepts chosen are potentially attractive for use in fusion reactors.

#### F. Units

The basic units used throughout the text are mks units. However, certain "standard" simplifications are introduced. First, wherever Boltzmann's constant  $K$  appears in the text it is absorbed into the temperature. Thus the symbol  $T$  refers to temperature measured in energy units. The permittivity  $\epsilon_0$  and the permeability  $\mu_0$

are maintained, up to the point in Sec. II where the ideal MHD equations are derived. In the final form of the MHD equations, only  $\mu_0$  appears. From this point on,  $\mu_0$  is set equal to unity. This implies, for instance, that magnetic pressure is  $B^2/2$  and that the magnetic field due to a uniform-current-carrying wire is  $B=I/2\pi r$ . Whenever critical dimensionless parameters appear, they are defined in terms of both the modified units and, in parenthesis, the actual mks units, maintaining  $\mu_0$ .

## II. THE MHD MODEL

### A. Introduction

The main goal of this section is to provide a physical understanding of the ideal MHD model. This includes: (1) a basic description of the model, (2) a derivation starting from a more fundamental kinetic description, and, most important, (3) a discussion of its range of validity.

As has been often pointed out, plasmas of fusion interest do not satisfy all the criteria for validity; in particular, they are not sufficiently collisional. On the other hand there is overwhelming empirical evidence that ideal MHD provides a very accurate description of the macroscopic behavior of fusion plasmas. This fact is more than a coincidence. It is explained here by the introduction of a slightly different model, the "perpendicular MHD model," which in most cases of interest makes predictions almost identical to those of ideal MHD but which is valid over a much wider parameter range of fusion interest.

Other discussions of the MHD model can be found in Rose and Clark (1961), Braginskii (1965), Boyd and Sanderson (1969), Krall and Trivelpiece (1973), and Bateman (1978).

### B. Ideal MHD equations

The ideal MHD model provides a single-fluid description of long-wavelength, low-frequency, macroscopic plasma behavior. The equations of ideal MHD are given by

$$\frac{\partial \rho}{\partial t} + \nabla \cdot \rho \mathbf{v} = 0 , \quad (2.1)$$

$$\rho \frac{d\mathbf{v}}{dt} = \mathbf{J} \times \mathbf{B} - \nabla p , \quad (2.2)$$

$$\frac{d}{dt}(p/\rho^\gamma) = 0 , \quad (2.3)$$

$$\mathbf{E} + \mathbf{v} \times \mathbf{B} = 0 , \quad (2.4)$$

$$\nabla \times \mathbf{E} = - \frac{\partial \mathbf{B}}{\partial t} , \quad (2.5)$$

$$\nabla \times \mathbf{B} = \mu_0 \mathbf{J} , \quad (2.6)$$

$$\nabla \cdot \mathbf{B} = 0 . \quad (2.7)$$

In these equations, the electromagnetic variables are the electric field  $\mathbf{E}$ , the magnetic field  $\mathbf{B}$ , and the current density  $\mathbf{J}$ . The fluid variables are the mass density  $\rho$ , the fluid velocity  $\mathbf{v}$ , and the pressure  $p$ . Also  $\gamma = \frac{5}{3}$  is the ratio of specific heats, and  $d/dt = \partial/\partial t + \mathbf{v} \cdot \nabla$  is the convective derivative.

Equations (2.5)–(2.7) indicate that in ideal MHD the electromagnetic behavior is governed by low-frequency, pre-Maxwell equations. Equations (2.1)–(2.3) govern the time evolution of mass, momentum, and energy, respectively. The basic physics of the momentum equation corresponds to that of a fluid with three interacting forces, the pressure gradient force  $\nabla p$ , the magnetic force  $\mathbf{J} \times \mathbf{B}$ , and the inertial force  $\rho d\mathbf{v}/dt$ . The energy equation expresses an adiabatic evolution characterized by a ratio of specific heats,  $\gamma = \frac{5}{3}$ . The remaining relation, Eq. (2.4), is Ohm's law, which implies that in a reference frame moving with the plasma the electric field is zero; that is, the plasma is a perfect conductor. In fact it is the perfect-conductivity assumption of Ohm's law that gives rise to the name "ideal" MHD.

Although many important plasma physics phenomena are neglected in the derivation of the ideal MHD model, the one critical phenomenon that remains is the effect of magnetic geometry on the macroscopic equilibrium and stability of fusion plasmas.

### C. Starting equations

In order to more fully appreciate the physics content of ideal MHD it is useful to derive the equations starting from more basic principles. A number of such derivations exists in the literature, and each, including the present one, follows the same general procedure. See, for instance, Braginskii (1965) and Boyd and Sanderson (1969). The starting point for the present derivation is the full set of Maxwell's equations coupled with a kinetic model of the plasma, described by a Boltzmann equation for each species [a discussion of the starting equations themselves can be found in Montgomery and Tidman (1964) and Krall and Trivelpiece (1973)]. These equations are given by

$$\frac{\partial f_\alpha}{\partial t} + \mathbf{u} \cdot \nabla f_\alpha + \frac{q_\alpha}{m_\alpha} (\mathbf{E} + \mathbf{u} \times \mathbf{B}) \cdot \nabla_{\mathbf{u}} f_\alpha = \left[ \frac{\partial f_\alpha}{\partial t} \right]_c , \quad (2.8)$$

$$\nabla \times \mathbf{E} = - \frac{\partial \mathbf{B}}{\partial t} , \quad (2.9)$$

$$\nabla \cdot \mathbf{B} = 0 , \quad (2.10)$$

$$\begin{aligned} \nabla \times \mathbf{B} &= \mu_0 \mathbf{J} + \frac{1}{c^2} \frac{\partial \mathbf{E}}{\partial t} \\ &= \mu_0 \sum_\alpha q_\alpha \int \mathbf{u} f_\alpha d\mathbf{u} + \frac{1}{c^2} \frac{\partial \mathbf{E}}{\partial t} , \end{aligned} \quad (2.11)$$

$$\nabla \cdot \mathbf{E} = \frac{\sigma}{\epsilon_0} = \frac{1}{\epsilon_0} \sum_\alpha q_\alpha \int f_\alpha d\mathbf{u} . \quad (2.12)$$

Here  $f_\alpha(\mathbf{r}, \mathbf{u}, t)$  is the distribution function for each species  $\alpha$ , and is in general a function of the spatial coordinate, the velocity, and time. It shall be assumed that the plasma is fully ionized and consists of two species; electrons and ions. Hence  $\alpha = e, i$ .

In the Boltzmann description there are two types of forces which act on the particles. First there are the long-range Lorentz forces  $q_\alpha(\mathbf{E} + \mathbf{u} \times \mathbf{B})$ , in which  $\mathbf{E}$  and  $\mathbf{B}$  are smoothly behaving fields calculated from the averaged current and charge density, as indicated in Eqs. (2.11) and (2.12). Second, the right-hand side of Eq. (2.8) represents the forces due to short-range interactions, or collisions. In the derivation presented here, the details of the collision operator are not important, only certain global conservation relations. For plasmas of fusion interest, the dominant collisions are elastic Coulomb collisions between both like and unlike particles. The conservation laws for elastic collisions can be summarized as follows. If the collision operator is defined in the usual way,

$$\left[ \frac{\partial f_\alpha}{\partial t} \right]_c = \sum_\beta C_{\alpha\beta} , \quad (2.13)$$

where  $C_{\alpha\beta}$  represents collisions of particles of species  $\alpha$  with particles of species  $\beta$ , then:

(1) Conservation of particles in like and unlike particle collisions implies

$$\int C_{ee} d\mathbf{u} = \int C_{ii} d\mathbf{u} = \int C_{ei} d\mathbf{u} = \int C_{ie} d\mathbf{u} = 0 ; \quad (2.14)$$

(2) Conservation of momentum and energy in collisions between like particles implies

$$\int m_e \mathbf{u} C_{ee} d\mathbf{u} = \int m_i \mathbf{u} C_{ii} d\mathbf{u} = 0 , \quad (2.15)$$

$$\int \frac{1}{2} m_e u^2 C_{ee} d\mathbf{u} = \int \frac{1}{2} m_i u^2 C_{ii} d\mathbf{u} = 0 ; \quad (2.16)$$

(3) Conservation of total momentum and energy in collisions between unlike particles implies

$$\int (m_e \mathbf{u} C_{ei} + m_i \mathbf{u} C_{ie}) d\mathbf{u} = 0 , \quad (2.17)$$

$$\int \frac{1}{2} (m_e u^2 C_{ei} + m_i u^2 C_{ie}) d\mathbf{u} = 0 . \quad (2.18)$$

More detailed discussions of collisions in a plasma have been given by Spitzer (1956), Rose and Clark (1961), and Krall and Trivelpiece (1973).

The full set of Boltzmann-Maxwell equations provides a very detailed and complete description of plasma behavior. On the one hand it contains microscopic information about the orbits of individual charged particles, while on the other hand it accurately describes the macroscopic behavior of large plasma experiments. Not surprisingly, the complexity arising from this breadth of information makes it virtually impossible, even numerically, to solve the Boltzmann-Maxwell system of equations in any nontrivial geometry. This realization has led to the development of several simpler models with narrower physical content. Ideal MHD is such a model.

## D. Two-fluid equations

The first step in the derivation of the MHD equations is to take appropriate moments of the Boltzmann equation. This leads to a set of “two fluid” equations. The appropriate moments correspond to mass, momentum, and energy; that is,

$$\int Q_i \left[ \frac{df_\alpha}{dt} - \left[ \frac{\partial f_\alpha}{\partial t} \right]_c \right] d\mathbf{u} = 0 \quad (i=1-3),$$

$$Q_1 = 1, \quad Q_2 = m_\alpha \mathbf{u}, \quad Q_3 = \frac{1}{2} m_\alpha u^2. \quad (2.19)$$

After some straightforward algebra the fluid equations for each species can be written as

$$\frac{\partial n_\alpha}{\partial t} + \nabla \cdot n_\alpha \mathbf{v}_\alpha = 0,$$

$$\frac{\partial}{\partial t} (m_\alpha n_\alpha \mathbf{v}_\alpha) + \nabla \cdot (m_\alpha n_\alpha \langle \mathbf{u} \mathbf{u} \rangle) - q_\alpha n_\alpha (\mathbf{E} + \mathbf{v}_\alpha \times \mathbf{B})$$

$$= \int m_\alpha \mathbf{u} C_{\alpha\beta} d\mathbf{u}, \quad \alpha \neq \beta, \quad (2.20)$$

$$\frac{\partial}{\partial t} (\frac{1}{2} m_\alpha n_\alpha \langle u^2 \rangle) + \nabla \cdot (\frac{1}{2} m_\alpha n_\alpha \langle u^2 \mathbf{u} \rangle) - q_\alpha n_\alpha \mathbf{v}_\alpha \cdot \mathbf{E}$$

$$= \int \frac{1}{2} m_\alpha u^2 C_{\alpha\beta} d\mathbf{u}, \quad \alpha \neq \beta.$$

Here  $n_\alpha$  and  $\mathbf{v}_\alpha$  are the macroscopic number density and fluid velocity defined by

$$n_\alpha(\mathbf{r}, t) \equiv \int f_\alpha d\mathbf{u},$$

$$\mathbf{v}_\alpha(\mathbf{r}, t) \equiv \frac{1}{n_\alpha} \int \mathbf{u} f_\alpha d\mathbf{u}. \quad (2.21)$$

The quantities  $\langle \mathbf{u} \mathbf{u} \rangle$ ,  $\langle u^2 \rangle$ , and  $\langle u^2 \mathbf{u} \rangle$  are higher moments of the distribution function defined by the general relation

$$\langle Q \rangle \equiv \frac{1}{n_\alpha} \int Q f_\alpha d\mathbf{u}. \quad (2.22)$$

As is customary in deriving fluid equations, a new velocity variable is introduced,  $\mathbf{w} = \mathbf{u} - \mathbf{v}_\alpha(\mathbf{r}, t)$ , representing the random motion of the particles, so that  $\langle \mathbf{w} \rangle = 0$ . By introducing this variable into Eq. (2.20), we can write the fluid equations in terms of more physical macroscopic quantities. In particular, it is useful to introduce the scalar part of the pressure,

$$p_\alpha \equiv \frac{1}{3} n_\alpha m_\alpha \langle w^2 \rangle, \quad (2.23)$$

the total pressure tensor,

$$\vec{P}_\alpha \equiv n_\alpha m_\alpha \langle \mathbf{w} \mathbf{w} \rangle, \quad (2.24)$$

the anisotropic part of the pressure tensor,

$$\vec{\Pi}_\alpha \equiv \vec{P}_\alpha - p_\alpha \vec{I}, \quad (2.25)$$

the temperature,

$$T_\alpha \equiv p_\alpha / n_\alpha, \quad (2.26)$$

the heat flux due to random motion,

$$\mathbf{h}_\alpha \equiv \frac{1}{2} n_\alpha m_\alpha \langle w^2 \mathbf{w} \rangle, \quad (2.27)$$

the mean momentum transfer between unlike particles due to the friction of collisions,

$$\mathbf{R}_\alpha \equiv \int m_\alpha \mathbf{w} C_{\alpha\beta} d\mathbf{w}, \quad (2.28)$$

and the heat generated due to collisions between unlike particles,

$$Q_\alpha \equiv \int \frac{1}{2} m_\alpha w_\alpha^2 C_{\alpha\beta} d\mathbf{w}. \quad (2.29)$$

Substituting these relations into Eq. (2.20) and performing some standard algebraic rearrangement then leads to the following set of two-fluid equations:

$$\frac{dn_\alpha}{dt} + n_\alpha \nabla \cdot \mathbf{v}_\alpha = 0,$$

$$n_\alpha m_\alpha \frac{d\mathbf{v}_\alpha}{dt} - q_\alpha n_\alpha (\mathbf{E} + \mathbf{v}_\alpha \times \mathbf{B}) + \nabla \cdot \vec{P}_\alpha = \mathbf{R}_\alpha,$$

$$\frac{3}{2} n \frac{dT_\alpha}{dt} + \vec{P}_\alpha \cdot \nabla \mathbf{v}_\alpha + \nabla \cdot \mathbf{h}_\alpha = Q_\alpha,$$

$$\nabla \times \mathbf{E} = - \frac{\partial \mathbf{B}}{\partial t},$$

$$\nabla \times \mathbf{B} = \mu_0 e (n_i \mathbf{v}_i - n_e \mathbf{v}_e) + \frac{1}{c^2} \frac{\partial \mathbf{E}}{\partial t},$$

$$\nabla \cdot \mathbf{E} = \frac{e}{\epsilon_0} (n_i - n_e),$$

$$\nabla \cdot \mathbf{B} = 0, \quad (2.30)$$

where it has been assumed that the ions are singly charged so that  $q_i = -q_e = e$ .

Equations (2.30) are exact, if not very useful, since there is as yet no prescription for closing the sequence of higher-order moments of the system. The particular prescription which leads to the ideal MHD equations consists of the following steps. First, certain asymptotic approximations are made which eliminate the very-high-frequency, short-wavelength information. These approximations are easily satisfied when considering macroscopic behavior of fusion plasmas. Next, the equations are rewritten as a set of single-fluid equations by the introduction of approximate single-fluid variables. By assuming the plasma is collision dominated, one can approximate the higher moments from standard transport theory. It is then possible to determine a set of validity conditions such that the remaining equations are those of ideal MHD.

## E. Asymptotic approximations

There are two important asymptotic approximations which can be made. They are asymptotic in that each one eliminates a leading-order time derivative, thus altering the basic mathematical structure describing the time evolution.

The first of these is the transformation of the full Maxwell's equations to the low-frequency Maxwell's

equations. This limit can be obtained formally by letting  $\epsilon_0 \rightarrow 0$ . As a result the displacement current  $\epsilon_0 \partial \mathbf{E} / \partial t$  and the charge  $\epsilon_0 \nabla \cdot \mathbf{E}$  can both be neglected. The neglect of the displacement current implies that the electromagnetic waves of interest will have phase velocities much slower than the speed of light,  $\omega/k \ll c$ . Also, the thermal velocities are assumed to be nonrelativistic,  $V_{Te}, V_{Ti} \ll c$ ,  $V_{T\alpha} = (2T_\alpha/m_\alpha)^{1/2}$ . The neglect of  $\epsilon_0 \nabla \cdot \mathbf{E}$  restricts attention to phenomena whose characteristic frequency is much less than the electron plasma frequency  $\omega \ll \omega_{pe}$ ,  $\omega_{pe} \equiv (ne^2/m_e \epsilon_0)^{1/2}$  and whose characteristic length is much longer than the Debye length  $L \gg \lambda_d$ ,  $\lambda_d \equiv V_{Te}/\omega_{pe}$ . Each of these assumptions is very well satisfied when considering the macroscopic behavior of fusion plasmas.

The neglect of  $\epsilon_0 \nabla \cdot \mathbf{E}$  implies that  $n_i = n_e \equiv n$ . This relationship is called the "charge neutral" approximation. Note that it does not imply that  $\mathbf{E}$  or  $\nabla \cdot \mathbf{E} = 0$ . What is implied is that the electric field must adjust itself so that charge neutrality persists. For example, in an electrostatic problem  $E = -\nabla\phi$ , and one can imagine calculating  $n_e = n_e(\phi, \mathbf{r})$  and  $n_i(\phi, \mathbf{r})$ . Equating  $n_e$  to  $n_i$  and inverting the relationship then gives  $\phi = \phi(\mathbf{r})$ . The neglect of  $\epsilon_0 \nabla \cdot \mathbf{E}$  corresponds to calculating  $\mathbf{E} = -\nabla\phi$  and showing that  $\epsilon_0 \nabla \cdot \mathbf{E}/en \ll 1$ .

The second asymptotic approximation neglects electron inertia in the electron momentum equation and is accomplished formally by letting  $m_e \rightarrow 0$ . This implies that on time scales of MHD interest the electrons have an infinitely fast response time because of their small mass. Specifically, time scales which are long compared to those of the electron plasma frequency  $\omega_{pe}$  and the electron cyclotron frequency  $\omega_{ce} = eB/m_e$  are required. Similarly, the length scales must be long compared to the Debye length  $\lambda_d$  and the electron Larmor radius  $r_{Le} = V_{Te}/\omega_{ce}$ . As before, these conditions are easily satisfied for macroscopic phenomena in fusion plasmas.

One somewhat subtle point should be made regarding the neglect of electron inertia. There is a class of low-frequency, long-wavelength modes in plasmas whose length and time scales are not too much shorter and faster than those of MHD. These modes, called drift waves, are strongly affected by resonant particles moving along field lines. Thus, even with their small mass, the electrons do not respond "instantaneously," since they have to move a long distance to traverse one wavelength. When electron inertia is neglected, the physics of the drift wave is no longer accurately treated. [The theory of drift waves has been reviewed by Mikhailovskii (1967) and Krall and Trivelpiece (1973).] Thus one should keep in mind that a complete study of low-frequency plasma stability may require several separate treatments of different phenomena.

## F. Single-fluid equations

Using the asymptotic approximations just described, one can derive a set of single-fluid equations by introducing appropriate fluid variables. To begin, it is cus-

tomary to introduce a mass density rather than a number density. Since  $m_e \rightarrow 0$  and  $n_i = n_e \equiv n$ , the mass density is defined as

$$\rho = m_i n . \quad (2.31)$$

Likewise, the momentum of the fluid is carried by the ions, so that the appropriate definition of the fluid velocity is given by

$$\mathbf{v} = \mathbf{v}_i . \quad (2.32)$$

The current density is proportional to the difference in flow velocity between electrons and ions

$$\mathbf{J} = en (\mathbf{v}_i - \mathbf{v}_e) \quad (2.33)$$

or

$$\mathbf{v}_e = \mathbf{v} - \mathbf{J}/en . \quad (2.34)$$

The final definitions required are for the total pressure and temperature

$$\begin{aligned} p &= nT = p_e + p_i , \\ T &= T_e + T_i . \end{aligned} \quad (2.35)$$

Equations (2.31)–(2.35) relate the single-fluid variables  $\rho, \mathbf{v}, \mathbf{J}, p, T$  to the two-fluid variables  $n, \mathbf{v}_i, \mathbf{v}_e, p_e, p_i, T_e, T_i$ .

The first of the MHD equations is obtained from the conservation-of-mass equations. Multiplying the ion mass equation by  $m_i$  one finds

$$\frac{\partial \rho}{\partial t} + \nabla \cdot \rho \mathbf{v} = 0 , \quad (2.36)$$

which is identical to Eq. (2.1), the ideal MHD mass conservation relation. The other information contained in these equations is obtained by multiplying the electron and ion equation by  $e$  and then subtracting. The result is

$$\nabla \cdot \mathbf{J} = 0 . \quad (2.37)$$

Equation (2.37) is consistent with charge conservation in the low-frequency form of Maxwell's equations.

The next set of MHD equations follows from the momentum equations. The electron and ion equations are first added together. Making use of the fact that  $\mathbf{R}_e = -\mathbf{R}_i$  leads to the relationship

$$\rho \frac{d\mathbf{v}}{dt} - \mathbf{J} \times \mathbf{B} + \nabla p = -\nabla \cdot [\hat{\Pi}_i + \hat{\Pi}_e] . \quad (2.38)$$

Here  $d/dt = \partial/\partial t + \mathbf{v} \cdot \nabla$  now represents the convective derivative moving with the (ion) fluid. The left-hand side of Eq. (2.38) corresponds to the ideal MHD momentum equation. The condition under which the right-hand side is negligible determines one range of validity for the MHD equations and will be discussed shortly. Note that there is no electric force  $\sigma \mathbf{E}$  acting on the fluid, since  $\sigma = 0$  as a result of the charge neutral approximation.

The other information contained in the two-fluid momentum equations is obtained by simply rewriting the electron equation in terms of the single-fluid variables.

This leads to the following relation:

$$\mathbf{E} + \mathbf{v} \times \mathbf{B} = \frac{1}{en} (\mathbf{J} \times \mathbf{B} - \nabla p_e - \nabla \cdot \vec{\Pi}_e + \mathbf{R}_e) . \quad (2.39)$$

The left-hand side of Eq. (2.39) corresponds to Ohm's law. The conditions under which the right-hand side is negligible determine another region of validity, to be discussed shortly.

The third set of MHD equations follows from the two-fluid energy equations. After some straightforward algebra one obtains

$$\frac{d}{dt} \left[ \frac{p_i}{\rho^\gamma} \right] = \frac{2}{3\rho^\gamma} (Q_i - \nabla \cdot \mathbf{h}_i - \vec{\Pi}_i \cdot \mathbf{v}) , \quad (2.40a)$$

$$\begin{aligned} \frac{d}{dt} \left[ \frac{p_e}{\rho^\gamma} \right] &= \frac{2}{3\rho^\gamma} \left[ Q_e - \nabla \cdot \mathbf{h}_e - \vec{\Pi}_e : \left[ \mathbf{v} - \frac{\mathbf{J}}{en} \right] \right] \\ &\quad + \frac{1}{en} \mathbf{J} \cdot \nabla \left[ \frac{p_e}{\rho^\gamma} \right] . \end{aligned} \quad (2.40b)$$

The last term in Eq. (2.40b) results from the relation  $(d/dt)_e = (d/dt) - (\mathbf{J}/en) \cdot \nabla$ . The left-hand side of Eq. (2.40) is closely related to the ideal MHD equation of state. There are a number of terms on the right-hand side; neglecting these imposes further conditions on the region of validity. Furthermore, since MHD is a single-fluid model, still other assumptions must be made to closely couple the electron and ion energies into a single-fluid energy.

The final equations of the single-fluid model are the remaining low-frequency Maxwell's equations given by

$$\begin{aligned} \nabla \times \mathbf{E} &= - \frac{\partial \mathbf{B}}{\partial t} , \\ \nabla \times \mathbf{B} &= \mu_0 \mathbf{J} , \\ \nabla \cdot \mathbf{B} &= 0 . \end{aligned} \quad (2.41)$$

As stated previously, Eq. (2.37) is consistent with the low-frequency form of Ampere's law.

The single-fluid model is described by Eqs. (2.36)–(2.41). No assumptions other than the asymptotic approximations have been made at this point. Although the left-hand side of the fluid equations is identical to the MHD model, the full set of equations is still incomplete because of the presence of the as yet undefined higher moments.

#### G. The ideal MHD limit

In this section the single-fluid equations are investigated quantitatively to determine the conditions under which the model reduces to ideal MHD, in particular, to determine when the right-hand sides of Eqs. (2.38)–(2.40) become negligible.

The basic requirement for the validity of ideal MHD is that both the electrons and the ions be collision dominated. This is the usual requirement for a fluid model to be useful. If there are sufficiently many collisions, a

given particle remains reasonably close to its neighboring particles during time scales of interest. In this case the division of the plasma into small, identifiable fluid elements provides a good description of the physics.

In the collision-dominated limit the distribution function for both electrons and ions is nearly locally Maxwellian in form. As a consequence, one can refer to well-established theories (e.g., Braginskii, 1965), in order to obtain expressions for the higher-order fluid moments in terms of appropriate transport coefficients. By defining the characteristic length and time scales of ideal MHD, it is possible to compare the MHD terms with the transport terms. This then determines the conditions under which the right-hand sides of the single-fluid equations are negligible, and the model reduces to ideal MHD.

A convenient place to begin the analysis is with the specification of the characteristic MHD length and time scales. Since the main goal of ideal MHD is the investigation of macroscopic phenomena, the length scales of interest correspond to the macroscopic dimensions of the plasma denoted by  $a$ . The typical time scale of MHD interest corresponds to  $a/V_{Ti}$ ,  $V_{Ti} = (2T_i/m_i)^{1/2}$ , the ion thermal transit time across a macroscopic plasma dimension. This time scale is characteristic of many MHD plasma instabilities. It should be noted that other MHD instabilities and phenomena can have time scales somewhat faster or slower than  $a/V_{Ti}$ . For the present purposes, however, it is not crucial to make these distinctions. In determining the scaling relations it is helpful to introduce the characteristic MHD frequency  $\omega$  and wave number  $k$  as follows:

$$\begin{aligned} \omega &\sim \frac{\partial}{\partial t} \sim \frac{V_{Ti}}{a} , \\ k &\sim \nabla \sim \frac{1}{a} , \end{aligned} \quad (2.42)$$

and similarly, the resulting velocity

$$\frac{\omega}{k} \sim \mathbf{v} \sim V_{Ti} . \quad (2.43)$$

The next step in the analysis is to consider the conditions necessary for the approximation of collision dominance to be valid. There are two such conditions. The first is that during MHD time scales of interest each species have sufficiently many collisions to make the distribution function nearly Maxwellian. For the ions the dominant collision mechanism is due to ion-ion interactions, characterized by a collision time  $\tau_{ii}$ . The electrons become Maxwellian by colliding with either other electrons or ions. Since  $\tau_{ee} \sim \tau_{ei}$ , it is not important to make this distinction. Hence the condition that each species be collision dominated is given by:

$$\text{Ions } \omega \tau_{ii} \sim V_{Ti} \tau_{ii} / a \ll 1 , \quad (2.44a)$$

$$\text{Electrons } \omega \tau_{ee} \sim V_{Ti} \tau_{ee} / a \sim (m_e/m_i)^{1/2} V_{Ti} \tau_{ii} / a \ll 1 . \quad (2.44b)$$

Here use has been made of the fact that  $\tau_{ee} \sim (m_e/m_i)^{1/2} \tau_{ii}$  when  $T_e \sim T_i$ . As might be expected,

this condition is more restrictive for ions than for electrons.

The second condition for collision dominance to be valid is that the macroscopic scale length be much longer than the mean-free path. Noting that the mean-free path for each species is given by  $\lambda_\alpha \sim V_{T\alpha} \tau_{\alpha\alpha}$ , the condition  $\lambda_\alpha \ll a$  reduces to Eq. (2.44a) for both electrons and ions; that is, for the ions both the time scale and length scale requirements yield the same condition for high collisionality. For the electrons, the length scale requirement is more restrictive and yields the same condition as for the ions. Thus the conditions for a collision-dominated plasma can be summarized as

$$V_{Ti} \tau_{ii} / a \sim V_{Te} \tau_{ee} / a \ll 1. \quad (2.45)$$

Consider now the effects of collision dominance on the single-fluid equations, starting with Eq. (2.38), the momentum equation. The matrix elements for  $\vec{\Pi}_i$  and  $\vec{\Pi}_e$  are a rather complicated series of terms. The leading-ordering effect, however, is viscosity. Moreover, the ion viscosity coefficient is larger than that of the electrons by a factor  $(m_i/m_e)^{1/2}$ . Using the results of Braginskii (1965), it follows that the largest elements of the  $\vec{\Pi}_i$  tensor have the form (in rectangular coordinates)

$$\begin{aligned} \Pi_{jj} &\sim \mu (2\nabla_{||} \cdot \mathbf{v}_{||} - \frac{2}{3} \nabla \cdot \mathbf{v}) \sim \mu V_{Ti} / a, \\ \mu &\sim n T_i \tau_{ii}. \end{aligned} \quad (2.46)$$

If the right-hand side of Eq. (2.38) is now compared with the  $\nabla p$  term one finds

$$|\nabla \cdot \vec{\Pi}_i / \nabla p| \sim V_{Ti} \tau_{ii} / a \ll 1. \quad (2.47)$$

Therefore, if collision dominance is satisfied, the viscosity is negligible and the momentum equation reduces to that of ideal MHD.

The next equation to consider is Ohm's law, given by Eq. (2.39). From the argument just given it is clear that the  $\vec{\Pi}_e$  term is negligible compared to the  $\nabla p_e$  term. From the momentum equation it also follows that the  $\mathbf{J} \times \mathbf{B}$  and  $\nabla p_e$  terms are comparable. The  $\mathbf{J} \times \mathbf{B}$  term represents the Hall effect, while the  $\nabla p_e$  term basically describes the electron diamagnetism. Comparing either of these terms with the  $\mathbf{v} \times \mathbf{B}$  term yields

$$\frac{|\nabla p_e / en|}{|\mathbf{v} \times \mathbf{B}|} \sim \frac{r_{Li}}{a}, \quad (2.48)$$

where  $r_{Li} = V_{Ti} / \omega_{ci}$  is the ion gyroradius. Thus if it is assumed that

$$\frac{r_{Li}}{a} \ll 1, \quad (2.49)$$

the  $\mathbf{J} \times \mathbf{B}$  and  $\nabla p_e$  terms can be neglected in Ohm's law. The remaining term on the right-hand side of Eq. (2.39),  $\mathbf{R}_e / en$ , represents the momentum transfer due to the friction of collisions between electrons and ions. The dominant contribution to  $\mathbf{R}_e$  is electrical resistivity. Using the results from transport theory,  $\mathbf{R}_e$  can be expressed as

$$\begin{aligned} \frac{1}{en} \mathbf{R}_e &\sim \eta \mathbf{J}, \\ \eta &\sim \frac{m_e}{ne^2 \tau_{ei}}. \end{aligned} \quad (2.50)$$

Using the scaling relation (from the momentum equation)  $|\mathbf{J}| \sim |\nabla p| / |\mathbf{B}|$  leads to the following condition for the  $\eta \mathbf{J}$  term to be negligible compared to the  $\mathbf{v} \times \mathbf{B}$  term:

$$\frac{|\eta \mathbf{J}|}{|\mathbf{v} \times \mathbf{B}|} \sim \frac{(m_e/m_i)^{1/2}}{\omega \tau_{ii}} \left[ \frac{r_{Li}}{a} \right]^2 \ll 1. \quad (2.51)$$

Equation (2.51) implies that, whereas a sufficient number of collisions is required for the theory to be valid, there should not be too many collisions or else the plasma will be dominated by resistive diffusion. Alternatively one can view Eq. (2.51) as a requirement that the macroscopic dimension  $a$  be large enough so that the resistive diffusion time is long compared to the characteristic MHD time. Thus, in order to apply the ideal MHD Ohm's law the small gyroradius and small resistivity conditions must both be satisfied.

The last equations to consider are the energy relations given by Eq. (2.40). With the assumptions already made, most of the terms on the right-hand sides are negligible. In particular,

$$\begin{aligned} \frac{\vec{\Pi}_e : \nabla (\mathbf{J}/en)}{\partial p_e / \partial t} &\sim \left[ \frac{m_e}{m_i} \right]^{1/2} \left[ \frac{r_{Li}}{a} \right] \left[ \frac{V_{Ti} \tau_{ii}}{a} \right] \ll 1, \\ \frac{(\mathbf{J} \cdot \nabla p_e) / en}{\partial p_e / \partial t} &\sim \frac{r_{Li}}{a} \ll 1, \\ \frac{\vec{\Pi}_e : \nabla \mathbf{v}}{\partial p_e / \partial t} &\sim \left[ \frac{m_e}{m_i} \right]^{1/2} \left[ \frac{V_{Ti} \tau_{ii}}{a} \right] \ll 1, \\ \frac{\vec{\Pi}_i : \nabla \mathbf{v}}{\partial p_i / \partial t} &\sim \left[ \frac{V_{Ti} \tau_{ii}}{a} \right] \ll 1. \end{aligned} \quad (2.52)$$

The remaining terms contain the heat flux  $\mathbf{h}$  and the collisional heating  $Q$ . The largest contribution to  $\mathbf{h}$  is due to thermal conductivity. For both electrons and ions there are separate conductivity coefficients along and perpendicular to the field. By far the largest coefficients are those along the field, so that  $\mathbf{h}_j \approx -\kappa_{||j} \nabla_{||j} T_j$ . The main contributions to the collisional heating  $Q$  are joule heating and electron and ion energy equilibration. If the condition to neglect resistive diffusion, Eq. (2.51), is satisfied, then joule heating is also negligible. Therefore what remains of the energy equations is

$$\begin{aligned} \frac{d}{dt} \left[ \frac{p_i}{\rho^\gamma} \right] &= \frac{2}{3\rho^\gamma} \left[ \nabla_{||} \cdot (\kappa_{||i} \nabla T_i) + \frac{n(T_e - T_i)}{\tau_{eq}} \right], \\ \frac{d}{dt} \left[ \frac{p_e}{\rho^\gamma} \right] &= \frac{2}{3\rho^\gamma} \left[ \nabla_{||} \cdot (\kappa_{||e} \nabla T_e) - \frac{n(T_e - T_i)}{\tau_{eq}} \right], \end{aligned} \quad (2.53)$$

where  $\tau_{eq}$  is the energy equilibration time. As they now

stand, these equations describe the separate time evolution of both the electrons and the ions. In order to obtain the MHD energy equation, a further assumption is required which couples the electron and ion energies together. This assumption corresponds to the condition that the energy equilibration time be short compared to the characteristic times of interest, so that  $T_e \approx T_i$ . This can be expressed as  $\omega \tau_{eq} \ll 1$  or, using the relation  $\tau_{eq} \sim (m_i/m_e)^{1/2} \tau_{ii}$ ,

$$\left[ \frac{m_i}{m_e} \right]^{1/2} \frac{V_{Ti} \tau_{ii}}{a} \ll 1. \quad (2.54)$$

Because the energy equilibration time is long compared to the momentum exchange time, Eq. (2.54) is even more restrictive in terms of collisionality than Eq. (2.44), the basic condition for the collision dominance expansion to be valid.

If Eq. (2.54) is satisfied, then Eq. (2.53) implies that  $T_i \approx T_e$ . The other information contained in Eq. (2.53) can be obtained by adding the equations and setting  $T_e = T_i = T/2$ . The result is

$$\frac{d}{dt} \left[ \frac{p}{\rho^{\gamma}} \right] = \frac{1}{3\rho^{\gamma}} \nabla_{||} \cdot [(\kappa_{||e} + \kappa_{||i}) \nabla_{||} T]. \quad (2.55)$$

The ideal MHD equation of state follows if the right-hand side of Eq. (2.55) can be neglected. The parallel electron thermal conductivity is larger by  $(m_i/m_e)^{1/2}$  than that of the ions. Thus, using the result from transport theory that  $\kappa_{||e} \sim n T_e \tau_{ei}/m_e$ , it follows that the right-hand side is negligible if

$$\frac{\nabla_{||} \cdot (\kappa_{||e} \nabla_{||} T)}{\partial p / \partial t} \sim \left[ \frac{m_i}{m_e} \right]^{1/2} \frac{V_{Ti} \tau_{ii}}{a} \ll 1, \quad (2.56)$$

which is identical to Eq. (2.54).

This completes the derivation of the ideal MHD equations. In summary, the validity of ideal MHD imposes several conditions on the plasma: (1) collision dominance, (2) characteristic dimensions much larger than an ion gyroradius, and (3) sufficient size that resistive diffusion is negligible, despite the high collisionality.

## H. Region of validity

At this point it is useful to list in detail the most restrictive conditions required for the derivation of the ideal MHD equations and to discuss their regions of validity. This can be conveniently accomplished by introducing the dimensionless variables,

$$y = \frac{r_{Li}}{a},$$

$$x = \left[ \frac{m_i}{m_e} \right]^{1/2} \frac{V_{Ti} \tau_{ii}}{a}. \quad (2.57)$$

As we have seen above, there are three independent conditions which must be satisfied for ideal MHD to be valid. They are:

- (1) Small gyroradius  $y \ll 1$
- (2) Large collisionality  $x \ll 1$
- (3) Small resistivity  $y^2/x \ll 1$ . (2.58)

These conditions are illustrated in Fig. 1. The shaded region on each of the curves indicates that the given condition has been satisfied. In the region labeled "ideal MHD" all three conditions are simultaneously satisfied. Although a significant number of approximations have been made in the derivation, there is a substantial region of parameter space where all the assumptions are satisfied and the ideal MHD equations are valid.

The next question to be asked is whether plasmas of fusion interest lie in the region of MHD validity. This can be answered by transforming the  $(x,y)$  diagram into an  $(n,T)$  diagram and observing whether values of  $n$  and  $T$  of fusion interest lie in the region of validity.

The first step is to define the parameter range of fusion interest. Past experiments and extrapolations to future fusion reactors indicate that the densities and temperatures of fusion plasmas lie in the range

$$10^{12} \text{ cm}^{-3} < n < 10^{16} \text{ cm}^{-3},$$

$$0.1 \text{ keV} < T < 10 \text{ keV}. \quad (2.59)$$

These conditions describe a rectangle in the  $(n,T)$  diagram.

The next step is to rewrite the conditions in Eq. (2.58) in terms of  $n$  and  $T$ . Since the  $B$  field explicitly appears, a prescription is needed to specify how  $B$  varies with  $n$  and  $T$ . A reasonable choice is to assume  $\beta = 2\mu_0 n T / B^2$  is held fixed. The parameter  $\beta$  measures the ratio of plasma energy to magnetic energy. Its value is important in fusion reactor designs and is often limited by

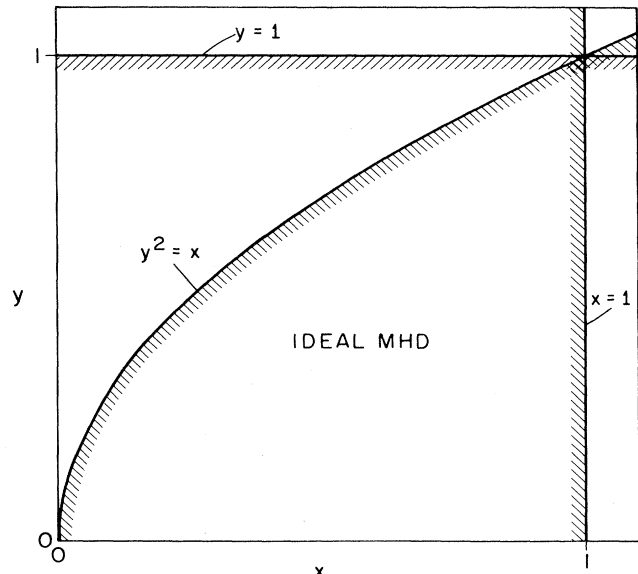


FIG. 1. Region of validity of the ideal MHD model in terms of the normalized variables  $y = r_{Li}/a$ , vs  $x = (m_i/m_e)^{1/2} \times (V_{Ti} \tau_{ii}/a)$ .

MHD instabilities. Consequently treating  $\beta$  and the scale length  $a$  as parameters leads to the following expressions for the three MHD criteria of validity:

(1) Small gyroradius

$$y = 2.28 \times 10^5 \left( \frac{\beta}{a^2 n} \right)^{1/2} \ll 1,$$

(2) Large collisionality

$$x = 9.88 \times 10^{17} \frac{T^2}{na} \ll 1,$$

(3) Small resistivity

$$y^2/x = 5.26 \times 10^{-8} \frac{\beta}{aT^2} \ll 1. \quad (2.60)$$

In these expressions the units are  $a$  (m),  $T$  (keV),  $n$  ( $\text{cm}^{-3}$ ). Also the Coulomb logarithm appearing in the expression for  $\tau_{ii}$  has been set to 18, and the ion mass corresponds to deuterium.

Equation (2.60) is illustrated in Fig. 2 for the case  $a=1$  m and  $\beta=0.05$ . Observe that the conditions of small gyroradius and small resistivity are well satisfied for plasmas of fusion interest. Note, however, that the large collisionality condition is not satisfied. Thus the region where ideal MHD is valid completely excludes plasmas of fusion interest. In fact, even if one puts aside the question of electron-ion equilibration and considers the less restrictive collisionality condition  $\omega\tau_{ii} = (m_e/m_i)^{1/2}x \ll 1$  (the dashed curve in Fig. 2), the region corresponding to plasmas of fusion interest is still almost completely excluded.

From the above analysis one is forced to conclude that, whatever virtues the ideal MHD model may have, the model is, strictly speaking, not valid for plasmas of fusion interest. However, as was stated previously, there is overwhelming empirical evidence that ideal MHD provides a rather accurate description of a wide variety of macroscopic plasma behavior. For examples of this, see,

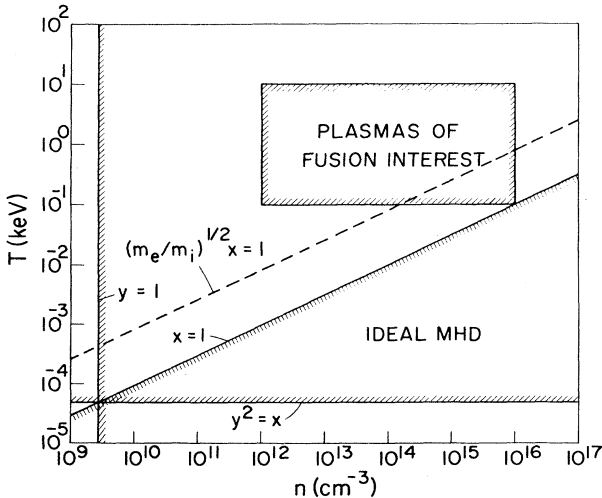


FIG. 2. Region of validity of the ideal MHD model in  $(n, T)$  parameter space for fixed  $\beta=0.05$  and  $a=1$  m.

Furth (1975), Bartsch *et al.* (1978), Bateman (1978), and Bodin and Newton (1980). There is good reason for this apparent good fortune, and the explanation is given in the next section with the introduction of the “perpendicular MHD” model.

## I. Perpendicular MHD

### 1. General discussion

The perpendicular MHD model has the property of making predictions which are almost identical to those of ideal MHD in almost all cases of interest. However, its region of validity includes plasmas of fusion interest. In those cases where the predictions are not similar, neither model is in general reliable.

The main difference in the models is that perpendicular MHD assumes that fusion plasmas are nearly collision free rather than collision dominated. In this limit the magnetic field in a certain sense plays the role of collisions; that is, perpendicular to the field, particles stay in the vicinity of a given magnetic line if their gyroradius is much smaller than the characteristic plasma length. Consequently, it is appropriate to treat the perpendicular behavior of the plasma with a fluid model.

However, the situation parallel to the field is much more complicated in a collisionless plasma. In fact, it is here that ideal MHD treats the physics very inaccurately and leads to the conclusion that the model, in particular the energy equation, is almost always invalid. The situation cannot be easily remedied by assuming a different expansion and proceeding with dimensional analysis. The reason is that the motion along field lines is kinetic, and the time scale describing such phenomena is typically  $a_{||}/V_{Ti}$ . This is identical to the time scale of MHD interest.

One way to correct the problem is with the guiding-center plasma model, as described, for instance, by Grad (1962, 1967b). Here the perpendicular motion is fluid-like, while a one-dimensional kinetic equation governs the behavior parallel to the field. This model is more general than ideal or perpendicular MHD in that anisotropic pressure is allowed. It is also more difficult to solve, particularly when parallel motion is involved. For the special subclass of isotropic equilibria, the guiding-center plasma model often makes macroscopic stability predictions remarkably close to those of ideal or perpendicular MHD. Similarly, there is another model, the guiding-center fluid model, described by Grad (1967b) and Chew, Goldberger, and Low (1956), in which the pressure is allowed to be anisotropic and there is a separate equation of state for  $p_{\perp}$  and  $p_{||}$ . This model also makes predictions similar to those of ideal MHD for the isotropic case, but its validity, like that of ideal MHD, should be questioned for collisionless plasmas, which in general are not fluidlike along the field.

The simplest model for investigating macroscopic stability in collisionless but approximately isotropic plasmas

is the perpendicular MHD model. Here the difficult question of behavior parallel to the field is resolved by restricting the class of allowable motions to those in which parallel disturbances do not occur. In other words, the perpendicular MHD model is valid over a wider and more useful parameter range than ideal MHD, but is more restrictive in the class of motions which it permits. Specifically, the essential difference is that the propagation of sound waves is suppressed in perpendicular MHD. Such an assumption is inherently more valid in a toroidal system, where large parallel transport quickly damps any substantial parallel gradients. It is a poor representation for an open-ended system, where the overall confinement is strongly coupled to the behavior parallel to the field.

The question, then, that naturally arises is why the stability predictions of perpendicular MHD should be so similar to those of ideal MHD, and even if so, why should either model be valid. The answer to the first part is related to the fact that in ideal MHD sound waves are very stable and involve motion which is predominantly parallel to the magnetic field. Since perturbations leading to macroscopic instabilities are nearly transverse to the field, they are only very weakly coupled, if at all, to the sound waves, and suppressing these waves from the model has almost no effect. This is not true for all MHD phenomena, but only those in which the equation of state (i.e., the appearance of  $\gamma$ , the ratio of specific heats) does not play an important role. One counterexample, for instance, is magnetoacoustic heating. If such heating takes place in a collisionless plasma, then neither model is reliable.

The answer to the second part of the question is more difficult. With respect to the perpendicular MHD model, the concern is whether relaxation of the constraint which restricts motion along the field lines can lead to much more severe instabilities when parallel kinetic effects are included. This is in general not the case. For static equilibria the effect of the ions is to produce a strong kinetic damping (ion Landau damping) of any perturbations along the field lines. [A discussion of this effect can be found in Krall and Trivelpiece (1973).] In these cases, as in ideal MHD, the least stable modes are only weakly coupled to the parallel motion, and hence perpendicular MHD is an accurate description. At somewhat higher frequencies and shorter perpendicular wavelengths, the electron kinetic effects become important and can drive new instabilities called drift waves [see, for instance, Mikhailovskii (1967) and Krall and Trivelpiece (1973)]. These waves lie outside the realm of any of the single-fluid MHD models and must be treated separately.

To summarize, the additional physics included in ideal MHD, the sound wave, is treated incorrectly for collisionless plasmas, leading one to conclude that the model is not valid. However, for MHD instabilities, the sound wave is almost completely decoupled from motion. Hence, even though the model is incorrect, the errors are usually unimportant. Similarly, completely suppressing

the sound wave in the perpendicular MHD model makes little difference in the results, but extends the region of validity to include low collisionalities.

## 2. Derivation from the Boltzmann equation

The perpendicular MHD model can be derived in a number of ways. One method starts with a hybrid model in which the ions are a fully collisionless kinetic species and the electrons are an isotropic massless electron fluid (Freidberg and Hewett, 1977; Pearlstein and Freidberg, 1978). For the present purposes the model can perhaps be most easily derived by making use of the moment equations. Assume first that the plasma is collisionless, so that

$$V_{Ti}\tau_{ii}/a \sim V_{Te}\tau_{ee}/a \gg 1 . \quad (2.61)$$

Consider now the closure of the set of moment equations. It is assumed that the configurations of interest are initially isotropic. The perpendicular part of the momentum equation can be written as

$$\rho \left[ \frac{d\mathbf{v}}{dt} \right]_{\perp} = \mathbf{J} \times \mathbf{B} - \nabla_{\perp} p - \left[ \nabla \cdot \left( \vec{\Pi}_i + \vec{\Pi}_e \right) \right]_{\perp} . \quad (2.62)$$

In a collisionless plasma the main contribution to  $\vec{\Pi}$  is the so-called magnetic viscosity coefficient, which is larger for ions than for electrons by  $m_i/m_e$ . The actual form for the  $\vec{\Pi}_i$  elements is somewhat complicated. For dimensional purposes it suffices to say that the perpendicular part of  $\nabla \cdot \vec{\Pi}_i$  scales as follows:

$$(\nabla \cdot \vec{\Pi}_i)_{\perp} \sim \frac{p_i}{\omega_{ci}} \nabla_{\perp}^2 (\mathbf{e}_b \times \mathbf{v}_{\perp}) \sim \left[ \frac{r_{Li}}{a_{\perp}} \right] \left[ \frac{p_i}{a_{\perp}} \right] , \quad (2.63)$$

where  $\mathbf{e}_b$  is a unit vector along  $\mathbf{B}$ . This term is negligible compared to  $\nabla_{\perp} p_i$  if

$$\frac{r_{Li}}{a_{\perp}} \ll 1 . \quad (2.64)$$

The parallel component of the momentum equation is very complicated because of the strong kinetic damping along the field, but it is not explicitly needed in the perpendicular MHD model. Instead, it is approximated by a relation in which  $v_{||}$  is determined so that there are no pressure perturbations allowed along  $B$ ; that is,

$$\mathbf{B} \cdot \nabla p = 0 . \quad (2.65)$$

The exact prescription for determining  $v_{||}$  will become apparent shortly.

The closure of Ohm's law for perpendicular MHD is very similar to that in ideal MHD. The dominant terms on the right-hand side of Eq. (2.39), the generalized form of Ohm's law, are still the Hall effect and the electron diamagnetism. Both of these are negligible if  $r_{Li}/a \ll 1$ .

The resistivity term is less important than in ideal MHD because the plasma is assumed to be collisionless. As before, a comparison of  $E_{||}$  and  $E_{\perp}$  indicates that  $E_{||}/E_{\perp} \sim r_{Li}/a \ll 1$ . The neglect of the small  $E_{||}$  is even less important in perpendicular MHD because the model is restricted so that no parallel perturbations occur.

Finally, as with the parallel momentum equation, the energy equation is also very complicated because of kinetic effects. In perpendicular MHD the energy equation has the form

$$\mathbf{B} \cdot \nabla T = 0, \quad (2.66)$$

which in an approximate sense can be viewed as the limit of "infinite parallel thermal conductivity." This is a much more accurate assumption than that of zero parallel thermal conductivity used in ideal MHD. Clearly Eqs. (2.65) and (2.66) imply that

$$\mathbf{B} \cdot \nabla \rho = 0. \quad (2.67)$$

In perpendicular MHD, Eqs. (2.65)–(2.67) constrain all density, temperature, and pressure perturbations to be constant along a field line. These relations can be cast in a more convenient form as follows. First Eq. (2.67) can be transformed into an equation for  $v_{||}$  by using conservation of mass and Faraday's law, with  $\mathbf{E}$  given by Ohm's law with perfect conductivity. The result is

$$\frac{d}{dt}(\mathbf{B} \cdot \nabla \rho) + 2\nabla \cdot \mathbf{v}(\mathbf{B} \cdot \nabla \rho) = -\rho \mathbf{B} \cdot \nabla(\nabla \cdot \mathbf{v}). \quad (2.68)$$

Thus, if  $\mathbf{B} \cdot \nabla \rho = 0$ , it follows that  $\mathbf{B} \cdot \nabla(\nabla \cdot \mathbf{v}) = 0$ . Assuming  $\mathbf{B} \cdot \nabla$  does not identically vanish

$$\nabla \cdot \mathbf{v} = 0 \quad (2.69)$$

or

$$\mathbf{B} \cdot \nabla \left[ \frac{v_{||}}{\mathbf{B}} \right] = -\nabla_{\perp} \cdot \mathbf{v}_{\perp}. \quad (2.70)$$

The condition  $\nabla \cdot \mathbf{v} = 0$  is sometimes assumed to be an equation of state, but in perpendicular MHD it is perhaps more appropriate to view it as the equation of parallel momentum flow which determines  $v_{||}$ .

A second convenient relation is obtained by substituting Faraday's law and Eq. (2.69) into Eq. (2.65). One finds

$$\frac{d}{dt}(\mathbf{B} \cdot \nabla p) = \mathbf{B} \cdot \nabla \frac{dp}{dt}. \quad (2.71)$$

Hence, if  $\mathbf{B} \cdot \nabla p = 0$  and  $\mathbf{B} \cdot \nabla$  does not identically vanish, Eq. (2.71) reduces to

$$\frac{dp}{dt} = 0 \quad (2.72)$$

and can be viewed as the energy equation for perpendicular MHD.

The equations of perpendicular MHD are summarized here and compared with ideal MHD. (Note that here and in the remainder of the text  $\mu_0 = 1$ .)

### Perpendicular MHD

$$\frac{d\rho}{dt} = 0$$

$$\rho \frac{D\mathbf{v}}{Dt} = \mathbf{J} \times \mathbf{B} - \nabla p$$

$$\nabla \cdot \mathbf{v} = 0$$

$$\frac{dp}{dt} = 0$$

$$\frac{\partial \mathbf{B}}{\partial t} = \nabla \times (\mathbf{v} \times \mathbf{B})$$

$$\nabla \times \mathbf{B} = \mathbf{J}$$

### Ideal MHD

$$\frac{d\rho}{dt} = -\rho \nabla \cdot \mathbf{v}$$

$$\rho \frac{d\mathbf{v}}{dt} = \mathbf{J} \times \mathbf{B} - \nabla p$$

$$\frac{dp}{dt} = -\gamma p \nabla \cdot \mathbf{v}$$

$$\frac{\partial \mathbf{B}}{\partial t} = \nabla \times (\mathbf{v} \times \mathbf{B})$$

$$\nabla \times \mathbf{B} = \mathbf{J}$$

Here the perpendicular inertial force is given by

$$\frac{D\mathbf{v}}{Dt} = \mathbf{e}_{\perp} \frac{dv_{\perp}}{dt} - \mathbf{e}_{\eta} \mathbf{v} \cdot \frac{d\mathbf{e}_{\eta}}{dt},$$

where  $\mathbf{v} = v_{\perp} \mathbf{e}_{\perp} + v_{||} \mathbf{e}_b$  and  $\mathbf{e}_{\eta} = \mathbf{e}_b \times \mathbf{e}_{\perp}$ . The second term, which is perpendicular to both  $\mathbf{e}_b$  and  $\mathbf{e}_{\perp}$ , represents the centrifugal effects. One can essentially go from ideal MHD to perpendicular MHD by replacing the equation of parallel momentum balance with the condition  $\nabla \cdot \mathbf{v} = 0$ .

In the derivation of perpendicular MHD there are essentially two basic assumptions which must be satisfied: low collisionality,  $V_{Ti}\tau_{ii}/a \gg 1$ , and small gyroradius,  $r_{Li}/a \ll 1$ . A reexamination of Fig. 2 indicates that these conditions are well satisfied for plasmas of fusion interest. A further point to emphasize is that in several places in the derivation it was assumed that the operator  $\mathbf{B} \cdot \nabla$  does not identically vanish. In almost all cases of interest this is indeed the situation. There are, however, several notable exceptions which will be discussed later. In these cases, the perpendicular MHD model is not reliable. Similarly, the ideal MHD model is not accurate in these cases, since the results are then rather strongly dependent on the energy equation.

The conclusion from this analysis is that plasmas whose ideal MHD stability properties are only weakly coupled to sound waves (i.e., whose perturbations are nearly incompressible,  $\nabla \cdot \mathbf{v} = 0$ ) will have almost identical stability properties when investigated in the perpendicular MHD model. However, when comparing the regions of validity for each model, it is clear that perpendicular MHD is much more appropriate for plasmas of fusion interest.

The remainder of the paper will deal primarily with ideal MHD, mainly for historical reasons, but at certain critical points detailed comparisons will be made to show the similarity of the models.

### 3. Derivation from single-particle orbit theory

A final topic of interest to the physics of the perpendicular MHD model is an intuitive derivation based on single-particle orbit theory. The derivation consists of

calculating the currents directly from the perpendicular guiding-center drifts in the low-frequency ( $\omega \ll \omega_{ci}$ ), small-gyroradius ( $r_{Li} \ll a$ ), collisionless limit. The cross product of this current with  $\mathbf{B}$  then gives the perpendicular MHD equations.

To show this explicitly, consider a particle gyrating about a magnetic field line with a velocity  $\mathbf{u} = \mathbf{u}_\perp + u_{||}\mathbf{e}_b + \mathbf{V}_{g\perp}$ . Here  $u_{||}$  is the velocity along the magnetic field,  $\mathbf{u}_\perp$  is the fast gyration velocity about the field line, and  $\mathbf{V}_{g\perp}$  is the slower drift velocity of the particles' guiding center. In particular,  $\mathbf{V}_{g\perp}$  is given by [see, for instance, Chen (1974)]

$$\mathbf{V}_{g\perp} = \mathbf{V}_E + \mathbf{V}_{\nabla B} + \mathbf{V}_\kappa + \mathbf{V}_p , \quad (2.73)$$

where  $\mathbf{V}_E$  is the " $\mathbf{E} \times \mathbf{B}$ " velocity

$$\mathbf{V}_E = \frac{\mathbf{E} \times \mathbf{B}}{B^2} , \quad (2.74)$$

$\mathbf{V}_{\nabla B}$  is the "grad- $B$ " velocity

$$\mathbf{V}_{\nabla B} = \frac{u_\perp^2}{2\omega_c} \frac{\mathbf{B} \times \nabla B}{B^2} , \quad (2.75)$$

$\mathbf{V}_p$  is the "polarization" drift

$$\mathbf{V}_p = \frac{\mathbf{e}_b}{\omega_c} \times \frac{d}{dt} \frac{\mathbf{E} \times \mathbf{B}}{B^2} , \quad (2.76)$$

and  $\mathbf{V}_\kappa$  is the "curvature" drift

$$\mathbf{V}_\kappa = -\frac{u_{||}^2}{\omega_c} \frac{\boldsymbol{\kappa} \times \mathbf{B}}{B} , \quad (2.77)$$

with  $\boldsymbol{\kappa} = \mathbf{e}_b \cdot \nabla \mathbf{e}_b = \mathbf{R}_c / R_c^2$  the curvature vector of the magnetic field line (i.e.,  $\mathbf{R}_c$  is the radius of curvature). These expressions are valid for both electrons and ions when one uses the appropriate magnitude and sign of  $q$  and  $m$  appearing in  $\omega_c$ . Also, the fields are to be evaluated at the guiding center of the particle.

In the MHD limit, the  $\mathbf{E} \times \mathbf{B}$  drift is assumed to be dominant, so that

$$\mathbf{V}_{1ge} \approx \mathbf{V}_{1gi} \equiv \mathbf{v}_\perp = \mathbf{E} \times \mathbf{B} / B^2 . \quad (2.78)$$

This is equivalent to Ohm's law in ideal MHD.

The total perpendicular current is calculated by integrating the guiding-center drift velocity over velocity space and adding the magnetization current

$$\mathbf{J}_1 = e \int [\mathbf{V}_{1gi} f_i(\mathbf{u}) - \mathbf{V}_{1ge} f_e(\mathbf{u})] d\mathbf{u} + \mathbf{J}_M . \quad (2.79)$$

Here

$$\mathbf{J}_M = \nabla \times \mathbf{M} ,$$

$$\mathbf{M} = -\frac{p_\perp}{B} \mathbf{e}_b . \quad (2.80)$$

The magnetization current arises even if there is no drift of the guiding centers. It occurs when there is a density gradient of guiding centers (more precisely, a gradient of their magnetic moments). A more detailed discussion of the magnetization current can be found in Longmire (1963).

One now computes the cross products of Eq. (2.79) with  $\mathbf{B}$ . Some simple manipulations yield

$$\rho \left[ \mathbf{e}_b \times \frac{d\mathbf{v}_\perp}{dt} \right] \times \mathbf{e}_b = \mathbf{J} \times \mathbf{B} - \nabla_\perp p_\perp - (p_{||} - p_\perp) \boldsymbol{\kappa} . \quad (2.81)$$

Equation (2.81) is the perpendicular momentum equation for the more general guiding-center plasma model and the guiding-center fluid model. For toroidal systems in which it can be assumed that the pressure is approximately isotropic, Eq. (2.81) essentially reduces to the momentum equation of perpendicular MHD; that is, setting  $p_\perp = p_{||} = p$  and noting that  $(\mathbf{e}_b \times \dot{\mathbf{v}}_\perp) \times \mathbf{e}_b = \mathbf{e}_b \dot{v}_\perp - \mathbf{e}_\eta (\mathbf{v}_\perp \cdot \dot{\mathbf{e}}_\eta)$ , it follows that only the  $-\mathbf{e}_\eta v_{||} (\mathbf{e}_b \cdot \dot{\mathbf{e}}_\eta)$  term, representing the parallel centrifugal force, need be "patched on" to Eq. (2.81) to obtain the perpendicular MHD equations. This effect was not included in the single-particle derivation.

To summarize, it has been shown that the perpendicular MHD model can be derived in an intuitive manner from collisionless single-particle orbit theory. In effect, from a single-particle point of view, the macroscopic MHD equilibrium and stability properties of a plasma are determined by the currents induced from the  $\mathbf{E} \times \mathbf{B}$ , grad- $B$ , curvature, and polarization guiding-center drifts.

### III. GENERAL PROPERTIES OF IDEAL MHD

#### A. Introduction

In this section several of the basic properties of ideal MHD are discussed. These properties form the physical foundation for the model and provide insight as to why the model is as reliable as it is when predicting experimental behavior.

First, a short description is given of three different classes of boundary conditions which show how a plasma can be coupled to its external surroundings. The most complex of these provides a quite accurate description of realistic experimental conditions.

Second, it is shown that despite the significant number of approximations made, the ideal MHD model still conserves mass, momentum, and energy, both locally and globally. This is one basic reason for the reliability of the model.

Finally, a short calculation shows that if one assumes perfect conductivity, the motion of the system can be interpreted as one in which the plasma and magnetic field are constrained to move together. This leads to important topological constraints on the model.

#### B. Boundary conditions

In order to fully specify an MHD problem, a set of appropriate boundary conditions is required to couple the plasma to its external surroundings. For problems of MHD stability there are three classes of boundary conditions, of varying complexity, which are often used. Each

is now discussed separately. Other discussions of ideal MHD boundary conditions can be found in Bernstein *et al.* (1958) and Goedbloed (1979).

### 1. Perfectly conducting wall

The first and simplest boundary condition assumes that the plasma extends out to a stationary, perfectly conducting wall, as shown in Fig. 3(a). In this case the electromagnetic boundary conditions require that the tangential electric field and normal magnetic field vanish on the conducting wall:

$$\mathbf{n} \times \mathbf{E} = 0, \quad (3.1)$$

$$\mathbf{n} \times \hat{\mathbf{B}} = 0. \quad (3.2)$$

Here  $\mathbf{n}$  is the outward-pointing normal vector. It then follows from Ohm's law in ideal MHD that  $\mathbf{n} \times \mathbf{E} = (\mathbf{n} \cdot \mathbf{B})\mathbf{v} - (\mathbf{n} \cdot \mathbf{v})\mathbf{B} = 0$ ; that is, the normal component of velocity also automatically vanishes on the wall:

$$\mathbf{n} \cdot \mathbf{v} = 0. \quad (3.3)$$

Thus, once appropriate initial data and the shape of the wall are specified, any two of the conditions given above completely specify the problem.

### 2. Insulating vacuum region

A somewhat more realistic set of boundary conditions assumes that the plasma is isolated from the conducting wall by a vacuum region, as shown in Fig. 3(b). In most cases this model is more appropriate than the previous one for describing "confined" plasmas.

In principle one solves the combined plasma-vacuum

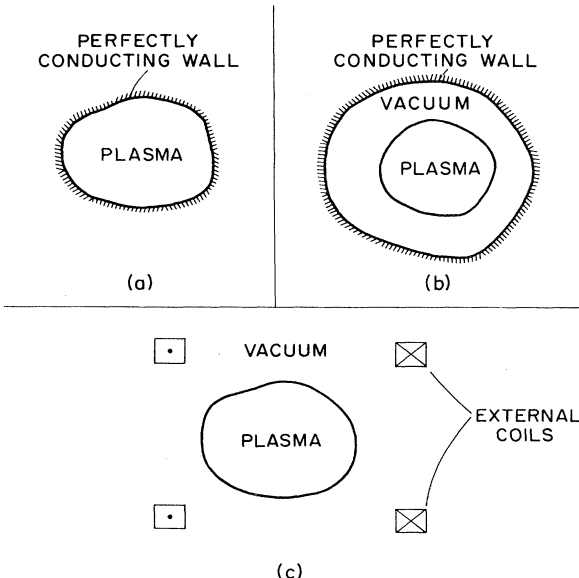


FIG. 3. Illustration of the three classes of boundary conditions often used in ideal MHD: (a) perfectly conducting wall, (b) plasma isolated from the wall by a vacuum region, and (c) plasma surrounded by external coils.

system as follows. In the plasma region the ideal MHD equations apply, while in the vacuum region, where the fluid variables are not defined, the relevant equations are given by

$$\begin{aligned} \nabla \times \hat{\mathbf{B}} &= 0, \\ \nabla \cdot \hat{\mathbf{B}} &= 0. \end{aligned} \quad (3.4)$$

Here quantities with a  $\hat{\phantom{A}}$  denote vacuum variables.

Assume that the equations can be solved in each region and consider the boundary conditions. On the perfectly conducting wall,  $r = R_w(\theta, z)$ ,

$$\hat{\mathbf{n}} \cdot \hat{\mathbf{B}} |_{R_w} = 0 \quad (3.5)$$

must be satisfied.

At the plasma-vacuum interface there are several conditions. Since the plasma surface  $r = R(\theta, z, t)$  is by definition a constant-pressure surface (i.e., a flux surface), it follows that

$$\hat{\mathbf{n}} \cdot \hat{\mathbf{B}} |_R = \mathbf{n} \cdot \mathbf{B} |_R = 0. \quad (3.6)$$

In general, the plasma surface can move, since the plasma is surrounded by vacuum. Hence  $\mathbf{n} \cdot \mathbf{v} |_R$  is arbitrary. It is possible, however, to have jumps in the pressure and the tangential magnetic field across the surface. Integration of the momentum equation and Ampere's law then requires

$$\left[ p + \frac{B^2}{2} \right]_R = 0, \quad (3.7)$$

$$[\mathbf{n} \times \mathbf{B}]_R = \mathbf{K} \quad (3.8)$$

where  $[Q]$  denotes  $\hat{Q} - Q$  and  $\mathbf{K}$  is the surface current density.

Although Eqs. (3.5)–(3.8) completely specify the boundary conditions, the plasma-vacuum problem is in practice difficult to solve. The reason is that a straightforward counting of boundary conditions indicates that there appears to be one condition too many. This is not actually the case. If one wants to independently specify the surface currents and the shape of the outer conductor, one must self-consistently determine the correct shape of the plasma surface. Therein lies the extra degree of freedom. Often in problems of this type it is easier to specify the shape of the plasma surface and then determine the appropriate shape of the outer perfect conductor.

### 3. Plasma surrounded by external coils

The most difficult and realistic set of boundary conditions corresponds to the situation where the plasma is confined by the magnetic fields created by a fixed set of external current-carrying conductors, as shown in Fig. 3(c). A convenient way to specify these currents is to assume they are located on a surface  $r = R_w(\theta, z)$  and correspond to a surface current density  $\mathbf{K}_w(\theta, z, t)$ .

This problem is more difficult than the previous one because the current-carrying conductors must necessarily have gaps between them. Consequently, the interior and exterior regions are no longer isolated from each other, and the MHD solution cannot be obtained unless the equations are solved in both domains.

In terms of the boundary conditions the requirements on the plasma-vacuum interface remain unchanged [i.e., Eqs. (3.6)–(3.8) still apply]. However, with external coils the wall condition, Eq. (3.5), is replaced by

$$\begin{aligned} [\hat{n} \cdot \hat{B}]_{R_w} &= 0, \\ [\hat{n} \times \hat{B}]_{R_w} &= K_w. \end{aligned} \quad (3.9)$$

In addition, the vacuum fields outside the wall must satisfy a regularity condition as  $r \rightarrow \infty$ .

Solutions to the MHD equations satisfying boundary condition 3 provide an accurate description of plasma behavior in realistic experimental situations. Because of their complexity it is perhaps not surprising that most applications of boundary condition 3 require substantial numerical computations.

The MHD equations and any set of the boundary conditions just discussed form a complete basis for investigating, the macroscopic equilibrium and stability of fusion plasmas.

### C. Local conservation relations

The original Boltzmann-Maxwell equations from which the MHD model was derived conserve mass, momentum, and energy, not only macroscopically, but microscopically as well. Since a considerable number of assumptions were made in the derivation of the MHD equations, it is useful to investigate whether the resulting model still satisfies the basic conservation laws. In this section the question of local conservation is treated by showing that both the ideal and the perpendicular MHD models can be written in conservation form. The implications for global conservation are discussed in the next section. An excellent review of ideal MHD conservation laws has been given by Goedbloed (1979).

In order to show local conservation it is necessary to write the mass, momentum, and energy equations in the form

$$\frac{\partial}{\partial t}(\ ) + \nabla \cdot (\ ) = 0. \quad (3.10)$$

Once this is accomplished, it is straightforward to derive the global conservation relations.

After some standard manipulations the ideal MHD equations can be expressed in conservation form,

$$\begin{aligned} \frac{\partial \rho}{\partial t} + \nabla \cdot \rho \mathbf{v} &= 0, \\ \frac{\partial}{\partial t} \rho \mathbf{v} + \nabla \cdot \vec{T} &= 0, \\ \frac{\partial u}{\partial t} + \nabla \cdot \mathbf{s} &= 0, \end{aligned} \quad (3.11)$$

where the stress tensor  $\vec{T}$ , energy  $u$ , and energy flux  $\mathbf{s}$  are given by

$$\begin{aligned} \vec{T} &= \rho \mathbf{v} \mathbf{v} + \left[ p + \frac{B^2}{2} \right] \vec{I} - \mathbf{B} \mathbf{B}, \\ u &= \frac{1}{2} \rho v^2 + \frac{B^2}{2} + \frac{p}{\gamma - 1}, \\ \mathbf{s} &= \left[ \frac{1}{2} \rho v^2 + \frac{\gamma}{\gamma - 1} p \right] \mathbf{v} + \mathbf{E} \times \mathbf{B}. \end{aligned} \quad (3.12)$$

Note that the stress tensor is composed of three terms. The  $\rho \mathbf{v} \mathbf{v}$  term is the Reynolds stress. In a local coordinate system in which  $\mathbf{v}$  is in the  $z$  direction, this part of the tensor has the form

$$\vec{T}_R = \begin{bmatrix} 0 & 0 & 0 \\ 0 & 0 & 0 \\ 0 & 0 & \rho v^2 \end{bmatrix}. \quad (3.13)$$

Thus the effect of the Reynolds stress is to produce a pressure along  $\mathbf{v}$ . This term represents an important contribution to systems with large fluid flow, but is usually not very important in studies of plasma stability where the flows are mostly small or zero.

The remaining part of the stress tensor includes the effect of the pressure and the magnetic field. In a local coordinate system in which  $\mathbf{B}$  is in the  $z$  direction, this part of the tensor can be expressed as

$$\vec{T}_B = \begin{bmatrix} p_\perp & 0 & 0 \\ 0 & p_\perp & 0 \\ 0 & 0 & p_{||} \end{bmatrix}, \quad (3.14)$$

where

$$\begin{aligned} p_\perp &= p + \frac{B^2}{2}, \\ p_{||} &= p - \frac{B^2}{2}. \end{aligned} \quad (3.15)$$

The quantities  $p_\perp$  and  $p_{||}$  represent the pressures perpendicular and parallel to the magnetic field, respectively. Equation (3.15) implies that the magnetic field adds to the pressure in the perpendicular direction while decreasing pressure, producing a tension, in the parallel direction.

Consider now the energy equation. The quantity  $u$  represents the sum of the plasma kinetic energy  $u_k$  and potential energy  $u_p$ ,

$$\begin{aligned} u &= u_k + u_p, \\ u_k &= \frac{1}{2} \rho v^2, \\ u_p &= \frac{B^2}{2} + \frac{p}{\gamma - 1}. \end{aligned} \quad (3.16)$$

Note that the potential energy is made up of two contributions, the magnetic energy and the internal energy of the plasma [ $(\frac{3}{2} n T)$  for  $\gamma = \frac{5}{3}$ ]. The total energy flux  $\mathbf{s}$  can be expressed as

$$\mathbf{s} = \left[ \frac{1}{2} \rho v^2 + \frac{p}{\gamma - 1} \right] \mathbf{v} + p \mathbf{v} + \mathbf{E} \times \mathbf{B}. \quad (3.17)$$

Here the first term represents the flow of plasma energy. The second term corresponds to the mechanical work done on or by the plasma as it moves, and the last term, the Poynting flux, represents the flow of electromagnetic energy.

To summarize, it has just been demonstrated that the ideal MHD equations can be written in local conservation form, in which each of the terms has a simple physical interpretation. A similar situation prevails for the perpendicular MHD model.

An important feature of the perpendicular MHD model is that the energy equation separates into two parts because of the decoupling of the sound waves. These are given by

$$\begin{aligned} \frac{\partial u}{\partial t} + \nabla \cdot \mathbf{s} &= 0, \\ \frac{\partial p}{\partial t} + \nabla \cdot p \mathbf{v} &= 0, \end{aligned} \quad (3.18)$$

where

$$\begin{aligned} u &= \frac{1}{2} \rho v_{\perp}^2 + \frac{B^2}{2}, \\ \mathbf{s} &= \frac{1}{2} \rho v_{\perp}^2 \mathbf{v} + p \mathbf{v} + \mathbf{E} \times \mathbf{B}. \end{aligned} \quad (3.19)$$

This decoupling of the plasma internal energy (i.e., the sound waves) from the remainder of the energy can easily be seen by comparing the ideal and perpendicular MHD models.

#### D. Global conservation laws

By integrating the local conservation laws just derived over a volume appropriate to any of the three sets of boundary conditions previously discussed, it is possible to obtain a set of global conservation laws for ideal MHD. These laws are exact and valid for general, nonlinear, multidimensional, time-dependent situations. Since they depend on the particular boundary conditions applied, it is useful to treat each of the three sets separately.

##### 1. Perfectly conducting wall

For this case it is appropriate to integrate the local conservation laws out to the conducting wall. Making use of the boundary conditions given by Eqs. (3.1)–(3.3) then leads to the following global conservation relations:

$$\frac{dM}{dt} = 0, \quad (3.20)$$

$$\frac{d\mathbf{P}}{dt} = - \int \left[ p + \frac{B^2}{2} \right] \mathbf{n} dS, \quad (3.21)$$

$$\frac{dW}{dt} = 0, \quad (3.22)$$

where  $M$  is the total mass of the plasma

$$M = \int \rho d\mathbf{r}, \quad (3.23)$$

$\mathbf{P}$  is the mechanical momentum of the plasma

$$\mathbf{P} = \int \rho \mathbf{v} d\mathbf{r}, \quad (3.24)$$

and  $W$  is the total kinetic and potential energy of the plasma and magnetic field

$$W = \int \left[ \frac{1}{2} \rho v^2 + \frac{p}{\gamma - 1} + \frac{B^2}{2} \right] d\mathbf{r}. \quad (3.25)$$

Equation (3.20) demonstrates that the total mass of the plasma is conserved. Equation (3.21) describes the conservation of momentum. The boundary term represents the total force exerted by the walls on the plasma. If the configuration is to remain in place, this force must vanish identically and  $d\mathbf{P}/dt = 0$ ; that is, mechanical momentum is conserved. The final equation, Eq. (3.22), shows that the total energy of the system is conserved. It implies that during a given plasma motion (an instability, for instance) energy can in general be transferred between the magnetic field, the plasma internal energy, and the plasma kinetic energy. This should be compared with the energy relations for perpendicular MHD, which have the form

$$\begin{aligned} \frac{dW}{dt} &= 0, \\ \frac{dU}{dt} &= 0, \end{aligned} \quad (3.26)$$

where

$$\begin{aligned} W &= \int \left[ \frac{1}{2} \rho v_{\perp}^2 + \frac{B^2}{2} \right] d\mathbf{r}, \\ U &= \int p d\mathbf{r}. \end{aligned} \quad (3.27)$$

In this model the suppression of sound waves implies that the total internal energy of the plasma remains constant during any plasma motion. If there is to be a transfer of energy, it can only occur between the magnetic field and the perpendicular kinetic energy.

##### 2. Insulating vacuum region

When the plasma is surrounded by a vacuum region it is of particular interest to focus attention on the conservation of energy. This relation is slightly more complicated than the case of the perfectly conducting wall, since the plasma boundary is now allowed to move. The result is that it is not the individual but the combined plasma-vacuum energy which is conserved.

To show this, first note that for a global quantity  $Z$ , defined by

$$Z(t) = \int z d\mathbf{r}, \quad (3.28)$$

the total time derivative in a volume whose boundary is moving with velocity  $\mathbf{u}$  is given by

$$\frac{dZ(t)}{dt} = \int_V \frac{\partial z}{\partial t} d\mathbf{r} + \int_S z \mathbf{n} \cdot \mathbf{u} dS. \quad (3.29)$$

Equation (3.29) is applied to the plasma volume moving with velocity  $\mathbf{u} = \mathbf{v}$  in the local energy conservation relation. If use is made of the ideal Ohm's law and the plasma-vacuum boundary conditions given by Eq. (3.6), it follows that

$$\frac{dW}{dt} = - \int \left[ p + \frac{B^2}{2} \right] \mathbf{n} \cdot \mathbf{v} dS. \quad (3.30)$$

Here the plasma energy  $W$  is given by Eq. (3.25). Note that if the plasma surface is moving, the boundary term is in general nonzero.

Consider now the vacuum region. Here the total energy is given by

$$\hat{W} = \int \frac{\hat{B}^2}{2} d\mathbf{r}, \quad (3.31)$$

from which it follows that

$$\frac{d\hat{W}}{dt} = \int \frac{1}{2} \left[ \hat{\mathbf{B}} \cdot \frac{\partial \hat{\mathbf{B}}}{\partial t} \right] d\mathbf{r} - \int \frac{\hat{B}^2}{2} \mathbf{n} \cdot \mathbf{v} dS. \quad (3.32)$$

This equation is simplified by substituting Faraday's law with  $\mathbf{E} = -\mathbf{v} \times \mathbf{B}$  for  $\partial \mathbf{B} / \partial t$ . After some straightforward algebra, where use is again made of the boundary conditions [Eq. (3.6)], one obtains

$$\frac{d\hat{W}}{dt} = \int \frac{\hat{B}^2}{2} \mathbf{n} \cdot \mathbf{v} dS. \quad (3.33)$$

The final energy relation is obtained by adding Eqs. (3.30) and (3.33),

$$\frac{d}{dt}(W + \hat{W}) = 0. \quad (3.34)$$

Here the boundary terms cancel by virtue of Eq. (3.7), which is the pressure balance jump condition.

Equation (3.34) implies that if an ideal MHD plasma is isolated from a conducting wall by a vacuum region, the combined energy of the plasma-vacuum system is conserved. The fact that only the total is conserved indicates that, in general, energy will flow from one region to the other as the plasma moves.

### 3. Plasma surrounded by external coils

If the conducting wall in the vacuum is replaced by a series of current-carrying conductors, the energy of the system is no longer conserved. The reason is, of course, that with external sources present, energy can be supplied or extracted from the system. Nevertheless, it is still possible to derive a relatively simple energy relation for the region interior to the conductors. The procedure is almost identical to that given for boundary condition 2. The main difference is that in the vacuum region the integration is carried out to a surface just inside the con-

ductors. The boundary term no longer vanishes on this surface since it is not a perfect conductor. Instead one obtains

$$\frac{d}{dt}(W + \hat{W}) = - \int (\mathbf{E} \times \mathbf{B}) \cdot \mathbf{n}_w dS_w. \quad (3.35)$$

Equation (3.35) can be simply interpreted as showing that the rate of increase of the total energy in the combined plasma-vacuum system is equal to the electromagnetic power flowing into the region.

### E. Conservation of flux

The final conservation law to be considered concerns the magnetic flux. The basic result, a consequence of the perfect conductivity assumed by Ohm's law, is that the magnetic flux passing through any arbitrary surface element moving with the plasma is constant; flux is conserved locally as well as globally.

To show this, note that the time rate of change of the flux passing through any moving surface  $S$  is given by

$$\frac{d\psi}{dt} = \int \frac{\partial \mathbf{B}}{\partial t} \cdot \mathbf{n} dS - \oint \mathbf{u} \times \mathbf{B} \cdot d\mathbf{l}. \quad (3.36)$$

Here  $\mathbf{u}$  is the velocity of the surface and

$$\psi = \int \mathbf{B} \cdot \mathbf{n} dS \quad (3.37)$$

is the magnetic flux.

If Ohm's law is substituted into Faraday's law,

$$\frac{\partial \mathbf{B}}{\partial t} = \nabla \times (\mathbf{v} \times \mathbf{B}), \quad (3.38)$$

and the velocity  $\mathbf{u}$  is chosen as the plasma velocity  $\mathbf{v}$ , a simple calculation then shows that

$$\frac{d\psi}{dt} = 0. \quad (3.39)$$

Since the derivation of Eq. (3.39) applies to any arbitrary surface area, it follows immediately, by considering the entire plasma cross section, that the total flux in an ideal MHD plasma is constant. A more interesting case is to allow the surface area to coincide with the cross section of a long thin flux tube. Application of Eq. (3.39) then leads to the well-known intuitive picture that, in an ideal MHD plasma, magnetic lines are "frozen into the fluid."

The relation for conservation of flux has very important implications for the structure of the magnetic field. This follows because, for any physically realizable motion of the plasma, neighboring fluid elements stay in the vicinity of one another; that is, fluid elements are not allowed to tear or break away into separate pieces. Since the magnetic lines move with the plasma, the field line topology cannot change during any physically allowable MHD motion. This is a very strict requirement on the structure of the magnetic fields. Other discussions of the structure of magnetic fields and the motion of magnetic field lines can be found in Grad and Rubin (1958), Newcomb (1958), Morozov and Solov'ev (1966), and

Bateman (1978).

There are many configurations in plasma physics in which it is intuitively clear that it is energetically favorable for field lines to break and reconnect into new configurations with lower potential energy. Such transitions are not allowed because of the constraint on the topology. It is for this reason that the introduction of even a small resistivity can have a dramatic effect on plasma stability, much larger than is indicated from simple dimensional arguments. A small dissipation removes the topological constraint and allows a much wider class of motions to take place. The inclusion of resistive effects is outside the scope of the present work, but is discussed in detail in the review article of Greene (1976).

We have seen in this section that the ideal MHD model conserves mass, momentum, energy, and magnetic flux. These conservation laws apply to general nonlinear, time-dependent, multidimensional systems. In view of the many assumptions made in the derivation of the model, the existence of such laws is a nontrivial result. However, having shown the existence of the conservation laws, one can proceed with some confidence to the crucial problems of equilibrium and stability of magnetic fusion configurations, knowing that the model should provide valuable insight because of its inherently sound foundation.

#### IV. EQUILIBRIUM

The goal of MHD equilibrium theory is the discovery of magnetic geometries which simultaneously (1) confine and isolate hot plasmas from material walls and (2) have good stability properties at sufficient values of  $\beta$  ( $\beta \equiv$  plasma energy/magnetic energy) to be promising for use in potential fusion reactors. There are a number of existing concepts which satisfy these criteria. Section IV begins with a discussion of the common features of such configurations resulting directly from MHD equilibrium requirements. Next, the specific properties of the most promising concepts are described in more detail. Included are the tokamak, stellarator, Elmo bumpy torus, and reversed field pinch.

##### A. General properties

###### 1. Basic equations

Consider first the MHD equilibrium equations given by

$$\mathbf{J} \times \mathbf{B} = \nabla p , \quad (4.1)$$

$$\nabla \times \mathbf{B} = \mathbf{J} , \quad (4.2)$$

$$\nabla \cdot \mathbf{B} = 0 . \quad (4.3)$$

These are just the time-independent form of the full MHD equations with  $v=0$ ; the equilibria of interest are static. Stationary equilibria with nonzero flow are possi-

ble, but are not considered here for two reasons. First, the kinetic energy of flow represents a source of free energy which often derives instabilities. Such instabilities in the ideal MHD model have been discussed by Taylor (1962), Freidberg and Wesson (1970), Spies (1978), and Hameiri (1981). Second, when plasma flows do occur, they are usually small and are caused by physics not included in the ideal MHD model (i.e., resistivity, finite Larmor radius effects, etc.). [See, for instance, Taylor (1962); Rosenbluth *et al.* (1962); Bowers and Haines (1971); and Freidberg and Pearlstein (1978).] It would be incorrect to include the dynamic effect of such small flows without including the physical effect itself which drives the flow.

Having made these points one should keep in mind that while flow is destabilizing in most cases of interest, this is not a universal result. Counterexamples have been investigated by Hameiri (1979) and Spies (1980).

Finally, note that for static equilibria the density  $\rho(\mathbf{r})$  is arbitrary.

##### 2. Virial theorem

The ideal MHD equilibrium equations satisfy a particular integral relation known as the virial theorem (Shafranov, 1966). A consequence of this is the basic requirement that any confined MHD equilibrium must be supported by external currents. It is not possible to create a configuration confined solely by currents flowing within the plasma itself.

To demonstrate this, recall that the equilibrium equations can be written in conservation form,

$$\nabla \cdot \vec{T} = 0 , \quad (4.4)$$

where the stress tensor  $\vec{T}$  is given by

$$\vec{T} = p_{\perp}(\vec{I} - \mathbf{e}_b \mathbf{e}_b) + p_{||} \mathbf{e}_b \mathbf{e}_b , \quad (4.5)$$

$$p_{\perp} = p + \frac{\mathbf{B}^2}{2} , \quad (4.6)$$

$$p_{||} = p - \frac{\mathbf{B}^2}{2} , \quad (4.7)$$

$$\mathbf{e}_b = \frac{\mathbf{B}}{B} . \quad (4.8)$$

Note that in a local rectangular coordinate system, with  $\mathbf{B}$  defined in the  $z$  direction,  $\vec{T}$  has the form

$$\vec{T} = \begin{bmatrix} p_{\perp} & 0 & 0 \\ 0 & p_{\perp} & 0 \\ 0 & 0 & p_{||} \end{bmatrix} , \quad (4.9)$$

so that  $p_{\perp}$  and  $p_{||}$  represent the pressures perpendicular and parallel to  $\mathbf{B}$ , respectively.

The next step in deriving the virial theorem is to integrate the identity

$$\nabla \cdot (\mathbf{r} \cdot \vec{T}) = \mathbf{r} \cdot (\nabla \cdot \vec{T}) + \text{Tr}(\vec{T}) \quad (4.10)$$

over an arbitrary volume  $V$ , surrounded by the surface  $S$ .

Setting  $\nabla \cdot \vec{T} = 0$  for equilibrium, one obtains

$$\int \left[ 3p + \frac{B^2}{2} \right] dV = \oint \left[ \left( p + \frac{B^2}{2} \right) (\mathbf{n} \cdot \mathbf{r}) - B^2(\mathbf{r} \cdot \mathbf{e}_b)(\mathbf{n} \cdot \mathbf{e}_b) \right] dS , \quad (4.11)$$

$$d\mathbf{S} = \mathbf{n} dS .$$

Assume now that the virial theorem is false; confined equilibria do exist without external currents. Let  $S$  be outside the confined plasma so that  $p(S) = 0$ . If no external currents are present,  $S$  can extend to infinity. Furthermore, if the equilibrium currents are indeed confined to the plasma, then  $B(S) \leq 1/r^3$  for large  $r$ . Under these circumstances the right-hand side of Eq. (4.11) vanishes. The resulting contradiction thus proves the virial theorem. When confined equilibria are surrounded by external conductors, Eq. (4.11) is no violated since the right-hand side must now be evaluated over the surface of the conductors.

### 3. Toroidal geometry

The most obvious common feature in current magnetic fusion concepts is that, with one important exception, each is toroidal. The intent is to create a configuration in which magnetic field lines remain contained within the toroidal volume; lines should not intersect the external current-carrying conductors or even the vacuum chamber, which is usually somewhat closer to the plasma.

The reason for building relatively complicated toroidal systems rather than simpler, linear, open-ended systems is the enormous difference in the energy loss rates perpendicular and parallel to a magnetic field. In an open-ended device, magnetic field lines leave the system and ultimately make contact with material walls [see Fig. 4(a)]. Both density and energy can be lost very quickly because charged particles move freely along magnetic field lines. Assuming that the potentially faster particle loss is eliminated by magnetic trapping, the dominant remaining energy-loss mechanism is parallel thermal conduction by electrons. In a toroidal device with contained lines, the dominant energy-loss mechanism is cross-field ion thermal conduction; Fig. 4(b). The ratio of the classical thermal conductivities is given by (Spitzer, 1956; Braginskii, 1965)

$$\frac{\kappa_{||e}}{\kappa_{\perp i}} = 1.12Z^3 \left( \frac{m_i}{m_e} \right)^{1/2} \left( \frac{T_e}{T_i} \right)^{5/2} (\omega_{ci} \tau_{ii})^2$$

$$\approx 4.35 \times 10^{21} \frac{T(\text{eV})^3 B(\text{G})^2}{n(\text{cm}^{-3})^2} , \quad (4.12)$$

where  $\omega_{ci}$  is the ion cyclotron frequency and  $\tau_{ii}$  is the ion-ion collision frequency for momentum exchange. In the numerical formula, it is assumed that (1) the ions are singly charged deuterons ( $Z = 1$ ,  $m_i = 2m_{\text{proton}}$ ), (2) the

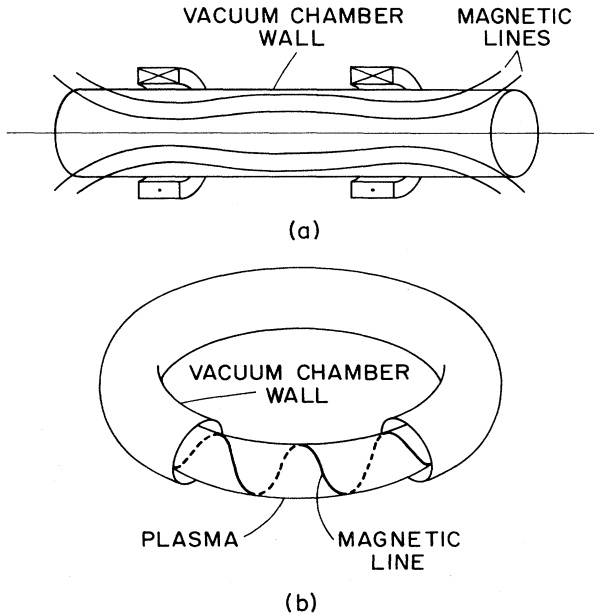


FIG. 4. Magnetic field line trajectories in (a) open-ended systems and (b) toroidal systems.

electrons and ions are at the same temperature ( $T_e = T_i = T$ ), and (3) the Coulomb logarithm appearing in  $\tau_{ii}$  has been set to 18 ( $\ln \Lambda = 18$ ). For plasma parameters corresponding to either current experimental operation or to reactor conditions, this ratio is enormous. As an example consider a tokamak with  $T = 2$  keV,  $B = 25$  kG, and  $n = 3 \times 10^{13} \text{ cm}^{-3}$ . In this case  $\kappa_{||e}/\kappa_{\perp i} = 2.4 \times 10^{13}$ .

In practice the actual values of perpendicular electron and ion thermal conductivities in toroidal devices can be substantially larger than their classical values. The reasons for this are twofold. First, the orbits of a relatively few particles are strongly modified by toroidal effects, leading to a disproportionately large contribution to  $\kappa_{\perp i}$  (neoclassical transport). [See, for instance, Hinton and Hazeltine (1976).] Second, anomalous effects due to plasma microinstabilities increase the effective collision frequency, leading to enhanced values of  $\kappa_{\perp i}$  (Molvig *et al.*, 1979). Experimental measurements of  $\kappa_{||e}$  indicate that its value is approximately classical (McKenna *et al.*, 1979). Even with these larger values of  $\kappa_{\perp i}$ , the ratio  $\kappa_{||}/\kappa_{\perp i}$  remains so large that the consensus in the magnetic fusion community is that, to avoid such losses, the magnetic configuration must be toroidal.

The one major exception to this consensus is the open-ended mirror confinement concept. [See, for instance, Baldwin (1977) and Baldwin and Logan (1979).] Here, by a combination of clever design and plasma operating regime, the plasma energy density at the point of material wall contact is sufficiently low so that the plasma electrostatically shields itself from the wall. One criterion of success for the mirror concept is the effectiveness of this shielding and its ability to keep the parallel losses to an acceptable level.

#### 4. Magnetic flux surfaces

In fusion devices of interest, the magnetic field lines lie in general on a set of closed nested toroidal surfaces. This follows from the equilibrium relation

$$\mathbf{B} \cdot \nabla p = 0 . \quad (4.13)$$

That is, for well-confined equilibria the pressure in most configurations is maximum near the center of the poloidal cross section and is approximately constant as a function of toroidal angle (Fig. 5). For such profiles the contours of constant pressure are nested toroidal surfaces. From Eq. (4.13) it follows that the magnetic lines lie on the  $p = \text{const}$  contours, and consequently these contours are usually referred to as either magnetic surfaces or flux surfaces. The limiting magnetic surface, which approaches a single magnetic line where the pressure is maximum, is called the magnetic axis.

There are two important classes of magnetic surfaces that must be distinguished; those in which a given magnetic field line exactly closes on itself after a finite number of toroidal circuits and those in which it does not. The first class consists of the rational surfaces. The second class contains magnetic lines which ergodically cover the surface and hence consists of ergodic surfaces. All configurations will in general have rational surfaces, although the number of such surfaces is usually of measure zero compared to the ergodic surfaces. The tokamak, stellarator, and reversed field pinch are configurations of this type. One notable counterexample which has only closed lines is the Elmo bumpy torus.

The usual way to characterize the two classes of surfaces is in terms of the rotational transform, defined as follows. Imagine the projection of a magnetic line on a given poloidal cross section, as shown in Fig. 6. After one transit around the torus, the magnetic line returns to a slightly different angle,  $\theta_0 + \Delta\theta$ , on the flux surface. In general,  $\Delta\theta$  depends upon the poloidal angle  $\theta_0$  where the line started. The rotational transform  $\iota$  is the average value of the angle  $\Delta\theta$  after an infinite number of transits

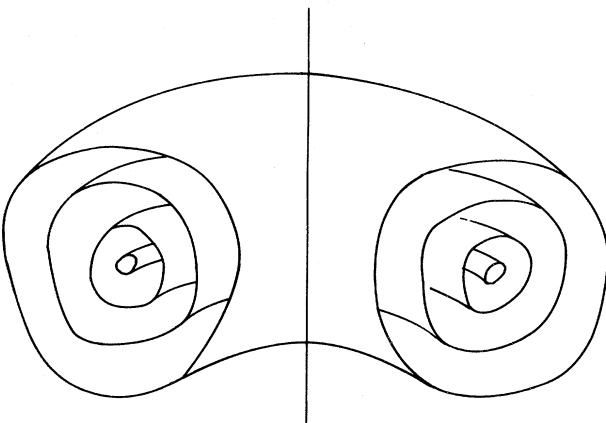


FIG. 5. Contours of constant pressure in a well-confined toroidal equilibrium.

FIELD LINE PROJECTIONS  
IN THE POLOIDAL PLANE

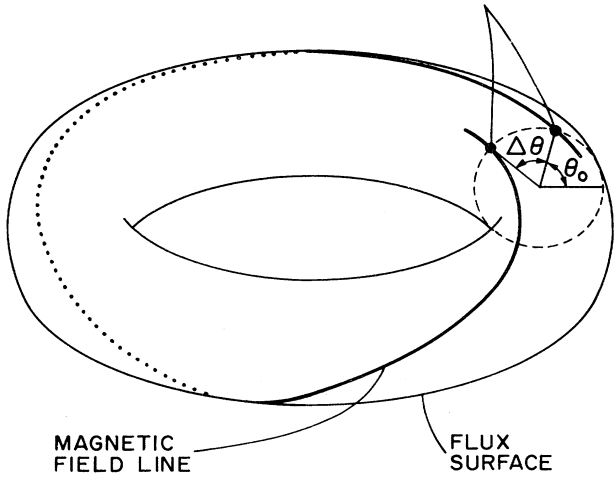


FIG. 6. Magnetic field line projection used in the definition of rotational transform.

$$\iota \equiv \lim_{N \rightarrow \infty} \frac{1}{N} \sum_1^N \Delta\theta_n . \quad (4.14)$$

If  $\iota$  is a rational fraction of  $2\pi$ , the line is closed. If it is not, the line is ergodic. The rotational transform plays an important role in both equilibrium and stability, and the procedures for calculating it are discussed later. Note that ergodic surfaces can be mapped out either by plotting  $p = \text{const}$  contours or by tracing magnetic field line trajectories around many circuits of the torus. For closed-line systems, however, the magnetic surfaces are defined only as  $p = \text{const}$  surfaces, since closed lines do not trace out complete surfaces.

#### 5. Freedom to specify an equilibrium

By utilizing the equilibrium equations it is possible to define certain quantities by performing appropriate integrals over the magnetic surfaces. In general these "surface quantities" describe special global properties of the equilibria. The number of global properties which can be independently specified is of great interest physically in distinguishing different equilibria and of great importance mathematically in correctly formulating a method of solution. It is this topic that is considered here.

To begin, note that the current lines as well as the magnetic lines lie on the  $p = \text{const}$  magnetic surfaces, a consequence of the equilibrium relation

$$\mathbf{J} \cdot \nabla p = 0 . \quad (4.15)$$

This has the simple interpretation that the current must flow between magnetic flux surfaces. Since  $\mathbf{J}$  and  $\mathbf{B}$  lie on the magnetic surfaces it follows that each of the quantities

$$\begin{aligned} I_t &= \int \mathbf{J} \cdot d\mathbf{S}_t \text{ toroidal current} \\ I_p &= \int \mathbf{J} \cdot d\mathbf{S}_p \text{ poloidal current} \\ \psi_t &= \int \mathbf{B} \cdot d\mathbf{S}_t \text{ toroidal flux} \\ \psi_p &= \int \mathbf{B} \cdot d\mathbf{S}_p \text{ poloidal flux} \end{aligned} \quad (4.16)$$

defined as an integral from the magnetic axis out to a given magnetic surface (see Fig. 7) is a function only of that magnetic surface (and not of the remaining nonintegrated toroidal or poloidal angle). Such quantities are called surface quantities. By definition, the pressure and rotational transform are surface quantities, while, for example, the poloidal magnetic field and current density are not.

These surface quantities, which often play an important role in equilibrium and stability, are not independent. Intuitively, one expects two surface quantities to be free. This intuition is based on the fact that there are two independent controls that can be exercised via the external circuits producing any given configuration; one in the toroidal field circuit (e.g., regulation of the toroidal flux) and one in the poloidal field circuit (e.g., regulation of the toroidal current). The existence of two arbitrary independent surface quantities has been shown explicitly in exact calculations of one- and two-dimensional equilibria and in asymptotic calculations of three-dimensional equilibria.

Therefore, in order to completely specify an equilibrium, one must be able to prescribe two independent surface quantities which reflect the history of the evolution to steady state of the toroidal and poloidal magnetic fields.

## 6. The basic problem of toroidal equilibrium

In an approximate sense the requirements for toroidal equilibrium separate into two parts. First the magnetic

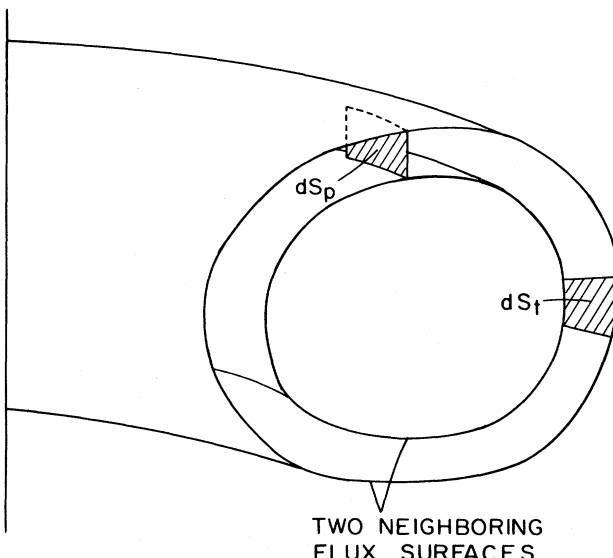


FIG. 7. Illustration of the poloidal and toroidal surface elements  $dS_p$  and  $dS_t$ .

configuration must provide radial confinement (i.e., radial pressure balance) in the poloidal plane so that the pressure contours form closed nested surfaces. Although the manners in which they do so are quite different, either toroidal or poloidal fields can easily accomplish this. The second, and by far the more difficult, problem is the design configurations which compensate for the force of outward expansion inherent in all toroidal configurations, without sacrificing stability. With this in mind, it is helpful to examine two opposing limiting cases which serve to illustrate the basic nature of the toroidal force balance problem.

First consider a configuration with a purely poloidal magnetic field, as shown in Fig. 8(a). There are two forces which cause the plasma to expand outward in the toroidal plane (i.e., in the  $+R$  direction): (1) an outward hoop force, just as would exist in a circular current-carrying loop of wire, produced by the toroidal current which generates the magnetic field; (2) a net outward force, even when the plasma pressure is constant, because the area on the outside of the torus is slightly larger than that on the inside. The situation is similar to that in a rubber tire tube. The combined outward force can be compensated for in two different ways. If a perfectly conducting shell surrounds the plasma, then as the plasma expands in response to the outward forces, the poloidal magnetic flux outside the plasma is compressed, thereby increasing the magnetic pressure [Fig. 8(b)]. Equilibrium is achieved when the plasma shifts far

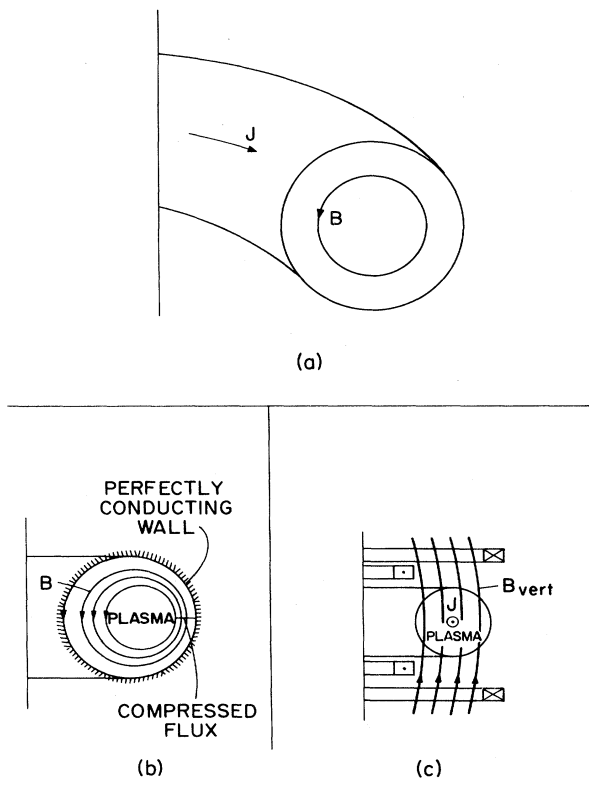


FIG. 8. Toroidal equilibrium in a configuration with purely poloidal field: (a) geometry, (b) equilibrium by a conducting wall, (c) equilibrium by a vertical field.

enough that, due to the increased magnetic pressure, the inward force balances the outward force.

A second way to balance the outward force is to replace the conducting wall with a set of fixed current-carrying vertical-field coils [Fig. 8(c)]. By a proper choice of magnitude and sign, the vertical fields generated by these coils can produce an inward compensating  $\mathbf{J} \times \mathbf{B}_{\text{vert}}$  force for equilibrium.

Thus configurations with purely poloidal magnetic fields can easily be designed with good toroidal equilibrium properties. However, it will be shown later that, in general, such configurations develop strong instabilities, which often lead to the destruction of the plasma.

Consider now the opposite limit, that of a pure toroidal field, as shown in Fig. 9(a). As will be demonstrated in Sec. V, this configuration has inherently better stability properties than the purely poloidal case. Nevertheless, from the simple calculation outlined below it follows that a purely toroidal configuration cannot be held in magnetohydrodynamic equilibrium. To show this, assume that all the current flows solely in a thin layer at the plasma surface and that the pressure  $p$  is a constant  $p_0$  in the plasma and zero outside. (Note that  $\mathbf{J} \times \mathbf{B} = \nabla p$  is trivially satisfied in the plasma.) Assume that the plasma is completely diamagnetic, so that the magnetic field in the plasma is zero. Outside, from Maxwell's equations, it follows that the toroidal field decreases inversely with  $R$ ; that is,  $\mathbf{B} = B_0(R_0/R)\mathbf{e}_\phi$  [see

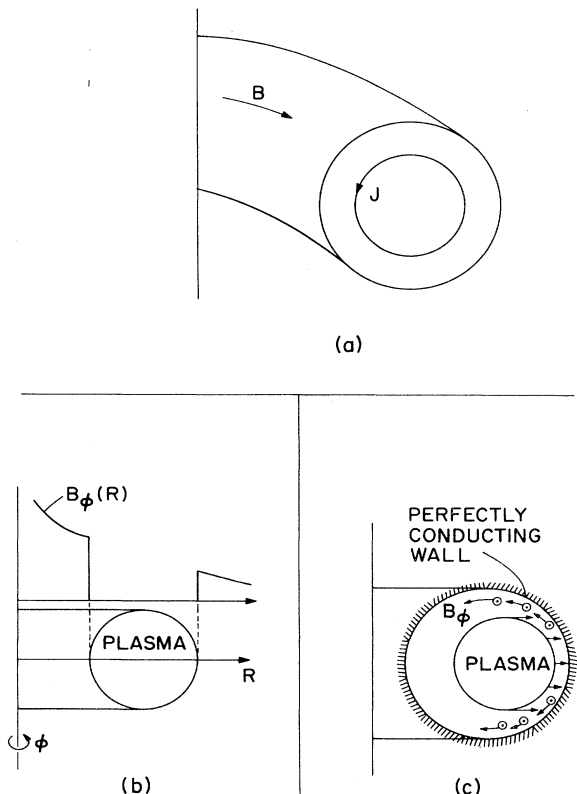


FIG. 9. Toroidal force balance in a configuration with purely toroidal field: (a) geometry, (b)  $1/R$  dependence of the toroidal field, (c) lack of toroidal equilibrium.

Fig. 9(b)]. Because of the  $1/R$  dependence, it is clear that the magnetic pressure on the inside of the torus ( $\pi/2 < \theta < 3\pi/2$ ) is always greater than that on the outside. This effect is partially compensated for by the slightly smaller area on the inside, but there always remains a net outward force. There is an additional outward force arising from the "rubber tire tube" effect, identical to that in the purely poloidal case. The combined outward force (in the  $+R$  direction) can easily be calculated by integrating the  $e_R$  component of the total pressure jump over the plasma surface [i.e.,  $2F_R = \int (2p - B^2) \cos\theta 2\pi R(\theta) a d\theta$ ]. For large aspect ratios,  $R/a \gg 1$ , the force per unit length, is given by

$$\frac{F_R}{2\pi R_0} = \pi \left[ p + \frac{B_0^2}{2} \right] \frac{a^2}{R_0}. \quad (4.17)$$

Since the magnetic field is in the toroidal direction, a conducting wall is not able to compensate for this force; that is, as the plasma moves outward, the magnetic lines simply slip around and let the plasma drift through [Fig. 9(c)]. Likewise, vertical fields do not help because by symmetry they cannot produce any net force.

The conclusion from this calculation is that a configuration with a purely toroidal magnetic field cannot be held in equilibrium because of the  $1/R$  dependence of the magnetic field resulting from the toroidal geometry. One question to be asked is whether or not the outward drift can be negligible on the time scale of interest if the aspect ratio is made sufficiently large. The answer is negative. If a vacuum chamber were located at a minor radius  $b$ , then the time required for the plasma to make contact would be given by

$$t = \left[ \frac{2b}{F_R/M} \right]^{1/2} = \left[ \frac{4bR_0\rho_0}{B_0^2 + 2p} \right]^{1/2}, \quad (4.18)$$

where  $\rho_0$  is the plasma mass density. Even in an extreme case ( $b = 1$  m,  $R_0 = 1$  km,  $B_0 = 5$  T,  $n_0 = 10^{15}$  cm $^{-3}$ ,  $2p = B_0^2$ , and deuterium mass),  $\tau = 18$   $\mu$ sec, which is much too short to be of practical interest.

The basic problem of finding satisfactory magnetic geometries for confining fusion plasmas can be summarized as follows. On the one hand, closed toroidal systems, where the predominant magnetic field is poloidal, have good toroidal equilibrium properties but poor stability properties. On the other hand, when the toroidal field is dominant, stability is inherently much better, but serious equilibrium problems exist. Attempts to resolve this dilemma have led to the discovery of a number of different configurations, often managing to combine the desirable features of both toroidal and poloidal systems while, to a reasonable extent suppressing the undesirable ones. In the remainder of this section the currently most promising configurations are discussed from the point of view of equilibrium, the stability questions being addressed in Sec. V.

## B. One-dimensional configurations

Even though the magnetic configurations of interest are toroidal, a very useful way to develop intuition is to first study their one-dimensional cylindrically symmetric analogs. In this way the two basic problems of MHD equilibrium, toroidal force balance and radial pressure balance, are isolated from each other, thereby making their understanding considerably simpler. The one-dimensional model focuses on radial pressure balance. The question of toroidal force balance does not appear, since by definition the geometry is linear. Consequently toroidal force balance can only be accounted for by considering multidimensional geometries. Also, note that certain configurations are inherently multidimensional (e.g., the stellarator, the Elmo bumpy torus) and hence have no simple one-dimensional analog.

Given below is a description of the basic one-dimensional configurations and how they provide radial pressure balance in a plasma.

### 1. $\theta$ pinch

The  $\theta$  pinch represents the one-dimensional analog of the toroidal configuration with a purely toroidal field. The "equivalent" torus consists of a section,  $2\pi R_0$  in length, of the infinitely long, cylindrically symmetric, linear plasma column. In a  $\theta$  pinch the only nonzero component of  $\mathbf{B}$  is in the  $z$  direction. It is applied externally and induces a large diamagnetic  $\theta$  current  $J_\theta = -dB_z/dr$  in the plasma, as shown in Fig. 10 (hence the name  $\theta$  pinch).

The basic equilibrium relation for the  $\theta$  pinch is obtained from the radial component of the pressure balance equation,  $J_\theta B_z = dp/dr$  (all other equations being trivially satisfied). The result is

$$\frac{d}{dr} \left[ p + \frac{B_z^2}{2} \right] = 0 \quad (4.19)$$

or, upon integrating,

$$p(r) + \frac{B_z^2(r)}{2} = \frac{B_0^2}{2}, \quad (4.20)$$

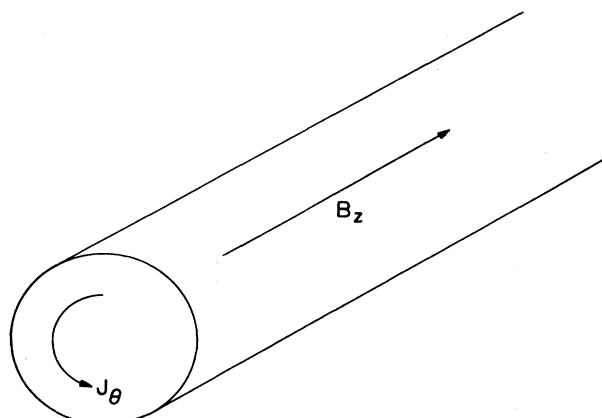


FIG. 10.  $\theta$ -pinch geometry.

where  $B_0$  is the externally applied field.

Equation (4.20) indicates that at any local value of  $r$  the sum of the particle pressure and the magnetic pressure is constant and equal to the externally applied magnetic pressure. Illustrated in Fig. 11 is a set of typical profiles. Note that the pressure is peaked at  $r=0$  and decreases rapidly for large  $r$ , thus isolating itself from the containing wall. This indicates good radial containment and closed nested pressure contours.

One measure of the effectiveness of plasma containment is the quantity  $\beta$ , which is the ratio of plasma energy to total energy,

$$\beta(r) \equiv \frac{p}{p + B^2/2}, \quad 0 \leq \beta \leq 1. \quad (4.21)$$

For a  $\theta$  pinch, the central  $\beta$  [i.e.,  $\beta_0 \equiv \beta(0) = 2p(0)/B_0^2$ ] can have any value between zero and unity. This flexibility, including access to high values of  $\beta_0$ , indicates that the  $\theta$  pinch is an excellent radial container of plasma.

Regarding toroidal equilibrium, the  $\theta$  pinch represents a highly degenerate configuration. Stability analysis indicates that the straight  $\theta$  pinch is neutrally stable in the ideal MHD model, and as has been previously shown, when it is bent into a torus, its equilibria do not exist. Therefore additional fields must be added to provide equilibrium, and since the basic configuration is neutrally stable, the overall stability will depend sensitively on the additional fields. Thus the important problems have yet to be faced. Nevertheless, the  $\theta$  pinch represents the radial pressure balance properties of a number of interesting fusion concepts, in particular, high- and low- $\beta$  stellarators, high- $\beta$  tokamaks, the central cell of the tandem mirror, and the Elmo bumpy torus.

### 2. $Z$ pinch

The  $Z$  pinch is a one-dimensional model of the toroidal configuration with purely poloidal field and is in many ways orthogonal to the  $\theta$  pinch. In a  $Z$  pinch, only  $B_\theta$  is nonzero and consists entirely of the self field

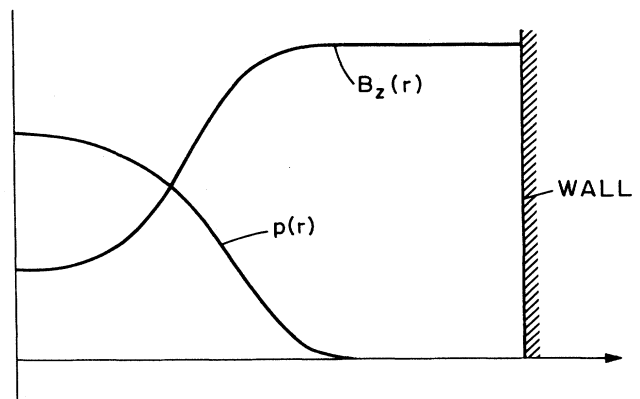


FIG. 11. Equilibrium profiles for a  $\theta$  pinch.

induced by the longitudinal current  $J_z = r^{-1}d(rB_\theta)/dr$  flowing in the plasma (hence the name  $Z$  pinch). See Fig. 12. Unlike the case of the  $\theta$  pinch, when the plasma current vanishes in the case of the  $Z$  pinch there is no background  $B$  field remaining.

As before, the only equilibrium equation that is not trivially satisfied is the radial component of pressure balance,  $J_z B_\theta = -dp/dr$ , which reduces to

$$\frac{d}{dr} \left[ p + \frac{B_\theta^2}{2} \right] + \frac{B_\theta^2}{r} = 0. \quad (4.22)$$

Equation (4.22) is somewhat similar to that of the  $\theta$  pinch, but an additional inward force arises because of the tension in the curved magnetic field lines. It is straightforward to generate simple, physically realizable  $B_\theta$  profiles which satisfy Eq. (4.22) and provide good radial containment. As a specific example, consider the well-known Bennett profiles (Bennett, 1934)

$$\begin{aligned} B_\theta &= \frac{I}{2\pi} \frac{r}{r^2 + a^2}, \\ J_z &= \frac{I}{\pi} \frac{a^2}{(r^2 + a^2)^2}, \\ p &= \frac{I^2}{8\pi^2} \frac{a^2}{(r^2 + a^2)^2}, \end{aligned} \quad (4.23)$$

where  $I$  is the total plasma current and  $a$  is the plasma scale length.

Note that the value of  $\beta$  on axis,  $\beta_0$ , is always unity for a pure  $Z$  pinch since  $B_\theta(0)=0$ . Although high  $\beta_0$  is in general desirable, the inability to achieve small to moderate  $\beta_0$  can be a disadvantage; that is, some classes of potentially dangerous MHD modes can be stabilized if  $\beta_0$  is sufficiently low. The fact that this cannot occur in a pure  $Z$  pinch is one reason why its stability properties are so poor.

The energy balance in a  $Z$  pinch can be more conveniently expressed in terms of certain macroscopic quantities, in what is known as the Bennett pinch relation,

$$W_p = \frac{I^2}{8\pi}, \quad (4.24)$$

where  $W_p = 2\pi \int pr dr$  (apart from a factor  $\gamma-1$ ) is the

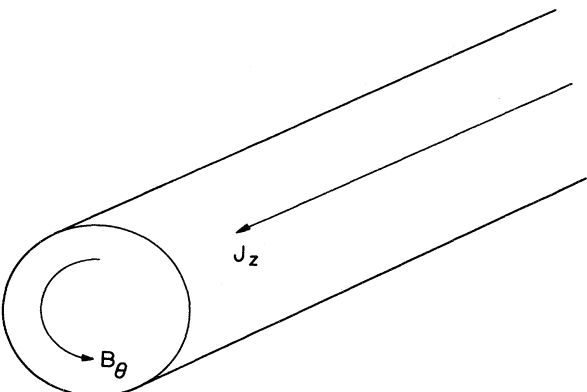


FIG. 12.  $Z$ -pinch geometry.

energy line density (i.e., plasma energy density integrated over the cross section). This relationship, which is valid for any self-consistent profile, indicates that the energies in the plasma and the magnetic field are comparable.

As stated previously, a  $Z$ -pinch equilibrium can easily be bent into a torus, although its stability properties remain poor. Nevertheless, the  $Z$  pinch represents the radial pressure balance properties of several interesting fusion concepts, including the conventional tokamak and reversed field pinch.

### 3. General screw pinch

It should come as no surprise that in the search for satisfactory toroidal equilibria, one approach of interest is to consider configurations with both toroidal and poloidal fields. The hope, of course, is to combine the favorable and suppress the unfavorable features of each field. The one-dimensional analogs of such systems have both  $B_\theta$  and  $B_z$  nonzero.

For the general screw pinch, with  $B_\theta$  and  $B_z$  arbitrary, the equilibrium pressure balance reduces to

$$\frac{d}{dr} \left[ p + \frac{B_z^2 + B_\theta^2}{2} \right] + \frac{B_\theta^2}{r} = 0 \quad (4.25)$$

and in a sense represents a simple superposition of the  $\theta$  pinch and  $Z$  pinch. Even this simple relation exhibits many of the features expected in more realistic, multidimensional toroidal calculations.

First, there are two free functions available to specify the equilibrium; for example,  $B_\theta(r)$  and  $B_z(r)$ . The  $\theta$  pinch and  $Z$  pinch are special choices where either  $B_\theta$  or  $B_z$  is set to zero, respectively. In the general case, once both profiles are specified, the pressure is calculated from Eq. (4.25).

Second, the contours of constant pressure are given by  $r=\text{const}$ . Thus the magnetic flux surfaces are cylinders whose cross sections are closed concentric circles.

Third, the  $\beta$  value can be varied over a wide range if  $B_z$  is not equal to zero.

Fourth, the magnetic lines wrap around the column along helical paths. See Fig. 13. This gives rise to a nonzero rotational transform which can be calculated as follows: the average value of the angle  $\Delta\theta$  [see Eq. (4.14)] is independent of  $\theta_0$ , the starting angle, because of

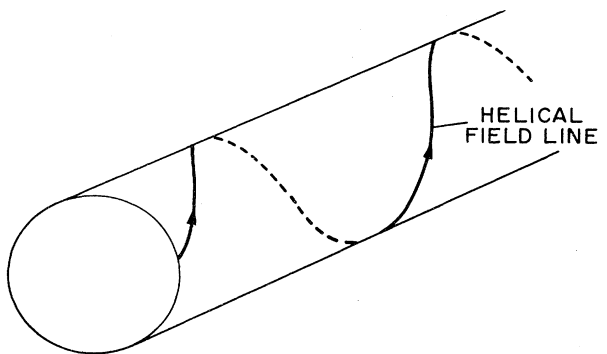


FIG. 13. Helical field line trajectory in a general screw pinch.

the circular symmetry. Thus to calculate  $\iota$  it is only necessary to integrate the field line trajectory a distance  $2\pi R_0$  in  $z$ , corresponding to one transit around the "equivalent" torus,

$$\iota \equiv \Delta\theta = \int_0^{\Delta\theta} d\theta = \int_0^{2\pi R_0} \frac{d\theta}{dz} dz. \quad (4.26)$$

Using the equations for the field line trajectories,

$$\begin{aligned} \frac{d\theta}{dz} &= \frac{B_\theta(r)}{rB_z(r)}, \\ \frac{dr}{dz} &= \frac{B_r(r)}{B_z(r)} = 0, \end{aligned} \quad (4.27)$$

then gives

$$\iota(r) = \frac{2\pi R_0 B_\theta(r)}{rB_z(r)}. \quad (4.28)$$

Oftentimes it is convenient to introduce a quantity  $q$  called the safety factor (for stability reasons to be discussed later), which is related to the inverse of  $\iota$ :  $q \equiv 2\pi/\iota$  or

$$q(r) = \frac{rB_z(r)}{R_0 B_\theta(r)}. \quad (4.29)$$

The quantity  $q$  can be interpreted as the ratio  $\Delta\phi/2\pi$  where  $\Delta\phi$  is the change in toroidal angle of a magnetic line as it traverses one complete poloidal circuit,  $\Delta\theta=2\pi$ . Note that  $\iota=0$  in a  $\theta$  pinch, since the field lines are straight, and that  $q=0$  in a  $Z$  pinch, since the field lines have no axial motion.

Equation (4.25) represents a complete leading-order approximation (i.e., appropriate combinations of  $B_\theta$  and  $B_z$  for radial pressure balance and stability) of toroidal devices with axisymmetry and nearly circular flux surfaces. Even within this subclass there are a great many possible configurations. However, current experimental and theoretical evidence indicates that several configurations in particular are potentially attractive for use in fusion reactors. They are the tokamak [see, for instance, Furth (1975), Wesson (1978), and Bateman (1978)], by far the most important fusion concept both nationally and internationally, and the reversed field pinch, a compact, high- $\beta$  device based on the early British experiment, Zeta (Butt *et al.*, 1958; Bodin and Newton, 1980).

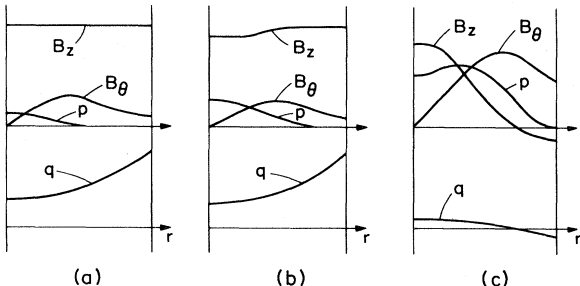


FIG. 14. One-dimensional equilibrium profiles for: (a) a conventional tokamak, (b) a high- $\beta$  tokamak, and (c) a reversed field pinch.

The specific combinations of  $B_\theta$  and  $B_z$  describing each of these devices are illustrated in Fig. 14. From the point of view of radial pressure balance and toroidal force balance, observe that a conventional tokamak is similar to a pure  $Z$  pinch but with a large vacuum  $B_z$  field to improve stability. On the other hand, plasma is contained in a high- $\beta$  tokamak by a small diamagnetic well in the  $B_z$  field. Even though the well is shallow, it is still sufficiently deep to enable a higher  $\beta$  to be contained than in a conventional tokamak because  $B_z \delta B_z \gg B_\theta^2$ . Thus a high- $\beta$  tokamak is both confined radially and stabilized as in a  $\theta$  pinch, the purpose of the small  $B_\theta$  field being only to provide toroidal force balance. The somewhat unusual profiles characterizing the reversed field pinch were observed first in the Zeta experiment, and later shown theoretically (Robinson, 1971) to have good ideal MHD stability properties. The reasons for this are discussed in Sec. V. In any event, the profiles have comparable  $B_\theta$  and  $B_z$  and the pressure is hollow rather than peaked. The plasma is compressed between the  $B_\theta$  pressure on the outside and the  $B_z$  pressure on the inside.

### C. Two-dimensional configurations

In the preceding section it was shown that a one-dimensional model could provide a reasonably good approximation to the radial pressure balance properties of certain axisymmetric toroidal configurations. This section contains a description of equilibria which are functions of two variables. In particular, a derivation is given of the Grad-Shafranov equation, the basic equation describing axisymmetric toroidal equilibrium. The solutions to this equation provide a complete ideal MHD equilibrium description (i.e., radial pressure balance, toroidal force balance, equilibrium  $\beta$  limits, rotational transform profiles, etc.) of the following toroidal devices: conventional tokamak, high- $\beta$  tokamak, noncircular tokamak, flux-conserving tokamak, and reversed field pinch.

In addition, an equation similar to the Grad-Shafranov equation, but for helically symmetric equilibria, is presented. This equation, which is at least as difficult to solve, represents the leading-order description of low- $\beta$  and high- $\beta$  stellarators and the Elmo bumpy torus. The solutions all correspond to infinitely long straight helices. Bending such a configuration into a torus requires a full three-dimensional calculation and is discussed in the next section.

#### 1. The Grad-Shafranov equation

The Grad-Shafranov equation is a two-dimensional, nonlinear, elliptic partial differential equation obtained from the reduction of the ideal MHD equilibrium equations [Eqs. (4.1)–(4.3)] for the case of toroidal axisymmetry (Grad and Rubin, 1958; Shafranov, 1960). It can be derived as follows. Consider the geometry illustrated

in Fig. 15. Here  $R, \phi, Z$  describe the usual right-handed cylindrical coordinate system. The assumption of toroidal axisymmetry implies that  $\partial/\partial\phi=0$ . It then follows from  $\nabla \cdot \mathbf{B}=0$  that  $\mathbf{B}$  can be written as

$$\mathbf{B} = B_\phi \mathbf{e}_\phi + \mathbf{B}_p, \quad \mathbf{B}_p = \frac{1}{R} \nabla \psi \times \mathbf{e}_\phi, \quad (4.30)$$

where  $B_\phi$  is the toroidal field,  $B_p$  is the poloidal field, and  $\psi/R = A_\phi$ , the toroidal component of the vector potential. It can also be easily shown that the poloidal flux  $\psi_p$  is related to  $\psi$  by  $\psi_p = 2\pi\psi$ . In axisymmetric tori it is convenient to label the magnetic flux surfaces with  $\psi$  rather than the pressure  $p$ .

Substituting Eq. (4.30) into Ampere's law yields

$$\mathbf{J} = -\frac{1}{R} \Delta^* \psi \mathbf{e}_\phi + \frac{1}{R} \nabla (RB_\phi) \times \mathbf{e}_\phi, \quad (4.31)$$

where  $\Delta^*$  is the elliptic operator given by

$$\Delta^* \psi \equiv R \frac{\partial}{\partial R} \left( \frac{1}{R} \frac{\partial \psi}{\partial R} \right) + \frac{\partial^2 \psi}{\partial Z^2}. \quad (4.32)$$

The last step in the derivation is to substitute Eqs. (4.30) and (4.31) into the momentum equation [Eq. (4.1)]. An efficient way to do this is to decompose Eq. (4.1) into three components, along  $\mathbf{B}$ ,  $\mathbf{J}$ , and  $\nabla\psi$  (normal to the flux surface). The  $\mathbf{B}$  component gives  $\mathbf{B} \cdot \nabla p = 0$  or  $\mathbf{e}_\phi \cdot \nabla \psi \times \nabla p = 0$ . As expected, this implies that  $p$  is a surface quantity,

$$p = p(\psi). \quad (4.33)$$

Similarly, the  $\mathbf{J}$  component gives  $\mathbf{J} \cdot \nabla p = 0$  or  $\mathbf{e}_\phi \cdot \nabla \psi \times \nabla (RB_\phi) = 0$ , so that  $RB_\phi$  is also a surface quantity,

$$RB_\phi = F(\psi). \quad (4.34)$$

It can easily be shown that  $F(\psi) = I_p / 2\pi$ , where  $I_p$  is the poloidal current passing through the surface bounded by  $R = \text{const}$ ,  $Z = 0$ .

The Grad-Shafranov equation is obtained by substituting these results into the  $\nabla\psi$  component. The result is

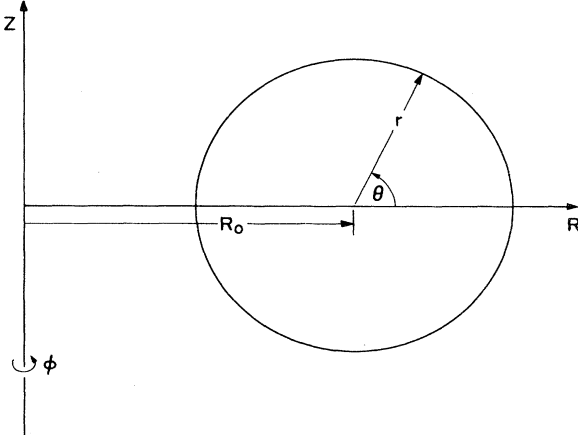


FIG. 15. Axisymmetric toroidal geometry.

$$\Delta^* \psi = -R^2 \frac{dp}{d\psi} - F \frac{dF}{d\psi}. \quad (4.35)$$

Equation (4.35) is a second-order nonlinear partial differential equation describing axisymmetric toroidal equilibria. The nature of the equilibria (i.e., tokamak, reversed field pinch, etc.) is to a large extent determined by the choice of the two free functions  $p(\psi)$  and  $F(\psi)$  and, of course, the boundary conditions. These issues are discussed in more detail on an individual basis in later sections.

Consider now the macroscopic plasma parameters  $\beta$  and  $q$ . There is no unique definition of  $\beta$  which is simultaneously meaningful in all geometries and simple to evaluate. The different definitions, which usually are not too dissimilar from each other or Eq. (4.21), are also discussed on an individual basis.

On the other hand, the safety factor  $q$  is uniquely defined and can be calculated as follows. The equation for a magnetic field line in toroidal coordinates  $r, \theta, \phi$  defined by (see Fig. 15)

$$R = R_0 + r \cos\theta, \quad Z = r \sin\theta \quad (4.36)$$

can be expressed as

$$\frac{R d\phi}{B_\phi} = \frac{dr}{B_r} = \frac{r d\theta}{B_\theta} = \frac{dl}{B_p}, \quad (4.37)$$

where  $dl = [(dr)^2 + (rd\theta)^2]^{1/2}$  is the poloidal arc length and  $B_p = (B_r^2 + B_\theta^2)^{1/2} = |\nabla\psi|/R$  is the poloidal magnetic field. As the magnetic line wraps exactly once around the poloidal cross section, the toroidal angle  $\Delta\phi$  along which it travels is given by

$$\Delta\phi = \int_0^{\Delta\phi} d\phi = \int_0^{2\pi} \left[ \frac{r B_\phi}{R B_\theta} \right]_S d\theta. \quad (4.38)$$

Thus the average fractional poloidal transit per single toroidal transit is just  $\iota = 2\pi(2\pi/\Delta\phi)$ , the rotational transform. The safety factor  $q = 2\pi/\iota$  then has the form

$$q(\psi) = \frac{1}{2\pi} \int_0^{2\pi} \left[ \frac{r B_\phi}{R B_\theta} \right]_S d\theta = \frac{F(\psi)}{2\pi} \int \frac{dl}{R^2 B_p}. \quad (4.39)$$

In Eqs. (4.38) and (4.39) the integrals are to be evaluated on the flux surface on which the magnetic line lies.

Because of the nonlinearity, the Grad-Shafranov equation must in general be solved numerically. Most of the major fusion laboratories around the world have developed such codes. They can be used for essentially arbitrary  $p(\psi)$  and  $F(\psi)$ , as well as for rather sophisticated boundary conditions. Examples of these numerical equilibria are presented later.

However, from the point of view of obtaining physical understanding, it is perhaps more instructive to perform asymptotic analysis of the Grad-Shafranov equation. The simplifications that arise often permit analytic solu-

tions which are of great aid in developing intuition. The basic expansion parameter is the inverse aspect ratio  $r/R$ . When  $r/R \ll 1$ , the toroidal effects are weak, allowing many configurations to be viewed as perturbations about a straight system. Extensive use of the inverse aspect ratio expansion is made in the remainder of this section.

Before proceeding with the applications it is useful to note that a "Grad-Shafranov" equation also exists for systems with helical symmetry. In such systems all quantities are functions of the two independent variables  $(r, \alpha \equiv l\theta + hz)$ , where  $2\pi/h$  is the helical period and  $l$  describes the order of the poloidal periodicity. The derivation of the equation is similar to that of the axisymmetric torus, and the results are as follows (Solov'ev, 1967):

$$\begin{aligned} B_r &= -\frac{1}{r} \frac{\partial \psi}{\partial \alpha}, \\ lB_\theta + hrB_z &= \frac{\partial \psi}{\partial r}, \\ lB_z - hrB_\theta &= F(\psi), \\ \Delta^* \psi &= \frac{2hlF}{(l^2 + h^2 r^2)^2} - \frac{dp}{d\psi} - \frac{F}{l^2 + h^2 r^2} \frac{\partial F}{d\psi}, \\ \Delta^* \psi &\equiv \frac{1}{r} \frac{\partial}{\partial r} \frac{r}{l^2 + h^2 r^2} \frac{\partial \psi}{\partial r} + \frac{1}{r^2} \frac{\partial^2 \psi}{\partial \alpha^2}. \end{aligned}$$

The equation for  $\psi$  is of comparable difficulty to the axisymmetric Grad-Shafranov equation. It provides a good zeroth-order description of stellarators and the Elmo bumpy torus, but does not include the effects of toroidal force balance. This requires a three-dimensional calculation and is discussed in the next section.

## 2. The reversed field pinch

It is convenient to begin discussions of individual concepts with the reversed field pinch because it, of all others, is the one most accurately described as a perturbation about a linear system. Application of the appropriate aspect ratio expansion leads to a relatively simple analytic solution to the Grad-Shafranov equation. Concerning boundary conditions, it is realistic to assume that the plasma is surrounded by a perfectly conducting circular wall of minor radius  $b$ . On such a surface  $\mathbf{n} \cdot \mathbf{B} = 0$ , implying that the wall is a flux surface. Hence the boundary conditions require (1) regularity throughout the domain and (2)  $\psi(b, \theta) = \text{const}$ .

The asymptotic expansion is defined in terms of the inverse aspect ratio

$$\epsilon \equiv a/R_0 \ll 1, \quad (4.40)$$

where  $a$  is the typical scale length of the minor plasma radius (i.e.,  $r \sim a$ ). Keeping in mind that the toroidal and poloidal fields are comparable in a reversed field pinch, the appropriate ordering is given by

$$\begin{aligned} \frac{B_\phi}{B_p} &\sim 1, \\ \beta &\sim \frac{2p}{B_p^2} \sim 1, \\ q &\sim \frac{rB_\phi}{RB_p} \sim \epsilon. \end{aligned} \quad (4.41)$$

This ordering implies that the reverse field pinch is a high- $\beta$  device, operating with a small safety factor, in which both poloidal and toroidal fields play an important role in radial pressure balance. Using Eq. (4.41), one can solve the Grad-Shafranov equation by expanding the flux function as follows:

$$\psi(r, \theta) = \psi_0(r) + \psi_1(r) \cos \theta + \dots, \quad (4.42)$$

where  $\psi_1/\psi_0 \sim \epsilon$  and  $\psi_0/rRB_p \sim 1$ .

In zeroth order  $B_{r0}(r) = 0$ ,  $B_{\theta 0}(r) = \psi'_0(r)/R_0$ ,  $F(\psi_0) = R_0 B_{\phi 0}(r)$ , and  $p(\psi_0) = p_0(r)$ . The corresponding contribution to the Grad-Shafranov equation is obtained by noting that, in  $r, \theta$  coordinates,

$$\begin{aligned} \Delta^* \psi &= \nabla^2 - \frac{1}{R} \left[ \cos \theta \frac{\partial}{\partial r} - \frac{\sin \theta}{r} \frac{\partial}{\partial \theta} \right], \\ \nabla^2 &= \frac{1}{r} \frac{\partial}{\partial r} r \frac{\partial}{\partial r} + \frac{1}{r^2} \frac{\partial^2}{\partial \theta^2}. \end{aligned} \quad (4.43)$$

The result is

$$\frac{d}{dr} \left[ p_0 + \frac{B_{\phi 0}^2}{2} \right] + \frac{B_{\theta 0}}{r} \frac{d}{dr} (rB_{\theta 0}) = 0, \quad (4.44)$$

which is just the radial pressure balance relation for the straight general screw pinch [Eq. (4.25)]. In place of  $p(\psi), F(\psi)$ , two of the four quantities  $p_0(r), B_{\phi 0}(r), B_{\theta 0}(r), \psi_0(r)$  can be specified as arbitrary free functions. For convenience assume that  $B_{\theta 0}$  and  $B_{\phi 0}$  are free, that  $p'_0$  is determined from Eq. (4.44), and that  $\psi_0$  is determined from  $\psi_0 = R_0 \int B_{\theta 0} dr$ .

Continuing, the order  $\epsilon$  contribution to the Grad-Shafranov equation can be written, after some algebra, as

$$\frac{d}{dr} \left[ rB_\theta^2 \frac{d}{dr} \left[ \frac{\psi_1}{B_\theta} \right] \right] = -2r^2 \frac{dp}{dr} + rB_\theta^2. \quad (4.45)$$

For simplicity the subscript 0 has been dropped from the zero-order quantities. The solution to Eq. (4.45) satisfying the boundary conditions is given by

$$\psi_1(r) = B_\theta(r) \int_r^b \frac{dx}{xB_\theta^2(x)} \int_0^x \left[ 2y^2 \frac{dp(y)}{dy} - yB_\theta^2(y) \right] dy. \quad (4.46)$$

The contribution of  $\psi_1$  to the total flux represents the toroidal correction to reversed field pinch equilibria.

Consider now the basic properties of such equilibria. Since  $B_\theta$  and  $B_\phi$  are both leading-order quantities, the values of  $\beta$  and  $q$  are essentially the same as in the straight system. In measuring the efficiency of magnetic field utilization it has been proven more useful to define

an average, rather than a local,  $\beta$ . A reasonable definition follows from an integral form of Eq. (4.44) given by

$$2\pi \int_0^b \left[ p + \frac{B_\phi^2}{2} \right] r dr = \frac{I^2}{8\pi} + \frac{1}{2}\pi b^2 B_\phi^2(b), \quad (4.47)$$

where  $I$  is the toroidal current.

First, a quantity known as the "poloidal beta" is introduced as follows:

$$\begin{aligned} \langle \beta_p \rangle &= W_p / W_I + O(\epsilon), \\ W_p &= 2\pi \int_0^b pr dr, \\ W_I &= I^2 / 8\pi. \end{aligned} \quad (4.48)$$

This quantity is useful in the understanding of both reversed field pinches and tokamaks. Now, since the reversal of the toroidal field  $B_\phi(b)$  is usually small in a reversed field pinch (see Fig. 14), a convenient definition of the average beta is given by  $\langle \beta \rangle \equiv \langle \beta_p \rangle$ . Note that  $\langle \beta \rangle$  is of order unity and can assume a wide range of values, depending upon the strength of the  $B_\phi$  field in the plasma interior. Also,  $\langle \beta_p \rangle = 1$  for a pure  $Z$  pinch.

The safety factor  $q$  is given approximately by its straight value

$$q(r) = \frac{rB_\phi(r)}{R_0 B_\theta(r)} + O(\epsilon^2). \quad (4.49)$$

$q$  is typically of order  $\epsilon$  and actually passes through zero where  $B_\phi$  reverses (see Fig. 14). The question of how a configuration with such a small safety factor can be made MHD stable is discussed in detail in Sec. V. Briefly, though, the answer is the high shear associated with the  $B_\phi$  reversal and the presence of a perfectly conducting wall close to the plasma.

Since  $q \sim 1/I$  is small, the toroidal current is large. This has the effect of requiring only a small outward shift of the plasma to compress sufficient flux for toroidal equilibrium, even with  $\langle \beta \rangle \sim 1$ . To see this, consider a realistic plasma model in which all the plasma currents effectively vanish outside a particular flux surface. Assume that this surface is a circle whose center is slightly shifted from the center of the wall located at  $R = R_0, Z = 0$ ; it is denoted by  $r_a = a + \Delta \cos\theta$ ,  $\Delta \ll a$ . The shift  $\Delta$  is determined from the condition  $\psi[r_a(\theta), \theta] = \text{const}$  or  $\Delta \sim -\psi_1(a)/\psi'_0(a)$ . After some straightforward algebra it follows that (Shafranov, 1966)

$$\frac{\Delta}{b} = \frac{b}{2R} \left[ \left( \langle \beta_p \rangle + \frac{l_i - 1}{2} \right) \left( 1 - \frac{a^2}{b^2} \right) + \ln \frac{b}{a} \right], \quad (4.50)$$

where  $l_i$  is the normalized internal inductance per unit length associated with the toroidal current,

$$\begin{aligned} l_i &= 2L/R_0 \rightarrow \left[ \frac{L}{2\pi R_0} \right] \Big/ \left[ \frac{\mu_0}{4\pi} \right], \\ \frac{1}{2}LI^2 &= 2\pi R_0 W_m, \quad W_m = 2\pi \int_0^a \frac{B_\theta^2}{2\mu_0} r dr. \end{aligned} \quad (4.51)$$

Note that  $\Delta$  is positive, indicating an outward shift. Since  $b/R \ll 1$  in the asymptotic expansion, Eq. (4.50) verifies that the equilibrium shift is indeed small.

The principal response to the outward shift can be seen by calculating the poloidal magnetic field on the plasma surface,

$$\begin{aligned} B_p[r_a(\theta), \theta] &\approx B_a \left[ 1 + \left( \frac{\psi'_1(a)}{R_0 B_a} - \frac{\Delta}{a} - \frac{a}{R_0} \right) \cos\theta \right] \\ &\approx B_a \left[ 1 + \frac{a}{R_0} \left[ \langle \beta_p \rangle + \frac{l_i}{2} - 1 \right] \cos\theta \right], \end{aligned} \quad (4.52)$$

where  $B_a = I/2\pi a$ . The first term, independent of  $\theta$ , represents the straight cylindrical contribution of the toroidal current. Of the  $\cos\theta$  terms, the  $(-1)$  contribution is a result of the toroidal geometry, which causes  $B_p$  to decrease slightly on the outside ( $\theta = 0$ ) and increase on the inside ( $\theta = \pi$ ). The  $l_i/2$  term represents a redistribution of the plasma currents and compression of the outer poloidal flux in response to the outward shift of the plasma. Hence it causes  $B_p$  to increase slightly on the outside and decrease on the inside. The  $\langle \beta_p \rangle$  term contains the combined response of the "tire tube" force and the  $1/R$  toroidal field force. If the toroidal field were zero, then  $\langle \beta_p \rangle$  would be unity [Eqs. (4.47) and (4.48)]. This term then represents a compression of the outer poloidal field caused by the outward shift of the plasma pressure. If the toroidal field is not zero, then  $\langle \beta_p \rangle$  is somewhat reduced, thereby decreasing this compression of the flux. Stated another way, the  $B_\phi$  field in a reversed field pinch is paramagnetic (i.e., large when the pressure is high and small when the pressure is low). Thus, in contrast to the  $\theta$  pinch, which is diamagnetic, the  $1/R$  force due to the toroidal field is actually inward. It partially compensates for the pressure force, resulting in a reduced compression of the outer poloidal flux.

"Exact" numerical solutions of the Grad-Shafranov equation indicate that the asymptotic expansion described above represents an excellent approximation of reversed field pinch equilibria. A typical example of a numerical equilibrium is shown in Fig. 16. Here the functions  $p(\psi)$  and  $F(\psi)$  were chosen to closely simulate experimental profiles. Note the small outward shift of the plasma pressure and the increase of the poloidal field on the outside of the torus.

In summary, the reverse field pinch is a high- $\beta$ , low- $q$  configuration in which the plasma is contained radially between the toroidal magnetic pressure on the inside and the poloidal magnetic pressure on the outside. A large toroidal current provides toroidal force balance by compressing the poloidal flux between the conducting wall and the slightly outward-shifted plasma.

### 3. The conventional tokamak

At the present time the conventional tokamak is the leading contender in the international magnetic fusion program. In particular, PLT, TFTR, Doublet III, Alca-

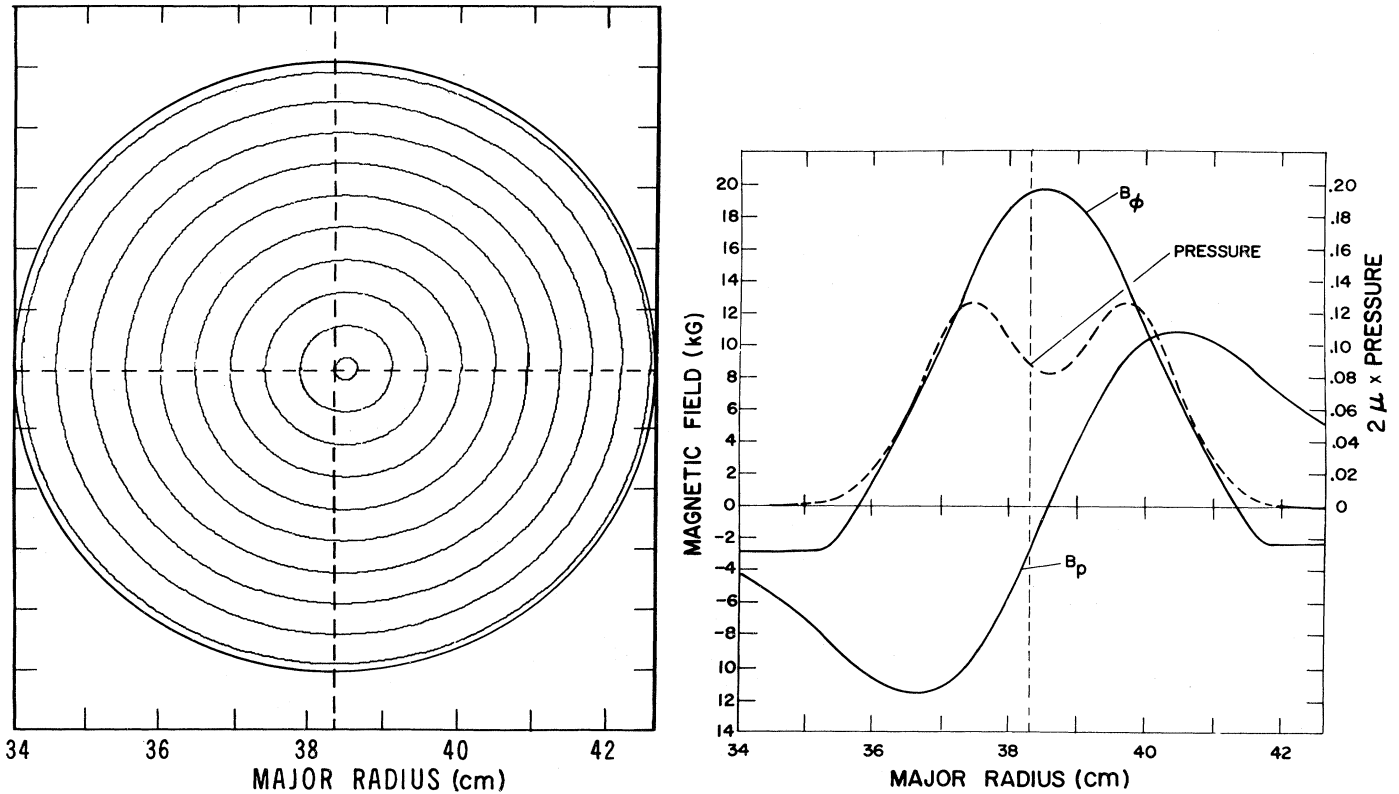


FIG. 16. Equilibrium flux plot for a reversed field pinch. Also shown are the pressure, toroidal field, and poloidal field along the midplane,  $Z=0$  (courtesy L. W. Mann, Los Alamos Scientific Laboratory, 1981).

tor, JET, T-10, TFR, ASDEX, and DIVA are major devices in the United States, Western Europe, Japan, and the Soviet Union, whose basic mode of operation is that of a conventional tokamak. [For a summary of the major fusion experiments throughout the world see IAEA (1976).]

Although the basic field configuration of the tokamak is quite different from the reversed field pinch, the analysis is nevertheless quite similar. The underlying reason is that the pressure is sufficiently small so that only a small outward shift is required for equilibrium, thus implying that the inverse aspect ratio expansion should be very accurate. [See, for instance, Shafranov (1966), Wesson (1978), and Bateman (1978).]

In applying the expansion it is initially assumed for simplicity that the plasma is surrounded by a perfectly conducting shell. This assumption is then relaxed and replaced by the condition that toroidal force balance is achieved by an external vertical field. Since the typical experimental time scales of tokamak operation are much greater than the skin penetration time of the surrounding walls, the vertical-field boundary condition is a much more realistic one.

In terms of the inverse aspect ratio,  $\varepsilon \equiv a/R_0$ , the appropriate expansion for the conventional tokamak is given as

$$\begin{aligned} \frac{B_p}{B_\phi} &\sim \varepsilon, \\ \beta \sim \frac{2p}{B_\phi^2} &\sim \varepsilon^2, \\ q \sim \frac{rB_\phi}{RB_p} &\sim 1. \end{aligned} \quad (4.53)$$

The configuration is dominated by a large toroidal vacuum field. The plasma pressure is contained radially primarily by the poloidal field, as in a pure  $Z$  pinch. This field is made as large as possible to facilitate toroidal equilibrium and to maximize  $\beta$  and ohmic heating, but is limited by the stability constraint that the safety factor be of order unity. Even so, the maximum pressure is still sufficiently low that the equilibrium toroidal shift is small. In practice the toroidal field can also enter the radial pressure balance either diamagnetically or paramagnetically. However, in a conventional tokamak, the deviation from the vacuum field is very small (i.e., of order  $\varepsilon^2$ ), leaving the  $Z$ -pinch nature of the radial confinement unchanged.

Under the conventional tokamak ordering, the Grad-Shafranov equation is solved by formally expanding as follows:

$$\begin{aligned}\psi(r, \theta) &= \psi_0(r) + \psi_1(r) \cos\theta \dots , \\ p(\psi) &= p_2(\psi_0) + \frac{dp_2(\psi_0)}{d\psi_0} \psi_1 \cos\theta \dots , \\ F(\psi) &= RB_\phi = R_0 B_0 + F_1(\psi_0) \dots ,\end{aligned}\quad (4.54)$$

where  $B_0 = \text{constant}$  is the toroidal vacuum field at  $R = R_0$  and  $\psi_1/\psi_0 \sim \epsilon$ ,  $\psi_0/rRB_0 \sim \epsilon$ ,  $p_2/B_0^2 \sim \epsilon^2$ ,  $F_1/rB_0 \sim \epsilon$ . The leading-order contribution to the Grad-Shafranov equation gives

$$\begin{aligned}\frac{d}{dr}(p_2 + B_0 B_{\phi 2}) + \frac{B_{\theta 1}}{r} \frac{d(rB_{\theta 1})}{dr} &= 0, \\ B_{\theta 1}(r) &= \frac{1}{R_0} \frac{d\psi_0}{dr}, \\ B_\phi(r) &= B_0 + B_{\phi 2}(r), \\ B_{\phi 2}(r) &= F_1(\psi_0)/R_0.\end{aligned}\quad (4.55)$$

As in the reversed field pinch, radial pressure balance is identical to that in a straight screw pinch. Likewise the basic plasma parameters are essentially given by their equivalent "straight" values. In particular, it follows that the safety factor  $q$  can be expressed as

$$q = \frac{rB_0}{R_0 B_{\theta 1}} \sim 1 \quad (4.56)$$

and is in general an increasing function of radius. The average  $\beta$  is defined in terms of the toroidal magnetic energy, since  $B_\phi \gg B_p$

$$\begin{aligned}\langle \beta \rangle &= \frac{W_p}{W_t} \sim \epsilon^2, \\ W_p &= 2\pi \int p_2 r dr, \\ W_T &= \frac{1}{2} \pi b^2 B_0^2.\end{aligned}\quad (4.57)$$

In tokamak theory it is also convenient to introduce the poloidal  $\beta$ , a quantity which measures the ratio of plasma energy to poloidal magnetic field energy,

$$\begin{aligned}\langle \beta_p \rangle &= \frac{W_p}{W_I} \sim 1, \\ W_I &= I^2/8\pi.\end{aligned}\quad (4.58)$$

An examination of the general, one-dimensional, equilibrium integral relation [Eq. (4.47)] indicates that when  $B_{\phi 2} = 0$  (i.e., for a purely vacuum toroidal field) then  $\langle \beta_p \rangle = 1$ . If  $B_{\phi 2} < 0$ , the plasma is diamagnetic and  $\langle \beta_p \rangle > 1$ , since part of the pressure is now contained by the toroidal field. Similarly, for a paramagnetic configuration,  $B_{\phi 2} > 0$  and  $\langle \beta_p \rangle < 1$ .

A further useful equilibrium relation can be obtained by considering the model where all the plasma pressure and currents vanish outside a radius  $r = a$ . In this case, it follows directly from the definitions that

$$\langle \beta \rangle = \frac{\langle \beta_p \rangle \epsilon^2}{q^2(a)}. \quad (4.59)$$

In conventional tokamak operation  $\langle \beta_p \rangle \approx 1$ . Equation (4.59) then implies that the total pressure that can be contained is proportional to  $I^2$ , and in this sense radial pressure balance in a conventional tokamak is similar to that in a pure  $Z$  pinch.

Consider now the toroidal corrections to  $\psi(r, \theta)$ . The equation which determines  $\psi_1(r)$  is obtained from the first-order contribution to the Grad-Shafranov equation. Not too surprisingly, this equation is identical to Eq. (4.45). If the plasma were surrounded by a perfectly conducting shell located at  $r = b$ , then the solution would be identical to Eq. (4.46), repeated here for convenience:

$$\psi_1(r) = B_{\theta 1}(r) \int_r^b \frac{dx}{xB_{\theta 1}^2(x)} \int_0^x \left[ 2y^2 \frac{dp_2(y)}{dy} - yB_{\theta 1}^2(y) \right] dy. \quad (4.60)$$

To simulate more realistic tokamak boundary conditions, assume that a set of vertical-field coils has been placed outside the conducting shell. In vacuum these coils produce an additional magnetic field,  $B_v \mathbf{e}_z$ .

In actual tokamak experiments, it is the interaction of this field with the toroidal current that produces the compensating force required for toroidal force balance; that is, the typical penetration time of a copper shell is sufficiently short compared to experimental times that the shell does not behave like a perfect conductor. One must thus use a vertical field for toroidal equilibrium.

Assume that the vertical-field coils have been energized for a sufficiently long time so that their fields have penetrated the conducting boundary. Keep in mind that, once this has occurred, the wall still acts as a perfect conductor on the faster MHD time scale. In this situation, the boundary condition on the flux function is modified so that  $\psi(b, \theta) = \text{const} + \psi_v(b, \theta)$ , where  $\psi_v(r, \theta) = R_0 B_v r \cos\theta$  is the flux function due to the vertical field.

The full toroidal correction to  $\psi$  is obtained by adding an appropriate homogeneous solution to  $\psi_1$  [Eq. (4.60)]. Writing  $\psi_1(\text{total}) = \hat{\psi}_1(r) \cos\theta$  one finds

$$\hat{\psi}_1(r) = \psi_1(r) + \left[ \frac{bR_0 B_v}{B_{\theta 1}(b)} \right] B_{\theta 1}(r). \quad (4.61)$$

The main effect of adding the vertical field is to change the toroidal shift of the plasma, which is now given by

$$\begin{aligned}\Delta &= -\hat{\psi}_1(a)/\psi'_0(a) \\ &= -\psi_1(a)/\psi'_0(a) - \Delta_v,\end{aligned}$$

where

$$\Delta_v = bB_v/B_{\theta 1}(b).$$

This can be written as

$$\frac{\Delta}{b} = \frac{b}{2R_0} \left[ \left( \langle \beta_p \rangle + \frac{l_i - 1}{2} \right) \left( 1 - \frac{a^2}{b^2} \right) + \ln \frac{b}{a} \right] - \frac{B_v}{B_b}, \quad (4.62)$$

where  $B_b = B_{\theta 1}(b) = I/2\pi b$ ,  $l_i$  is given by Eq. (4.51), and typically  $l_i \gtrsim \frac{1}{2}$ .

It is of particular interest to determine the vertical field required to make the plasma shift with respect to the geometric axis  $R = R_0$  equal to zero. This is easily accomplished by setting  $\Delta = 0$  in Eq. (4.62) and solving for  $B_v$ . Even more important is determining the vertical field required to hold the plasma in equilibrium with its center and  $R = R_0$  when no conducting shell is present. To obtain this result it is necessary to set  $\Delta = 0$  and take the limit  $b/a \gg 1$ . This limit is smooth for the first group of terms in Eq. (4.62). The logarithmic term is more complicated, since as  $b$  gets larger it eventually reaches its geometric limit  $b = R_0$ . In fact, a reasonable estimate of the required vertical field is obtained by setting  $\Delta = 0$  and  $b = R_0$  in the logarithmic term (i.e.,  $\ln(b/a) \rightarrow \ln(R_0/a)$ ).

The exact value of  $B_v$  requires a lengthy calculation (Shafranov, 1966; Mills, 1970; and Bateman, 1978). See also Sec. V.D.1.g. However, a more accurate value than the heuristic one just given is obtained by noting that the  $\ln(b/a)$  term represents the force due to the change in magnetic energy between the plasma and the wall as the plasma shifts outward by a small amount  $dR_0 = \Delta$ . It is the analog of the  $l_i$  term, except applied to the external flux. This force can be written as

$$F = -\frac{d}{dR_0} \int_a^b \frac{B_{\theta 1}^2}{2} d\mathbf{r} = -\frac{1}{2} \frac{d}{dR_0} (L_e I^2), \quad (4.63)$$

where  $L_e$  is the external inductance associated with the poloidal flux  $\psi_e$  between the plasma and the wall. Since  $\psi_e = L_e I$  is constant under this displacement,  $F = (1/2)I^2(dL_e/dR_0)$ .

If the wall is reasonably near the plasma, then

$$L_e = \mu_0 R_0 \ln \left( \frac{b}{a} \right). \quad (4.64)$$

If the wall is removed from the plasma, then the value of  $L_e$  to be used should correspond to that of a circular current-carrying loop of wire with major radius  $R_0$  and minor radius  $a$ . This value of  $L_e$  can be found in standard electromagnetic textbooks (Stratton, 1941). For  $a/R_0 \ll 1$ ,

$$L_e = \mu_0 R_0 \left[ \ln \frac{8R_0}{a} - 2 \right]. \quad (4.65)$$

After carrying out the differentiation with respect to  $R_0$  and equating the forces, it follows that the appropriate limit for  $\ln(b/a)$  as  $b \rightarrow R_0$  is given by

$$\ln \frac{b}{a} \rightarrow \ln \frac{8R_0}{a} - 1 = \ln \frac{R_0}{a} + 1.079. \quad (4.66)$$

Note that this differs from the heuristic assumption only by the factor 1.079. Substituting Eq. (4.66) into Eq. (4.62) and setting  $\Delta = 0$  yields the value of  $B_v$  required for toroidal equilibrium with no conducting shell:

$$B_v = \frac{\mu_0 I}{4\pi R_0} \left[ \langle \beta_p \rangle + \frac{1}{2} l_i - \frac{3}{2} + \ln \frac{8R_0}{a} \right]. \quad (4.67)$$

The results described above have proven to be a very reliable guide for the operation of tokamak experiments. They have also been shown to be quite accurate when compared to exact numerical solutions of the Grad-Shafranov equation. In fact, because of the importance of tokamaks to the international fusion program, a number of sophisticated numerical codes have been developed to solve the Grad-Shafranov equation. [See, for instance, Callan and Dory (1972), Helton and Wang (1978), and Johnson *et al.* (1979).] One important feature incorporated in these codes is the ability to solve the more difficult, but realistic, problem in which the plasma is surrounded by a set of external coils rather than a perfect conductor. An example of such a numerical calculation is illustrated in Fig. 17 for the PLT experiment. Note the small shift of the flux surfaces and the compression of the poloidal field on the outside of the torus, in agreement with the asymptotic theory.

To summarize, a conventional tokamak is a device in which both radial containment and toroidal force balance are achieved almost entirely by the poloidal field, as in a Z pinch. The toroidal current is limited in amplitude by the requirement that the safety factor  $q$  be of order unity for stability. The sole purpose (from the ideal MHD point of view) of the large, technically and economically expensive, toroidal field is stability. Since all the heating and confinement are provided by the relatively small poloidal field, the resulting pressure is very small ( $p \sim \epsilon^2$ ), requiring only a small shift or small vertical field for toroidal force balance.

#### 4. The high- $\beta$ tokamak

The progress in physics of conventional tokamaks has been impressive over the last few years, particularly in

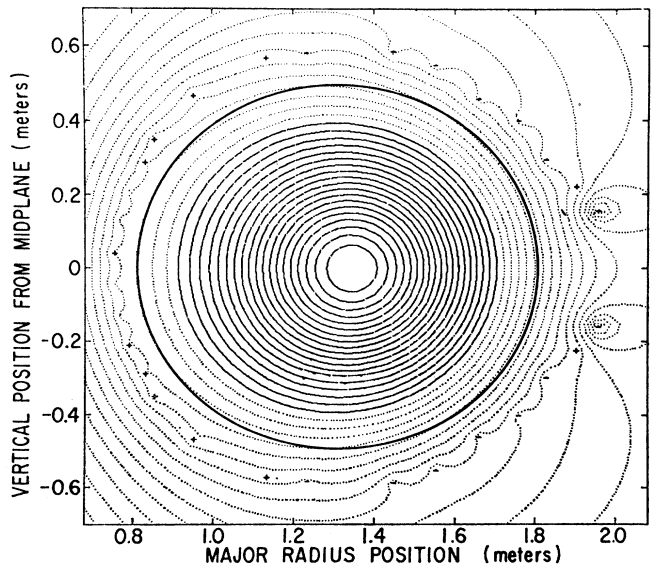


FIG. 17. Equilibrium flux plot of the PLT tokamak. The '+'s and '-'s correspond to the location of vertical-field coils (from Johnson *et al.*, 1979).

the achievement of high temperatures and long energy-confinement times. [See, for instance, Eubank *et al.* (1979) and Gondhaleker *et al.* (1979).] In fact, if it were not for the inherently low  $\langle\beta\rangle$ 's (from the reactor physics requirement point of view), the conventional tokamak would be a much more desirable axisymmetric toroidal system. However, since the  $\langle\beta\rangle$ 's are low, it is worthwhile to investigate variations of the basic tokamak configuration which attempt to correct this problem. At present, two separate methods have received serious consideration.

The first method requires the application of external heating sources such as neutral beams or rf power. Even putting the question of  $\langle\beta\rangle$  aside, such external heating will almost certainly be required, since ohmic heating alone will probably not be able to raise the temperature in a tokamak sufficiently high to cause ignition. With external heating the plasma  $\langle\beta\rangle$  can be raised substantially, leading to a class of configurations described as "high- $\beta$  tokamaks." [See, for instance, Shafranov (1971); Freidberg and Haas (1973); Clark and Sigmar (1977).] These are discussed here and in Sec. IV.C.6 on "The flux-conserving tokamak."

The second method of raising  $\langle\beta\rangle$  is to allow the cross section of the plasma to become noncircular. Optimizing over this new degree of freedom leads to higher  $\langle\beta\rangle$ 's and is discussed in Sec. IV.C.5 on "noncircular tokamaks."

The basic idea of the high- $\beta$  tokamak is as follows. Application of an independent source of external heating at fixed toroidal current and toroidal field causes an increase in the plasma pressure. The higher  $\langle\beta\rangle$  that results is contained by poloidal diamagnetic currents induced in the plasma. When sufficient heating is applied, radial pressure balance is provided almost entirely by the toroidal field. This is the regime of the high- $\beta$  tokamak. The plasma pressure is decoupled from the ohmic heating current (in contrast to the conventional tokamak), and confinement is more closely related to that in a  $\theta$  pinch rather than a  $Z$  pinch. The key feature of the high- $\beta$  tokamak is that the  $\langle\beta\rangle$  is raised to the maximum value that can be supported in toroidal force balance by a toroidal current satisfying the stability condition  $q \gtrsim 1$ .

Taking these requirements into account leads to the following inverse aspect ratio expansion for the high- $\beta$  tokamak:

$$\begin{aligned} \frac{B_p}{B_\phi} &\sim \varepsilon, \\ \beta &\sim \frac{2p}{B_\phi^2} \sim \varepsilon, \\ q &\sim \frac{rB_\phi}{RB_p} \sim 1, \\ \beta_p &\sim \frac{2p}{B_p^2} \sim \frac{1}{\varepsilon}. \end{aligned} \quad (4.68)$$

Note that  $\beta$  is one order larger than in a conventional

tokamak. Also  $\beta_p \sim 1/\varepsilon$  indicates that the poloidal field has only a minor role in radial pressure balance. The confinement is provided by a small diamagnetic well in the toroidal field. Even though the well is small, of order  $\varepsilon$ , it still confines  $1/\varepsilon$  more plasma than the poloidal field.

Because of the higher  $\beta$ 's, the toroidal shift of the flux surfaces is of order unity, and the flux surfaces themselves are no longer small deviations from circles. Consequently, although the inverse aspect ratio expansion does somewhat simplify the Grad-Shafranov equation, the leading-order equilibrium remains inherently two dimensional; that is, radial pressure balance and toroidal force balance enter simultaneously.

As a result of this feature, only the leading-order contribution to the Grad-Shafranov equation is required. The appropriate formal expansion for the high- $\beta$  tokamak is given by

$$\begin{aligned} \psi(r, \theta) &= \psi_0(r, \theta) \dots, \\ p(\psi) &= p_1(\psi_0) \dots, \end{aligned} \quad (4.69)$$

where  $\psi_0/rRB_\phi \sim \varepsilon$  and  $p_1/B_0^2 \sim \varepsilon$ . The expansion for  $F(\psi)$  is slightly subtle because the Grad-Shafranov equation basically determines the poloidal field, whereas the primary radial pressure balance is dominated by the toroidal field. The expansion for  $F(\psi)$  must automatically take this into account. The procedure is to introduce a new function,  $G_2(\psi)$ , in place of  $F(\psi)$ ,

$$\begin{aligned} 2R_0^2 p(\psi) + F^2(\psi) &= R_0^2 [B_0^2 + G_2(\psi)] \\ &= R_0^2 [B_0^2 + G_2(\psi_0) \dots], \end{aligned} \quad (4.70)$$

where, as before,  $B_0$  is the vacuum toroidal field at  $R = R_0$ . Equation (4.70) implies that the deviation from a  $\theta$ -pinch pressure balance relation is of order  $G_2/B_0^2 \sim \varepsilon^2$ , which is one order smaller than the pressure itself. Substituting into the Grad-Shafranov equation leads to a two-dimensional partial differential equation for high- $\beta$  tokamak equilibria. This equation is given by

$$\nabla^2 \psi_0 = -\frac{1}{2} R_0^2 \left[ G'_2 + 4p'_1 \left( \frac{r}{R_0} \right) \cos\theta \right], \quad (4.71)$$

where prime denotes differentiation with respect to  $\psi_0$ .

Since Eq. (4.71) is a nonlinear two-dimensional partial differential equation, it must in general be solved numerically. However, for special choices of  $G_2(\psi_0), p_1(\psi_0)$ , Eq. (4.71) can be solved analytically, and it is such solutions that provide a great deal of the insight into the nature of high- $\beta$  tokamak equilibria. The model discussed below was first investigated by Haas (1972). Other simple high- $\beta$  tokamak equilibria have been given by Shafranov (1966), Laval *et al.* (1970), Strauss (1971), and Solov'ev (1976).

Consider the case where  $G_2(\psi_0)$  and  $p_1(\psi_0)$  are linear in  $\psi_0$ , so that  $G'_2(\psi_0) = -A$ ,  $p'_1(\psi_0) = -C$ . Assume the plasma surface is circular, with radius  $a$ , and is surrounded by vacuum. The linear dependence of  $G_2$  implies that the toroidal current density is nearly uniform

in the plasma (at least for low  $\beta$ ) and abruptly jumps to zero across the plasma surface. The function  $\psi_0(r, \theta)$  must be regular for  $r \leq a$  and is normalized so  $\psi_0(a, \theta) = 0$ . The solution to Eq. (4.71) inside the plasma is given by

$$\begin{aligned}\psi_0 &= -\frac{a^2}{2\langle\beta\rangle q^*} p_1 = \frac{a^2 B_0}{2q^*} [u^2 - 1 + v(u^3 - u) \cos\theta], \\ B_\theta &= \frac{\epsilon B_0}{q^*} \left[ u + \frac{v}{2}(3u^2 - 1) \cos\theta \right], \\ u &= \frac{r}{a}, \quad v = \langle\beta\rangle q^{*2}/\epsilon \sim 1.\end{aligned}\quad (4.72)$$

Equation (4.72) is expressed in terms of the plasma parameters  $\langle\beta\rangle, q^*$ , rather than the constants  $A, C$ :

$$\begin{aligned}\frac{1}{q^*} &\equiv \frac{1}{\epsilon B_0} \left( \frac{I}{2\pi a} \right) = \frac{1}{2\pi\epsilon B_0} \int_0^{2\pi} B_\theta(a, \theta) d\theta = \frac{R_0}{4B_0} A \\ \langle\beta\rangle &= \frac{2}{\pi a^2 B_0^2} \int p_1 r dr d\theta = \frac{a^2}{2q^*} C.\end{aligned}$$

Here the quantity  $q^*$  is by definition inversely proportional to  $I$ . It is similar but not equal to the safety factor. The exact relationship is discussed shortly.

There are a number of points to be made concerning the solution. First, note that the pressure profile is basically parabolic. The shift of the magnetic axis [i.e., the radius where  $\partial\psi(r=\Delta, \theta=0)/\partial r = 0$ ] with respect to the plasma surface is given by

$$\frac{\Delta}{a} = \frac{v}{1 + (1 + 3v^2)^{1/2}}. \quad (4.73)$$

Since  $v \sim 1$  in the high- $\beta$  ordering, the shift of the magnetic axis is finite, not small as in the conventional tokamak.

Second, if  $\langle\beta_p\rangle$  is defined as in Eq. (4.58), then the equilibrium relation between  $\langle\beta\rangle$  and  $\langle\beta_p\rangle$  has the form

$$\langle\beta\rangle = \langle\beta_p\rangle \epsilon^2 / q^{*2}. \quad (4.74)$$

This is analogous to Eq. (4.59) except that in the present case  $\langle\beta\rangle$  and  $\langle\beta_p\rangle$  are each one order larger in  $\epsilon$ . Furthermore, from the definition of  $v$  [Eq. (4.72)] it follows that  $v = \epsilon \langle\beta_p\rangle$ .

The third point to note is that in the high- $\beta$  ordering the variation of  $B_\theta$  around the cross section is of order unity, in order to support the higher pressure in toroidal force balance. This variation by definition averages to zero when calculating  $1/q^*$ , so that  $q^* \sim 1/I$ . However, when calculating  $q(a)$  as defined by Eq. (4.39), the integrand is more strongly weighted on the inside of the torus where  $B_\theta(a, \theta)$  is small. This leads to the result that  $q(a) > q^*$ . More explicitly,

$$q(a) = \frac{\epsilon B_0}{2\pi} \int_0^{2\pi} \frac{d\theta}{B_\theta(a, \theta)} = \frac{q^*}{(1-v^2)^{1/2}}. \quad (4.75)$$

In the limit of low  $\langle\beta\rangle$ ,  $v \rightarrow 0$  and  $q(a) \rightarrow q^*$ . Nevertheless, in the high- $\beta$  regime it is important to distinguish between  $q^*$  and  $q(a)$ , particularly since  $1/q(a)$

is not simply proportional to  $I$ .

The next and perhaps most interesting feature of high- $\beta$  tokamak equilibria is the appearance of an upper limit on the value of  $\langle\beta\rangle$  that can be contained for a given current. This can be seen in Eq. (4.75), which requires  $v < 1$  for reality of the solutions. At the limiting value  $v = 1$ , the plasma parameters are given by

$$\begin{aligned}\langle\beta\rangle &= \epsilon/q^{*2}, \quad \langle\beta_p\rangle = 1/\epsilon, \\ q(a) &\rightarrow \infty, \quad \Delta/a = 1/3.\end{aligned}\quad (4.76)$$

For a given inverse aspect ratio  $\epsilon$ , the actual numerical value of  $\langle\beta\rangle$  is obtained from the minimum allowable  $q^*$ , as determined from stability considerations.

The origin of the equilibrium limit can be understood by examining the fields in the vacuum region. The solution which matches Eq. (4.71) and satisfies the vacuum equation  $\nabla^2\psi_0 = 0$  is given by

$$\hat{\psi}_0 = \frac{a^2 B_0}{q^*} \left[ \ln u + \frac{v}{2} \left[ u - \frac{1}{u} \right] \cos\theta \right]. \quad (4.77)$$

The first term represents the equivalent "straight" contribution of the toroidal current, while the last two terms correspond to the vertical field and its diamagnetic response, respectively. Note that the vacuum field has a separatrix at the point defined by  $B_\theta(r_s, \theta_s) = B_r(r_s, \theta_s) = 0$ , where  $\theta_s = \pi$  and

$$\frac{r_s}{a} = u_s = \frac{1 + (1 - v^2)^{1/2}}{v}. \quad (4.78)$$

For low  $\langle\beta\rangle$ ,  $v \ll 1$ , and the separatrix  $u_s \approx 2/v$  is far from the plasma surface. As  $\langle\beta\rangle$  (i.e.,  $v$ ) increases, the vertical field increases, and the separatrix moves in towards the plasma. When  $v = 1$ , the separatrix moves onto the plasma surface. Since it can move no further, this corresponds to the equilibrium limit. The existence of the separatrix is shown graphically in Fig. 18; it is obtained by summing the contributions of the vertical field and the  $1/r$  field of the toroidal current.

From the results presented above, one might conjecture that all high- $\beta$  tokamaks have an equilibrium  $\langle\beta\rangle$  limit with similar scaling in  $\epsilon$ . This is only true if increasing values of  $\langle\beta\rangle$  are maintained in toroidal force balance by increasing the vertical field, but *keeping the toroidal current fixed*. Such a procedure is very convenient for numerical calculations, but does not in general represent the physical evolution of a given experimental discharge. This problem is addressed in Sec. IV.C.6 on "The flux-conserving tokamaks," where it is shown that an equilibrium limit of the type discussed does not exist for interesting regimes of tokamak operation, although the nature of such equilibria changes qualitatively when  $\langle\beta\rangle q^{*2}/\epsilon \gtrsim 1$ .

Another interesting point to note about high- $\beta$  tokamak equilibria is that the toroidal current can reverse on the inside of the torus before the equilibrium limit is reached. For the special model discussed, the current reverses for  $\frac{1}{2} < v < 1$  on the cylindrical surface,

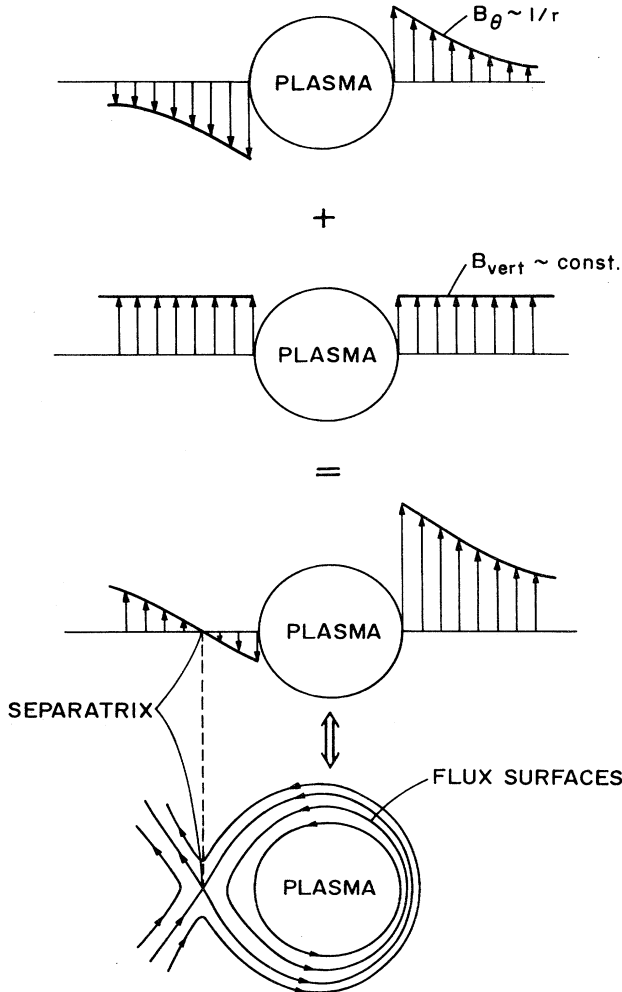


FIG. 18. The appearance of a separatrix in a high- $\beta$  tokamak.

$$R = R_0(1 - \epsilon/2\nu). \quad (4.79)$$

A current reversal may be difficult to realize in systems with finite conductivity, but this question lies outside the scope of ideal MHD.

The question of the vertical field required for toroidal force balance is easily answered by examining Eq. (4.77). Since the  $u \cos\theta$  term explicitly represents the vertical-field source, it follows that

$$B_v = \frac{I}{4\pi R_0} \langle \beta_p \rangle. \quad (4.80)$$

This result is consistent with the corresponding result for the conventional tokamak given by Eq. (4.67) if one keeps in mind that the  $\langle \beta_p \rangle$  term would be  $1/\epsilon$  times larger than other terms in the high- $\beta$  ordering.

The final point to be discussed is a slightly subtle one concerning the maximum  $\langle \beta \rangle$  limit and its relation to  $q^*$  and the safety factor. Consider a system with a given aspect ratio, whose most dangerous modes can be stabilized by keeping the current below some critical value (i.e.,  $q^* > q_c$ ). Thus, if we set  $q^* = q_c$  in the relation

$\langle \beta \rangle q^{*2}/\epsilon = \epsilon \langle \beta_p \rangle$ ,  $\langle \beta \rangle / \epsilon$  becomes linearly dependent on  $\epsilon \langle \beta_p \rangle$  and in fact achieves its maximum value at the equilibrium limit  $\epsilon \langle \beta_p \rangle = 1$ . Consider now another realistic situation in which the most severe stability limitations arise, not from the current, but from the value of the safety factor on axis [i.e.,  $q(0) > q_c$  for stability]. In this case the relationship for  $\langle \beta \rangle$  should be written as

$$\frac{\langle \beta \rangle}{\epsilon} q^2(0) = \epsilon \langle \beta_p \rangle \frac{q^2(0)}{q^{*2}}, \quad (4.81)$$

where, after expanding the flux function about the magnetic axis and substituting into Eq. (4.39), it can be shown that

$$q(0) = \Delta B_0 (\psi_{rr} \psi_{\theta\theta})^{-1/2} = q^* \left[ \frac{3}{\eta(2+\eta)} \right]^{1/2}, \\ \eta = (1+3\nu^2)^{1/2} = (1+3\epsilon^2 \langle \beta_p \rangle^2)^{1/2}. \quad (4.82)$$

Here the flux function is to be evaluated on the magnetic axis,  $r = \Delta, \theta = 0$ . After substituting Eq. (4.82) into Eq. (4.81) it is clear that the right-hand side is no longer a simple linear function of  $\epsilon \langle \beta_p \rangle$ , but is now more complicated. In fact the right-hand side has a maximum when  $\epsilon \langle \beta_p \rangle = 0.842$ , and gives

$$\langle \beta \rangle q^2(0)/\epsilon |_{\max} = \langle \beta \rangle q_c^2/\epsilon = 0.379.$$

The curves of maximum  $\langle \beta \rangle$  vs  $\langle \beta_p \rangle$  are shown in Fig. 19 for the two cases  $q_c = q^*$  and  $q_c = q(0)$ . These results show that when stability is determined by  $q(0)$ , the maximum  $\langle \beta \rangle$  is not achieved at the equilibrium limit  $\epsilon \beta_p = 1$ , but at some slightly smaller value. This somewhat surprising result is a consequence of the fact that, for the given profiles, as  $\beta_p$  is increased the current must be decreased in order to keep  $q(0)$  fixed, thereby weakening the restoring force for toroidal force balance.

An important conclusion from the above analysis is that, in order to make predictions in the regime of the

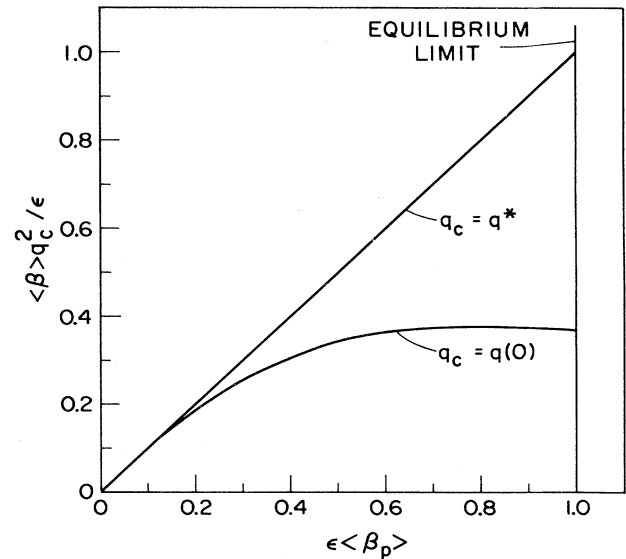


FIG. 19. Plot of  $\langle \beta \rangle$  vs  $\langle \beta_p \rangle$  for the two cases  $q_c = q^*$  and  $q_c = q(0)$ .

high- $\beta$  tokamak, one must exercise caution in distinguishing the various  $q$ 's which appear and their relation to stability, since they can lead to qualitatively different results.

A number of numerical studies have been carried out which investigate the equilibrium properties of high- $\beta$  tokamaks. [See, for instance, Callan and Dory (1972), D'Ippolito *et al.* (1977), and Dory and Peng (1977).] A particular example of a plasma with a circular cross section is illustrated in Fig. 20. Note the large shift of the peak plasma pressure. Also, to contain such high  $\langle\beta\rangle$ 's, the toroidal current peaks on the outside of the torus, and reverses on the inside. The corresponding  $B_\phi$  profile indicates that a diamagnetic well has formed and is primarily responsible for radial pressure balance.

To summarize, a high- $\beta$  tokamak is a configuration in which radial pressure balance is provided almost entirely by the toroidal field, as in a  $\theta$  pinch. The toroidal current provides toroidal force balance but is limited in magnitude by the stability condition  $q \geq 1$ . The large, nearly vacuum, toroidal field is responsible for stability, as in the conventional tokamak. In the regime of the high- $\beta$  tokamak, the  $\langle\beta\rangle$  is raised to the largest value that can be held in toroidal force balance by a current satisfying  $q \geq 1$ . This leads to a scaling  $\langle\beta\rangle \sim \epsilon$ ,  $\langle\beta_p\rangle \sim 1/\epsilon$ , which is one order larger in  $\epsilon$  than a conventional tokamak. There will in general be an upper limit on the achievable  $\langle\beta\rangle$ 's if, as  $\langle\beta\rangle$  is raised, toroidal force balance is maintained by increasing the applied vertical field but keeping the toroidal current and toroidal field fixed. In this case a separatrix forms and ultimately moves onto the plasma surface.

A more realistic description of the plasma behavior as  $\langle\beta\rangle$  increases is given in Sec. IV.C.6 on "The flux-conserving tokamak." This discussion begins with a summary of the properties of noncircular tokamaks.

## 5. Noncircular tokamaks

The second method which has received serious attention for increasing  $\beta$  in a tokamak is that of using a noncircular cross section. It is clear that if one allows an additional degree of freedom in the equilibrium, a

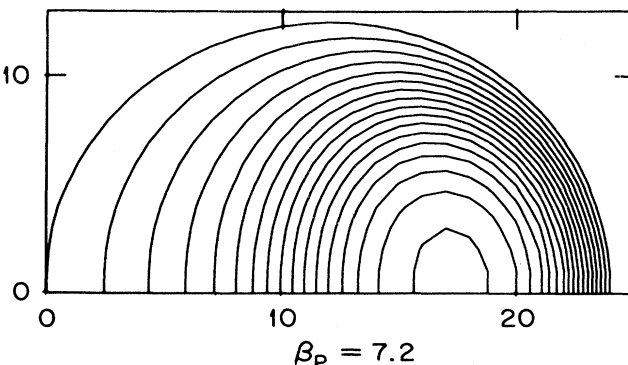


FIG. 20. Equilibrium flux plot for a high- $\beta$  tokamak (from Callan and Dory, 1972).

further optimization can be performed, leading to higher  $\beta$ 's (see, for instance, Solov'ev *et al.*, 1969; Laval *et al.*, 1971, 1972, 1974; Freidberg and Haas, 1974). The intuitive prescription for optimization follows from the modification of the basic equilibrium relation given by Eq. (4.59). For noncircular configurations, this relation (which is derived later for a specific model) has the form

$$\langle\beta\rangle = \left[ \frac{\langle\beta_p\rangle\epsilon^2}{q^{*2}} \right] G(C/2\pi a). \quad (4.83)$$

Here  $\epsilon \equiv a/R_0$ , and  $a$  is the width of the minor plasma radius. The quantity  $G$  is a geometric factor describing the effects of noncircularity and is a function of  $C/2\pi a$ , where  $C$  is the poloidal plasma circumference. For a circular cross section  $G \rightarrow 1$ , whereas for highly elongated shapes  $G \sim (C/2\pi a)^2$ .

It thus follows that, for fixed  $\langle\beta_p\rangle$  and inverse aspect ratio  $\epsilon$ , the value of  $\langle\beta\rangle$  increases quadratically with minor circumference *if the value of  $q^*$  required for stability is independent of elongation*; that is, either conventional or high- $\beta$  tokamaks with highly elongated cross sections should be capable of achieving much higher  $\langle\beta\rangle$  values. In practice, however, the critical  $q^*$  for stability is also an increasing function of elongation, so that the gains in  $\langle\beta\rangle$  are not as large as might initially be anticipated. Nevertheless, these gains still remain significant.

A brief description is now given of a simple noncircular equilibrium from which the function  $G$  can be explicitly calculated. If one reexamines the high- $\beta$  equilibrium discussed in Sec. IV.C.4 one can easily see by direct substitution that, for  $G'(\psi_0) = -A$  and  $p'(\psi_0) = -C$ , the solution to the corresponding Grad-Shafranov equation [Eq. (4.71)] for an elliptically shaped plasma is given by

$$\psi = \frac{abB_0}{2q^*} \left[ \frac{x^2}{a^2} + \frac{y^2}{b^2} - 1 \right] \left[ 1 + \nu \frac{x}{a} \right]. \quad (4.84)$$

Here  $x$  and  $y$  are horizontal and vertical rectangular coordinates,  $a$  is the width of the ellipse, and  $b$  is the height of the ellipse. The quantity  $q^*$  is defined by

$$\frac{1}{q^*} = \left[ \frac{IR_0}{2\pi abB_0} \right] \left[ \frac{2ab}{a^2+b^2} \right]. \quad (4.85)$$

The geometric factor associated with  $q^*$  has been chosen so that, in the limit of low  $\beta$  (i.e.,  $\nu \rightarrow 0$ ),  $q^* \rightarrow q(a)$ . For arbitrary  $\nu$ ,  $q^*$  and  $q(a)$  are related by

$$q(a) = \frac{q^*}{(1-\nu^2)^{1/2}}, \quad (4.86)$$

where, in Eqs. (4.84) and (4.86),

$$\nu = \left[ \frac{4a^2}{3b^2+a^2} \right] \left[ \frac{\langle\beta\rangle q^{*2}}{\epsilon} \right]. \quad (4.87)$$

Using these relations, one can define  $\langle\beta_p\rangle$  as

$$\langle\beta_p\rangle = \left[ \int p dx dy \right] (gI^2/8\pi)^{-1}, \quad (4.88)$$

where  $g$  is a geometric factor chosen so that  $\langle\beta_p\rangle = 1$

when  $\nu \rightarrow 0$ ,

$$g = 2ab / (a^2 + b^2). \quad (4.89)$$

Combining these results, one obtains the basic equilibrium relation

$$\langle \beta \rangle = \left[ \frac{\langle \beta_p \rangle \varepsilon^2}{q^{*2}} \right] \left[ \frac{b^2 + a^2}{2a^2} \right]. \quad (4.90)$$

Consider the application of Eq. (4.90) to a conventional tokamak,  $\langle \beta_p \rangle = 1$ . For fixed inverse aspect ratio  $\varepsilon$ , the value of  $\langle \beta \rangle$  increases quadratically with  $b/a$  for  $b/a \gg 1$  if the value of  $q^*$  for stability is independent of elongation. In the high- $\beta$  regime, there is an equilibrium limit, as in the circular case. For the noncircular case, the equilibrium limit  $\nu=1$  is given by

$$\langle \beta \rangle = \left[ \frac{\varepsilon}{q^{*2}} \right] \left[ \frac{3b^2 + a^2}{4a^2} \right]. \quad (4.91)$$

Here also the limiting  $\langle \beta \rangle$  scales quadratically with  $b/a$  for  $b/a \gg 1$  and  $q^*$  fixed.

There have been a number of recent analytical and numerical investigations of the stability of noncircular tokamaks (Sykes *et al.*, 1977; D'Ippolito *et al.*, 1978; Todd *et al.*, 1979; and Bernard *et al.*, 1980). However, there is still no uniquely defined, optimal cross section. There are strong indications that the critical  $q^*$  for stability is an increasing function of elongation, thus nullifying much of the gain anticipated for  $b/a \gg 1$ . This, coupled with various technological constraints and vertical-stability requirements, leads one to infer that elongations on the order of 2:1 may be optimum in the practical sense.

The theoretical studies have also shown that a combination of elongation and outward-pointing triangularity can have a net stabilizing effect on certain classes of internal instabilities. A particular example of a major tokamak which makes use of this stabilization is the JET experiment being built in England (IAEA, 1976). A numerically computed equilibrium of this device is shown in Fig. 21.

A more detailed discussion of the effects of noncircularity on MHD stability is given in Sec. V.

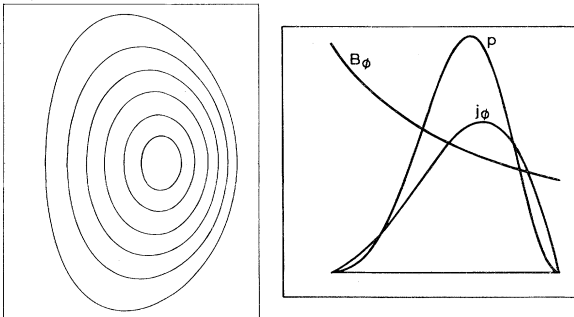


FIG. 21. Equilibrium flux plot of the JET tokamak showing both elongation and triangularity. Also shown are the pressure, toroidal field, and toroidal current along the midplane  $Z=0$ . (Courtesy J. A. Wesson, Culham Laboratory, 1981).

## 6. The flux-conserving tokamak

The existence of an equilibrium  $\langle \beta \rangle$  limit for high- $\beta$  tokamaks has been shown to be strongly coupled to the constraint imposed on the safety factor. In particular, for fixed profiles, if the current (i.e.,  $1/q^*$ ) or the safety factor on axis is kept fixed, there exists an equilibrium limit. However, it has also been pointed out that numerically computed equilibria satisfying either of these constraints do not in general represent the actual evolution of a given plasma discharge. Shafranov (Shafranov, 1971; Mukhovatov and Shafranov, 1971), in fact, first noted that a tokamak surrounded by a perfectly conducting shell could not evolve in such a way as to form a separatrix if one did not originally exist because of the topological constraints of ideal MHD; thus it would appear that such systems do not have an equilibrium  $\langle \beta \rangle$  limit.

This problem has been resolved by the concept of the flux-conserving tokamak (Clarke and Sigmar, 1977; Dory and Peng, 1977). Here the evolution to higher  $\beta$  is governed by a different set of constraints and leads to the conclusion that no equilibrium  $\langle \beta \rangle$  limit exists. The basic idea is to model the actual evolution of a single plasma discharge by devising a realistic prescription for choosing the free functions  $p(\psi)$  and  $F(\psi)$ . This is done as follows. Consider a system which is initially operated as a conventional tokamak,  $\beta \sim \varepsilon^2, \beta_p \sim 1$ . The plasma is then heated by a high-power external source, neutral beams for instance. It is assumed that the time scale for heating is long compared to characteristic Alfvén times. Thus MHD inertial effects are negligible, and the plasma evolution can be viewed as a series of quasistatic equilibria, each one satisfying the Grad-Shafranov equation. On the other hand, the time scale for heating is assumed to be short compared to the magnetic diffusion time, whether it is classical or anomalous. In this situation the plasma behaves like a perfect conductor during the heating process.

Keeping these assumptions in mind, the function  $p(\psi)$  can be modeled by a weighted scaling of the initial pressure distribution associated with the conventional tokamak operation; that is,  $p(\psi) = W(\psi)p_i(\psi)$ , with  $p_i(\psi)$  the initial pressure distribution and  $W(\psi)$  the weight factor. Since the theory and computation of neutral-beam deposition are reasonably well understood, it is not very difficult to obtain good approximations for  $W(\psi)$ . These approximations directly specify the evolution of  $p(\psi)$  in the Grad-Shafranov equation and thus eliminate the need for solving the energy transport equation.

The interesting new feature of the flux-conserving tokamak is the specification of  $F(\psi)$ . Since the plasma behaves like a perfect conductor during the heating process, both the toroidal and poloidal fluxes are conserved, and it is this condition which determines  $F(\psi)$ . To find the relationship for  $F(\psi)$ , first imagine that in each quasistatic equilibrium the flux surfaces are labeled by  $\psi = \text{const}$ . Since the poloidal flux  $\psi_p = 2\pi\psi$ , flux surfaces with the same  $\psi$  label in different equilibria by def-

initially conserve poloidal flux. Now consider the toroidal flux contained within any of these surfaces:

$$\psi_t(\psi) = \int B_\phi(r, \theta) r dr d\theta = \int_0^\psi d\psi' \int_0^{2\pi} \frac{rB_\phi}{RB_\theta} d\theta' , \quad (4.92)$$

where in the second integral an implicit transformation of integration variables has been made,  $\psi' = \psi'(r, \theta), \theta' = \theta$ , and the integrand is assumed to be a function of  $\psi'$  and  $\theta'$ . Note that [see Eq. (4.39)]

$$\begin{aligned} \frac{d\psi_t(\psi)}{d\psi} &= \int_0^{2\pi} \frac{rB_\phi}{RB_\theta} d\theta' = 2\pi q(\psi) , \\ \psi_t(\psi) &= 2\pi \int_0^\psi q(\psi') d\psi' . \end{aligned} \quad (4.93)$$

It follows from Eq. (4.93) that, in order for the toroidal flux to be conserved as the system evolves (i.e., in order for the toroidal flux contained within a given  $\psi$  surface to be the same for every equilibrium), the function  $F(\psi)$  must be chosen so that  $q(\psi)$  is identical in each quasi-static state. Since this applies in particular to the initial state, the actual functional dependence of  $q(\psi)$  corresponds to conventional tokamak operation. Using Eq. (4.39), it then follows that the Grad-Shafranov equation for  $\psi$  is given by

$$\Delta^* \psi = -R^2 \frac{d}{d\psi} (W p_i) - \frac{1}{2} \frac{d}{d\psi} \left[ q_i^2 \left( \frac{1}{2\pi} \oint \frac{dl}{R |\Delta\psi|} \right)^{-2} \right] , \quad (4.94)$$

where  $q_i(\psi)$  is the initial safety factor and  $dl$  is poloidal arc length.

Equation (4.94) is a nonlinear integro-differential equation which must in general be solved numerically. Nevertheless, one can gain some insight into the flux-conserving tokamak, without actually having to solve Eq. (4.94), by considering a modification of the special profiles discussed in the previous section. The basic idea is as follows. As a simple approximation to flux conservation, assume that as the plasma evolves only  $q(0)$  and  $q(a)$  are exactly conserved. Since the  $q(\psi)$  profile is a simple monotonically increasing function, fixing the end points  $q(0)$  and  $q(a)$  should be sufficient to ascertain the main features of the evolution, even if the exact profiles are not conserved.

The first important point concerns the circular high- $\beta$  tokamak discussed in Sec. IV.C.4. Note that this equilibrium has only two free parameters. One represents the plasma heating and is proportional to  $\langle \beta \rangle$ . The other represents an appropriate form of the safety factor. Consequently, in this simple model, there is freedom to fix one, but not both, of the quantities  $q(0)$  and  $q(a)$  as  $\langle \beta \rangle$  increases. Nevertheless, even making the rather gross approximation that flux conservation requires only  $q(a)$  to be conserved, the model no longer exhibits an equilibrium limit; that is, well-behaved solutions exist for arbitrarily large  $\langle \beta \rangle$ . This can be seen ex-

plicitly by introducing the heating parameter  $\nu^* = \langle \beta \rangle q^2(a)/\epsilon$ . In this case  $\langle \beta_p \rangle$  and  $I \sim 1/q^*$  can be written as

$$\begin{aligned} \left[ \frac{I}{I_0} \right]^2 &= \frac{1}{2q_a^2} [1 + (1 + \nu^{*2})^{1/2}] , \\ \epsilon \langle \beta_p \rangle &= \frac{2\nu^*}{1 + (1 + 4\nu^{*2})^{1/2}} , \end{aligned} \quad (4.95)$$

where  $q_a \equiv q(a)$  and  $I_0 = 2\pi a^2 B_0 / R_0$ . These functions are shown graphically in Fig. 22. Also shown are the equivalent relations for the high- $\beta$  tokamak with fixed current rather than fixed  $q_a$ . Here the appropriate heating factor is  $\nu^* = \nu = \langle \beta \rangle q^{*2}/\epsilon$  and the corresponding relations are given by  $\epsilon \langle \beta_p \rangle = \nu^*, I/I_0 = \text{const}$ .

Observe that equilibria exist for arbitrarily large  $\langle \beta \rangle$  (i.e.,  $\nu^*$ ) when  $q_a$  is held fixed, whereas there is an upper equilibrium limit on  $\langle \beta \rangle$  when  $q^*$  is held fixed. The reason for this is that, in the flux-conserving case, the current  $I$  increases as  $\langle \beta \rangle$  increases to keep  $q_a$  constant. The increased current, along with a corresponding increased vertical field, supports higher values of  $\langle \beta \rangle$  in toroidal force balance. However, since both increase simultaneously, the separatrix does not move onto the plasma surface.

Another point to note is that  $\langle \beta_p \rangle$  reaches a plateau

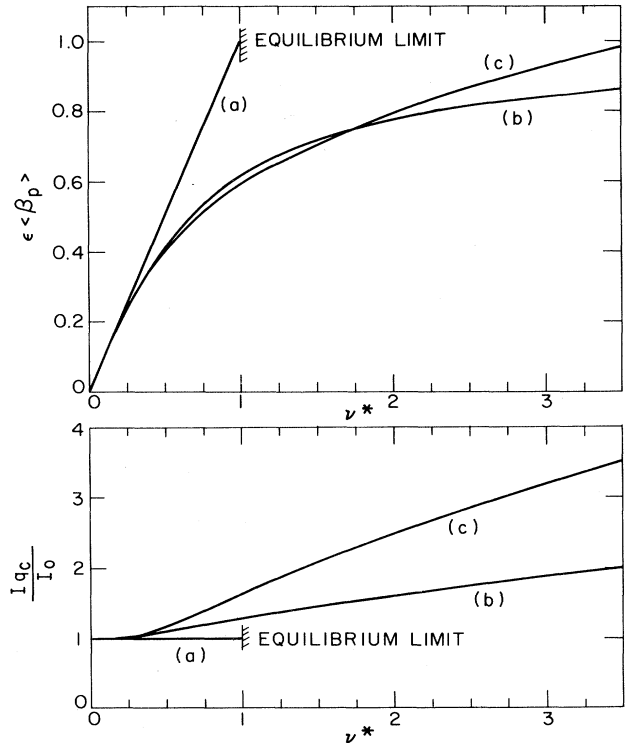


FIG. 22. Plot of  $\epsilon \langle \beta_p \rangle$  and  $I/I_0$  vs the heating parameter  $\nu^*$  (i.e.,  $\nu^* \sim \langle \beta \rangle$ ) for: (a) high- $\beta$  tokamak;  $q^* = \text{const}$ , (b) simple flux-conserving tokamak;  $q_a = \text{const}$ , circular, (c) flux-conserving tokamak;  $q_a, q_0 = \text{const}$ , elliptical. Case (c) is computed for the case  $q_0 = 1, q_a = 1.2$ . Also, for cases (b) and (c),  $q_c = q_a$ , while for case (a),  $q_c = q^*$ .

as  $\langle\beta\rangle \rightarrow \infty$ . This is in contrast to what one might expect from the equilibrium relation, Eq. (4.74), which would indicate  $\langle\beta_p\rangle$  and  $\langle\beta\rangle$  increasing in unison. The explanation is again associated with the fact that, for large  $\langle\beta\rangle$  both the pressure and current are increasing, causing the ratio  $\langle\beta_p\rangle \sim p/I^2$  to saturate.

Although the simple model just described predicts the correct qualitative behavior of the flux-conserving tokamak, the results can be further quantified by adding an additional degree of freedom which allows both  $q_a$  and  $q_0 \equiv q(0)$  to remain fixed as  $\langle\beta\rangle$  increases.

An intuitive choice for this freedom is as follows. Recall that the explicit choices  $p'_1(\psi) = \text{const}$ ,  $G'_2(\psi) = \text{const}$  give rise to a current profile with a jump at the surface [see Eq. (4.72) and the accompanying discussion]. This model thus describes the core of a more realistic plasma in which the current vanishes on the boundary. In a realistic plasma, as  $\langle\beta\rangle$  increases, the flux surfaces are shifted further outward. As a consequence one would expect the plasma core to be compressed, assuming a vertically elongated shape. As an approximation to this behavior, the simple circular model is generalized to allow for an elliptical cross section (of width  $a$  and height  $b$ ). The ellipticity represents the extra degree of freedom and must be adjusted to keep  $q(0)$  constant as  $\langle\beta\rangle$  increases.

Using the results of the previous section, the critical relations for the flux-conserving tokamak can be easily derived. Assume that  $q_a$ ,  $q_0$ , and the plasma cross-sectional area  $\pi ab$  are held fixed during the external heating. An appropriate definition of the heating parameter is then  $\nu^* \equiv \langle\beta\rangle q_a^2/\varepsilon$ , where  $\varepsilon = (ab)^{1/2}/R_0$ . One then calculates:

(1)  $q_a$  [Eq. (4.86)]

$$q_a = \frac{q^*}{(1-\nu^2)^{1/2}} ; \quad (4.96)$$

(2)  $q_0$  [Eqs. (4.82) and (4.84)]

$$q_0 = \left[ \frac{3}{\eta(2+\eta)} \right]^{1/2} q^*, \quad \eta = (1+3\nu^2)^{1/2} ; \quad (4.97)$$

(3) general equilibrium [Eq. (4.90)]

$$\varepsilon \langle\beta_p\rangle = \left[ \frac{2\alpha(1-\nu^2)}{1+\alpha^2} \right] \nu^* ; \quad (4.98)$$

(4)  $\nu^*$

$$\frac{3+\alpha^2}{4\alpha^{3/2}} = \left[ \frac{1-\nu^2}{\nu} \right] \nu^* . \quad (4.99)$$

Here  $\alpha = a/b$  and  $\nu$  and  $q^*$  are defined in Eqs. (4.85) and (4.87). These should be viewed as four equations for the four unknowns,  $\nu$ ,  $\alpha$ ,  $q^*$ , and  $\varepsilon \langle\beta_p\rangle$ , which are functions of  $\nu^*$  for fixed  $q_a, q_0$ .

Dividing Eq. (4.97) by Eq. (4.96) indicates that  $\nu$  is independent of  $\nu^*$  and is a function only of ratio  $k = q_a^2/q_0^2$ :

$$\nu^2 = \frac{1}{3} \frac{(k-1)(3k+1)}{(k+1)^2} . \quad (4.100)$$

The dependence of  $\alpha$  on  $\nu^*$  now follows directly from Eq. (4.99). For simplicity assume that the initial state corresponds to a conventional tokamak,  $\nu^* \ll 1$ . In such a state, the constant-current model predicts  $q_a \approx q_0$ , leading to a value of  $\nu \ll 1$ . Thus the heating process begins with  $\nu^* \approx \nu \ll 1$  and a circular cross section  $\alpha \approx 1 - (\nu^*/\nu - 1) \dots$ . After substantial heating has taken place (i.e.,  $\langle\beta\rangle \sim \nu^* \rightarrow \infty$ ), the cross section becomes quite elongated:  $\alpha \approx (3\nu/4\nu^*)^{2/3}$ .

Assuming  $\alpha = \alpha(\nu^*)$  is known, it is straightforward to calculate  $\varepsilon \langle\beta_p\rangle$  from Eq. (4.98) and  $I/I_0$  from the relation

$$\frac{I}{I_0} = \frac{(1-\nu^2)^{-1/2}}{q_a} \left[ \frac{1+\alpha^2}{2\alpha} \right] ,$$

where, for this case,  $I_0 = 2\pi abB_0/R_0$ . Note that in the initial low- $\langle\beta\rangle$  state,  $\varepsilon \langle\beta_p\rangle \approx \nu^*$  and  $I/I_0 \approx 1/q_a$ . For large heating ( $\nu^* \rightarrow \infty$ ) there is again no equilibrium limit and

$$\varepsilon \langle\beta_p\rangle \approx [2(3\nu/4)^{2/3}] \nu^{*1/3} ,$$

$$\frac{I}{I_0} \approx \left[ \frac{(4/3\nu)^{2/3}}{2q_a} \right] \nu^{*2/3} . \quad (4.101)$$

These results are also illustrated in Fig. 22. As in the simpler model, the current  $I$  increases with  $\langle\beta\rangle$ , thereby allowing higher  $\langle\beta\rangle$ 's to be maintained in toroidal force balance without the appearance of a separatrix on the plasma surface. The quantity  $\varepsilon \langle\beta_p\rangle$  increases linearly with  $\langle\beta\rangle$  for  $\nu^* \ll 1$ . At large  $\nu^*$  the curve bends over, but does not saturate as in the simple model.

The basic features of the flux-conserving tokamak discussed above were first found in a more sophisticated analytic theory by Clarke and Sigmar (1977) and a series of numerical computations by Dory and Peng (1977). The results just presented are in qualitative agreement with the analytic theory, although the scaling of  $I$  with  $\langle\beta\rangle$  is slightly different, presumably because of different assumptions regarding the shape of the cross section. An example of a series of numerically computed flux-conserving equilibria is illustrated in Fig. 23. Note the large shift and elongation of the flux surfaces as  $\langle\beta\rangle$  increases. This is accompanied by a strong peaking of the current on the outside of the torus. Also plotted for comparison is the behavior of  $\varepsilon \langle\beta_p\rangle$  and  $I/I_0$  as a function of the heating parameter  $\nu^*$ . This should be compared with Fig. 22. In all cases, substantial increases in the toroidal current and vertical field are required to maintain equilibrium as the plasma evolves.

To summarize, a flux-conserving tokamak is an externally heated high- $\beta$  tokamak in which the heating rate is slow compared to Alfvén times and fast compared to the magnetic diffusion time. In this regime the plasma behaves like a perfect conductor, passing through a series of quasistatic equilibria during the heating phase. The requirements of flux conservation, in addition to a sim-

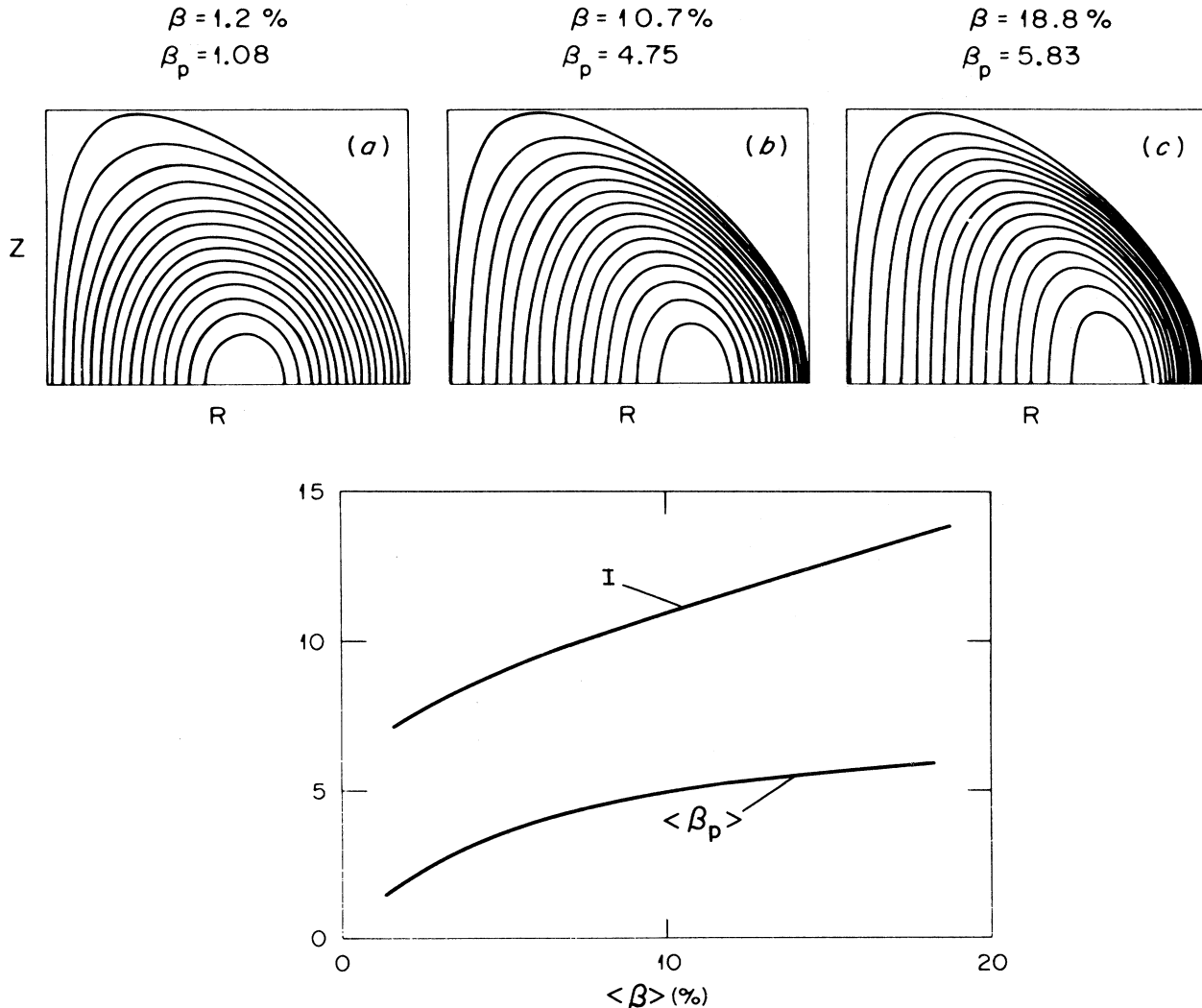


FIG. 23. Series of flux-conserving equilibria for increasing values of  $\langle \beta \rangle$  (from Dory and Peng, 1977). Also shown are plots of  $\epsilon \langle \beta_p \rangle$  and  $I$  vs  $\langle \beta \rangle \sim v^*$ , which should be compared with Fig. 22.

ple modeling of the heating, serve to determine the functions  $p(\psi)$  and  $F(\psi)$  for each quasistatic state. The most interesting feature of the flux-conserving tokamak is that no equilibrium  $\langle \beta \rangle$  limit exists, although when  $\epsilon \langle \beta_p \rangle \sim 1$ , the profiles become quite peaked on the outside of the torus. The avoidance of the equilibrium limit is accomplished by a combination of increased toroidal current, increased vertical field, and reshaping of the plasma core. In practice the assumption of slow magnetic diffusion will likely break down at some point because of anomalies created by the increased  $\langle \beta \rangle$ . Such questions lie outside the realm of ideal MHD. Nevertheless, the fact that no equilibrium limit is set by ideal MHD must be viewed as an optimistic result for tokamaks.

#### D. Three-dimensional configurations

In the previous section it was shown that toroidal MHD equilibria possessing axisymmetry could be con-

structed from the ideal MHD model. Specifically, the RFP and the various types of tokamaks are of this class. Although radial pressure balance could be predominantly that of a  $\theta$  pinch or a  $Z$  pinch, each configuration requires sufficient toroidal current to counterbalance the outward toroidal drift force.

The present section considers toroidal MHD equilibria which are inherently three dimensional. The motivation for investigating such obviously more complicated equilibria is that they possess the potential for providing toroidal confinement without the need of a net toroidal current. This makes the possibility of ultimately achieving a steady-state fusion reactor more feasible, since such configurations no longer require a toroidal current transformer.

The basic configurations of interest are: (1) the Elmo bumpy torus, (2) the conventional stellarator, and (3) the high- $\beta$  stellarator. Although they appear physically quite different, each can be reasonably accurately

categorized as a toroidal helix. For all three configurations, radial pressure balance corresponds to that of a  $\theta$  pinch, while toroidal force balance results from the development of slightly subtle helically induced restoring forces. There are two such forces, each one important, representing the basic mechanisms for providing toroidal force balance in configurations with no net toroidal current.

Because of the lack of symmetry, no exact Grad-Shafranov-like equation can be derived for any of these concepts. As a result, equilibrium investigations have relied either on asymptotic expansions or on numerical computations. Regarding the analytic studies, there is evidence that "exact" three-dimensional equilibria may not even exist (Grad, 1967a); that is, small changes in the boundary conditions can lead to large changes in the topological structure of the flux surfaces—for example, the formation of fine-scale magnetic islands. Although such phenomena may be unimportant or dominated by other physics in a real experiment, the inevitability of their existence in three-dimensional MHD equilibria implies that asymptotic analysis may not only be mathematically simpler but may represent the most useful and accurate procedure for practical applications. It is this approach which is followed here. For each of the configurations of interest, an appropriate asymptotic expansion is formulated which demonstrates the basic nature of the radial pressure balance and the toroidal force balance.

It should be noted that the existence of exact three-dimensional equilibria raises no problems if all the magnetic field lines are closed (Lortz, 1970).

### 1. Flux function in a closed-line system

The first configuration to be investigated is the Elmo bumpy torus (EBT). One basic feature of this concept is that all the magnetic lines exactly close on themselves (i.e., the rotational transform  $\iota$  equals zero). In this connection it is useful to derive a general equilibrium relation, valid for any closed-line toroidal system, before proceeding with the specific formulation of the EBT configuration.

In a system with ergodic field lines, the constant-pressure surfaces can be traced out by following magnetic field line trajectories many transits around the torus. In the axisymmetric torus, these surfaces are labeled by the poloidal flux,  $\psi$ , and  $p=p(\psi)$ . Consequently contours of constant flux also correspond to surfaces of constant pressure. In a closed-line system, however, a magnetic line by definition does not trace out a surface. The question that is then posed is whether or not an equivalent "flux function" for determining the pressure contours exists for closed-line systems. The answer is that there is such a function, and its specific form is obtained from the following derivation (Shafranov, 1966).

Consider two contours of constant pressure in a closed-line system, as illustrated in Fig. 24. Upon integrating  $\nabla \cdot \mathbf{J} = 0$  over the shaded volume, one obtains

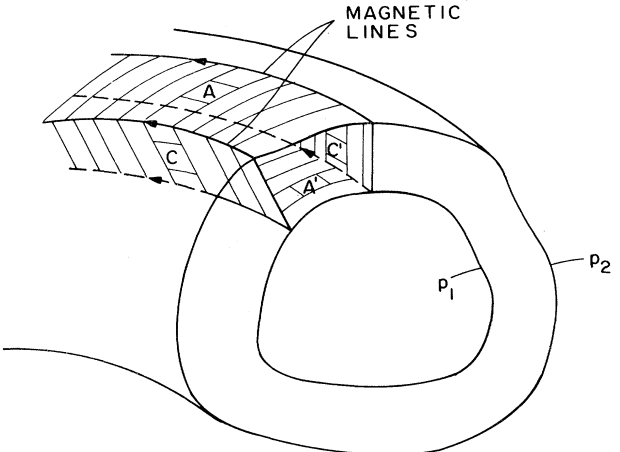


FIG. 24. Geometry for calculating the closed-line "flux function."

$$\int \nabla \cdot \mathbf{J} d\mathbf{r} = \int \mathbf{J} \cdot d\mathbf{S} = 0. \quad (4.102)$$

On surfaces  $A$  and  $A'$ , lying on the  $p=\text{const}$  contours, the differential area element  $d\mathbf{S}$  points in the  $\nabla p$  direction. Since  $\mathbf{J} \cdot \nabla p = 0$  in equilibrium, the surface contribution on  $A$  and  $A'$  must vanish; that is, the current flows parallel to constant-pressure surfaces. Keeping in mind that the magnetic lines lie on constant- $p$  surfaces, the differential area element on  $C$  and  $C'$  can be written as

$$d\mathbf{S} = \frac{\mathbf{B} \times \nabla p}{B |\nabla p|^2} dp dl. \quad (4.103)$$

Here  $dl = (\mathbf{B}/B)dl$  represents the arc length along the magnetic field, and  $d\mathbf{r} = (\nabla p / |\nabla p|^2)dp$  represents the "radial" line element expressed in terms of  $p$ . Using the fact that  $\mathbf{J}_\perp = (\mathbf{B} \times \nabla p)/B^2$ , it then follows from Eq. (4.102) that

$$\int_C \frac{dp dl}{B} = \int_{C'} \frac{dp dl}{B}. \quad (4.104)$$

Equation (4.104) expresses the condition that the current  $I$  flowing into  $C'$  equals the current  $I$  flowing out of  $C$ . Consider the limit in which the two pressure surfaces are arbitrarily close to one another,  $p_2 = p_1 + \delta p, \delta p/p_1 \rightarrow 0$ . In this limit, the current  $I$  flowing out of  $C$  is given by

$$I = \int_C \frac{dp dl}{B} = \delta p \oint \frac{dl}{B}, \quad (4.105)$$

where the line integral is taken along the magnetic line contained in the surface  $C$  as it shrinks when  $\delta p \rightarrow 0$ . Equation (4.104) implies that  $I$  will be the same for any other arbitrary surface  $C'$  bounded by  $p_1$  and  $p_1 + \delta p$ . This can only be true if the quantity

$$U = \oint \frac{dl}{B} \quad (4.106)$$

is constant on every magnetic line lying on the constant-pressure surface. Note that the differential volume  $dV$  of a small flux tube with cross-sectional area  $dA$  and flux  $d\Psi = B dA$  is given by  $dV(\Psi) = d\Psi \int dl/B$ ;  $U$  is the

volume per unit flux.

To summarize, in a closed-line system,  $U$  plays the role of the flux function. It is determined directly from the magnetic field, and surfaces of constant  $U$  correspond to surfaces of constant  $p$ , so that  $p = p(U)$ .

## 2. The Elmo bumpy torus (EBT)

The Elmo bumpy torus is the simplest of the three-dimensional configurations discussed in this section. Even so, analysis of EBT equilibrium properties requires very lengthy algebraic calculations (Hedrick, 1979; Grad, 1971; and Freidberg, 1980). For this reason it is more appropriate to outline the main features of the analysis and then summarize the results.

The Elmo bumpy torus is a large-aspect-ratio, closed-line, toroidal configuration consisting of a series of linked mirrors, as shown schematically in Fig. 25 (McAlee et al., 1976; Hedrick et al., 1977). The mirror coils produce a magnetic field with periodic variation in the toroidal direction, thus producing localized mirror cells or "bumps." There is no net toroidal current in the EBT configuration. Midway between each mirror coil, in the bulge region, is a hot electron ring generated by a high-power rf source resonant with the electron cyclotron frequency. The resonant radius where the ring is formed determines the radial boundary of the main toroidal plasma. The electron rings have several crucial roles in the EBT concept. First, they must ultimately provide a large fraction of the heating in the main toroidal plasma, since they themselves are typically at several hundred keV due to their resonant formation. Second, they are vital for the stability of the main plasma core. Without the rings, the system would be unstable to both gross and localized MHD modes. Interestingly enough, the rings are not required to produce the equilibrium itself, only to stabilize it. For this reason the treatment of the rings can be greatly simplified for equilibrium calculations by assuming the ring pressure is isotropic. Consequently the pressure  $p$  appearing in the MHD equilibrium equations consists of two contributions  $p = p_c + p_e$ , where  $p_c$  is the pressure of the toroidal plasma core and  $p_e$  is the electron ring pressure.

The basic physical issues associated with Elmo bumpy torus equilibria can be investigated by means of the EBT expansion. This expansion provides a reasonable approx-

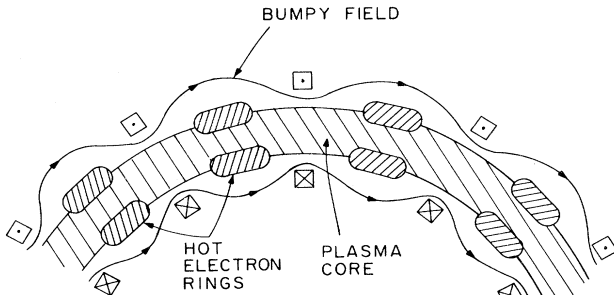


FIG. 25. Schematic diagram of the Elmo bumpy torus.

imation to the actual experiments and serves to separate a number of physical phenomena such as radial pressure balance, toroidal force balance, maximum  $\beta$ , scaling with aspect ratio, etc. The basic expansion parameter is the amplitude of the bumpy fields created by the mirror coils,

$$\delta = \frac{B_{\max} - B_{\min}}{B_{\max} + B_{\min}} \ll 1 . \quad (4.107)$$

Typically  $\delta \approx \frac{1}{3}$  in actual experiments, so that while the expansion may be qualitatively correct it should not be used for quantitative predictions. In the EBT expansion it is necessary to carry out the calculation to fifth order in  $\delta$  in order to account for the small, but nevertheless unavoidable, toroidal effects. As for axisymmetric toroidal equilibrium, the calculation is carried out in  $(r, \theta)$  poloidal coordinates (see Fig. 15). In terms of  $\delta$ , the basic EBT expansion is given by

$$\begin{aligned} \beta &\sim \delta^2, \quad a/R_0 \sim \delta^3, \quad ha \sim 1 , \\ \nabla &= \nabla_0 + (a/R_0)\nabla_T, \quad \nabla_0 \sim \nabla_T \sim 1 . \end{aligned} \quad (4.108)$$

Here  $L = 2\pi/h$  is the spacing between the mirror coils, and the gradient operator has been expanded as a straight cylindrical part  $\nabla_0$  plus a toroidal correction  $(a/R_0)\nabla_T$ . In the expansion, the toroidal effects are assumed to be very small,  $a/R_0 \sim \delta^3$ , thus spreading out the calculation over several orders. This has been deliberately done to demonstrate that toroidicity is required only as a mechanism to close the magnetic lines and has no significant effects on the stability.

Consider now the EBT expansion, order by order. In zeroth order the only field present is a uniform vacuum field pointing in the toroidal direction. Hence

$$\begin{aligned} \mathbf{B}_0 &= B_0 \mathbf{e}_\phi, \quad B_0 = \text{const} , \\ \mathbf{J}_0 &= p_0 = 0 . \end{aligned} \quad (4.109)$$

In first order a small bumpy vacuum field is added representing the effect of the mirror coils. This field satisfies

$$\begin{aligned} \nabla_0 \times \mathbf{B}_1 &= \nabla_0 \cdot \mathbf{B}_1 = 0 , \\ \mathbf{J}_1 &= p_1 = 0 . \end{aligned} \quad (4.110)$$

In this order the fields are azimuthally symmetric, so that  $\mathbf{B}_1 = \mathbf{B}_1(r, z)$ , where  $z = R_0\phi$  represents length along the toroidal direction. Because of the symmetry, one can write  $\mathbf{B}_1 = (\nabla\psi_1 \times \mathbf{e}_\theta)/r$ . For sinusoidal bumps,  $\psi_1(r, z) = \psi_1(r)\cos(hz)$  with  $\psi_1(r)$  satisfying

$$r \left[ \frac{\psi'_1}{r} \right]' - h^2 \psi_1 = 0 . \quad (4.111)$$

A regularity condition at  $r = 0$  and specification of the amplitude of the bumps is sufficient to uniquely determine  $\psi_1$ .

In second order the effects of the pressure first enter the calculation. The inverse aspect ratio is ordered sufficiently small so that in this order the pressure contours

are nested circles (i.e., toroidal distortions of the plasma appear in higher order). Consequently all quantities are functions only of  $r$ , and the second-order equations describe the radial pressure balance of EBT, which corresponds to that of a low- $\beta$   $\theta$  pinch:

$$\mathbf{B}_2 = \mathbf{B}_2(r)\mathbf{e}_\phi, \quad \mathbf{J}_2 = \mathbf{J}_2(r)\mathbf{e}_\theta, \quad p_2 = p_2(r), \\ (\nabla_0 \times \mathbf{B}_2) \times \mathbf{B}_0 - \nabla_0 p_2 = 0, \quad (p_2 + B_0 B_2)' = 0. \quad (4.112)$$

The pressure is ordered as  $\delta^2$  so that the “magnetic well” contribution due to the electron rings is comparable to the average destabilizing effect of the bumpy field. Here a magnetic well refers to the sign of the quantity  $\partial U/\partial r$ ,  $U$  being the “flux function” for closed-line systems defined in Eq. (4.106). It has been shown that the magnetic well quantity  $\partial U/\partial r$  plays a very important role in the stability of closed-line systems. [See, for instance, Kadomtsev (1960), Nelson and Hedrick (1979).] For the present, it is sufficient to note that a bumpy field of order  $\delta$  produces destabilizing effects of order  $\delta^2$ . These can be compensated for by electron rings with  $p \sim \delta^2$  by adjusting the profile and  $\beta$  to produce a magnetic well (i.e.,  $\partial U/\partial r < 0$ ). It should also be noted that equilibria exist with  $\beta_c \equiv 2p_c/B_0^2 \sim 1$  and  $\beta_e \equiv 2p_e/B_0^2 \sim \delta^2$ , still possessing a magnetic well. Such equilibria are more complicated to analyze; for simplicity,  $\beta_c$  has been ordered so that  $\beta_c \sim \beta_e \sim \delta^2$ .

Continuing, in third order, the equilibrium equations are given by

$$(\nabla_0 \times \mathbf{B}_3) \times \mathbf{B}_0 - \nabla_0 p_3 \\ = -(\nabla_0 \times \mathbf{B}_2) \times \mathbf{B}_1 - (a/R_0)(\nabla_T \times \mathbf{B}_0) \times \mathbf{B}_0, \\ \nabla_0 \cdot \mathbf{B}_3 = -(a/R_0)\nabla_T \cdot \mathbf{B}_0. \quad (4.113)$$

There are a number of inhomogeneous terms driving the third-order fields. First, the  $(\nabla_0 \times \mathbf{B}_2) \times \mathbf{B}_1$  gives rise to a diamagnetic correction to the bumpy vacuum field of order  $\beta \mathbf{B}_1 \sim \delta^3$ . The resulting field  $\tilde{\mathbf{B}}_3$  is only a function of  $(r, z)$  and hence can be written as  $\tilde{\mathbf{B}}_3(r, z) = (\nabla \psi_3 \times \mathbf{e}_\theta)/r$  with  $\psi_3$  satisfying

$$r \left[ \frac{\psi'_3}{r} \right]' - h^2 \psi_3 = -\frac{r}{2} \left[ \frac{\beta'}{r} \right]' \psi_1(r), \\ \beta(r) = 2p_2/B_0^2 \sim \delta^2. \quad (4.114)$$

Second, it is here that the toroidal effects first enter the calculation, and the last term in Eq. (4.113) gives rise to the well-known  $(r/R_0) \cos\theta$  correction to  $B_\phi$ , resulting from the  $1/R$  dependence associated with the geometry.

Finally, there are homogeneous solutions of the form  $\hat{\mathbf{B}}_3(r, \theta)\mathbf{e}_\phi, \hat{p}_3(r, \theta)$  which must be included. It is a fairly common occurrence in three-dimensional equilibrium calculations that homogeneous solutions must be allowed at some intermediate order to satisfy a periodicity constraint occurring at some higher order. This “higher order” corresponds to the condition for toroidal force balance. Since the outward toroidal force is of order  $\beta(a/R_0)$  [see Eq. (4.17)], the EBT expansion must be carried out to fifth order to determine the homogeneous terms. The results of this calculation show that  $\hat{\mathbf{B}}_3$  and  $\hat{p}_3$  are of the form  $\hat{\mathbf{B}}_3 = \hat{\mathbf{B}}_3(r) \cos\theta$  and  $\hat{p}_3 = \hat{p}_3(r) \cos\theta$ , indicating that the distortion of the flux surfaces has the form of a small toroidal shift. Combining these results, one can write the total third-order fields as

$$\mathbf{B}_3 = \tilde{\mathbf{B}}_3(r, z) + [\hat{\mathbf{B}}_3(r) - B_0(r/R_0)] \cos\theta \mathbf{e}_\phi, \\ p_3 = \tilde{p}_3(r, z) + \hat{p}_3(r) \cos\theta, \quad (\hat{p}_3 + B_0 \hat{\mathbf{B}}_3)' = 0. \quad (4.115)$$

The fourth-order equations are quite complicated:

$$(\nabla_0 \times \mathbf{B}_4) \times \mathbf{B}_0 - \nabla_0 p_4 \\ = -(\nabla_0 \times \mathbf{B}_3) \times \mathbf{B}_1 - (\nabla_0 \times \mathbf{B}_2) \times \mathbf{B}_2 \\ - (a/R_0)[(\nabla_T \times \mathbf{B}_0) \times \mathbf{B}_1 - (\nabla_T \times \mathbf{B}_1) \times \mathbf{B}_0], \\ \nabla_0 \cdot \mathbf{B}_4 = -(a/R_0)\nabla_T \cdot \mathbf{B}_1. \quad (4.116)$$

Of the many driving terms, the only ones which ultimately affect the fifth-order toroidal force balance are those with explicit  $\theta$  dependence. There are two such contributions. One represents the toroidal correction to the bumpy vacuum field (i.e., the terms multiplied by  $a/R_0$ ). Since these are corrections to a vacuum field, their contribution eventually cancels when one computes force balance. The most important contribution arises from the  $(\nabla_0 \times \mathbf{B}_3) \times \mathbf{B}_1$  term and represents the development of sideband fields resulting from the fact that the plasma is no longer centered in the bumpy vacuum fields; that is, because of the  $\cos\theta$  shift of the flux surfaces associated with the homogeneous terms  $(\hat{\mathbf{B}}_3, \hat{p}_3)$ , the basic bumpy field develops sidebands of the form  $B_4 = B_4(r, z) \exp(\pm i\theta)$ . It is the currents associated with these sideband fields that ultimately provide the toroidal force balance (Ribe, 1969; Miller, 1977). The solution to Eq. (4.116) is somewhat tedious; it suffices to say that after a straightforward but lengthy calculation the  $\theta$ -dependent, fourth-order fields can be explicitly determined.

Finally, consider the fifth-order momentum equation,

$$(\nabla_0 \times \mathbf{B}_5) \times \mathbf{B}_0 - \nabla_0 p_5 = -(\nabla_0 \times \mathbf{B}_4) \times \mathbf{B}_1 - (\nabla_0 \times \mathbf{B}_3) \times \mathbf{B}_2 - (\nabla_0 \times \mathbf{B}_2) \times \mathbf{B}_3 \\ - (a/R_0)[(\nabla_T \times \mathbf{B}_0) \times \mathbf{B}_2 + (\nabla_T \times \mathbf{B}_1) \times \mathbf{B}_1 + (\nabla_T \times \mathbf{B}_2) \times \mathbf{B}_0]. \quad (4.117)$$

The toroidal force balance periodicity constraint arises because the fifth-order fields  $\mathbf{B}_5$  and  $p_5$  vanish when the operation  $\mathbf{B}_0 \cdot \nabla_0 \times \langle \rangle$  is performed. Here  $\langle \rangle$  denotes an average over one period of the bumpy field, and performing this average focuses attention on the net

toroidal forces. The toroidal constraint can only be satisfied by properly choosing the as yet undetermined homogeneous field  $\hat{\mathbf{B}}_3$ . Note that when the operation  $\mathbf{B}_0 \cdot \nabla_0 \times \langle \rangle$  is performed on any of the lower-order equations, the resulting constraints are trivially satisfied,

so that no other homogeneous terms are required. Evaluation of the toroidal constraint again involves considerable algebra. The details of this calculation show that there are two outward toroidal forces, one due to the  $1/R$  effect of the geometry and one due to the "rubber tire tube" effect (see Sec. IV.A.6), just as in a toroidal  $\theta$  pinch. As previously stated, there is only one force to compensate for this outward force. It arises from the  $(\nabla_0 \times \mathbf{B}_4) \times \mathbf{B}_1$  term and corresponds to the interaction of the basic bumpy field with the sideband current.

The overall results of the calculation are summarized below. The magnetic field and pressure, correct to third order, are given by (Freidberg, 1980)

$$\begin{aligned} \mathbf{B} &= B_0 \left[ 1 - \frac{1}{2} \beta - \left( \frac{1}{2} \beta_s + \frac{r}{R_0} \right) \cos \theta \right] \mathbf{e}_\phi \\ &\quad + \frac{1}{r} \nabla_0 [(\psi_1 + \psi_3) \cos(hz)] \times \mathbf{e}_\theta, \\ \frac{2p}{B_0^2} &= \beta + \beta_s \cos \theta + \beta' \left( \frac{\psi_1}{r B_0} \right) \cos(hz), \end{aligned} \quad (4.118)$$

where  $\beta(r)$  is assumed given and

$$\begin{aligned} \psi_1(r) &= \left[ \frac{B_0 \delta}{h^2} \right] \left[ r \frac{d}{dr} I_0(hr) \right], \\ \psi_3(r) &= \frac{1}{2} \psi_1(r) \int_r^\infty \frac{x dx}{\psi_1^2(x)} \int_0^x \left[ \frac{\beta(y)'}{y} \right]' \psi_1^2(y) dy, \\ \beta_s(r) &\equiv \frac{2\hat{p}_3(r)}{B_0^2} = \left[ \frac{2B_0^2}{h^2 R_0} \right] \left[ \frac{r^4 \beta'}{\psi_1(2r\psi_1' - \psi_1)} \right]. \end{aligned} \quad (4.119)$$

An examination of these results indicates the following. Toroidal closed-line EBT equilibria with no net toroidal current exist in the asymptotic sense. For these equilibria radial pressure balance is similar to that in a low- $\beta$  toroidal  $\theta$  pinch. The outward toroidal drift force is balanced by the sideband force resulting from the interaction of the basic bumpy field with the sideband currents generated by the toroidal shift of the plasma. The toroidal shift  $\Delta = -\beta_s/\beta'$ , as given by Eq. (4.119), is, perhaps surprisingly, inward. This is a clear indication of instability (i.e., displacement and restoring force in the same direction), and were it not for a special treatment of the electron rings in the stability analysis, this would indeed be so. This question is discussed in more detail in Sec. V. In the EBT expansion,  $\beta \sim \delta^2 \sim (a/R)^{2/3}$ , indicating that  $\beta$  is higher than in the high- $\beta$  tokamak. Finally, it is interesting to note that evaluation of the toroidal force balance constraint yields an algebraic expression for  $\beta_s(r)$  rather than a partial differential equation such as the Grad-Shafranov equation for axisymmetric tokamak equilibria. The question of whether toroidal force balance is algebraic or differential is of fundamental importance in distinguishing different configurations. Analysis of the conventional and high- $\beta$

stellarator sheds further light on this question, and a more complete discussion is deferred until later.

### 3. The high- $\beta$ stellarator (HBS)

Although the high- $\beta$  stellarator effort in the international fusion program has been greatly reduced in recent years, the concept itself remains of significant scientific interest, particularly for aiding in the understanding of the relation between EBT, the conventional stellarator, and the high- $\beta$  tokamak. In fact, the basic physical idea of achieving toroidal force balance by means of a helical sideband field originated with the analysis of high- $\beta$  stellarator equilibria (Blank *et al.*, 1969; Rosenbluth *et al.*, 1969; Ribe, 1969; Miller, 1977; Freidberg *et al.*, 1979).

A high- $\beta$  stellarator is a large-aspect-ratio, high- $\beta$  toroidal device whose magnetic field configuration consists primarily of: (1) a large toroidal field, (2) a moderate sized helical field characterized by  $l\theta + hz$ , (3) one or two small, externally applied helical sideband fields characterized by  $(l \pm 1)\theta + hz$ , and (4) no net toroidal current. Here  $z = R_0\phi$ ,  $L = 2\pi/h$  is the helical period, and  $l$  describes the multipolarity of the helical field. Since high- $\beta$  stellarators operate as short pulse devices ( $\tau \lesssim 100 \mu\text{sec}$ ), the required helical fields can be generated not only by externally applied coils, as in the ISAR experiment (Funfer *et al.*, 1975), but equally well by shaping the surface of the surrounding copper wall, as in the Scyllac experiment (Ellis *et al.*, 1974). A typical example of a Scyllac conducting shell is shown in Fig. 26. Here, as in all high- $\beta$  stellarators, the main helical field corresponds to  $l=1$  (for stability reasons), and in this particular case the sideband field corresponds to  $l=0$ .

The basic physical questions associated with high- $\beta$  stellarator equilibria are addressed by the HBS expansion. Conceptually, the Elmo bumpy torus and high- $\beta$  stellarator expansions are very similar. However, because of the high  $\beta$ , the HBS expansion is significantly compressed, so that one need only carry out the calculation to second order to compute toroidal force balance. In this connection, it is worthwhile pointing out that with regard to MHD equilibria, the EBT can be considered as the low- $\beta$  limit of an  $l=0$ , high- $\beta$  stellarator. Similarly, if the hot electron rings are ignored, then a finite- $\beta$  EBT is equivalent to an  $l=0$ , high- $\beta$  stellarator.

The basic parameter of the HBS expansion is the ratio of the helical field amplitude to the main toroidal field (Blank *et al.*, 1969; Rosenbluth *et al.*, 1969).

$$\delta = B_{\text{hel}}/B_\phi \ll 1. \quad (4.120)$$

Note that the amplitudes of the sideband fields and the main helical field are assumed to be comparable. In terms of  $\delta$ , the HBS expansion is given by

$$\begin{aligned} \beta &\sim 1, \quad a/R_0 \sim \delta^2, \quad ha \sim 1, \\ \nabla &= \nabla_0 + (a/R_0) \nabla_T, \quad \nabla_0 \sim \nabla_T \sim 1. \end{aligned} \quad (4.121)$$

As in EBT,  $\nabla_0$  is the straight cylindrical operator and

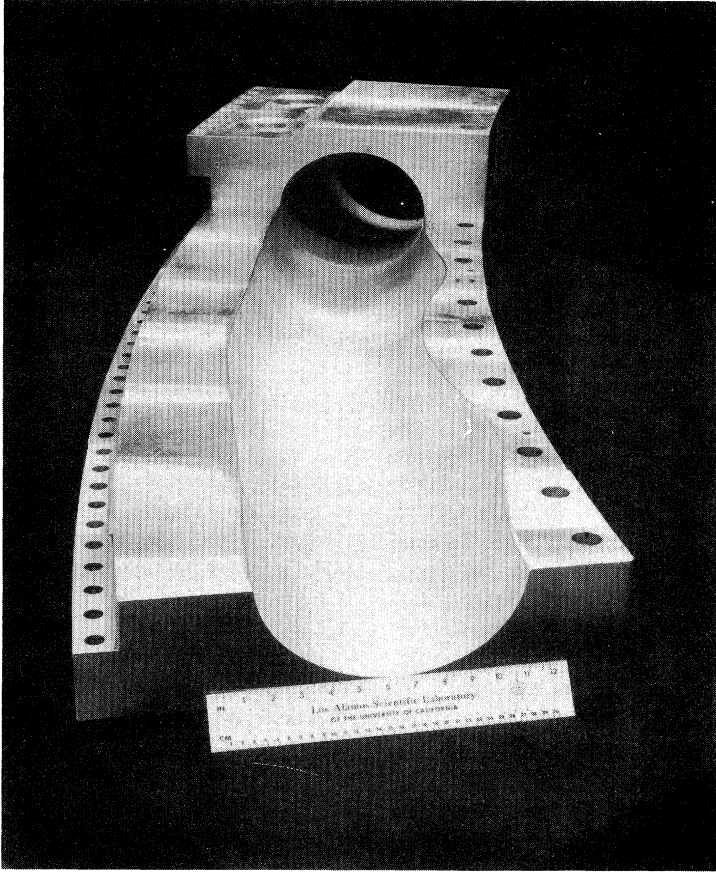


FIG. 26. Shaped conducting wall for producing an  $l=1,0$  high- $\beta$  stellarator configuration in the Scyllac experiment (courtesy K. F. McKenna, Los Alamos Scientific Laboratory, 1981).

$(a/R_0)\nabla_T$  is the toroidal correction. Since the outward toroidal force is of order  $\beta(a/R_0)$ , the expansion must be carried out to second order to include the effects of toroidal force balance. [Nonlinear high- $\beta$  stellarator equilibria without expansions have been calculated numerically by Brackbill and Pracht (1973), Betancourt and Garabedian (1976), and Barnes and Brackbill (1977).]

Consider now the HBS expansion order by order. The zeroth-order equations describe radial pressure balance. As no net current flows in a high- $\beta$  stellarator, the zeroth-order field is purely in the toroidal direction,  $\mathbf{B}_0 = B_0 \mathbf{e}_\phi$ . Since  $\beta \sim 1$ , there is also a nonzero pressure  $p_0$  and current  $\mathbf{J}_0$ . A crucial feature of the HBS expansion is that the lowest-order quantities must all be functions of  $(r,\theta)$ ; that is, the tempting hypothesis which assumes all zero-order quantities to be cylindrically symmetric (i.e., only functions of  $r$ ) leads to an overdetermined system with no solutions. The zeroth-order equations are given by

$$(\nabla_0 \times \mathbf{B}_0) \times \mathbf{B}_0 - \nabla_0 p_0 = 0, \quad \nabla_0 \cdot \mathbf{B}_0 = 0, \\ p_0 = p_0(r, \theta), \quad \mathbf{B}_0 = B_0(r, \theta) \mathbf{e}_\phi, \quad (4.122)$$

which simplify to

$$\nabla_0(p_0 + B_0^2/2) = 0. \quad (4.123)$$

Equation (4.123) shows that radial pressure balance in a high- $\beta$  stellarator corresponds to that in a  $\theta$  pinch. Since  $p_0 = p_0(r, \theta)$ , the zeroth-order pressure surfaces are allowed to have finite noncircular distortions which are as yet undetermined. In fact, the function  $p_0(r, \theta)$  exactly corresponds to the third-order homogeneous solution of the EBT expansion. Because of the high  $\beta$  and the assumption  $a/R_0 \sim \delta^2$  rather than  $\delta^3$ , the homogeneous solutions appear in zeroth order. Also the toroidal effects on the flux surfaces are finite and in general distort the shape of the surfaces as well as shifting them.

In first order the main helical field and all helical sideband fields are added. These fields satisfy

$$(\nabla_0 \times \mathbf{B}_0) \times \mathbf{B}_1 + (\nabla_0 \times \mathbf{B}_1) \times \mathbf{B}_0 - \nabla_0 p_1 = 0, \\ \nabla_0 \cdot \mathbf{B}_1 = 0. \quad (4.124)$$

The first-order fields are assumed to contain an arbitrary number of helical fields with different  $l$  values but all with the same pitch number  $h$ . These fields can be expressed as

$$\mathbf{B}_1(r, \theta, z) = \hat{\mathbf{B}}_1(r, \theta) \exp(izh) + \text{c.c.}, \\ p_1(r, \theta, z) = \hat{p}_1(r, \theta) \exp(izh) + \text{c.c.} \quad (4.125)$$

Straightforward analysis shows that the first-order quan-

tities can be expressed in terms of a single scalar function  $\Phi(r, \theta)$  as follows:

$$\begin{aligned}\hat{\mathbf{B}}_{1\perp}(r, \theta) &= (1/B_0)\nabla_\perp\Phi, \\ \hat{p}_1(r, \theta) &= ih\Phi, \\ \hat{\mathbf{B}}_{1\phi} &= (i/h)\nabla_\perp\cdot\hat{\mathbf{B}}_{1\perp},\end{aligned}\quad (4.126)$$

where  $\perp$  refers to the poloidal plane. The function  $\Phi$  satisfies

$$\begin{aligned}\nabla_\perp^2\Phi - h^2\Phi + (\nabla_\perp\beta\cdot\nabla_\perp\Phi)/(1-\beta) &= 0, \\ \beta(r, \theta) = 2p_0(r, \theta)/B_a^2 &= 1 - B_0^2/B_a^2,\end{aligned}\quad (4.127)$$

where  $B_a$  is the externally applied toroidal field.

For the boundary conditions it is assumed that the plasma is surrounded by a shaped conducting shell whose surface is given by  $r=b[1-\Sigma_l\Delta_l\cos(l\theta+hz)]$ , with  $\Delta_l\sim\delta$ . Specification of the helical distortions  $\Delta_l$ , combined with regularity at the origin, is sufficient to uniquely determine  $\Phi$  for a given  $\beta$ .

In second order the toroidal effects first enter the calculation. The corresponding equations are given by

$$\begin{aligned}(\nabla_0\times\mathbf{B}_0)\times\mathbf{B}_2 + (\nabla_0\times\mathbf{B}_2)\times\mathbf{B}_0 - \nabla_0p_2 &= \mathbf{R}, \\ \mathbf{R} = -(\nabla_0\times\mathbf{B}_1)\times\mathbf{B}_1 - (a/R_0)[(\nabla_T\times\mathbf{B}_0)\times\mathbf{B}_0 - \nabla_Tp_0],\end{aligned}\quad (4.128)$$

There are two inhomogeneous terms driving the second-order fields. The  $(a/R_0)$  term represents the outward toroidal force on the plasma. The  $(\nabla_0\times\mathbf{B}_1)\times\mathbf{B}_1$  term represents the force associated with the helical field interaction. This restoring force is slightly more complicated than for EBT because the expansion has been compressed. Thus the term includes the interaction of any given helical field component with both its own current and its sideband currents. As with EBT, the most important information contained in Eq. (4.128) arises from the  $z$ -averaged part of  $\mathbf{R}$ . In particular, if one performs the operation  $\mathbf{B}_0\cdot\nabla_0\times\langle\mathbf{R}\rangle$ , the explicit second-order fields vanish, leading to the toroidal force balance constraint  $\mathbf{e}_\phi\cdot\nabla_0\times\langle\mathbf{R}\rangle=0$ . After considerable algebra, this constraint can be written as (Freidberg *et al.*, 1979)

$$|\nabla_\perp\Phi|^2 + h^2|\Phi|^2 = B_a^4(1-\beta)^2[G(\beta) - (r/R_0)\cos\theta].\quad (4.129)$$

Here  $G(\beta)$  is an arbitrary free function resulting from an integration of the constraint equation. Before discussing Eq. (4.129), it should be pointed out that  $\mathbf{B}_0\cdot\langle\mathbf{R}\rangle$  is in general nonzero (although it is zero for the special case of closed-line symmetry corresponding to EBT). To balance this term, a second-order field of the form  $\mathbf{B}_2=\mathbf{e}_\phi\times\nabla_0\mathcal{A}$  is required. After another lengthy calculation it can be shown that  $\mathcal{A}$  is given by

$$\mathcal{A} = \frac{i}{hB_a^3} \frac{\mathbf{e}_\phi\cdot\nabla_\perp\Phi^*\times\nabla_\perp\Phi}{(1-\beta)^{3/2}} + H(\beta),\quad (4.130)$$

where  $H(\beta)$  is a second free integration function.

Thus the equilibrium of a high- $\beta$  stellarator is given by the simultaneous solution of Eqs. (4.127) and (4.129), a set of coupled nonlinear partial differential equations for the unknowns  $\Phi$  and  $\beta$ . In conjunction with Eq. (4.130) there are, as expected, two free functions  $G(\beta)$  and  $H(\beta)$  to specify the equilibrium. The function  $H(\beta)$  is directly coupled to the vector potential  $\mathcal{A}$  and hence the toroidal current. Assuming  $\Phi$  and  $\beta$  have been calculated,  $H(\beta)$  can then be adjusted to give any prescribed averaged toroidal current distribution as a function of pressure contour, including the pure stellarator case where  $\langle J_{\text{tor}} \rangle = 0$  on each surface.

Consider now the toroidal force balance relation, Eq. (4.129). There are basically two different ways in which the toroidal drift force [i.e., the  $(r/R_0)\cos\theta$  term] can be balanced. First, as in the case of EBT, a single helical field can be used to create an equilibrium. In this situation, the plasma shifts with respect to the center of the helical field, generating self-induced sideband currents. In this limit an approximate solution can be obtained by assuming  $\beta\approx\beta_0(r)+\beta_s(r)\cos\theta$  with  $\beta_s<\beta_0$  and  $\Phi\approx\Phi_l(r)\exp(il\theta)$ . The purely radial parts of Eq. (4.127) and (4.129) become

$$\Phi_l'' + \left[ \frac{1}{r} + \frac{\beta'_0}{1-\beta_0} \right] \Phi_l' - \left[ \frac{l^2}{r^2} + h^2 \right] \Phi_l = 0,\quad (4.131)$$

$$(1-\beta_0)^2 G(\beta_0) = \left[ \frac{1}{B_a^4} \right] \left[ \Phi_l'^2 + \left[ \frac{l^2}{r^2} + h^2 \right] \Phi_l^2 \right].\quad (4.132)$$

If one now treats  $\beta_0(r)$  as the given free function, Eq. (4.131) can be easily solved numerically for  $\Phi_l$ , and Eq. (4.132) can be used to determine  $\hat{G}(\beta_0)=(1-\beta_0)^2G(\beta_0)$ . Note that the self-interaction of a single helical field leads to a purely radial dependence for the left-hand side of Eq. (4.129) and a cylindrically symmetric  $\beta_0(r)$ ; that is, the basic purpose of the main helical field is to remove the degeneracy of the pure  $\theta$  pinch by creating a well-defined set of closed flux surfaces. The nature of the toroidal force balance can now be ascertained by expanding  $\hat{G}(\beta)\approx\hat{G}(\beta_0)+\hat{G}'(\beta_0)\beta_s\cos\theta$  and equating the  $\cos\theta$  terms. After some algebra one finds

$$\begin{aligned}\beta_s(r) &= (1-\beta_0)^2(r\beta'_0)(r/R_0)D^{-1}, \\ D &= \frac{2}{B_a^4} \left[ 2 \frac{(l^2+h^2r^2)}{r} \Phi_l \Phi_l' - \frac{l^2}{r^2} \Phi_l^2 - \left[ 1 + \frac{r\beta'_0}{1-\beta_0} \right] \Phi_l'^2 \right].\end{aligned}\quad (4.133)$$

This relationship is a high- $\beta$ , arbitrary- $l$  generalization of the EBT shift given by Eq. (4.119) and reduces exactly to Eq. (4.119) in the limit of low  $\beta$ ,  $l=0$ .

For practical cases the predicted shift of the flux surfaces for a high- $\beta$ ,  $l=1$  system is quite large. This leads to a second method of creating toroidal force balance and requires the addition of one or two small, externally applied, helical sideband fields; that is, since the plasma shift is determined by the induced sideband currents, it should be possible to control the shift by applying external sideband fields (Ribe, 1969). An approximate solu-

tion for this case can be obtained by writing

$$\beta(r) \approx \beta_0(r) + \beta_s(r) \cos \theta$$

and

$$\begin{aligned} \Phi &= \Phi_l(r) \exp(i l \theta) \\ &+ \Phi_{l \pm 1}(r) \exp[i(l \pm 1)\theta] \end{aligned}$$

with  $\beta_s < \beta_0$  and  $\Phi_{l \pm 1} < \Phi_l$ . The purely radial part of the equilibrium is identical to the single helical field case, and the same results and interpretation apply. The nature of the toroidal force balance can again be ascertained by expanding  $\hat{G}(\beta)$  and equating the  $\cos \theta$  terms. One finds

$$\begin{aligned} \beta_s(r) &= \frac{r\beta'_0}{D} [(1 - \beta_0)^2(r/R_0) + F_{l,l \pm 1}], \\ F_{l,l \pm 1} &= \frac{2}{B_a^2} \left[ \Phi'_l \Phi'_{l \pm 1} + \left( \frac{l(l \pm 1)}{r^2} + h^2 \right) \Phi_l \Phi_{l \pm 1} \right]. \end{aligned} \quad (4.134)$$

Note that the interaction of a helical field  $l$  with either of its sidebands  $l \pm 1$  gives rise to a force  $F_{l,l \pm 1}$  in the same (or exactly opposite) direction as the toroidal drift force. The  $\Phi_{l \pm 1}$  are determined by equating the  $\exp(\pm i \theta)$  components of Eq. (4.127) to zero. The resulting second-order, ordinary differential equations are linear in  $\Phi_{l \pm 1}$ , with an inhomogeneous term linearly dependent on  $\beta_s$ . Thus these equations, coupled with Eq. (4.134), must be solved simultaneously. This requires a lengthy calculation. However, it is intuitively clear from Eq. (4.134) that by adjusting the amplitudes of the main helical field and the externally applied sidebands one can set the shift of any given flux surface to zero. In particular, if the center of gravity of the plasma coincides with the geometric center of the conducting wall (i.e.,  $\int r^2 \beta_s dr = 0$ ) then the equilibrium relation for a "zero-shift" high- $\beta$  stellarator is given by

$$g_{l,l+1} \Delta_l \Delta_{l+1} + g_{l,l-1} \Delta_l \Delta_{l-1} = -1/h^2 b R_0. \quad (4.135)$$

Here the  $g_{l,l \pm 1}$  are functions of  $\langle \beta_0 \rangle$ ,  $a/b$ , and  $ha$ , and are usually determined numerically. In general the dependence on  $a/b$  and  $ha$  is weak. For the special example of an  $l=1$  system with a step-function pressure profile, the coefficients can be obtained analytically in the limit  $a/b, ha \ll 1$ . The results are (Blank *et al.*, 1969; Rosenbluth *et al.*, 1969)

$$\begin{aligned} g_{12} &= \frac{2}{2 - \langle \beta_0 \rangle}, \\ g_{10} &= \frac{(3 - 2\langle \beta_0 \rangle)}{(2 - \langle \beta_0 \rangle)(1 - \langle \beta_0 \rangle)}, \end{aligned} \quad (4.136)$$

where  $\langle \beta_0 \rangle = [2\pi \int p_0 r dr] / [\pi a^2 B_a^2 / 2]$ .

A final point to note in the theory of high- $\beta$  stellarators is that the toroidal force balance constraint, given by Eq. (4.129), is algebraic (in  $\beta$ ) and not a partial differential equation as for tokamaks. This is another indication of the similarity between EBT and high- $\beta$  stellarator

equilibria. The question of algebraic versus differential is addressed at the end of the next section.

To summarize, large-aspect-ratio, toroidal, high- $\beta$  stellarator equilibria without net toroidal current have been shown to exist in the asymptotic sense. The radial pressure balance of these equilibria corresponds to that of a  $\theta$  pinch. Toroidal force balance is achieved by the addition of a helical magnetic field. The interaction of this helical field with either a shift-induced or externally applied sideband field produces a restoring force for toroidal force balance.

In practice high- $\beta$  stellarators have great difficulty in achieving stable operation (Funfer *et al.*, 1975; Ellis *et al.*, 1979). The high  $\beta$  leads to relatively strong instabilities, even for the optimized  $l=1$  system, and can only be stabilized by a very close conducting wall [see, for instance, Davidson and Freidberg (1976)] or by feedback stabilization (Ribe and Rosenbluth, 1970). Neither of these can easily be achieved in a technologically attractive way, and as a result much, if not all, of the high- $\beta$  stellarator research has been stopped.

#### 4. Stellarators, heliotrons, and torsatrons

The final three-dimensional concept to be discussed is the conventional stellarator. This configuration, one of the earliest suggested in the fusion program, is a large-aspect-ratio, low-to-moderate- $\beta$ , toroidal device whose main field components are a large toroidal field and a single, somewhat smaller helical field, usually  $l=2$  or  $l=3$  (Spitzer, 1958). It can in principle operate with no net toroidal current, although in practice such currents are often present for purposes of ohmic heating [see Miyamoto (1978) for a review of stellarator experiments].

Typical time scales for stellarator experiments are tens of milliseconds, and future extrapolations are thought of in terms of steady-state operation. Consequently the helical fields must be generated by means of external coils (rather than a shaped copper shell), and three different methods have been suggested—the stellarator, the heliotron, and the torsatron, as illustrated schematically in Fig. 27. The stellarator consists of  $2l$  helical wires with alternating direction of current flow, situated in a large toroidal field. This is perhaps the most flexible configuration from the point of view of physics, but there exist very large forces, alternating inward and outward on the helical coils, making extrapolations to higher fields and larger experiments very unattractive, if not impossible. The constraints imposed by the radially inward forces are more severe, since the helical coils are usually mounted on a relatively fragile vacuum chamber. If the appropriate set of alternate helical coils is eliminated, the remaining coil set experiences only outward forces. This is the heliotron. Although not quite as efficient as a stellarator in generating helical fields, it has a considerable structural advantage. Note that the helical coil system itself produces a net toroidal field, since all the currents flow in one direction. If in fact the external

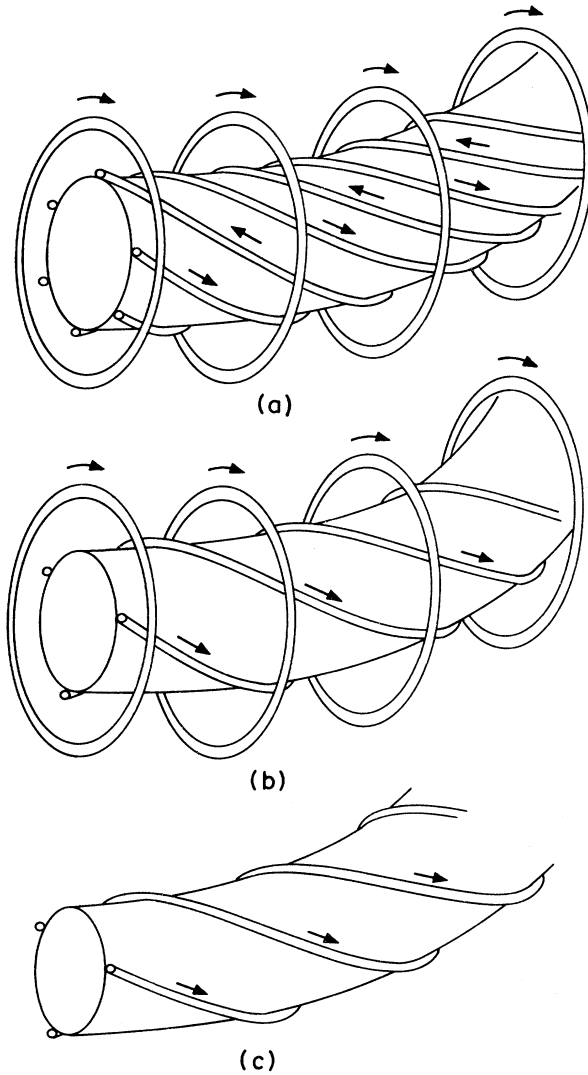


FIG. 27. Schematic diagram of: (a) stellarator, (b) heliotron, and (c) torsatron windings.

toroidal field is eliminated, the heliotron is transformed into a torsatron. This is the least flexible method of generating helical fields, in that the ratio of the helical field amplitude to the toroidal field amplitude can no longer be varied independently. However, by appropriately choosing the pitch of the windings one can make the torsatron configuration essentially force free, thereby dramatically reducing the structural support problem. Although quite different in physical appearance, the stellarator, heliotron, and torsatron each produce virtually the same field in the region occupied by the plasma. Consequently, in the theoretical analysis, these configurations are usually indistinguishable.

It is also useful to note that there has been considerable interest recently in designing modular stellarator coils (as opposed to the continuous types just discussed) in order to alleviate the access problem in large (reactor-size) configurations. This type of coil can, however, be acted upon by large forces. The ultimate desirability of

continuous versus modular is as yet unresolved and remains an area of active research.

The basic physical issues associated with MHD equilibria of stellarators are addressed by means of the "stellarator expansion" (Greene and Johnson, 1961). This expansion is very similar in mathematical detail to the high- $\beta$  stellarator expansion. In fact many of the relevant equations are simply obtained by taking the  $\beta \rightarrow 0$  limit in the HBS expansion. There is, however, one crucial difference, which ultimately implies that, from the point of view of physics, the conventional stellarator is much more closely related to the high- $\beta$  tokamak.

As in the high- $\beta$  stellarator, the basic parameter of the stellarator expansion is  $\delta$ , the ratio of helical field amplitude to toroidal field. The appropriate ordering is given by

$$\beta \sim a/R_0 \sim \delta^2, \quad ha \sim 1, \\ \nabla = \nabla_0 + (a/R_0)\nabla_T, \quad \nabla_0 \sim \nabla_T \sim 1. \quad (4.137)$$

This differs from the EBT expansion in that the inverse aspect ratio is assumed to be one order larger in  $\delta$ . Likewise, the main difference from the HBS expansion is that  $\beta$  is assumed to be two orders smaller in  $\delta$ . In fact, the scaling  $\beta \sim a/R_0$  is identical to the high- $\beta$  tokamak.

Consider now the stellarator expansion, order by order. In zeroth order there is a uniform toroidal vacuum field  $\mathbf{B}_0 = B_a \mathbf{e}_\phi$ . In first order a small, helical vacuum field is added,  $\mathbf{B}_1 = (1/B_a)\nabla\phi$ . Writing  $\Phi(r, \theta, z) = \Phi(r, \theta) \times \exp(ihz)$ , it follows that  $\Phi(r, \theta)$  satisfies

$$\nabla_\perp^2 \Phi - h^2 \Phi = 0, \quad (4.138)$$

which is just the low- $\beta$  limit of the corresponding HBS relation given by Eq. (4.127).

The second-order equations show that radial pressure balance is similar to that in a low- $\beta$   $\theta$  pinch,

$$\nabla_\perp(p_2 + B_a B_2) = 0. \quad (4.139)$$

Here  $p_2 = p_2(r, \theta)$ , so that the shift and distortions of the surfaces are assumed to be finite. As in the EBT and the high- $\beta$  stellarator, the explicit shape of the flux surfaces is determined in higher order, fourth to be precise, since toroidal force balance occurs for  $\beta(a/R_0) \sim \delta^4$ .

The third-order equations describe the diamagnetic contribution to the helical fields and the development of the sideband currents. The details are similar to those previously given for the EBT and the high- $\beta$  stellarator. Continuing, the fourth-order equations are given by

$$(\nabla_0 \times \mathbf{B}_4) \times \mathbf{B}_0 - \nabla_0 p_4 = \mathbf{R}, \\ \mathbf{R} = -(\nabla_0 \times \mathbf{B}_3) \times \mathbf{B}_1 - (\nabla_0 \times \mathbf{B}_2) \times \mathbf{B}_2 \\ - (a/R_0)[(\nabla_T \times \mathbf{B}_2) \times \mathbf{B}_0 + (\nabla_T \times \mathbf{B}_1) \times \mathbf{B}_1 \\ + (\nabla_T \times \mathbf{B}_0) \times \mathbf{B}_2 - \nabla_T p_2]. \quad (4.140)$$

As before, the important information contained in Eq. (4.140) is obtained by appropriately averaging over  $z$ . In fact, if one computes  $\mathbf{B}_0 \cdot \langle \mathbf{E} \rangle = 0$ , there results

a nonzero contribution from the right-hand side which can only be balanced by adding a homogeneous term to  $\mathbf{B}_2$  of the form  $\mathbf{e}_\phi \times \nabla_0 A$ . After a lengthy calculation,  $A$  is found to be

$$A = \frac{i}{hB_a^3} \mathbf{e}_\phi \cdot \nabla_\perp \Phi^* \times \nabla_\perp \Phi + H(\beta), \quad (4.141)$$

which is just the low- $\beta$  limit of Eq. (4.13) in the HBS expansion. In conventional stellarators, it is customary to label the pressure contours with a quantity  $\psi_0$ , the total averaged poloidal flux. This is accomplished by noting that  $H(\beta) = -\psi_0/2\pi R_0$  and hereafter treating  $\beta = \beta(\psi_0)$  as a free function.

The important difference between the high- and low- $\beta$  stellarator occurs in the toroidal force balance relation  $\mathbf{B}_0 \cdot \nabla_0 \times \langle \mathbf{R} \rangle = 0$ . The difference arises because of the additional force associated with the transverse field  $A$ . In both cases, this force,  $(\nabla_0 \times \mathbf{B}_2) \times \mathbf{B}_2$ , is of fourth order. However, in the HBS scaling the toroidal forces are of second order, and hence the additional force is negligible. This is not so for the conventional stellarator. After a lengthy calculation the force balance relation can be written as (Greene and Johnson, 1961; Strauss, 1979)

$$\nabla_\perp^2 A = \frac{2\pi R_0}{B_a^2} \frac{d\beta}{d\psi_0} \left[ |\nabla_\perp \Phi|^2 + h^2 |\Phi|^2 + B_a^4 \left( \frac{r}{R_0} \cos\theta + G(\beta) \right) \right]. \quad (4.142)$$

Note that the term in the bracket is just the low- $\beta$  limit of the HBS result given by Eq. (4.129). The additional force due to the transverse field  $A$  appears as the  $\nabla^2 A$  term and would be negligible if  $\beta \sim 1$  as in the HBS. This term completely changes the structure of the force balance relation, converting it from an algebraic relation, as for the EBT and HBS, into a partial differential equation similar to the Grad-Shafranov equation. In fact, if one sets  $\Phi = 0$  (i.e., eliminates the helical fields), Eq. (4.142) becomes identical to the equation for the high- $\beta$  tokamak given by Eq. (4.71).

The procedure for solving the conventional stellarator equations is as follows. First, Eq. (4.138) is solved for  $\Phi$ . Equation (4.141) then gives  $\psi_0 = \psi_0(A, r, \theta)$ . This is substituted into Eq. (4.142), which is basically a nonlinear elliptic partial differential equation. Here  $\beta(\psi_0)$  can be chosen arbitrarily, and by iteration  $G[\beta(\psi_0)]$  can be determined to give any specified net toroidal current distribution as a function of flux surface, including the important case  $\langle J_\phi \rangle = 0$ . Because of this complexity, the stellarator equations must in general be solved numerically. One interesting analytic limit is that in which  $\beta(\psi_0)/\epsilon$  is treated as small. In this limit one expands all quantities as  $Q = Q_0(r) + Q_s(r, \theta)$  with  $Q_s/Q_c \ll 1$ . For the case of a single helical field [i.e.,  $\phi \sim I_l(hr) \exp(il\theta)$ ], the toroidal contribution to the stellarator equations is given by

$$\begin{aligned} \iota_H \nabla_\perp^2 \left[ \frac{A_s}{B_a} \right] &= -\beta'_0(r) \cos\theta, \\ A_s(0, \theta) \text{ regular; } \\ A_s(r \rightarrow \infty, \theta) &= B_v r \cos\theta, \end{aligned} \quad (4.143)$$

where  $B_v$  is the externally applied vertical field,  $\beta_0(r)$  is a free function representing the leading-order contribution to the pressure, and  $\iota_H = 2\pi\mu_H$  is the vacuum helical rotational transform. Note that for  $ha \ll 1$ ,  $\iota_H(r) \approx \iota_H(a)[r/a]^{2l-4}$ .

The solution for  $A_s$  is related to the toroidal shift  $\Delta = -\beta_s/\beta'_0$  as follows:

$$\begin{aligned} \Delta(r) &= -\frac{R_0}{r\iota_H B_a} A_s \\ &= -\frac{R_0}{\iota_H} \left[ \frac{B_v}{B_a} + \int_r^\infty \frac{dx}{x^3} \int_0^x \frac{y^2 \beta'(y)}{\iota_H(y)} dy \right]. \end{aligned} \quad (4.144)$$

There are several points worth discussing about the solution. First, the helical sideband force found in the EBT and the high- $\beta$  stellarator is not present; that is, the contribution of  $|\nabla_\perp \phi|^2 + h^2 |\phi|^2$  proportional to  $\cos\theta$  does not appear when  $\beta/\epsilon \ll 1$ . It may, however, make a contribution when  $\beta/\epsilon \sim 1$ . The conclusion is that in a conventional stellarator the helical sideband force may make quantitative changes in the equilibrium, but is not fundamental in producing toroidal force balance.

Second, the basic force that balances the outward toroidal force [i.e., the  $\beta'_0(r) \cos\theta$  term in Eq. (4.143)] is proportional to  $\iota_H \nabla^2 A_s$ . This can be interpreted as follows. To understand the restoring force, one must identify the  $\mathbf{J}$  and  $\mathbf{B}$  which interact to produce an inward  $\mathbf{J} \times \mathbf{B}$  force. The  $\mathbf{B}$  in this relation corresponds to  $\iota_H$ ; that is, in an approximate sense  $\iota_H$  represents the average helical field on a given pressure contour. The leading-order helical field, of order  $\delta$ , averages to zero because of the helical symmetry. However, since the surface itself has a small helical distortion, there is a higher-order  $\delta^2$  contribution which does not average to zero. This nonzero average is directly related to  $\iota_H$ , the helical vacuum transform. The  $\mathbf{J}$  appearing in the restoring force corresponds to  $\nabla^2 A_s$ . This quantity represents the so-called Pfirsch-Schluter toroidal dipole current, induced by the shift of the plasma and required to maintain  $\mathbf{J}$  divergence free. Thus the  $\iota_H \nabla^2 A$  term describing the interaction of the Pfirsch-Schluter currents with the average poloidal helical field represents the second of the helical restoring forces to provide toroidal force balance in current-free configurations.

The third point of interest concerns the effect of the vertical field. From the form of Eq. (4.143) it is apparent that the effect of an external vertical field  $B_v$  can be accounted for by adding the term  $B_v r \cos\theta$  to  $A_s$ . Since  $\nabla^2(B_v r \cos\theta) = 0$  it follows that the vertical field does not produce a net body force on the plasma. This should not be surprising, since there is no net current

flowing in a stellarator.

Fourth, a perhaps paradoxical point is that, even though a vertical field produces no net body force on the plasma, it does shift the plasma flux surfaces, as evidenced by Eq. (4.144). One possible resolution of this "paradox" is that, as the vertical field changes from one value to another, transient electric fields are induced which drive parallel currents. It is these currents interacting with the vertical field that produce a force. Once the transients decay, the vertical-field force vanishes. However, in evolving from one state to another, the Pfirsch-Schluter current continuously readjusts itself, so that after the transient there remains the correct dipole current to hold the plasma in its new equilibrium position. One conclusion from this discussion is that, regardless of its influence on stability, a vertical field is not required to produce toroidal stellarator equilibrium.

Nevertheless, the presence of the transverse fields  $A$  in the toroidal force balance relation completely alters the structure of the equilibrium equations; that is, in a conventional stellarator one has the freedom to apply whatever external transverse fields are desired, zero being a particular case. This freedom results because Eq. (4.142) is a partial differential equation with a corresponding freedom to specify boundary conditions. In a high- $\beta$  stellarator, the order of solving the equations is reversed, and  $A$  is only determined afterwards from Eq. (4.130). Since this is an algebraic relation, one is not free to specify boundary conditions and must simply apply whatever field is required. Because of the additional freedom, the conventional stellarator expansion constitutes a maximal ordering, as compared to the high- $\beta$  stellarator.

Whether the toroidal force balance is to be described by a partial differential equation or by an algebraic relation is determined by whether or not the transverse poloidal fields play a major role in producing the restoring force. This issue has been considered by Lortz and Nührenberg (1978), Spies (1978a) and Freidberg (1980). It appears that the transition criterion for any two- or three-dimensional toroidal configuration is given by

$$\beta q^2/\epsilon \begin{cases} \lesssim 1 & \text{differential equation} \\ \gg 1 & \text{algebraic relation} \end{cases} .$$

In summary, conventional stellarators, heliotrons, and torsatrons are toroidal helices, capable of achieving toroidal equilibria with no net toroidal current. Their  $\beta$ 's are in general lower than that in the EBT and the high- $\beta$  stellarator, but are comparable to those of the high- $\beta$  tokamak. In fact, if one considers a generalized hybrid tokamak-stellarator concept, then the high- $\beta$  tokamak and the pure stellarator (i.e.,  $\langle J_\phi \rangle = 0$ ) are both special examples corresponding to particular choices of  $\Phi$  and  $G$  in Eq. (4.142). As with other three-dimensional configurations, radial pressure balance is similar to that in a  $\theta$  pinch. However, the helical sideband force is not basic to toroidal force balance in these configurations as it is for the EBT and the high- $\beta$  stellarator. Instead, the interaction of the Pfirsch-Schluter

currents with the average helical field produces the restoring force. This force is negligible in the EBT and the high- $\beta$  stellarator. Moreover, a vertical field is not required for toroidal equilibrium, as it is in the tokamak.

## 5. The parallel current constraint

A final point of interest concerns the periodicity constraint which appears in the analysis of each of the three-dimensional concepts investigated: the EBT, the high- $\beta$  stellarator, and the conventional stellarator. Recall that, in each case, in order to calculate the fields to a certain given order, the analysis must be carried out several orders higher. Ultimately, a solvability condition arises in the form of a periodicity constraint, which then serves to determine the lower-order pressure contours.

The periodicity constraint occurs in a straightforward, natural way in the analysis and provides valuable insight into the nature of the toroidal restoring force. Nevertheless, substantial extra calculations of higher-order fields must be carried out to explicitly evaluate the constraint. This disadvantage can be eliminated by the derivation of a general form of the constraint which is valid for arbitrary toroidal geometry. The resulting expression is known as the "parallel current constraint," and its derivation is outlined below.

There are two methods by which the general constraint can be derived. The first is an obvious generalization of that used in the asymptotic analysis. Here one substitutes  $\mathbf{J} = \nabla \times \mathbf{B}$  into the momentum equation and then applies the operator  $(\mathbf{B} \cdot \nabla \times)$ . At this point no averaging along field lines is as yet carried out. In the second method, which is completely equivalent, one writes  $\nabla \cdot \mathbf{J} = \nabla \cdot (J_{||} \mathbf{e}_b + \mathbf{J}_\perp) = 0$  and then substitutes  $J_{||}$  from the momentum equation. Either procedure leads to the following equation for  $J_{||}$ :

$$\mathbf{e}_b \cdot \nabla \left( \frac{J_{||}}{B} \right) = \frac{1}{B^2} (\mathbf{e}_b \cdot \nabla p \times \boldsymbol{\kappa}) . \quad (4.145)$$

Note that there are a number of ways to rewrite the right-hand side using the equilibrium relations. The specific form shown has been chosen so that the leading-order contribution to the right-hand side is already small in any of the standard expansions. For this reason it is unnecessary to calculate explicit higher-order fields to evaluate the periodicity constraint.

Consider now two different situations. In the first, assume that the configurations of interest have closed lines or, for ergodic systems, that attention is focused on the rational surfaces. One now integrates Eq. (4.145) along one full circuit of a magnetic line (i.e., until it closes on itself). Since  $J_{||}$  must be single-valued, the left-hand contribution vanishes. What remains is the parallel current constraint, which must be satisfied on each magnetic line,

$$\oint \frac{dl}{B^2} (\mathbf{e}_b \cdot \nabla p \times \boldsymbol{\kappa}) = 0 . \quad (4.146)$$

Equation (4.146) can be viewed as a constraint on the line-averaged toroidal forces, which, when satisfied, guarantees that the  $J_{||}$  required to make  $\nabla \cdot \mathbf{J} = 0$  is single valued.

For the second situation, when the flux surfaces are ergodic, the constraint is slightly modified. Equation (4.145) is multiplied by  $B$  and then integrated over the volume enclosed by a given flux surface. Again, the left-hand contribution vanishes, since  $\mathbf{n} \cdot \mathbf{B} = 0$  on a  $\psi = \text{const}$  surface. The remaining expression is a flux surface average generalization of the parallel current constraint given by

$$\int_S \frac{dS}{B |\nabla\psi|} (\mathbf{e}_b \cdot \nabla p \times \boldsymbol{\kappa}) = 0. \quad (4.147)$$

Here the integration is carried out over the area of the flux surface. Equation (4.147) must be satisfied for every value of  $\psi$ .

In summary, the periodicity constraint appearing in the asymptotic analysis of certain three-dimensional configurations can be generalized to arbitrary toroidal geometries. The resulting parallel current constraint is significantly simpler to evaluate, since its leading-order contribution is already small. This can save considerable effort in the analysis.

### E. Summary

In this section it has been shown how the MHD model can be used to describe the basic equilibrium properties of magnetically confined plasmas.

The equilibria of interest are in general toroidal and are characterized by a set of nested, closed, magnetic flux surfaces. The problem of achieving equilibrium in such systems separates into two distinct parts. First, the plasma must be held in radial pressure balance in order that it be isolated from the surrounding walls. This can be accomplished by either  $\theta$ -pinch or  $Z$ -pinch confinement, or any combination thereof. Second, the magnetic configuration must be such that the outward toroidal drift force, inherent in any toroidal system, is somehow compensated for.

Concerning toroidal force balance, it was pointed out that the  $Z$  pinch has favorable toroidal equilibrium properties but poor stability. The opposite is true for the  $\theta$  pinch. This basic conflict has led to a wide variety of different concepts which attempt, by various combinations, to optimize the good features while minimizing the unfavorable ones.

Three basic methods were described to compensate for the toroidal drift force. First, if sufficient toroidal current flows, toroidal force balance may be achieved by the interaction of this current with image currents induced by a perfectly conducting shell or with an externally applied vertical field. Such configurations can possess toroidal axisymmetry and include the various types of tokamaks and the RFP. In the second method, toroidal force balance is achieved by the generation of a helical sideband force induced when the plasma shifts

away from the geometric center of the applied helical field or when an additional sideband field is externally applied. This type of equilibrium is in general three-dimensional and thus considerably more difficult to analyze. Nevertheless, it is of considerable interest since it can exist without any net toroidal current. Included in this case are the EBT and the high- $\beta$  stellarator. Third, in conventional, low- $\beta$  stellarators the dominant restoring force is not the helical sideband force, but the force resulting from the interaction of the Pfirsch-Schlüter currents and the poloidal component of the helical magnetic field averaged over the surface.

In summary, the MHD model provides a very reliable description of the equilibria of magnetically confined fusion plasmas.

## V. STABILITY

### A. Introduction

This section is concerned with determining the stability of ideal MHD equilibria. The goal is to develop an understanding of the various mechanisms which drive instabilities and to discuss possible ways to avoid them. Equally important, it is shown why many of the particular equilibria discussed in Sec. IV have favorable stability properties, thus at least partially justifying their prominence in the international fusion program.

There are a number of techniques available for investigating ideal MHD stability. By far the greatest effort is devoted to linear stability analysis. Because of this and the fact that physical intuition is most easily acquired when analytic treatment is possible, the present review is almost exclusively concerned with linear stability. Other techniques, which are only briefly mentioned, include nonlinear analysis and large-scale numerical simulation.

The beginning of Sec. V outlines the basic concepts and formulates the general linearized MHD stability problem. In addition there is a discussion of some general properties common to all geometries.

The second part discusses applications to various equilibria. Because of the enormous volume of literature available, this discussion is restricted to the currently most promising concepts in the United States fusion program: the tokamak, the EBT and the RFP. While there is renewed interest in the stellarator, as a result of some very encouraging results from the W VIIA experiments (Bartlett *et al.*, 1980), this concept still remains a relatively minor part of the national fusion program. Thus the stellarator is not included in the stability discussion. A recent review of stellarator theory and experiment is that of Miyamoto (1978). Note again that the important mirror concept is not included because of the basic inapplicability of the ideal MHD model. For a summary of the mirror concept one should refer to the recent articles by Baldwin (1977), Fowler and Logan (1977), and Baldwin and Logan (1979).

It is also useful to mention that a number of more de-

tailed reviews of the MHD stability theory for specific concepts have appeared recently. In particular, for tokamaks one should see Furth (1975), Wesson (1978), Bateman (1978), and Bateman and Sigmar (1982). The stability of the EBT has been summarized by Nelson and Hedrick (1979), while reviews of the RFP have been given by Robinson (1971) and Bodin and Newton (1980).

## B. Basic theoretical concepts

### 1. Exponential stability: the homogeneous plasma

As a useful starting point for stability analysis, consider the configuration in which the magnetic field is infinite, homogeneous, and unidirectional. This system, which is not toroidal and does not confine plasma, is nonetheless very useful to investigate, for its stability corresponds to a determination of the basic waves which propagate in an MHD plasma and thus forms the foundation upon which intuition is developed.

The equilibrium of the homogeneous system is given by

$$\begin{aligned} \mathbf{B} &= B_0 \mathbf{e}_z, \quad \rho = \rho_0, \\ \mathbf{J} &= 0, \quad \mathbf{v} = 0, \\ p &= p_0, \end{aligned} \quad (5.1)$$

where  $B_0$ ,  $\rho_0$ , and  $p_0$  are constants and where it has been assumed that  $\mathbf{B}$  points in the  $\mathbf{e}_z$  direction. Note that this "equilibrium" has no gradients, so that  $\nabla p = \nabla \rho = \mathbf{J} = 0$ .

The linear stability of this configuration is determined by linearizing all quantities as follows:  $Q(\mathbf{r}, t) = Q_0 + Q_1(\mathbf{r}, t)$  with  $Q_1$  being a small first-order perturbation. Since the equilibrium is both time- and space-independent, the most general form of perturbation can be written as

$$\begin{aligned} Q_1(\mathbf{r}, t) &= \hat{Q}_1 \exp[-i(\omega t - \mathbf{k} \cdot \mathbf{r})], \\ \mathbf{k} &= k_{\perp} \mathbf{e}_y + k_{||} \mathbf{e}_z, \\ \mathbf{k} \cdot \mathbf{r} &= k_{\perp} y + k_{||} z. \end{aligned} \quad (5.2)$$

Here, without loss in generality, it has been assumed that the wave vector  $\mathbf{k}$  lies in the  $(y, z)$  plane. Also, the subscripts  $\perp$  and  $||$  refer, respectively, to directions perpendicular and parallel to the *equilibrium* magnetic field.

It is appropriate at this point to more precisely define stability and instability. With very few exceptions the simplest and most reliable definition corresponds to exponential stability; that is, if any of the eigenfrequencies  $\omega$  correspond to exponential growth, the system is exponentially unstable. If not, it is exponentially stable:

$$\text{Im}\omega > 0 \text{ exponential instability.} \quad (5.3)$$

Implicit in this definition is the assumption that the modes are discrete with distinguishable eigenfrequencies. This is not true in general. However, no difficulties arise for the homogeneous equilibrium. Perhaps more impor-

tant, no problems exist for the general case if one is interested only in the unstable part of the spectrum (i.e., in whether or not a plasma is exponentially unstable). These questions and the frequency spectrum of ideal MHD are discussed in more detail in Sec. V.B.3. [More detailed discussions of the MHD spectrum include those of Grad (1973), Goedbloed (1975), Tataronis and Grossmann (1977), and Goedbloed (1979).]

Continuing with the homogeneous problem, one substitutes Eq. (5.2) into the linearized MHD equations. After some straightforward algebra (not using the momentum equation), all quantities can be expressed in terms of the perturbed velocity  $\mathbf{v}_1$ . The result is

$$\begin{aligned} \omega \rho_1 &= -\rho_0 (\mathbf{k} \cdot \mathbf{v}_1), \\ \omega p_1 &= -\gamma p_0 (\mathbf{k} \cdot \mathbf{v}_1), \\ \omega \mathbf{B}_1 &= \mathbf{k} \times (\mathbf{v}_1 \times \mathbf{B}_0), \\ \omega \mathbf{J}_1 &= i \mathbf{k} \times [\mathbf{k} \times (\mathbf{v}_1 \times \mathbf{B}_0)]. \end{aligned} \quad (5.4)$$

Substituting this into the linearized momentum equation and setting the resultant determinant to zero yields the following dispersion relation:

$$\begin{aligned} \omega^2 &= k_{||}^2 V_a^2, \\ \omega^2 &= \frac{1}{2} k^2 (V_s^2 + V_a^2) [1 \pm (1 - \alpha^2)^{1/2}], \\ \alpha^2 &= 4 \frac{k_{||}^2}{k^2} \frac{V_s^2 V_a^2}{(V_s^2 + V_a^2)^2}, \end{aligned} \quad (5.5)$$

where  $k^2 = k_{\perp}^2 + k_{||}^2$ ,  $V_s = (\gamma p_0 / \rho_0)^{1/2}$  is the adiabatic sound speed, and  $V_a = (B_0^2 / \rho_0)^{1/2}$  is the Alfvén speed. Note that there are three branches to the dispersion relation, and since  $0 \leq \alpha^2 \leq 1$  they all correspond to purely oscillatory solutions. Consequently  $\text{Im}(\omega) = 0$  for each mode, and the homogeneous magnetic field configuration is exponentially stable. This is not surprising, since this system is in thermodynamic equilibrium, and there are no sources of free energy available to drive instabilities.

The first branch of the dispersion relation  $\omega_a^2 = k_{||}^2 V_a^2$  is known as the shear Alfvén wave. Its polarization is such that the perturbed magnetic field and velocity are always perpendicular to  $\mathbf{B}_0$  and  $\mathbf{k}$ ; the wave is purely transverse. This produces a shear in the magnetic field and causes the magnetic field lines to bend. It also results in an incompressible flow,  $\nabla \cdot \mathbf{v}_1 = p_1 = 0$ . The shear Alfvén wave describes a basic oscillation between perpendicular plasma kinetic energy and perpendicular "line bending" magnetic energy.

The second branch of the dispersion relation (i.e., the  $+$  sign) describes the fast magnetoacoustic wave  $\omega_f^2$ . A simple calculation shows that  $\omega_f^2 \geq \omega_a^2$ . This is a wave in which both the magnetic field and the plasma pressure are compressed, so that  $\nabla \cdot \mathbf{v}_1 \neq 0$ , and  $\mathbf{B}_1$  has both  $y$  and  $z$  components. In the interesting limit  $\beta \sim V_s^2 / V_a^2 \ll 1$ , the fast magnetoacoustic wave reduces to the compressional Alfvén wave  $\omega_f^2 \approx (k_{\perp}^2 + k_{||}^2) V_a^2$ . Here the wave is nearly transverse ( $v_{1y} \gg v_{1z}$ ) and describes an oscillation between perpendicular plasma ki-

netic energy and the combined magnetic compressional and line bending energies.

The third branch of the dispersion relation corresponds to the slow magnetoacoustic wave  $\omega_s^2$ . This wave always satisfies  $\omega_s^2 \leq \omega_a^2$ . Its polarization is similar to that of the fast magnetoacoustic wave and thus also represents a compression of both plasma and magnetic energy. In the limit  $V_s^2/V_a^2 \ll 1$  the slow magnetoacoustic wave reduces to a sound wave  $\omega_s^2 \approx k_{\parallel}^2 V_s^2$ . Here the mode is nearly longitudinal (i.e.,  $v_{1z} \gg v_{1y}$ ) and describes a basic oscillation between parallel plasma kinetic energy and plasma internal energy.

It is interesting to note that if one repeats this calculation for the perpendicular MHD model, the resulting dispersion relation consists of two branches given by

$$\begin{aligned}\omega^2 &= k_{\parallel}^2 V_a^2 \\ \omega^2 &= (k_{\perp}^2 + k_{\parallel}^2) V_a^2.\end{aligned}\quad (5.6)$$

These correspond to the shear Alfvén and compressional Alfvén waves, respectively. The sound wave is suppressed. This result can be obtained from the ideal MHD dispersion relation by setting  $\gamma=0$  and suppressing the slow magnetoacoustic wave.

The three waves given by Eq. (5.5) describe the basic wave propagation characteristics of an ideal MHD plasma. In the homogeneous geometry, all are stable. In more physically interesting inhomogeneous geometries, each of these waves is modified and can couple to the others. An important result concerning stability is that, for reasons to be discussed later, the most unstable perturbations almost always involve the shear Alfvén wave.

## 2. General linearized stability equations

The stability of an arbitrary MHD equilibrium can be investigated by means of the general linearized equations of motion. [See, for instance, Bernstein *et al.* (1958), Goedbloed (1979).] These equations can be formulated either as an initial-value problem or a normal-mode problem. To begin with, consider the initial-value formulation and assume that a static, ideal MHD equilibrium, satisfying

$$\begin{aligned}\mathbf{J}_0 \times \mathbf{B}_0 &= \nabla p_0, \quad \nabla \times \mathbf{B}_0 = \mathbf{J}_0, \\ \nabla \cdot \mathbf{B}_0 &= 0, \quad v_0 = 0,\end{aligned}\quad (5.7)$$

is given. All quantities are then linearized about this background state:  $Q(\mathbf{r}, t) = Q_0(\mathbf{r}) + \tilde{Q}_1(\mathbf{r}, t)$ , with  $\tilde{Q}_1/Q_0 \ll 1$ . When substituting into the MHD equations, it is convenient to express all perturbed quantities in terms of a vector  $\tilde{\xi}$  defined by

$$\tilde{\mathbf{v}}_1 \equiv \frac{\partial \tilde{\xi}}{\partial t}. \quad (5.8)$$

Note that  $\tilde{\xi}$  represents the displacement of the plasma away from equilibrium. In an initial-value formulation one needs to specify appropriate initial data. A very useful (but not completely general) choice of initial data for

stability problems is as follows:

$$\begin{aligned}\tilde{\xi}(\mathbf{r}, 0) &= \tilde{\mathbf{B}}_1(\mathbf{r}, 0) = \tilde{\rho}_1(\mathbf{r}, 0) = \tilde{p}_1(\mathbf{r}, 0) = 0, \\ \frac{\partial \tilde{\xi}}{\partial t}(\mathbf{r}, 0) &= \tilde{\mathbf{v}}_1(\mathbf{r}, 0) \neq 0.\end{aligned}\quad (5.9)$$

This corresponds to the situation where, at  $t=0$ , the plasma is in its exact equilibrium position but is moving away with a small velocity  $\tilde{\mathbf{v}}_1(\mathbf{r}, 0)$ . Under such conditions the linearized form of the equation for conservation of mass, the energy relation, and Faraday's law give, respectively,

$$\begin{aligned}\tilde{\rho}_1 &= -\nabla \cdot (\rho_0 \tilde{\xi}), \\ \tilde{p}_1 &= -\tilde{\xi} \cdot \nabla p_0 - \gamma p_0 \nabla \cdot \tilde{\xi}, \\ \tilde{\mathbf{B}}_1 &= \nabla \times (\tilde{\xi} \times \mathbf{B}_0).\end{aligned}\quad (5.10)$$

These quantities can be substituted into the momentum equation yielding a single, vector equation for the displacement  $\tilde{\xi}$ :

$$\rho_0 \frac{\partial^2 \tilde{\xi}}{\partial t^2} = \mathbf{F}(\tilde{\xi}), \quad (5.11)$$

where  $\mathbf{F}(\tilde{\xi}) = \mathbf{J}_0 \times \tilde{\mathbf{B}}_1 + \tilde{\mathbf{J}}_1 \times \mathbf{B}_0 - \nabla \tilde{p}_1$  can be written as

$$\mathbf{F}(\tilde{\xi}) = (\nabla \times \mathbf{B}_0) \times \tilde{\mathbf{Q}} + (\nabla \times \tilde{\mathbf{Q}}) \times \mathbf{B}_0 + \nabla(\tilde{\xi} \cdot \nabla p_0 + \gamma p_0 \nabla \cdot \tilde{\xi}) \quad (5.12)$$

and  $\tilde{\mathbf{Q}} \equiv \tilde{\mathbf{B}}_1 = \nabla \times (\tilde{\xi} \times \mathbf{B}_0)$ . Equation (5.11), subject to  $\tilde{\xi}(\mathbf{r}, 0) = 0$ ,  $\partial \tilde{\xi}(\mathbf{r}, 0)/\partial t = \tilde{\mathbf{v}}_1(\mathbf{r}, 0)$ , and appropriate boundary conditions (as discussed in Sec. III.B), constitutes the formulation of the general linearized stability equation as an initial-value problem. The initial-value approach has the advantage of directly determining the actual time evolution of a given initial perturbation. It is also useful in a number of ways when numerically formulating the full nonlinear problem (Sykes and Wesson, 1974, and Bateman *et al.*, 1974). The drawbacks are that it often contains much more information than is required to determine stability, one consequence of which is that numerical calculations are often very time consuming.

A more efficient way to investigate linear stability is to reformulate Eq. (5.11) as a normal-mode problem (Bernstein *et al.*, 1958). This can easily be done by letting all perturbed quantities vary as follows:  $\tilde{Q}_1(\mathbf{r}, t) = Q_1(\mathbf{r}) \exp(-i\omega t)$ . Since the right-hand sides of Eqs. (5.10) and (5.11) contain no explicit time derivatives, the normal-mode formulation of ideal MHD stability, expressed in terms of the transformed variables has the form

$$\rho_1 = -\nabla \cdot \rho_0 \tilde{\xi}, \quad (5.13)$$

$$p_1 = -\tilde{\xi} \cdot \nabla p_0 - \gamma p_0 \nabla \cdot \tilde{\xi}, \quad (5.14)$$

$$\mathbf{Q} \equiv \mathbf{B}_1 = \nabla \times (\tilde{\xi} \times \mathbf{B}_0), \quad (5.15)$$

$$\begin{aligned}-\omega^2 \rho_0 \tilde{\xi} &= \mathbf{F}(\tilde{\xi}) \\ &= (\nabla \times \mathbf{Q}) \times \mathbf{B}_0 + (\nabla \times \mathbf{B}_0) \times \mathbf{Q} - \nabla p_1.\end{aligned}\quad (5.16)$$

In this approach only appropriate boundary conditions

on  $\xi$  need be specified, so that Eq. (5.16) can be solved as an eigenvalue equation for the eigenvalue  $\omega^2$ . The normal-mode method is more amenable to analysis than the initial-value approach, and more efficient with respect to numerical computations (Freidberg and Marder, 1973; Grimm *et al.*, 1976; and Berger *et al.*, 1977a). However, there is no obvious way to exploit these advantages in a full nonlinear formulation. Finally, there is a subtlety involved with the normal-mode approach; its usefulness is strongly coupled to the assumption that for the problems of interest the eigenvalues are discrete and distinguishable, so that the concept of exponential stability is valid. While this is likely true for the unstable part of the spectrum, the full situation is more complicated, and to obtain a more complete understanding, additional detailed knowledge of the properties of the force operator  $\mathbf{F}$  is required. These questions are discussed in the next section.

### 3. Properties of the force operator $\mathbf{F}$

The force operator  $\mathbf{F}$  possesses an important mathematical property which greatly aids in the analysis of linearized MHD stability. In particular,  $\mathbf{F}$  is a self-adjoint operator. This implies that the eigenvalues  $\omega^2$  are purely real. Hence stability transitions always occur when  $\omega^2$  crosses zero, rather than at some general point on the real axis where  $\text{Re}(\omega) \neq 0$ . This fact ultimately leads to an elegant and efficient formulation for testing linear stability known as the Energy Principle, which is discussed in the next section.

Finally, a further examination of the properties of  $\mathbf{F}$  shows that the frequency spectrum consists not only of discrete modes, but of continua as well. Fortunately, in most cases of interest so far investigated, the continua lie on the stable side of the  $\omega$  plane or at most reach the origin,  $\omega^2 = 0$ . Thus when attention is restricted to exponential instabilities there is strong justification for using the normal-mode approach.

Each of these issues is now discussed separately.

#### a. Self-adjointness of $\mathbf{F}$

As stated, the self-adjointness of  $\mathbf{F}$  has a major impact on both the analytic and the numerical formulation of linearized MHD stability. To demonstrate this property, it is necessary to show that for any vectors  $\tilde{\xi}$  and  $\tilde{\eta}$  satisfying appropriate boundary conditions, such as those discussed in Sec. III.B, the following relation holds:

$$\int \tilde{\eta} \cdot \mathbf{F}(\tilde{\xi}) d\mathbf{r} = \int \tilde{\xi} \cdot \mathbf{F}(\tilde{\eta}) d\mathbf{r}. \quad (5.17)$$

Equation (5.17) can be derived by a direct but lengthy calculation. A more elegant derivation has been given by Bernstein *et al.* (1958), and it is this calculation which is outlined here.

The proof is based on the fact that the total energy of the system is an exact nonlinear constant; that is, as shown in Sec. III,

$$\frac{dH}{dt} = \frac{d}{dt} \int \left[ \frac{1}{2} \rho v^2 + \frac{1}{2} \mathbf{B}^2 + \frac{p}{\gamma - 1} \right] d\mathbf{r} = 0. \quad (5.18)$$

For simplicity, it is assumed that the plasma is surrounded by a perfectly conducting wall. However, the proof can easily be generalized to include boundary conditions which allow a vacuum region between plasma and wall.

The integrand in Eq. (5.18) is linearized and expanded to second order in amplitude. The zeroth-order contribution trivially vanishes, since the equilibrium quantities are time independent. The first-order contribution, combined with Eq. (5.10), yields the ideal MHD equilibrium equations. The second-order energy can be written as  $H_2 = K + \delta W$ , where

$$K = \frac{1}{2} \int \rho_0 \left[ \frac{\partial \tilde{\xi}}{\partial t} \right]^2 d\mathbf{r},$$

$$\delta W = \delta W(\tilde{\xi}, \tilde{\xi}). \quad (5.19)$$

Although  $\delta W$  can be calculated, its specific form is not required. The important feature is that  $\delta W$  is quadratic in  $\tilde{\xi}$  and is not explicitly dependent on  $\partial \tilde{\xi} / \partial t$ . The latter point, which is crucial in the derivation, follows because the relevant part of the integrand is a function of  $\tilde{\mathbf{B}}_1$ ,  $\tilde{\mathbf{B}}_2$ ,  $\tilde{p}_1$ , and  $\tilde{p}_2$ . Equation (5.10) shows that  $\tilde{\mathbf{B}}_1$  and  $\tilde{p}_1$  are independent of  $\partial \tilde{\xi} / \partial t$ . As a result it is straightforward to show that  $p$  and  $\mathbf{B}$  are independent of  $\partial \tilde{\xi} / \partial t$  to all orders in the amplitude (Bernstein *et al.*, 1958). The conservation of energy then implies that  $H_1 = K + \delta W = 0$ , or

$$\int \rho_0 \frac{\partial \tilde{\xi}}{\partial t} \cdot \frac{\partial \tilde{\xi}}{\partial t} d\mathbf{r} = -\delta W \left[ \tilde{\xi}, \frac{\partial \tilde{\xi}}{\partial t} \right] - \delta W \left[ \frac{\partial \tilde{\xi}}{\partial t}, \tilde{\xi} \right]. \quad (5.20)$$

Substituting Eq. (5.11) into the left-hand side of equation (5.20) leads to

$$\int \frac{\partial \tilde{\xi}}{\partial t} \cdot \mathbf{F}(\tilde{\xi}) d\mathbf{r} = -\delta W \left[ \tilde{\xi}, \frac{\partial \tilde{\xi}}{\partial t} \right] - \delta W \left[ \frac{\partial \tilde{\xi}}{\partial t}, \tilde{\xi} \right]. \quad (5.21)$$

Since  $\tilde{\xi}$  and  $\partial \tilde{\xi} / \partial t$  are in general independent vectors, each satisfying the boundary conditions,  $\partial \tilde{\xi} / \partial t$  can be replaced by  $\tilde{\eta}$ . The self-adjointness property then follows immediately by interchanging  $\tilde{\xi}$  and  $\tilde{\eta}$  and noting the symmetry on the right-hand side of Eq. (5.21).

Finally, for the special choice  $\tilde{\eta} = \tilde{\xi}$ , it follows that

$$\delta W(\tilde{\xi}, \tilde{\xi}) = -\frac{1}{2} \int \tilde{\xi} \cdot \mathbf{F}(\tilde{\xi}) d\mathbf{r}. \quad (5.22)$$

Thus the relation  $K + \delta W = 0$  has the following simple interpretation. The quantity  $K$  represents the kinetic energy of the perturbation.  $\delta W$  represents the change in the potential energy associated with the perturbation and is equal to the work done against the force  $\mathbf{F}$  in displacing the plasma by an amount  $\tilde{\xi}$ . Since the total energy is conserved, the change in the kinetic plus potential energy must equal zero.

### b. Real $\omega^2$

By making use of the self-adjointness of  $F$ , it is straightforward to show that for any discrete normal mode, the corresponding eigenvalue  $\omega^2$  is purely real (Bernstein *et al.*, 1958). The proof is obtained by forming the dot product of Eq. (5.16) with  $\xi^*(\mathbf{r})$  and integrating over the plasma volume. The result is

$$\omega^2 \int \rho_0 |\xi|^2 d\mathbf{r} = - \int \xi^* \cdot \mathbf{F}(\xi) d\mathbf{r}. \quad (5.23)$$

The procedure is then repeated with the vector  $\xi(\mathbf{r})$  and the complex conjugate of Eq. (5.16). Using the self-adjoint property of  $F$ , it follows that

$$(\omega^2 - \omega^{*2}) \int \rho_0 |\xi|^2 d\mathbf{r} = 0 \quad (5.24)$$

or  $\omega^2 = \omega^{*2}$ ; that is,  $\omega^2$  is purely real. Furthermore, the fact that the differential operators in Eq. (5.16) are real implies that  $\xi(\mathbf{r})$  itself is real.

In terms of the definition of exponential stability, a normal mode with  $\omega^2 > 0$  corresponds to a pure oscillation and hence would be considered stable. Conversely, for a mode with  $\omega^2 < 0$ , one branch must grow exponentially and thus would correspond to instability. Clearly, the transition from stability to instability occurs when  $\omega^2 = 0$ . It is worthwhile emphasizing the importance of this result. In general, a stability transition occurs when  $\text{Im}(\omega) = 0$  with  $\text{Re}(\omega) \neq 0$ . This makes the determination of marginal stability boundaries considerably more complicated, since  $\text{Re}(\omega)$  must also be calculated. However, in ideal MHD the self-adjointness of  $F$  guarantees that, at any stability boundary  $\text{Im}(\omega) = 0$ , the  $\text{Re}(\omega)$  must also be zero simultaneously.

Finally, it is worth noting that a derivation similar to the one given above shows that for two discrete normal modes  $(\xi_n, \omega_n^2), (\xi_m, \omega_m^2)$  the following relation must hold:

$$(\omega_n^2 - \omega_m^2) \int \rho_0 \xi_m^* \xi_n d\mathbf{r} = 0$$

where use has been made of the self-adjointness of  $F$ . This demonstrates that the normal modes are orthogonal.

### c. Spectrum of $F$

Because of the self-adjointness of  $F$ , one is strongly motivated to choose the normal-mode approach rather than the initial-value approach when considering the linearized stability of ideal MHD plasmas. In fact, if the operator  $F$  allowed only discrete eigenvalues, the concept of exponential stability could easily be extended to include both oscillatory and damped motions of the plasma. However, this is not the case. To show this in detail would require a complete spectral analysis of the force operator  $F$ , a task beyond the scope of the present work and one which has indeed only been carried out for special MHD equilibria. Nevertheless, it is worthwhile to indicate typical spectral properties which can occur and their influence on stability, based on these calculations (Grad, 1973; Goedbloed, 1975, 1979).

The spectral properties of  $F$  follow from an examination

of the operator  $(F/\rho_0 - \lambda)^{-1}$  for all complex  $\lambda$ . If this operator exists and is bounded for a given  $\lambda$ , the linearized inhomogeneous MHD equations  $(F/\rho_0 - \lambda)\xi = \mathbf{a}$  (which would occur when solving an initial-value problem by Laplace transforms) can be inverted to yield  $\xi = (F/\rho_0 - \lambda)^{-1}\mathbf{a}$ . The spectrum of  $F$  consists of those values of  $\lambda$  for which the operator  $(F/\rho_0 - \lambda)^{-1}$  cannot be inverted. There are two important cases. First, the familiar situation when  $\lambda$  is such that  $(F/\rho_0 - \lambda)\xi = 0$  possesses a nontrivial solution. These values of  $\lambda$  correspond to the point or discrete spectra of  $F$  and represent the normal-mode eigenvalues to be examined for exponential stability. In this case it is clear that the operator  $(F/\rho_0 - \lambda)^{-1}$  does not exist.

In the second case of interest,  $\lambda$  is such that  $(F/\rho_0 - \lambda)^{-1}$  exists but is unbounded [e.g.,  $(F/\rho_0 - \lambda) = k_{||} V_d^2(r) - \lambda = 0$ ]. Usually there is a continuous range of  $\lambda$  (determined by varying  $r$  in the range of  $0 < r < r_{\text{wall}}$ ) over which the operator is ill behaved. A typical ideal MHD spectrum is illustrated schematically in Fig. 28. Notice that the continuous spectra could significantly increase the complexity of determining plasma stability if the corresponding frequencies were located in that part of the complex  $\omega$  plane where  $\text{Im}(\omega) > 0$ . Fortunately this appears not to be the case. In most problems of interest thus far investigated containing continua, the frequencies are located on the real axis (i.e.,  $\omega^2 > 0$ ). Grad has conjectured that this should be true for any arbitrary static ideal MHD equilibrium. Recent studies show that this conjecture is still unresolved and somewhat controversial. A calculation by Spies (1979) indicates that in certain special cases unstable continua exist. A recent calculation by Tataronis and Salat (1981) implies that for general three-dimensional geometries no unstable continua exist.

One consequence of the existence of a continuum is that discrete modes can accumulate at either of its boundaries. If one boundary extends to the origin  $\omega^2 = 0$ , as it often does, it is possible to have an accumulation of unstable modes with growth rates approaching zero (see Fig. 28). Although such behavior is perfectly acceptable mathematically, if not accounted for properly it can obscure the concept of marginal stability. On the other hand, if it is known that a continuum extends to the origin, it is often possible to derive an analytic criterion, depending only upon the equilibrium quantities, which determines whether or not there is an accumulation of unstable modes. This procedure is far simpler than computing normal modes and gives rise to sufficient conditions for instability.

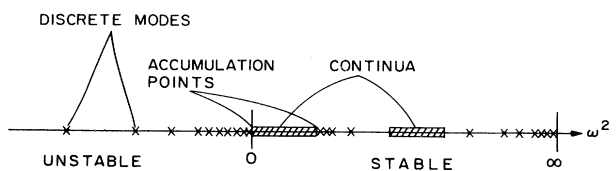


FIG. 28. Schematic diagram of a typical ideal MHD spectrum.

In summary, the spectrum of the force operator  $\mathbf{F}(\xi)$  contains both discrete eigenvalues and continua. It is very likely that the continua exist only for  $\omega^2 > 0$ . This assertion provides further motivation for examining plasma stability by the normal-mode approach, restricting attention only to the question of whether or not exponentially growing modes exist. Even so, the situation can become somewhat complicated as  $\omega^2 \rightarrow 0$ , since unstable modes can either accumulate or make smooth transitions from instability to stability.

#### 4. The Energy Principle

The stability of any given magnetic configuration as determined by the normal-mode approach requires the solution of ordinary or partial differential equations. In this section it is shown that the general stability problem can be recast in the form of a variational principle, thus providing an integral description of linearized MHD. Furthermore, if the primary goal is a determination only of whether a system is stable or not, as opposed to a calculation of specific growth rates (which can often be easily estimated), one can derive a powerful minimizing principle based on the conservation of energy. This formulation is known as the Energy Principle and represents the most efficient and often the most intuitive method of determining plasma stability (Bernstein *et al.*, 1958). It receives wide application in the literature and will be used extensively in the remainder of Sec. V.

The Energy Principle can be applied in a direct manner to systems in which the plasma is surrounded by a conducting wall. It also applies, in principle, to the situation where a vacuum region is present. However, in this case the actual calculations can become somewhat cumbersome because of the complicated boundary conditions across the plasma-vacuum interface, specifically the linearized pressure balance condition. These difficulties are resolved by means of the extended Energy Principle, in which the vacuum contribution is explicitly isolated, thereby eliminating the need for the pressure balance jump condition.

With the establishment of the extended Energy Principle, it then becomes useful to display several convenient forms of the energy integral which are often utilized in carrying out specific calculations. Finally, the concept of  $\sigma$  stability is discussed briefly; this variation of the Energy Principle provides a useful procedure for numerically calculating MHD stability and, in particular, avoids the problems that occur when  $\omega^2 \rightarrow 0$  (Goedbloed and Sakanaka, 1974).

##### a. Variational formulation

The linearized normal-mode equations describing ideal MHD stability can be cast in a variational form as follows [see, for instance, Bernstein *et al.* (1958) or Goedbloed (1979)]. Consider  $\Omega^2(\xi^*, \xi)$  to be a functional of  $\xi$  defined by

$$\begin{aligned}\Omega^2(\xi^*, \xi) &= \frac{\delta W(\xi^*, \xi)}{K(\xi^*, \xi)}, \\ \delta W(\xi^*, \xi) &= -\frac{1}{2} \int \xi^* \cdot \mathbf{F}(\xi) d\mathbf{r}, \\ K(\xi^*, \xi) &= \frac{1}{2} \int \rho_0(\xi^* \cdot \xi) d\mathbf{r}. \end{aligned}\quad (5.25)$$

Although  $\xi(\mathbf{r})$  has been shown to be real, it is treated as complex in Eq. (5.25) in anticipation of cases where, because of symmetry, several spatial coordinates can be Fourier analyzed. The variational principle states that any allowable function  $\xi$  for which  $\Omega^2$  becomes stationary is an eigenfunction of the ideal MHD normal-mode equations with eigenvalue  $\omega^2 = \Omega^2(\xi^*, \xi)$ . The proof follows by letting  $\xi \rightarrow \xi + \delta\xi$  and setting the resulting  $\delta\Omega^2 = 0$  (corresponding to  $\Omega^2$  being stationary). After some simple rearranging, one finds

$$\frac{\delta W(\delta\xi^*, \xi) + \delta W(\xi^*, \delta\xi)}{K(\delta\xi^*, \xi) + K(\xi^*, \delta\xi)} = \frac{\delta W(\xi^*, \xi)}{K(\xi^*, \xi)} \equiv \omega^2. \quad (5.26)$$

Using the self-adjoint property of  $\mathbf{F}$ , Eq. (5.26) can be written as

$$\int d\mathbf{r} \{ \delta\xi^* \cdot [\mathbf{F}(\xi) + \omega^2 \rho_0 \xi] + \delta\xi \cdot [\mathbf{F}(\xi^*) + \omega^2 \rho_0 \xi^*] \} = 0. \quad (5.27)$$

Since  $\delta\xi$  is arbitrary, Eq. (5.27) implies that

$$-\omega^2 \rho_0 \xi = \mathbf{F}(\xi). \quad (5.28)$$

This completes the proof and shows that the normal-mode eigenvalue equation [Eq. (5.16)] and the variational principle [Eq. (5.25)] are equivalent formulations of linearized ideal MHD stability.

##### b. Statement and proof of the Energy Principle

It is often of primary interest to determine whether a given system is stable or unstable, without being particularly concerned about the specific values of growth rates. The reason is that the growth times ( $\tau \lesssim 50 \mu\text{sec}$ ) are typically much shorter than experimental times ( $\tau \gtrsim 1 \text{ msec}$ ). Thus it is far more important to determine the conditions for avoiding instability than to calculate precise growth rates. In such cases, the variational formulation just derived can be further simplified, leading to a more convenient procedure which exactly determines stability boundaries but only estimates growth rates. This simplified formulation is known as the Energy Principle (Bernstein *et al.*, 1958).

The physical basis for the Energy Principle is the fact that energy is exactly conserved in the ideal MHD model. As a consequence, the most negative stationary value of  $\Omega^2(\xi, \xi)$  actually corresponds to a minimum in the potential energy. This in turn implies that the question of stability or instability can be determined by analyzing only the sign of  $\delta W(\xi, \xi)$  and not the full variational problem. Specifically, the Energy Principle states that an equilibrium is stable if and only if

$$\delta W(\xi, \xi) \geq 0 \quad (5.29)$$

for all allowable displacements (i.e.,  $\xi$  bounded in energy and satisfying boundary conditions). The proof of this assertion will be given shortly. Assuming the proof, consider the advantages that follow. First, if one has some intuition about the form of an unstable perturbation, this form can be substituted into  $\delta W$  as a trial function. If  $\delta W < 0$ , the minimizing principle guarantees that the actual eigenvalue  $\omega^2$  must be smaller (i.e., more unstable) than the value  $\omega^2 = \delta W/K < 0$  calculated by using the trial function; that is, the existence of an allowable trial function which makes  $\delta W < 0$  is sufficient for instability. Second, the Euler-Lagrange equations following from  $\delta W$  correspond to the marginal stability form (i.e.,  $\omega^2 = 0$ ) of the normal-mode equations and are usually far simpler to analyze. Third, in the integral form of  $\delta W$ , the various stabilizing and destabilizing mechanisms appear quite transparently, thus helping in the development of physical intuition.

Finally, there exists a very practical method based on the Energy Principle, for numerically testing MHD stability. In this procedure one chooses a suitable set of basis functions  $\xi_n$  and writes  $\xi$  as an arbitrary sum of these functions,  $\xi = \sum a_n \xi_n$ . Substituting into the expression for  $\delta W$  then yields  $\delta W = \sum A_{mn} a_m a_n$  where the  $A_{mn} = \delta W(\xi_m, \xi_n)$  are well defined, computable matrix elements. Once the  $A_{mn}$  are known, the expression for  $\delta W$  can be minimized with respect to the coefficients  $a_m$ , given some suitable normalization. Clearly a clever choice and/or a sufficient number of basis functions gives an increasingly accurate indication of whether or not  $\delta W$  can be made negative. Note that the minimization with respect to the  $a_m$  can be carried out for any convenient choice of normalization, not necessarily  $K(\xi, \xi) = \text{const}$ . This procedure for determining stability is very effective in multidimensional geometries, where numerical shooting methods are not possible (Freidberg and Marder, 1973; Grimm *et al.*, 1976; and Berger *et al.*, 1977a).

The proof of the Energy Principle would be straightforward if  $\mathbf{F}$  allowed only discrete normal modes, constituting a complete set of basis functions  $\xi_n$ . In this case, any arbitrary  $\tilde{\xi}(t)$  could be expanded as  $\tilde{\xi} = \sum a_n \xi_n \exp(-i\omega_n t)$ , where  $\omega_n$  are the normal-mode eigenvalues. If the  $\xi_n$  are chosen orthonormal with respect to a weight function  $\rho_0$ , then  $\delta W$  has the value

$$\delta W = \sum |a_n|^2 \omega_n^2. \quad (5.30)$$

Thus if a  $\tilde{\xi}(t)$  could be found for which  $\delta W < 0$ , at least one  $\omega_n^2$  is negative, indicating instability. Conversely, if  $\delta W \geq 0$  for all  $\tilde{\xi}(t)$ , then each  $\omega_n^2 \geq 0$ , indicating exponential stability. Unfortunately, this proof, first given by Bernstein *et al.* (1958), is not completely valid for the general case because of the existence of continua.

An elegant proof of the Energy Principle has been given by Laval *et al.* (1965), which does not assume a complete set of discrete normal modes. The proof is based on the conservation of energy  $H = K(\tilde{\xi}, \tilde{\xi}) + \delta W(\tilde{\xi}, \tilde{\xi})$ ,  $\dot{H} = 0$ . To show sufficiency, assume that  $\delta W$

is positive for all allowable  $\tilde{\xi}(\mathbf{r}, t)$ . Energy conservation implies  $\delta W = H - K > 0$ ,  $H = \text{const}$ . Hence unbounded exponential growth of the kinetic energy  $K$  (i.e., exponential instability) would violate energy conservation.

To show necessity, assume a perturbation  $\eta(\mathbf{r})$  exists such that  $\delta W(\eta, \eta) < 0$ . Consider a displacement  $\tilde{\xi}(\mathbf{r}, t) = \eta(r, \tilde{\xi}(r, 0))$ . Energy conservation implies that  $H(t) = H(0) = \delta W(\eta, \eta) < 0$ . This is substituted into the relation  $\ddot{I} = 2K(\tilde{\xi}, \tilde{\xi}) - 2\delta W(\tilde{\xi}, \tilde{\xi})$ , where  $I = K(\tilde{\xi}, \tilde{\xi})$ . Setting  $\delta W(\tilde{\xi}, \tilde{\xi}) = H(t) - K(\tilde{\xi}, \tilde{\xi})$  leads to the result  $\ddot{I} = 4K(\tilde{\xi}, \tilde{\xi}) - 2H > -2H > 0$ ; that is,  $I$  grows without bound as  $t \rightarrow \infty$ , indicating that  $\tilde{\xi}$  increases at least as fast as  $t$ . Laval *et al.* (1965) showed by a somewhat more complicated analysis that if  $\delta W(\eta, \eta) < 0$ , there exists a  $\xi$  which grows exponentially [i.e.,  $\xi \sim \exp(\lambda t)$ ], with a growth rate at least as fast as  $\lambda = [-\delta W(\eta, \eta)/K(\eta, \eta)]^{1/2}$ .

### c. The extended Energy Principle

The Energy Principle, calculated with  $\mathbf{F}(\xi)$  given by Eq. (5.16), is valid if the plasma is directly surrounded by a conducting wall or if there is an isolating vacuum region. In the first case, application of the Energy Principle is straightforward, since the only boundary condition that need be satisfied is

$$(\eta \cdot \xi_\perp)|_{\text{wall}} = 0. \quad (5.31)$$

When a vacuum region is present, the situation is more complicated because the vacuum fields do not appear explicitly in  $\delta W$  but enter only through the boundary conditions at the plasma surface.

To see this, consider the full set of linearized boundary conditions, obtained by expanding Eqs. (3.5)–(3.7) about the perturbed surface  $\mathbf{r}_s = \mathbf{r} + \xi$ ,

$$(\mathbf{n} \cdot \hat{\mathbf{B}}_1)|_{\text{wall}} = 0, \quad (5.32)$$

$$(\mathbf{n} \cdot \hat{\mathbf{B}}_1)|_{\text{surf}} = \mathbf{n} \cdot \nabla \times (\xi_\perp \times \hat{\mathbf{B}}_0)|_{\text{surf}}, \quad (5.33)$$

$$(\mathbf{n} \cdot \mathbf{B}_1)|_{\text{surf}} = \mathbf{n} \cdot \nabla \times (\xi_\perp \times \mathbf{B}_0)|_{\text{surf}}, \quad (5.34)$$

$$(\mathbf{B}_0 \cdot \mathbf{B}_1 + \frac{1}{2} \xi \cdot \nabla B_0^2 - \gamma p_0 \nabla \cdot \xi)|_{\text{surf}} \\ = (\hat{\mathbf{B}}_0 \cdot \hat{\mathbf{B}}_1 + \frac{1}{2} \xi \cdot \nabla \hat{B}_0^2)|_{\text{surf}}. \quad (5.35)$$

Here the notation  $\hat{\cdot}$  represents the vacuum region, and the subscript “surf” refers to the unperturbed surface. As intuitively obvious as Eqs. (5.33) and (5.34) may seem, their derivation is nontrivial. Each result is derived in an identical manner, in which not only must  $\mathbf{B}$  be evaluated on the perturbed surface, but the normal vector must be expanded as  $\mathbf{n} = \mathbf{n}_0 + \mathbf{n}_1$  with  $\mathbf{n}_1 = -(\nabla \xi) \cdot \mathbf{n}_0 + \mathbf{n}_0 [\mathbf{n}_0 \cdot (\nabla \xi) \cdot \mathbf{n}_0]$ . Note that, for the plasma, Eq. (5.34) is automatically satisfied by virtue of Eq. (5.15). Equation (5.33) couples the vacuum field  $\hat{\mathbf{B}}_1$  to the plasma displacement  $\xi$  and is an important relation, since  $\xi$  is not defined in the vacuum. The pressure balance jump condition is straightforward to derive, but has

a rather complicated form. As a consequence, direct application of the Energy Principle to a system with a vacuum region can be cumbersome, first because of the complexity of Eq. (5.35), and second because the form of  $\delta W$  with  $F$  given by Eq. (5.16) is not very intuitive (as the vacuum contribution does not appear explicitly).

These issues are resolved by a reformulation of  $\delta W$  known as the extended Energy Principle (Bernstein *et al.*, 1958 and Goedbloed, 1979), in which the vacuum contribution explicitly appears and Eq. (5.35) is no longer needed. The first step in the reformulation is to perform an integration by parts of the  $\xi^* \cdot \nabla p_1$  and  $\xi^* \cdot (\nabla \times \mathbf{Q}) \times \mathbf{B}_0$  terms in  $\delta W$ . After some algebra one obtains

$$\begin{aligned} \delta W &= W_F + \text{B.T.}, \\ \delta W_F &= \frac{1}{2} \int_P d\mathbf{r} [ |\mathbf{Q}|^2 - \xi_\perp^* \cdot (\mathbf{J}_0 \times \mathbf{Q}) \\ &\quad + \gamma p_0 |\nabla \cdot \xi|^2 + (\xi_\perp \cdot \nabla p_0) \nabla \cdot \xi_\perp^* ], \\ \text{B.T.} &= \frac{1}{2} \int_S dS (\mathbf{n} \cdot \xi_\perp^*) (\mathbf{B}_1 \cdot \mathbf{B}_0 - \gamma p_0 \nabla \cdot \xi - \xi_\perp \cdot \nabla p_0). \end{aligned} \quad (5.36)$$

Here  $\mathbf{Q} \equiv \mathbf{B}_1 = \nabla \times (\xi_\perp \times \mathbf{B}_0)$  and  $\xi = \xi_\perp + \xi_{||}$ , where  $\perp$  and  $||$  refer to the equilibrium magnetic field  $\mathbf{B}_0$ . Also, the labels  $P$ ,  $S$ , and  $V$  appearing on the integrals correspond to the unperturbed plasma volume, plasma surface, and vacuum volume, respectively. Using Eq. (5.35) in (5.36) leads to the following expression for the boundary terms:

$$\begin{aligned} \text{B.T.} &= \delta W_S + \frac{1}{2} \int_S dS (\mathbf{n} \cdot \xi_\perp^*) \hat{\mathbf{B}}_0 \cdot \hat{\mathbf{B}}_1, \\ \delta W_S &= \frac{1}{2} \int_S dS |\mathbf{n} \cdot \xi_\perp|^2 \mathbf{n} \cdot [\nabla(p_0 + \frac{1}{2} B_0^2)], \end{aligned} \quad (5.37)$$

where  $[T]$  denotes the jump in  $T$  from vacuum to plasma. In deriving Eq. (5.37), use has been made of the equilibrium relation  $[p_0 + B_0^2/2] = 0$  to infer that the tangential jump in  $\nabla(p_0 + B_0^2/2)$  also vanishes. The quantity  $\delta W_S$  is usually referred to as the surface contribution and vanishes unless surface currents flow on the plasma-vacuum boundary. [This last result is implied by Eq. (3.8).]

The remaining term in Eq. (5.37) is identical to the perturbed magnetic energy in the vacuum region,

$$\delta W_V = \frac{1}{2} \int_V d\mathbf{r} |\hat{\mathbf{B}}_1|^2. \quad (5.38)$$

To show this, write  $\hat{\mathbf{B}}_1$  as  $\hat{\mathbf{B}}_1 = \dot{\nabla} \times \hat{\mathbf{A}}_1$  with  $\nabla \times \dot{\nabla} \times \hat{\mathbf{A}}_1 = 0$ . Integrating by parts then converts  $\delta W_V$  into a surface integral,

$$\delta W_V = -\frac{1}{2} \int_S dS \mathbf{n} \cdot (\hat{\mathbf{A}}_1^* \times \hat{\mathbf{B}}_1). \quad (5.39)$$

Note that the contribution on the outer conductor vanishes by virtue of Eq. (5.32). On the surface  $\hat{\mathbf{A}}_1$  can be expressed in terms of  $\mathbf{n} \cdot \xi$  by using the relation  $\mathbf{n} \cdot \hat{\mathbf{B}}_1 = \mathbf{n} \cdot \nabla \times \hat{\mathbf{A}}_1 = \mathbf{n} \cdot \nabla \times (\xi \times \hat{\mathbf{B}}_0)$ ; that is,  $\hat{\mathbf{A}}_1 = \xi \times \mathbf{B}_0 + \nabla \phi$ . If  $\phi$  is chosen so that the gauge condition is  $\mathbf{B}_1 \cdot (\mathbf{n} \times \nabla \phi) = 0$ , then Eq. (5.38) reduces to

$$\delta W_V = \frac{1}{2} \int_S dS (\mathbf{n} \cdot \xi_\perp^*) \hat{\mathbf{B}}_0 \cdot \hat{\mathbf{B}}_1, \quad (5.40)$$

which is identical to the remaining term in Eq. (5.37).

This completes the derivation. To summarize, in the extended Energy Principle a system is exponentially stable if and only if  $\delta W \geq 0$  for all allowable perturbations with

$$\delta W = \delta W_F + \delta W_S + \delta W_V, \quad (5.41)$$

where

$$\begin{aligned} \delta W_F &= \frac{1}{2} \int_P d\mathbf{r} [ |\mathbf{Q}|^2 - \xi_\perp^* \cdot (\mathbf{J}_0 \times \mathbf{Q}) + \gamma p_0 |\nabla \cdot \xi|^2 \\ &\quad + (\xi_\perp \cdot \nabla p_0) \nabla \cdot \xi_\perp^* ], \end{aligned} \quad (5.42a)$$

$$\delta W_S = \frac{1}{2} \int_S dS |\mathbf{n} \cdot \xi_\perp|^2 \mathbf{n} \cdot [\nabla(p_0 + \frac{1}{2} B_0^2)], \quad (5.42b)$$

$$\delta W_V = \frac{1}{2} \int_V d\mathbf{r} |\hat{\mathbf{B}}_1|^2. \quad (5.42c)$$

The vacuum contribution appears explicitly and is coupled to the plasma displacement by solving  $\nabla \times \hat{\mathbf{B}}_1 = \nabla \cdot \hat{\mathbf{B}}_1 = 0$  subject to the conditions

$$\mathbf{n} \cdot \hat{\mathbf{B}}_1|_{\text{wall}} = 0, \quad (5.43)$$

$$\mathbf{n} \cdot \hat{\mathbf{B}}_1|_{\text{surf}} = \mathbf{n} \cdot \nabla \times (\xi \times \hat{\mathbf{B}}_0)|_{\text{surf}}. \quad (5.44)$$

Note that the complicated pressure balance condition is no longer needed; that is, the boundary term in Eq. (5.37) has been rewritten in a form which is self-adjoint by construction. Hence, the contributions  $\delta W_S$  and  $\delta W_V$  are variational so that Eq. (5.35) need no longer be explicitly satisfied by any given minimizing function  $\xi$ . Furthermore, after a somewhat lengthy calculation it can be shown that Eq. (5.44) can be expressed only in terms of  $\mathbf{n} \cdot \xi_\perp$  on the boundary by the relation

$$\mathbf{n} \cdot \hat{\mathbf{B}}_1|_{\text{surf}} = \hat{\mathbf{B}}_0 \cdot \nabla(\mathbf{n} \cdot \xi_\perp) - (\mathbf{n} \cdot \xi_\perp)[\mathbf{n} \cdot (\mathbf{n} \cdot \nabla) \hat{\mathbf{B}}_0]|_{\text{surf}}. \quad (5.45)$$

Thus, in a plasma-vacuum system, one can specify an arbitrary surface distortion  $\mathbf{n} \cdot \xi_\perp$ , which is then sufficient to determine both the surface and vacuum contributions to  $\delta W$ . For the special case where there is no vacuum (i.e., where the plasma extends to the wall),  $\mathbf{n} \cdot \xi_\perp$  on the boundary must vanish and  $\delta W = \delta W_F$ . Equation (5.41) is the standard form of the extended Energy Principle and is used widely throughout the literature.

#### d. Forms of $\delta W_F$

The extended Energy Principle, described by Eqs. (5.41) and (5.42), is completely adequate for application to any magnetic geometry. Nevertheless, in order to further clarify some of the mathematical and physical issues, it is useful to present several alternate forms of  $\delta W_F$ . In particular, there are several forms of  $\delta W_F$  which explicitly show the self-adjointness of  $F$  and one which provides a simple physical interpretation of the different phenomena occurring in plasmas. Each of these forms requires a lengthy manipulation of Eq. (5.42). For present purposes it suffices to state the required forms. Finally, a brief comparison is given of the forms of the energy and variational principles for the ideal and perpendicular MHD models.

To begin, consider the question of self-adjointness.

The first explicit form demonstrating this property was given by Bernstein *et al.* (1958):

$$\delta W_F = \frac{1}{2} \int d\mathbf{r} [ |\mathbf{Q} + (\mathbf{n} \cdot \boldsymbol{\xi})(\mathbf{J}_0 \times \mathbf{n})|^2 + \gamma p_0 |\nabla \cdot \boldsymbol{\xi}|^2 - 2(\mathbf{J}_0 \times \mathbf{n}) \cdot (\mathbf{B}_0 \cdot \nabla \mathbf{n}) |\mathbf{n} \cdot \boldsymbol{\xi}|^2 ]. \quad (5.46)$$

Here the definition  $\mathbf{n} \equiv \nabla p_0 / |\nabla p_0|$  is extended over the whole plasma volume and represents the unit vector normal to the magnetic surfaces. When  $\boldsymbol{\xi}^*$  is considered as an independent vector  $\boldsymbol{\eta}$ , it follows by inspection that  $\delta W$  remains unchanged if  $\boldsymbol{\xi}$  and  $\boldsymbol{\eta}$  are interchanged. A different self-adjoint form of  $\delta W_F$  has been given by Berge and Freidberg (1975):

$$\delta W_F = \frac{1}{2} \int d\mathbf{r} [ |\mathbf{B}_0 \cdot \nabla \boldsymbol{\xi}_\perp|^2 + B_0^2 |\nabla \cdot \boldsymbol{\xi}_\perp + 2\boldsymbol{\xi}_\perp \cdot \boldsymbol{\kappa}|^2 + \gamma p_0 |\nabla \cdot \boldsymbol{\xi}|^2 + \boldsymbol{\xi}_\perp^* \cdot (\boldsymbol{\xi}_\perp \cdot \nabla) \nabla \hat{p}_0 - 4B_0^2 |\boldsymbol{\xi}_\perp \cdot \boldsymbol{\kappa}|^2 ], \quad (5.47)$$

where  $\nabla \hat{p}_0 \equiv \nabla(p_0 + B_0^2/2) = \mathbf{B}_0 \cdot \nabla \mathbf{B}_0$  and  $\boldsymbol{\kappa} = \mathbf{e}_b \cdot \nabla \mathbf{e}_b$ , with  $\mathbf{e}_b = \mathbf{B}_0/B_0$ .  $\boldsymbol{\kappa}$  is the curvature vector of the magnetic field lines. This form has proven very useful in the asymptotic analysis of helically symmetric geometries.

Perhaps the most intuitive form of  $\delta W$  has been given by Furth *et al.* (1965) and Greene and Johnson (1968):

$$\delta W_F = \frac{1}{2} \int d\mathbf{r} [ |\mathbf{Q}_\perp|^2 + B_0^2 |\nabla \cdot \boldsymbol{\xi}_\perp + 2\boldsymbol{\xi}_\perp \cdot \boldsymbol{\kappa}|^2 + \gamma p_0 |\nabla \cdot \boldsymbol{\xi}|^2 - 2(\boldsymbol{\xi}_\perp \cdot \nabla p_0)(\boldsymbol{\kappa} \cdot \boldsymbol{\xi}_\perp^*) - \frac{\mathbf{J}_0 \cdot \mathbf{B}_0}{B_0^2} (\boldsymbol{\xi}_\perp^* \times \mathbf{B}_0) \cdot \mathbf{Q}_\perp ]. \quad (5.48)$$

The terms in Eq. (5.48) have the following simple physical interpretation. The  $|\mathbf{Q}_\perp|^2$  term represents the energy required to bend magnetic field lines. It is the dominant potential energy contribution to the shear Alfvén wave. The second term corresponds to the energy necessary to compress the magnetic field and describes the major potential energy contribution to the compressional Alfvén wave. The  $\gamma p_0 |\nabla \cdot \boldsymbol{\xi}|^2$  term represents the energy required to compress the plasma. It is the main source of potential energy for the sound wave. Each of the contributions just described is stabilizing. The remaining two terms can be positive or negative and thus can drive instabilities. The first of these is proportional to  $\nabla p_0 \sim \mathbf{J}_\perp \times \mathbf{B}_0$ , while the second is proportional to  $\mathbf{J}_0 \cdot \mathbf{B}_0 \sim J_{||}$ . Thus, while a vacuum field is MHD stable, either perpendicular or parallel currents represent potential sources of instability. The former type are sometimes referred to as pressure-driven modes and the latter as current-driven modes. A more detailed discussion of the classification of MHD instabilities is given in Sec. V.B.7.

As a final point, it is useful to note that each of the four forms of  $W_F$  can be written as

$$\delta W_F(\boldsymbol{\xi}^*, \boldsymbol{\xi}) = \delta W_\perp(\boldsymbol{\xi}_\perp^*, \boldsymbol{\xi}_\perp) + \frac{1}{2} \int \gamma p_0 |\nabla \cdot \boldsymbol{\xi}|^2 d\mathbf{r}. \quad (5.49)$$

Similarly, the ideal MHD normalization  $K$  can be expressed as

$$K(\boldsymbol{\xi}^*, \boldsymbol{\xi}) = K_\perp(\boldsymbol{\xi}_\perp^*, \boldsymbol{\xi}_\perp) + \frac{1}{2} \int \rho_0 |\boldsymbol{\xi}_{||}|^2 d\mathbf{r}. \quad (5.50)$$

Both  $\delta W_\perp$  and  $K_\perp$  are independent of  $\boldsymbol{\xi}_{||}$ . It is now possible to make a direct comparison of the energy and variational principles corresponding to the ideal and perpendicular MHD models. For the energy principle, a necessary and sufficient condition for exponential stability is

$$\begin{aligned} \delta W_F + \delta W_S + \delta W_V &\geq 0 \text{ (ideal MHD),} \\ \delta W_\perp + \delta W_S + \delta W_V &\geq 0 \text{ (perpendicular MHD).} \end{aligned} \quad (5.51)$$

The corresponding variational principles are given by

$$\begin{aligned} \omega^2 &= (\delta W_F + \delta W_S + \delta W_V)/K \text{ (ideal MHD),} \\ \omega^2 &= (\delta W_\perp + \delta W_S + \delta W_V)/K_\perp \text{ (perpendicular MHD).} \end{aligned} \quad (5.52)$$

As might be expected, the quantity  $\boldsymbol{\xi}_{||}$  never appears in the perpendicular MHD formulation. The only difference between these models is the plasma compressibility contribution, which is almost always very small if not identically zero. A more detailed comparison is made in Sec. V.B.5, where the significance of incompressibility,  $\nabla \cdot \boldsymbol{\xi} = 0$ , is discussed.

#### e. $\sigma$ stability

The extended Energy Principle is perhaps the most elegant and efficient method for examining MHD stability. There is, however, one additional modification that can be made, which further increases its usefulness, particularly for numerical calculations. This modification, introduced by Goedbloed and Sakanaka (1974), is known as  $\sigma$  stability.

Application of the  $\sigma$  stability criterion, rather than the extended Energy Principle, eliminates the following difficulty. Even though it is very likely that no continua exist in the unstable portion of the  $\omega$  plane, there are many cases where one or more continuum may extend to the origin. When this occurs, discrete modes can accumulate from the unstable side of the spectrum, in which case the marginal point  $\omega^2 = 0$  becomes singular. In numerical studies, one wishes to avoid such singularities whenever possible. This is the purpose of the  $\sigma$  stability concept.

The basic idea is to use a more practical definition of stability; that is, a configuration is said to be  $\sigma$  stable if there are no exponential modes growing faster than  $\exp(\sigma t)$ . Here  $1/\sigma$  represents some important limiting physical time scale, such as the decay time of the external circuits, the decay time of the plasma currents, the particle or energy loss time, the time scale for validity of the MHD model, etc. If modes grow on a time scale slower than  $1/\sigma$ , they are likely to be unimportant or significantly altered in an actual experiment. To incorporate this feature into the stability analysis one considers a modified form of  $\delta W$  given by

$$\delta W_\sigma(\xi^*, \xi) = \delta W(\xi^*, \xi) + \sigma^2 K(\xi^*, \xi). \quad (5.53)$$

Equation (5.53) states that the potential energy available to derive any MHD instabilities is reduced by an amount  $\sigma^2 K$ . An analysis similar to that given by Laval *et al.* (1965) demonstrates that the necessary and sufficient condition for  $\sigma$  stability is

$$\delta W_\sigma(\xi, \xi) \geq 0 \quad (5.54)$$

for all allowable  $\xi$ . [A detailed discussion of this topic, including examples, has been given by Goedbloed (1979)].

The additional term added to  $\delta W$  in Eq. (5.53) eliminates a small portion of the  $\omega$  plane, near  $\omega^2=0$ , from stability considerations. Thus the problems associated with modes accumulating at the origin are avoided. Furthermore, since modes cannot accumulate at  $\omega^2=-\sigma^2$ , a transition in  $\sigma$  stability always occurs for an isolated mode, a distinct advantage numerically. These features are illustrated schematically in Fig. 29.

Observe that the variational form, or the equivalent Euler-Lagrange equations associated with  $\sigma$  stability, are identical to the full MHD equations with  $\omega^2$  replaced by  $-\sigma^2$ . The similarity is deceptive, since  $\sigma^2$  is not an eigenvalue to be determined. On the contrary, one sets a value for  $\sigma^2$  and then applies any of the well-established minimizing techniques to ascertain the sign of  $\delta W_\sigma$ . This is particularly useful for multidimensional geometries. One drawback to  $\sigma$  stability is that the presence of the additional terms increases the complexity of the equations (i.e., more terms, more complicated coefficients, etc.) This is usually not important in numerical investigations.

In summary, the concept of  $\sigma$  stability should receive serious consideration if one intends to investigate MHD stability primarily by numerically means. For problems in which analysis is the main method of investigation, the additional complications introduced by  $\sigma$  stability suggest that the extended Energy Principle is a more convenient formulation. Most of the cases considered in the remainder of this section fall into the latter category, leading to frequent use of the extended Energy Principle.

## 5. Incompressibility

Because of the simple way in which  $\xi_{||}$  appears in  $\delta W$ , it is possible to minimize the potential energy once and for all with respect to  $\xi_{||}$  for essentially arbitrary geometry. The resulting form of  $\delta W$  is only a function of  $\xi_{\perp}$ , and thus the number of unknown dependent vari-

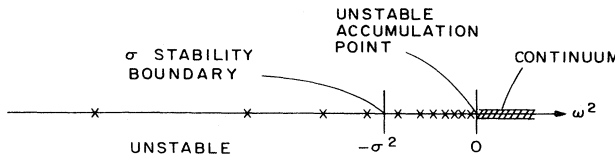


FIG. 29. Schematic diagram of the  $\omega$  plane, indicating the advantages of the  $\sigma$  stability concept.

ables is reduced from three to two.

The minimizing condition follows from letting  $\xi_{||} \rightarrow \xi_{||} + \delta \xi_{||}$  in Eq. (5.49) and then setting the corresponding variation equal to zero. The result is

$$\mathbf{B}_0 \cdot \nabla (\nabla \cdot \xi) = 0. \quad (5.55)$$

In fact, since  $\xi_{||}$  also appears in a simple form in the MHD normalization  $K$  [see Eq. (5.50)], the actual equation of motion for arbitrary  $\omega^2$  can be calculated similarly. The full equation is given by

$$\omega^2 \rho_0 \xi_{||} + (\gamma p_0 / B_0) \mathbf{B}_0 \cdot \nabla (\nabla \cdot \xi) = 0. \quad (5.56)$$

As expected, at marginal stability,  $\omega^2=0$ , the condition to minimize  $\delta W$  is identical to the equation of motion.

For most configurations, the operator  $\mathbf{B}_0 \cdot \nabla$  is non-singular, and consequently Eq. (5.55) implies that the general minimizing condition is

$$\nabla \cdot \xi = 0, \quad (5.57)$$

that is, the most unstable perturbations (i.e., those with the lowest thresholds) are incompressible.

In a sense this is obvious from Eq. (5.49), since the only term containing  $\xi_{||}$  is positive. Thus its smallest value is zero and is obtained by setting  $\nabla \cdot \xi = 0$ . However, it is the components of  $\xi$  which are the physical quantities and not  $\nabla \cdot \xi$  itself. Therefore, in order to set  $\nabla \cdot \xi = 0$ , one must be able to choose such a  $\xi_{||}$  for any given  $\xi_{\perp}$ . This  $\xi_{||}$  is given by the solution of  $\mathbf{B}_0 \cdot \nabla (\xi_{||}/B_0) = -\nabla \cdot \xi_{\perp}$ . Physically acceptable solutions for  $\xi_{||}$  are possible only if the operator  $\mathbf{B}_0 \cdot \nabla$  is nonsingular, as is the case in most configurations of interest. (Even if  $\mathbf{B}_0 \cdot \nabla$  vanishes on *isolated* magnetic surfaces, a  $\xi_{||}$  can be constructed which is bounded in the vicinity of the surface but which makes a vanishingly small contribution to the plasma compressional energy.)

It is worth noting that there are two special cases where the operator  $\mathbf{B}_0 \cdot \nabla$  cannot be simply inverted. In the first case, if there exists sufficient equilibrium symmetry, the operator  $\mathbf{B}_0 \cdot \nabla$  identically vanishes for certain special modes. As an example, consider a pure Z pinch with equilibrium magnetic fields  $\mathbf{B}_0 = B_\theta(r)\mathbf{e}_\theta$ . If the perturbations are Fourier analyzed with respect to  $\theta$  and  $z$  so that  $\xi \sim \xi(r)\exp[i(m\theta + kz)]$ , then for the  $m=0$  mode the operator  $\mathbf{B}_0 \cdot \nabla$  (scalar) identically vanishes. In this situation  $\nabla \cdot \xi = \nabla \cdot \xi_{\perp} + \mathbf{B}_0 \cdot \nabla (\xi_{||}/B_0) = \nabla_{\perp} \cdot \xi_{\perp}$ ; that is,  $\xi_{||}$  does not appear in  $\delta W$ , and the compressibility term  $\gamma p_0 |\nabla_{\perp} \cdot \xi_{\perp}|^2$  must be maintained and included in the minimization with respect to  $\xi_{\perp}$ .

The second case corresponds to the situation of closed-line symmetry, where the operator  $\mathbf{B}_0 \cdot \nabla$  is not in general singular, but there is a periodicity constraint requiring  $\xi_{||}(l) = \xi_{||}(l+L)$  on every magnetic line, since the lines are closed. (Here  $l$  is arc length and  $L$  is the total length of a given field line.) In this case it is necessary to add a homogeneous solution to Eq. (5.55) so that

$$\nabla \cdot \xi = F(U),$$

$$U = \oint \frac{dl}{B_0}, \quad (5.58)$$

where  $F$  is an arbitrary function of  $U$ , and  $U$  satisfies the homogeneous equation  $\mathbf{B}_0 \cdot \nabla U = 0$  (see Sec. IV.D.1). Solving Eq. (5.58) for  $\xi_{||}$  yields

$$\frac{\xi_{||}}{B_0} = \int_0^l \frac{dl}{B_0} [F(U) - \nabla \cdot \xi_{\perp}] . \quad (5.59)$$

The periodicity constraint requires that  $F(U)$  be chosen as follows:

$$F(U) = \langle \nabla \cdot \xi_{\perp} \rangle ,$$

$$\langle Q \rangle = \frac{\oint Q dl / B_0}{\oint dl / B_0} . \quad (5.60)$$

The end result is that in closed-line systems the minimum value of the plasma compressibility term cannot be made zero, but has the value

$$\int \gamma p_0 |\nabla \cdot \xi|^2 d\mathbf{r} = \int \gamma p_0 |\langle \nabla \cdot \xi_{\perp} \rangle|^2 d\mathbf{r} . \quad (5.61)$$

Note that, for the general case where  $\nabla \cdot \xi = 0$ ,  $\delta W(\text{ideal MHD}) = \delta W(\text{perpendicular MHD})$ , indicating that both models predict identical stability boundaries. For either of the special cases discussed, there is an additional stabilizing term in ideal MHD proportional to  $\gamma$ . Considering the lack of validity of the ideal MHD energy equation in most cases of physical interest, the contribution of this term is likely to be unreliable. Similarly in the perpendicular MHD model, the assumptions made restricting the class of allowable motions are also violated for the two special cases, indicating that this model is no more reliable than ideal MHD. In summary, for cases where  $\nabla \cdot \xi = 0$ , both models give the same predictions; for either special case, neither model is particularly reliable.

Finally, it is worth pointing out the following mathematical result. For the full variational problem, applied to the general or either special case, it can be shown that for unstable modes

$$\omega^2(\text{perp MHD}) \leq \omega^2(\text{ideal MHD}) . \quad (5.62)$$

Thus the perpendicular MHD model is more pessimistic with regard to growth rates.

## 6. Vacuum versus force-free plasma

One important but somewhat subtle issue is the general stability relationship between configurations which are surrounded by a vacuum or by a force-free plasma [a detailed discussion of this topic, including examples, has been given by Goedbloed (1979)]. This problem arises physically as follows. Many confinement configurations consist of a hot core of plasma carrying nearly all of the plasma current. This core is often surrounded by a cold, low-density, current-free plasma which ultimately makes contact with the first wall. Since the electrical conductivity of the outer plasma is much less than that of the core, it might appear not unreasonable to treat this region as a perfect insulator (i.e., a vacuum). However, it is more often the case that the conductivity of the outer

region is still sufficiently high that the resistive diffusion time is long compared to characteristic MHD time. It would thus seem more realistic to treat this region, not as a vacuum, but as an ideal MHD plasma with low pressure (i.e., force-free), carrying no equilibrium current.

The replacement of a perfectly insulating region with a perfectly conducting region might be expected to have a large effect on the overall stability. While this is often true, there are many cases where there is no effect at all. To understand this situation, compare the outer region contribution to  $\delta W$  for each case: (a) the vacuum, given by Eq. (5.42c), and (b) the force-free, currentless plasma, given by  $\delta W_F$  [Eq. (5.42a)] with  $\mathbf{J}_0 p_0 \rightarrow 0$ .

$$\delta W_V = \frac{1}{2} \int_V |\mathbf{B}_1|^2 d\mathbf{r} \quad (\text{vacuum}),$$

$$\delta W_F = \frac{1}{2} \int_V |\mathbf{Q}|^2 d\mathbf{r} \quad (\text{force-free plasma}) . \quad (5.63)$$

Since  $\mathbf{Q} \equiv \mathbf{B}_1 = \nabla \times (\xi_{\perp} \times \mathbf{B}_0)$ , both energy contributions are identical in form. One might then be led to conclude that the magnetic perturbation  $\mathbf{B}_1$ , which minimizes the vacuum energy, also minimizes the force-free plasma energy, and thus both contributions should always be identical. Although this is true for the magnetic perturbation, there is an additional constraint in the case of the force-free plasma. In particular, the plasma displacement resulting from the minimizing magnetic perturbation must correspond to a physically allowable motion [i.e.,  $K(\xi_{\perp}^*, \xi_{\perp})$  must be bounded]. No such constraint exists in the vacuum, since  $\xi_{\perp}$  is not defined in this region.

For a well-defined, bounded magnetic perturbation, the force-free-plasma topological constraint arises when attempting to invert the relationship  $\mathbf{B}_1 = \nabla \times (\xi_{\perp} \times \mathbf{B}_0)$  to determine  $\xi_{\perp}$ . Whether or not the inversion is singular, is closely related to the properties of the  $\mathbf{B}_0 \cdot \nabla$  operator. For example, in a general one-dimensional screw pinch, the relation between  $B_{1r}$  and  $\xi_r$  is given by  $B_{1r} = \mathbf{B}_0 \cdot \nabla \xi_r$ . After Fourier analyzing with respect to  $\theta$  and  $z$ , one can invert this relationship, yielding  $\xi_r = -iB_{1r}/F$ ,  $F = kB_z(r) + mB_\theta(r)/r$ . Hence, if  $F(r)$  vanishes anywhere in the outer region,  $\xi_r$  is singular. When this situation occurs, the stability of the force-free region must be recomputed with  $\mathbf{n} \cdot \mathbf{B}_1$  set to zero, not on the outer conductor, but on the singular surface. The force-free plasma is now more stable than the vacuum, since the new boundary condition is equivalent to moving the conducting boundary inward.

Even with the above distinction between vacuum and force-free plasma, there still remains one crucial physics issue. Each of the two cases discussed represents a limiting description of the outer region. In reality, the outer plasma has a small but finite resistivity. If such an effect is included in Ohm's law, the plasma can diffuse through the magnetic field, and the ideal MHD topological constraint of perfect conductivity is no longer required. In this situation, the marginal stability boundaries are identical with those of the vacuum case (since no additional constraints are necessary), but the growth rates are much lower and depend upon the value of the resistivity in the region of the singular surface.

In summary, the stability behavior of the outer region is as follows. The most pessimistic description corresponds to the vacuum case. Here no additional constraints need be imposed, and the characteristic growth times are those of ideal MHD. If the vacuum region is replaced by a force-free plasma, the stability may or may not change, depending upon whether the particular mode under consideration has a singular surface in the outer region. With no singular surface, the situation is identical to the vacuum case. If there is a singular surface, the force-free plasma is considerably more stable because of the topological constraint. Finally, when the outer region is replaced with a resistive force-free plasma, the topological constraint is eliminated. The marginal stability boundaries are again identical to the vacuum case, but growth rates are much lower when a singular surface exists.

The resistive force-free plasma provides the most realistic description of the outer region. Therefore, since the remainder of this section is primarily concerned with the determination of stability boundaries, whenever the outer region plays an important role in the stability of a given mode, we shall treat this region as a vacuum.

## 7. Classification of MHD instabilities

In this section the various methods used to classify MHD instabilities are summarized. Also, wherever appropriate, those properties of an equilibrium magnetic configuration which are effective in reducing or eliminating a given instability are discussed. Note that many modes have descriptive names based on the physical issues involved, but do not have precise mathematical definitions except in special limits (e.g., ballooning mode, high- $\beta$  interchange mode). Similarly certain "modes" correspond to specific choices of trial functions which are likely to cause instabilities, but which are not the true minimizing functions (e.g., interchange mode, rigid shift displacement). Such trial functions give rise to conditions which are necessary for stability and sufficient for instability. In general, a complete and exact minimization of  $\delta W$  for any nontrivial geometry requires numerical computation.

Because of the imprecisions discussed above, any classification system should be viewed as providing general guidelines for understanding MHD instabilities rather than providing a unique prescription for distinguishing different MHD modes.

The first step in classification is to note that all MHD modes can be reasonably well distinguished by their main driving source of instability. Thus a given mode can be either pressure driven or current driven.

### a. Current-driven modes

It was shown in Sec. V.B.1 that a homogeneous, unidirectional magnetic field is always MHD stable. Furthermore, it was shown by Eq. (5.48) that there are two

possible sources of MHD instability. Those modes in which the dominant destabilizing term is the one proportional to  $\mathbf{J}_0 \cdot \mathbf{B}_0$  are known as current-driven modes. They are driven by parallel currents and can exist even in a zero-pressure, force-free plasma.

### b. Pressure-driven modes

Similarly unstable MHD modes in which the dominant destabilizing term in Eq. (5.48) is the one proportional to  $\nabla p_0$  are known as pressure-driven modes. They are driven by perpendicular currents and can exist even if no parallel currents are present in the equilibrium.

The second step in the classification procedure is to determine whether or not a given MHD mode causes the plasma surface to move from its equilibrium position. This feature distinguishes internal and external modes (also referred to as fixed-boundary and free-boundary modes, respectively), which can be described as follows:

### c. Internal/fixed-boundary modes

Consider a magnetic configuration in which the plasma is surrounded by a vacuum. Perturbations which maintain the plasma-vacuum boundary fixed at its equilibrium position are called internal or fixed-boundary modes. The boundary condition applicable to such modes is  $\mathbf{n} \cdot \boldsymbol{\xi}|_{\text{surf}} = 0$  and is equivalent to moving a conducting wall onto the plasma-vacuum interface. For internal modes it is only necessary to minimize  $\delta W_F$ , since  $\delta W_S = \delta W_V = 0$ .

### d. External/free-boundary modes

If the plasma-vacuum interface is moved from its equilibrium position during an unstable MHD perturbation, the corresponding modes are known as external or free-boundary modes. For such instabilities  $\delta W_S$  and  $\delta W_V$  must be evaluated as well as  $\delta W_F$ , since  $\mathbf{n} \cdot \boldsymbol{\xi}|_{\text{surf}} \neq 0$ . Although an internal mode can be viewed as the special case of an external mode with  $\mathbf{n} \cdot \boldsymbol{\xi}|_{\text{surf}} = 0$ , the definition assumed here makes each mode mutually exclusive; that is, if  $\mathbf{n} \cdot \boldsymbol{\xi}|_{\text{surf}} = 0$ , the mode is an internal mode. If not, it is an external mode.

These categorizations represent a general classification system for MHD instabilities. There are, however, alternate categorizations which distinguish MHD modes in somewhat more detail. The most important of these are: (1) the kink instability, (2) the interchange instability, and (3) the ballooning mode. Most MHD instabilities can be described by one or more of these basic modes. A brief discussion of each is given below.

### e. Kink modes

The designation "kink mode" refers to either an internal or an external current-driven mode. The internal

mode is important in the RFP. The external mode is dominant (at least theoretically) for the tokamak, although the internal mode also plays an important role experimentally.

Consider first the external kink mode. The main destabilizing term for high- $m$  modes ( $m$  is the azimuthal wave number) is the radial gradient in the parallel current. For low- $m$  numbers,  $m=1$  in particular, the current profile is not as important as the total current itself. The basic form of the perturbation is such that the plasma surface "kinks" into a helix as illustrated in Fig. 30. The unstable modes occur for long parallel wavelengths (i.e.,  $k_{\parallel}/k_{\perp} \ll 1$ ), minimizing line bending. Usually the most dangerous kinks correspond to low perpendicular wave numbers (i.e.,  $k_{\perp}a \sim m \sim 1$ ).

There are several ways to improve the stability of a given configuration to external kink modes. First, for a prescribed geometry there is usually a critical parallel current indicating the onset of instability. Stability can be achieved by keeping the parallel current below this value. Likewise, for a fixed parallel current, a toroidal device with sufficiently small major circumference will prohibit the formation of long-wavelength kinks. Second, to the extent that one can experimentally control the field profiles, higher- $m$  kink modes can be stabilized by peaking the parallel current profile, keeping the total current fixed. Third, since low- $m$  kinks have a broad radial extent, they can be stabilized if a perfectly conducting shell is placed sufficiently close to the plasma surface.

The internal kink has many properties similar to those of the external kink, although it is in general a weaker instability. In fact, for a tokamak it is usually only  $m=1$  that can become unstable. As before, a combination of low current and/or tight aspect ratio can help to stabilize internal kink modes, particularly in a tokamak. Neither of these methods is effective in the RFP; there, interestingly enough, a broad profile helps to provide stability. That is, for internal modes, broadening the current profile at fixed total current effectively moves a conducting wall closer to the current channel, thereby providing stability. Although broad profiles would be

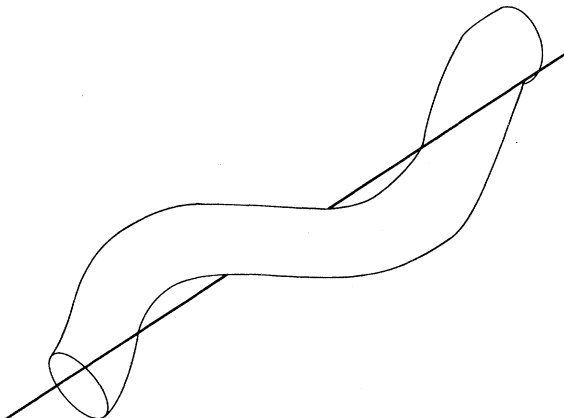


FIG. 30. Illustration of an  $m=1$  kink instability.

detrimental for external kink stability, such modes are not expected to be important in the RFP since the plasma is in fact surrounded by a conducting shell.

#### f. Interchange instabilities

Interchange instabilities are internal modes driven by the pressure gradient and are very similar in nature to the Rayleigh-Taylor instability [see, for instance, Chandraseker (1961), Bateman (1978)]. Actually, except in special asymptotic limits, the interchange perturbation is not a true mode of the system but represents a special choice of trial functions which attempts to minimize the line bending contribution in  $\delta W_F$  (i.e., for an interchange  $B_{\perp\perp} \approx 0$ ). The interchange instability is important in the RFP, the Elmo bumpy torus, the stellarator, and sometimes the tokamak.

The interchange perturbation can lead to instability, depending upon the relative sign of the magnetic field line curvature and the pressure gradient. If the field lines are convex towards the plasma, their tension tends to make them shorten and collapse inward. The plasma pressure, on the other hand, has a natural tendency to expand outward. In such cases a perturbation which "interchanges" two flux tubes at different radii leads to a system with lower potential energy and hence instability (see Fig. 31). Because of the way the surfaces are fluted, the perturbations are also sometimes known as "flute modes." When the field lines are concave to the plasma, the system is stable to interchange perturbations.

From this description it follows that interchanges represent plasma perturbations which are nearly constant along a field line (i.e., which have no line bending). Perpendicular to the field, the most unstable perturbations

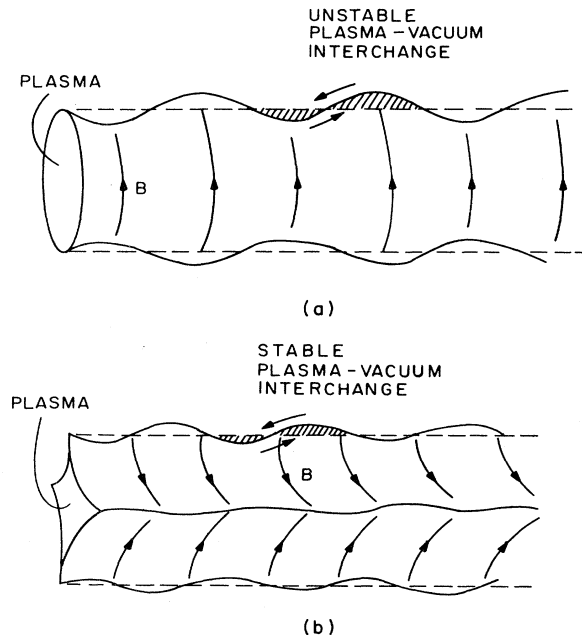


FIG. 31. Illustration of (a) unstable and (b) stable interchange perturbations.

have very rapid variations (i.e.,  $k_{||}/k_{\perp} \ll 1, k_{\perp}a \gg 1$ ) if  $J_{||}=0$ . These are known as localized interchanges and are very amenable to analysis. In general, they lead to necessary conditions for stability which can be expressed solely in terms of local values of the equilibrium quantities. Examples of such conditions are the Suydam criterion (for one dimension) and the Mercier criterion (for two dimensions). Interchanges with more moderate or global variation perpendicular to the field can also exist, but in general require numerical computation. One special case which can be solved analytically is the  $m=0$  "sausage" mode in a pure Z pinch, discussed in Sec. V.C.2.

There are several features of the magnetic geometry which can be effective in stabilizing interchanges. First, if there is shear in the magnetic field from one flux surface to another, it is not possible to interchange two neighboring flux tubes without some line bending occurring. If the pressure gradient is sufficiently small compared to the shear, the interchange can be stabilized. A second method makes use of the fact that on the inside of a torus the local field line curvature is often favorable. Thus, as a given magnetic line encircles the torus, it in general passes through alternating regions of favorable and unfavorable curvature. By carefully designing the configuration, one can make the average curvature favorable, thus stabilizing interchanges. Such configurations are said to possess a "magnetic well." [An early discussion of interchange instability has been given by Rosenbluth and Longmire (1957)].

#### *g. Ballooning modes*

Ballooning modes are also driven by the pressure gradient and can occur either externally or internally, although in recent years most of the interest has focused on the latter. These instabilities occur in tori or other multidimensional configurations and are important in that they determine one set of criteria which limits the value of  $\beta$  due to MHD behavior.

The designation "ballooning" refers to the fact that in multidimensional geometries the curvature of the magnetic field line often alternates between regions which are favorable and unfavorable. Thus a perturbation which is not constant, but varies slowly along a field line in such a way that the mode is concentrated in the unfavorable curvature region, can lead to more unstable situations than the simple interchange perturbation. In effect, the ballooning nature of the perturbation in the unfavorable curvature region increases the pressure-driven, destabilizing contribution to  $\delta W_F$ . If the localization is not too severe, the increase in stability from line bending cannot compensate for this destabilizing effect.

Magnetic shear is somewhat effective in stabilizing ballooning modes. However, once in the regime where ballooning modes are important, the most effective way to stabilize given magnetic field profiles is to keep  $\beta$  below some critical value.

In general ballooning modes are difficult to calculate

because they are inherently multidimensional. The stability problem is greatly simplified by considering the asymptotic limit  $k_{||}/k_{\perp} \ll 1, k_{\perp}a \gg 1$ , where there is very rapid variation of the perturbation perpendicular to the field, although less than in an interchange perturbation. In this case the stability problem reduces to the solution of a one-dimensional differential equation on each flux surface. Substantial progress has been made, using this procedure, in the study of ballooning modes in tokamaks. One interesting feature of the ballooning mode equation is that, in a special limit, it reduces to the localized interchange criterion (i.e., the Mercier criterion).

#### 8. Summary

In this section the general features of MHD stability theory have been described. Starting from the linearized equations of motion, it was shown that a powerful method, known as the Energy Principle, exists for determining linear MHD stability. The existence of this principle is directly related to the self-adjointness of the force operator  $F(\xi)$  and the exact, nonlinear conservation of total energy.

An examination of the Energy Principle indicates that, except in certain special cases, the perturbations which minimize  $\delta W_F$  are incompressible. It was also pointed out that it is important to distinguish whether the region surrounding the main plasma core is a vacuum, an ideal MHD plasma, or a resistive MHD plasma. The ideal MHD plasma often predicts considerably greater stability because the class of allowable perturbations is restricted as a result of the topological constraints of perfect conductivity.

Finally, the various types of MHD instabilities that can occur were described and discussed. In general, instabilities can be driven by currents flowing parallel to the field (current-driven modes) or perpendicular to the field (pressure-driven modes). They are also distinguished by whether or not the unstable displacement perturbs the plasma surface (external versus internal modes). These classifications were further categorized into kinks, interchanges, and ballooning modes. Depending on the mode in question, such equilibrium features as a conducting wall, maximum current, maximum  $\beta$ , shear, magnetic well, or tight aspect ratio could be used to improve stability. As a general feature, essentially all MHD instabilities correspond to plasma displacements which are nearly constant along a field line (i.e.,  $k_{||} \approx 0$  to minimize line bending). However, perpendicular to the field they can vary macroscopically (as in kinks) or very rapidly (as in interchange and ballooning modes).

#### C. Application to 1D configurations

This section describes the application of the Energy Principle to one-dimensional cylindrical configurations. First, the stability of the two basic configurations, the  $\theta$

pinch and the  $Z$  pinch, is investigated. It is shown that the  $\theta$  pinch has inherently favorable stability properties, while the opposite is true for the  $Z$  pinch. Next, the Energy Principle is applied to the general screw pinch. Even this relatively basic configuration exhibits a rather high level of complexity. Three important results which are discussed are Suydam's criterion for localized interchanges, Newcomb's general procedure for testing stability, and the oscillation theorem describing the eigenvalue behavior for the full linearized stability equations.

Based on these results, a relatively complete description of the stability of the reversed field pinch is then given. The ordering of the fields in the aspect ratio is such that the one-dimensional stability analysis is essentially all that is required for the reversed field pinch, the toroidal effects leading only to small corrections. Finally, a discussion is given of the "straight" tokamak. Although a relatively complete stability picture is again obtained, the results must be used cautiously since, for the tokamak, there are toroidal modifications which are of comparable importance.

### 1. The $\theta$ pinch

As a first application of the Energy Principle, consider the  $\theta$  pinch. Recall that the equilibrium is described by  $p(r), \mathbf{B} = B_z(r)\mathbf{e}_z$ , where

$$p(r) + \frac{1}{2}B_z^2(r) = \frac{1}{2}B_a^2 \quad (5.64)$$

and  $B_a^2$  is the externally applied field. Since the equilibrium is symmetric with respect to  $\theta$  and  $z$ , the plasma displacement can be Fourier analyzed as follows:

$$\xi(\mathbf{r}) = \xi(r)\exp[i(m\theta + kz)]. \quad (5.65)$$

Here  $m$  and  $k$  correspond to the "poloidal" and "toroidal" wave numbers, respectively.

The first step in the minimization of  $\delta W$  is to note that the incompressibility condition,  $\nabla \cdot \xi = 0$ , yields the following expression for  $\xi_{||} \equiv \xi_z$ :

$$\xi_z = \frac{1}{kr}[(r\xi_r)' + im\xi_\theta]. \quad (5.66)$$

Hence, as long as  $k \neq 0$ , the minimizing perturbations are incompressible.

Consider now the general internal modes of the  $\theta$  pinch. Straightforward substitution into  $\delta W = \delta W_F$  [i.e., Eq. (5.48)] gives

$$\frac{\delta W_F}{L} = \pi \int_0^a I(r)r dr, \quad (5.67)$$

$$I(r) = B_z^2 \left[ k^2(|\xi_r|^2 + |\xi_\theta|^2) + \frac{1}{r^2} |(r\xi_r)'|^2 + \frac{m^2}{r^2} |\xi_\theta|^2 \right. \\ \left. + \frac{im}{r^2} (r\xi_r')' \xi_\theta - \frac{im}{r^2} (r\xi_r)' \xi_\theta^* \right],$$

where  $a$  is the outer radius of the plasma and  $L$  is the length of the column. Note that  $\xi_\theta$  appears only algebra-

ically in this expression. Consequently  $\delta W_F$  is minimized by choosing

$$\xi_\theta = \frac{im}{m^2 + k^2 r^2} (r\xi_r)' . \quad (5.68)$$

$\delta W_F$  then has the form

$$\frac{\delta W_F}{L} = \pi \int_0^a r dr \frac{k^2 B_z^2}{k_0^2 r^2} [ |(r\xi_r)'|^2 + k_0^2 r^2 |\xi|'^2 ]. \quad (5.69)$$

Here  $k_0^2 r^2 \equiv k^2 r^2 + m^2$  and  $\xi \equiv \xi_r$ .

Observe that  $\delta W_F > 0$  for any nonzero  $k^2$ , and  $\delta W_F \rightarrow 0$  as  $k^2 \rightarrow 0$ ; that is, the  $\theta$  pinch is positively stable for finite wavelengths and approaches marginal stability for very long wavelengths. These are the favorable stability properties previously mentioned.

A simple physical explanation for the stability is as follows. A  $\theta$ -pinch equilibrium has no parallel currents, so that current-driven modes cannot be excited. Likewise, since the field lines are straight, their curvature is zero (i.e., radius of curvature is infinite) and pressure-driven modes cannot be excited. Any perturbation to the equilibrium either bends or compresses the magnetic field lines, and both are stabilizing influences.

### 2. The $Z$ pinch

For the next application of the Energy Principle consider the  $Z$  pinch described by  $p(r), \mathbf{B} = B_\theta(r)\mathbf{e}_\theta$ , where

$$\frac{dp}{dr} + \frac{B_\theta}{r} \frac{d}{dr}(rB_\theta) = 0 . \quad (5.70)$$

As before, the equilibrium symmetry implies that the perturbations can be Fourier analyzed with respect to  $\theta$  and  $z$ :

$$\xi(r) = \xi(r)\exp[i(m\theta + kz)].$$

The first step in the minimization procedure is to examine the incompressibility condition. For  $m \neq 0$  it follows from  $\nabla \cdot \xi = 0$  that  $\xi_{||} \equiv \xi_\theta$  is given by

$$\xi_\theta = \frac{i}{m} [(r\xi_r)' + ikr\xi_z] . \quad (5.71)$$

For  $m = 0$  the general minimizing condition  $\mathbf{B} \cdot \nabla(\nabla \cdot \xi) = 0$  is automatically satisfied, and  $\xi_\theta$  never explicitly appears in the calculation. In this case,  $\nabla \cdot \xi = \nabla \cdot \xi_\perp$  and the plasma compressibility must be maintained.

Thus the two cases  $m \neq 0$  and  $m = 0$  must be treated separately. Consider first internal modes with  $m \neq 0$ . In analogy with the  $\theta$ -pinch case, the Energy Principle yields a quadratic expression in which  $\xi_z$  appears only algebraically. The minimizing  $\xi_z$  is given by

$$\xi_z = \frac{ikr^3}{m^2 + k^2 r^2} \left[ \frac{\xi_r}{r} \right]',$$

which, when substituted into  $\delta W_F$ , yields

$$\frac{\delta W_L}{L} = \pi \int_0^a r dr \left[ \frac{1}{r^2} (2rp' + m^2 B_\theta^2) |\xi|^2 + \frac{m^2 r^2 B_\theta^2}{m^2 + k^2 r^2} \left| \left( \frac{\xi}{r} \right)' \right|^2 \right],$$

where  $\xi \equiv \xi_r$ . Note that  $k^2$  only appears in a positive term, so that the minimizing perturbation occurs for  $k^2 \rightarrow \infty$ .  $\delta W_F$  thus reduces to

$$\frac{\delta W_F}{L} = \pi \int_0^a \frac{dr}{r} (2rp' + m^2 B_\theta^2) |\xi|^2. \quad (5.72)$$

Equation (5.72) implies that the necessary and sufficient condition for stability in the case when  $m \neq 0$  is  $2rp' + m^2 B_\theta^2 > 0$  [see, for instance, Kadomtsev (1966)]. Using the equilibrium relation, this can be rewritten as

$$\frac{r^2}{B_\theta} \left( \frac{B_\theta}{r} \right)' < \frac{1}{2} (m^2 - 4). \quad (5.73)$$

The standard Z-pinch profile has  $B_\theta/r$  as a decreasing function of radius. For such profiles Eq. (5.73) predicts stability for  $m \geq 2$ . It also predicts stability for  $m=1$  in the outer low-current regions where  $B_\theta \sim 1/r$ . However, near the axis  $B_\theta \sim r$ . Consequently the inner core of the Z pinch is always  $m=1$  unstable.

The source of the instability can be seen in Fig. 32. As the plasma undergoes an  $m=1$  deformation, the magnetic lines concentrate in the tighter portion of the column. The corresponding increased magnetic pressure produces a destabilizing force in the direction to further increase the  $m=1$  deformation—hence, instability.

Although the plasma distortion has the appearance of a helix, it does not correspond to a kink mode, since  $J_{||}=0$ . The mode is perhaps best described as a pressure-driven interchange in which line bending and magnetic compression are minimized by choosing  $k_{||} \equiv m/r$  as small as possible (i.e.,  $m=1$ ) and  $k_\perp \equiv k \rightarrow \infty$  so that  $\xi_z \rightarrow 0$ .

Consider now the  $m=0$  mode. The evaluation of  $\delta W_F$  again shows that  $\xi_z$  appears only algebraically. Minimizing  $\delta W_F$  yields

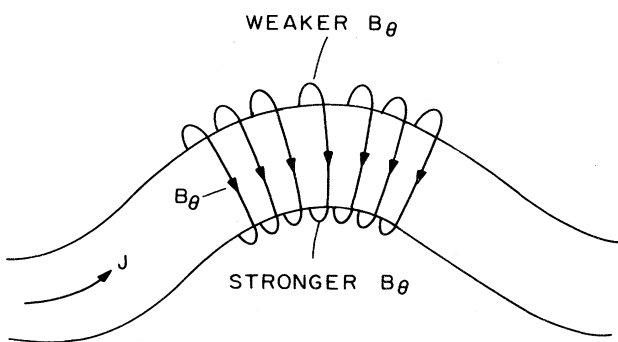


FIG. 32. Physical mechanism of the  $m=1$  instability in a pure Z pinch.

$$k\xi_z = \frac{i}{\gamma p + B_\theta^2} \left[ r B_\theta^2 \left( \frac{\xi_r}{r} \right)' + \frac{\gamma p}{r} (r \xi_r)' \right]$$

and

$$\frac{\delta W_F}{L} = \pi \int_0^a \frac{dr}{r} \left( \frac{4\gamma p B_\theta^2}{\gamma p + B_\theta^2} + 2rp' \right) |\xi|^2. \quad (5.74)$$

The necessary and sufficient condition for stability when  $m=0$  is thus given by (Kadomtsev, 1966)

$$-\frac{rp'}{p} < \frac{2\gamma B_\theta^2}{\gamma p + B_\theta^2}. \quad (5.75)$$

This condition can be satisfied for sufficiently gradual pressure profiles. Note, however, that the criterion is a strong function of the ideal MHD energy equation, which provides a poor description of the physics in a collisionless plasma. The corresponding condition from perpendicular MHD, equally unreliable since  $\mathbf{B} \cdot \nabla \equiv 0$ , is obtained by setting  $\gamma=0$ . The resulting stability criterion,  $-rp'/p < 0$ , is always violated for a confined plasma.

The  $m=0$  instability is an interchange mode often known as the “sausage instability.” The basic nature of the mode is illustrated in Fig. 33. When an  $m=0$  “sausage” perturbation is superimposed on the Z-pinch equilibrium, the magnetic field in the throat region increases, since the plasma carries the same current in a smaller cross section. The increased magnetic pressure produces a force which tends to further constrict the column.

In summary, a Z pinch is always unstable to  $m=1$  perturbations and is likely to be unstable to  $m=0$  as well. The unstable modes basically have the form of pressure-driven interchanges. These results form the basis of earlier statements attributing very poor stability characteristics to the Z pinch.

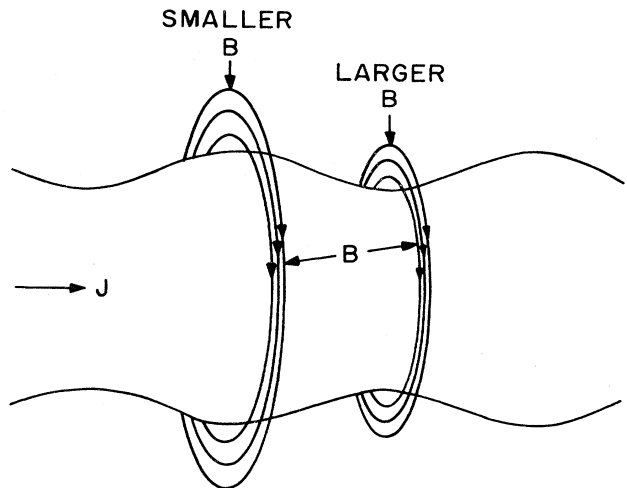


FIG. 33. Physical mechanism of the  $m=0$  sausage instability in a pure Z pinch.

### 3. The general screw pinch

#### a. Evaluation of $\delta W$

As a first step in finding configurations which combine the favorable equilibrium properties of the  $Z$  pinch with the favorable stability properties of the  $\theta$  pinch, consider the general screw pinch. The relevant equilibrium quantities are  $p(r)$  and  $\mathbf{B}=B_\theta(r)\mathbf{e}_\theta+B_z(r)\mathbf{e}_z$ ; they satisfy

$$\frac{d}{dr}[p + \frac{1}{2}(B_\theta^2 + B_z^2)] + \frac{B_\theta^2}{r} = 0. \quad (5.76)$$

Although two field components are present, the system still possesses  $(\theta, z)$  symmetry, so that the perturbations can be Fourier analyzed:  $\xi(\mathbf{r})=\xi(r)\exp[i(m\theta+kz)]$ . In fact, it is this dual symmetry that is ultimately responsible for the algebraic elimination of two components of  $\xi$  in the minimization procedure.

For the screw pinch it is convenient to decompose the displacement vector as follows:

$$\xi = \xi_r \mathbf{e}_r + \eta \mathbf{e}_\theta + \xi_{||} \mathbf{e}_b, \quad (5.77)$$

where  $\mathbf{e}_b$  is the unit vector along  $\mathbf{B}$  and

$$\begin{aligned} \xi_{||} &= (\xi_r B_\theta + \xi_z B_z)/B, \\ \eta &= (\xi_r B_z - \xi_z B_\theta)/B, \\ \mathbf{e}_\eta &= (B_z \mathbf{e}_\theta - B_\theta \mathbf{e}_z)/B. \end{aligned} \quad (5.78)$$

The first step in the minimization procedure is to examine the incompressibility condition. For a given  $m$  and  $k$ , setting  $\nabla \cdot \xi = 0$  yields

$$\xi_{||} = i \frac{B}{F} \nabla \cdot \xi_\perp, \quad (5.79)$$

where

$$F = \mathbf{k} \cdot \mathbf{B} = m B_\theta / r + k B_z. \quad (5.80)$$

Excluding the very special case of zero shear [i.e.,  $(B_\theta/rB_z)'=0$ ],  $F$  will in general be nonzero except perhaps at a finite number of discrete radii. If  $F$  is nonzero everywhere, a well-behaved  $\xi_{||}$  can be chosen in accordance with Eq. (5.79), and the plasma compressibility term in  $\delta W_F$  vanishes. Even when  $F=0$  singular points exist (as they almost always do), the compressibility term can be made negligibly small with a well-behaved  $\xi_{||}$ ,

$$\xi_{||} = \frac{iBF}{F^2 + \sigma^2} \nabla \cdot \xi_\perp, \quad (5.81)$$

where  $\sigma^2 > 0$  is small but nonzero. In this case the compressibility term is approximately given (for one singular point located at  $r=r_s$ ) by

$$\frac{1}{2} \int \gamma p |\nabla \cdot \xi|^2 d\mathbf{r} \approx \frac{\sigma}{2} \pi^2 L \left( \frac{\gamma p r |\nabla \cdot \xi_\perp|^2}{F'} \right)_{r_s} \quad (5.82)$$

and becomes arbitrarily small as  $\sigma \rightarrow 0$ .

The remaining terms in  $\delta W_F$  are functions only of  $\xi$  and  $\eta$ . As in previous cases, straightforward substitution shows that  $\eta$  appears only algebraically. The minimizing condition gives

$$\eta = \frac{i}{rk_0^2 B} [G(r\xi)' + 2kB_\theta \xi] \quad (5.83)$$

with  $k_0^2 = k^2 + m^2/r^2$  and  $G = mB_z/r - kB_\theta$ . After a slightly tedious calculation, one can write  $\delta W_F$  in the following form (Newcomb, 1960):

$$\frac{\delta W_F}{L} = \pi \int_0^a dr (f \xi'^2 + g \xi^2), \quad (5.84)$$

where

$$\begin{aligned} f &= \frac{rF^2}{k_0^2}, \\ g &= 2 \frac{k^2}{k_0^2} p' + \left( \frac{k_0^2 r^2 - 1}{k_0^2 r^2} \right) r F^2 + 2 \frac{k^2}{r k_0^4} \left[ kB_z - \frac{m B_\theta}{r} \right] F. \end{aligned} \quad (5.85)$$

Equation (5.84) is the usual form of the Energy Principle for internal modes [i.e.,  $\xi(a)=0$ ].

Consider now the generalization to external modes. First, when  $\xi(a) \neq 0$  there is an additional boundary term to  $\delta W_F$  resulting from the several integrations by parts required to obtain the form given by Eq. (5.84). The full  $\delta W_F$  can be written as

$$\frac{\delta W_F}{L} (\text{ext}) = \frac{\delta W_F}{L} (\text{int}) + \pi \left[ \frac{k^2 r^2 B_z^2 - m^2 B_\theta^2}{k_0^2 r^2} \right]_a \xi^2(a). \quad (5.86)$$

Here  $\delta W_F(\text{int})/L$  is given by Eq. (5.84). These must be combined with the surface and vacuum contributions to  $\delta W$ . If the assumption is made that no surface currents flow in the plasma, then  $\delta W_S=0$ . The remaining vacuum term is calculated, as follows. In the vacuum,  $\hat{\mathbf{B}}_1 = \nabla \hat{\phi}_1$  with  $\hat{\phi}_1$  satisfying  $\nabla^2 \hat{\phi}_1 = 0$ . The solution for  $\hat{\phi}_1$ , assuming a conducting wall at  $r=b$ , is given by

$$\hat{\phi}_1 = A \left[ K_r - \left( \frac{K'_b}{I'_b} \right) I_r \right] \exp[i(m\theta+kz)], \quad (5.87)$$

where  $K_z = K_m(kz)$  and  $I_z = I_m(kz)$ . The amplitude  $A$  is related to  $\xi(a)$  through the boundary condition  $\mathbf{n} \cdot \mathbf{B}_1 = \mathbf{B} \cdot \nabla \xi - \xi \mathbf{n} \cdot (\mathbf{n} \cdot \nabla) \mathbf{B}$  [see Eq. (5.45)]. One finds

$$A = \frac{iF(a)\xi(a)}{K_a} \left[ 1 - \left( \frac{K'_b}{I'_b} \right) \left( \frac{I_a}{K_a} \right) \right]^{-1}. \quad (5.88)$$

The last step in the computation is to make use of the fact that  $\nabla^2 \hat{\phi}_1 = 0$  and transform  $\delta W_V$  into a surface integral. The result is

$$\delta W_V = \frac{1}{2} \int_V d\mathbf{r} |\hat{\mathbf{B}}_1|^2 = -\frac{1}{2} \int_S dS (\mathbf{n} \cdot \nabla \hat{\phi}_1) \hat{\phi}_1^*. \quad (5.89)$$

Substituting into Eq. (5.89) and combining the results with Eq. (5.86) yields the following expression for  $\delta W$ :

$$\frac{\delta W}{\pi L} = \int_0^a dr [f\xi'^2 + g\xi^2] + \left[ \left( \frac{krB_z - mB_\theta}{k_0^2 r^2} \right) rF + \frac{r^2 \lambda}{m} F^2 \right]_a \xi^2(a), \quad (5.90)$$

where

$$\begin{aligned} \lambda &= -\frac{mK_a}{kaK'_a} \left( \frac{1 - (K'_b I_a)/(I'_b K_a)}{1 - (K'_b I'_a)/(I'_b K'_a)} \right) \\ &\approx \frac{1 + (a/b)^{2m}}{1 - (a/b)^{2m}}, \quad kb \ll 1. \end{aligned} \quad (5.91)$$

To summarize, the Energy Principle for the general screw pinch reduces to a quadratic form in one dependent variable,  $\xi$ . This expression, given by Eq. (5.90), is exact in that the minimizations with respect to  $\xi_{||}$  and  $\eta$  have been carried out without approximation. Equation (5.90) is valid for either external modes or internal modes if  $\xi(a)$  is nonzero or zero, respectively.

An examination of Eq. (5.90) indicates that screw-pinch stability is rather complicated because of the complexity of  $g(r)$ . Nevertheless, there are a number of general properties that can be proven for arbitrary profiles. First, necessary and sufficient conditions for stability based on the behavior of  $\xi$  have been given by Newcomb (1960). Second, a general oscillation theorem proving the Sturmian and anti-Sturmian behavior of the eigenvalues has been given by Goedbloed and Sakanaka (1974). Both of these properties are extremely valuable, not only for their physical content, but for their practical usefulness in devising numerical schemes for testing stability. The third property of interest is known as Suydam's criterion (Suydam, 1958). This is a purely analytical criterion, depending only on the equilibrium profiles, which provides a test of stability to the special class of perturbations corresponding to localized interchanges.

### b. Suydam's criterion

The Suydam criterion is derived by assuming that  $\xi(r)$  is a highly localized function of radius when evaluating  $\delta W$ . Since this corresponds to a special subclass of trial functions, the Suydam criterion is necessary but not sufficient for stability. The motivation for a localized eigenfunction follows from the observation that if  $F=0$  at some radius  $r=r_s$ , then each term in  $f$  and  $g$  vanishes except the  $p'$  term, which is almost always negative (i.e., destabilizing). Thus a perturbation localized about  $r=r_s$  has a reasonable likelihood of causing a pressure-driven instability. Note that  $F \equiv \mathbf{k} \cdot \mathbf{B} = 0$  corresponds to  $k_{||} \approx 0$ , so that such perturbations tend to minimize the bending of the magnetic lines. Consequently the Suydam criterion describes the stability of internal localized interchange perturbations.

The first step in the derivation is to assume that  $\xi(r)$  is localized about the singular surface  $F(r_s)=0$ . All quantities in  $\delta W_F$  are then expanded about  $x=r-r_s$ . The leading-order contribution is given by

$$\begin{aligned} \frac{\delta W_F}{L} &\approx \pi \left[ \frac{rF'^2}{k_0^2} \right]_{r_s} \delta W_f, \\ \delta W_f &= \int_{-\Delta}^{\Delta} dx \left[ x^2 \left( \frac{d\xi}{dx} \right)^2 + \alpha \xi^2 \right], \end{aligned} \quad (5.92)$$

where

$$\alpha = \left[ \frac{2k^2 p'}{rF'^2} \right]_{r_s} = \left[ \frac{2p' \mu^2}{rB_z^2 \mu'^2} \right]_{r_s}. \quad (5.93)$$

$\mu=B_\theta/rB_z$  is the pitch number of the magnetic field, and  $\mu'$  is the shear. The quantity  $\Delta \ll a$  is a measure of the localization. The function  $\xi$ , which minimizes  $\delta W_f$ , satisfies the Euler-Lagrange equation

$$\frac{d}{dx} \left[ x^2 \frac{d\xi}{dx} \right] - \alpha \xi = 0 \quad (5.94)$$

and has as its solution

$$\begin{aligned} \xi &= C_1 x^{p_1} + C_2 x^{p_2}, \\ p_{1,2} &= -\frac{1}{2} \pm \frac{1}{2}(1+4\alpha)^{1/2}. \end{aligned} \quad (5.95)$$

Since at least one solution for  $\xi$  is always singular, one cannot simply use the solution to Eq. (5.95) as a trial function in  $\delta W_f$ . Whether or not  $\xi$  can be modified very near  $x=0$  so that it becomes a well-behaved, allowable trial function, still capable of making  $\delta W_f < 0$ , depends upon the sign of  $1+4\alpha$ .

For  $1+4\alpha < 0$  the roots are complex and

$$\begin{aligned} \xi &= \frac{1}{|x|^{1/2}} [C_1 \sin(k_r \ln |x|) + C_2 \cos(k_r \ln |x|)], \\ k_r &= \frac{1}{2} [-(1+4\alpha)]^{1/2}. \end{aligned} \quad (5.96)$$

The solution as  $x \rightarrow 0$  oscillates infinitely rapidly with a diverging envelope proportional to  $1/|x|^{1/2}$ . Because of the oscillatory behavior, it is possible to construct a well-behaved  $\xi$  such that  $\delta W_f$  is always negative (i.e., unstable). The modified  $\xi$  is illustrated in Fig. 34. In regions I and V,  $\xi=0$  so that  $\delta W_f(I)=\delta W_f(V)=0$ . In regions II and IV,  $\xi$  satisfies the Euler-Lagrange equation. The corresponding contributions to  $\delta W_f$  are obtained by multiplying Eq. (5.94) by  $\xi$  and integrating over each region. Since either  $\xi$  or  $\xi'$  is zero at the end points of both regions, one finds

$$\delta W_f(II) = \int_{x_1}^{x_2} (x^2 \xi'^2 + \alpha \xi^2) dx = x^2 \xi \xi' \Big|_{x_1}^{x_2} = 0,$$

$$\delta W_f(IV) = \int_{x_3}^{x_4} (x^2 \xi'^2 + \alpha \xi^2) dx = x^2 \xi \xi' \Big|_{x_3}^{x_4} = 0. \quad (5.97)$$

The total contribution to  $\delta W_f$  arises from region III, where  $\xi=\text{const}$  and is given by

$$\delta W_f = \int_{x_2}^{x_3} (x^2 \xi'^2 + \alpha \xi^2) dx = \alpha \xi_0^2 (x_3 - x_2). \quad (5.98)$$

By assumption  $\alpha < -1/4$ . Therefore  $\delta W_f < 0$  and the system is unstable.

When  $1+4\alpha > 0$ , the indicial roots are real and at least

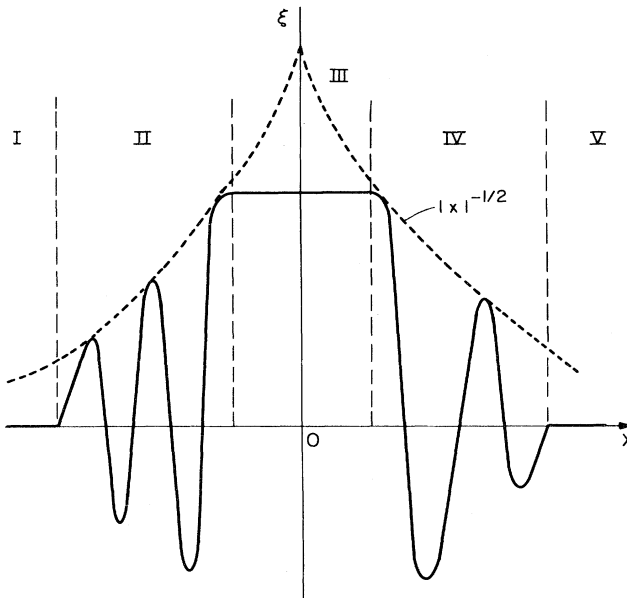


FIG. 34. Trial function leading to violation of Suydam's stability criterion.

one solution is singular. In this case oscillatory solutions do not exist, and a localized, well-behaved trial function cannot be constructed; that is, if  $1 + 4\alpha > 0$  the system is stable to localized interchange perturbations.

The stability boundary  $1 + 4\alpha > 0$  is known as Suydam's criterion. If it is violated for any  $r_s$  in the interval  $(0, a)$ , the plasma is unstable. The usual form for Suydam's criterion is given by (Suydam, 1958)

$$rB_z^2 \left[ \frac{\mu'}{\mu} \right]^2 + 8p' > 0. \quad (5.99)$$

Equation (5.99) indicates that the stability boundary involves two competing effects. The destabilizing term, corresponding to the interchange drive, results from the combination of a negative pressure gradient and the unfavorable curvature of the  $B_\theta$  field. The stabilizing term, proportional to  $\mu'^2$ , represents the work done in bending the field lines when interchanging two flux tubes in a system with shear.

One final question to be addressed is whether a mode with such highly localized structure would be important in an actual experiment and not be dominated by other physics. The answer is connected with the oscillation theorem discussed later. Briefly, the theorem shows that violation of Suydam's criterion corresponds to the existence of an accumulation point of discrete eigenvalues at  $\omega^2 = 0$  from the unstable side of the spectrum. In addition, the theorem proves that the unstable eigenvalues and eigenfunctions have Sturmian behavior; that is, if a highly oscillatory localized mode with a certain growth rate exists (as implied by violation of Suydam's criterion), a gross mode with zero nodes must also exist and have the maximum growth rate. Thus it is the guarantee that such a large-scale mode must exist that makes the violation of Suydam's criterion important.

### c. Newcomb's analysis

A general analysis of the Energy Principle for the screw pinch has been given by Newcomb (1960). In this investigation a set of necessary and sufficient conditions for the behavior of  $\xi$  are derived for determining MHD stability of arbitrary internal modes. Although the end results do not yield analytical criteria, such as the Suydam criterion, they provide a simple general prescription, which can easily be implemented numerically, for testing stability of arbitrary screw-pinch profiles. A key feature of the analysis is the use of ideas associated with Sturm's separation theorem. A brief outline of Newcomb's theory is given below.

To begin, consider  $\delta W_F$  given by Eq. (5.84) and assume that  $m$  and  $k$  are such that  $F(r) \neq 0$  in the interval  $(0, a)$ . In this case, the Euler-Lagrange equation

$$\frac{d}{dr} \left[ f \frac{d\xi}{dr} \right] - g\xi = 0 \quad (5.100)$$

is nonsingular and has two independent solutions:

$$\xi = C_1 \xi_1(r) + C_2 \xi_2(r). \quad (5.101)$$

Here  $\xi_1(r)$  can be chosen to be regular at  $r=0$ , but  $\xi_1(a)$  is not in general zero. Similarly  $\xi_2(r)$  can be chosen so that  $\xi_2(a)=0$  but  $\xi_2(0)$  is not in general regular at  $r=0$ .

In the first part of the analysis it is shown that when  $\xi_1(r)$  has a zero anywhere in the interval  $(0, a)$ , a trial function can be constructed which makes  $\delta W_F < 0$ . If no zero exists, the system is stable to the given  $m$  and  $k$ . The analysis is based on the separation theorem, which proves that the zeros of any two independent solutions of Eq. (5.100) [ $\xi_1(r)$  and  $\xi_2(r)$ , for instance] must alternate.

This is easily demonstrated by assuming the opposite; that is,  $\xi_1(r)$  has two consecutive zeros,  $r_1$  and  $r_2$ , and  $\xi_2'(r) \neq 0$  in the interval  $(r_1, r_2)$  (see Fig. 35). Clearly,  $\xi_1'=0$  for some intermediate  $r_0, r_1 < r_0 < r_2$ . Therefore the well-behaved function  $Y = \xi_1(r)/\xi_2(r)$  also has zeros at  $r_1$  and  $r_2$  and an intermediate zero derivative. If one now computes

$$Y' = \frac{\xi_2 \xi_1' - \xi_1 \xi_2'}{\xi_2^2}, \quad (5.102)$$

it follows that  $Y'$  can equal zero only if the Wronskian  $\xi_2 \xi_1' - \xi_1 \xi_2' = 0$  somewhere in the interval. However, should this occur, the assumption that  $\xi_1$  and  $\xi_2$  are independent is contradicted. Hence, the zeros must alternate.

Using this result, a trial function can be constructed using  $\xi_1(r)$  and  $\xi_2(r)$  in different parts of the interval  $(0, a)$  as shown in Fig. 36(a). Here it is assumed that  $\xi_1(r)$  has one zero at  $r_1$ . (The results can easily be generalized to include more than one zero.) The separation theorem guarantees that an  $r_2$  must exist such that  $\xi_2(r_2)=0$  with  $0 < r_2 < r_1$ . Likewise, in the interval  $r_2 < r < a$ ,  $\xi_2(r)$  cannot have a second zero:  $\xi_2(r) \neq 0$ ,  $r_2 < r < a$ . The trial function is constructed using  $\xi_1(r)$  to the left of the intersection point  $r_0$  and  $\xi_2(r)$  to the right. The value of  $\delta W_F$  is obtained by multiplying Eq.

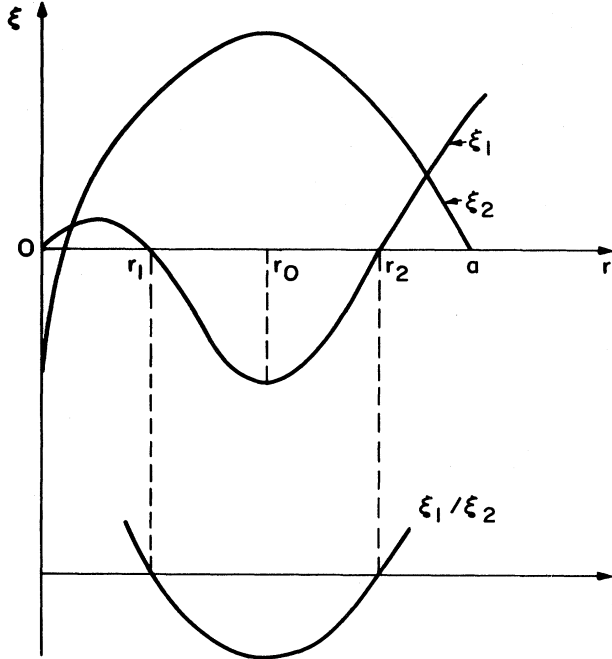


FIG. 35. Illustration of the separation theorem.

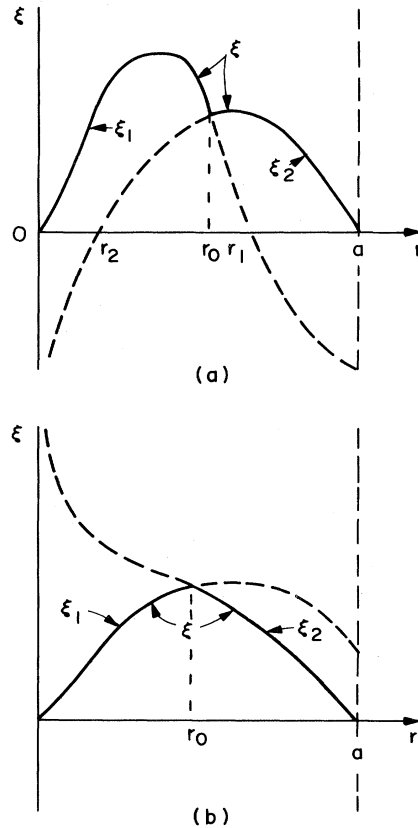
(5.100) by  $\xi$  and integrating over the separate regions. The result is

$$\begin{aligned} \frac{\delta W_F}{L} &= \pi f \xi_1 \xi'_1 \Big|_0^{r_0} + \pi f \xi_2 \xi'_2 \Big|_{r_0}^a \\ &= \pi f(r_0) \xi(r_0) [\xi'_1(r_0) - \xi'_2(r_0)]. \end{aligned} \quad (5.103)$$

Because of the separation theorem,  $\xi'_1(r_0) - \xi'_2(r_0) < 0$ , implying  $\delta W_F < 0$ , the system is unstable. If, however,  $\xi_1(r_0)$  has no zeros in the interval  $(0, a)$ , the only type of trial functions that can be constructed consistent with the separation theorem and the boundary conditions are shown in Fig. 36(b). In this case Eq. (5.103) still applies, but  $\xi'_1(r_0) - \xi'_2(r_0) > 0$  and the system is stable.

The first part of Newcomb's analysis can thus be summarized as follows. For values of  $k$  and  $m$  such that  $F(r) \neq 0$  in the interval  $(0, a)$ , the screw pinch is stable if and only if the nontrivial solution of the Euler-Lagrange equation [i.e., Eq. (5.100)], which is regular at  $r=0$ , does not have a zero for  $0 < r < a$ .

The situation is slightly more complicated if  $F(r_s) = 0$ ,  $0 < r_s < a$ . In this case, the Euler-Lagrange equation is singular, and the proper prescription for calculating  $\xi$  in the vicinity of the singular surface must be determined. Recall that in the vicinity of  $r_s$  the behavior of  $\xi$  is given by  $\xi = C_1 x^{p_1} + C_2 x^{p_2}$ , where  $x = r - r_s$  and  $p_{1,2} = -(\frac{1}{2}) \pm (\frac{1}{2})(1 + 4\alpha)^{1/2}$  [see Eq. (5.95)]. To determine the conditions for stability one must assume  $(1 + 4\alpha)_{r_s} > 0$  or else Suydam's criterion is violated. The proper choice of  $\xi$  is then determined by the physical condition that the potential energy remain bounded. Hence the root  $p_1 > -\frac{1}{2}$  is allowable, while  $p_2 < -\frac{1}{2}$

FIG. 36. Trial functions showing: (a) instability, and (b) stability by means of Newcomb's analysis for the case where  $F(r) \neq 0$ ,  $0 \leq r \leq a$ .

leads to a divergent energy. That is,

$$\int dx (x^2 \xi'^2 + \alpha \xi^2) = - \left[ \frac{p}{2p+1} \right] x^{2p+1} \rightarrow \begin{cases} 0 & \text{for } p_1 > -\frac{1}{2} \\ \infty & \text{for } p_2 < -\frac{1}{2}. \end{cases}$$

The conclusion is that in connecting through a singular point one must choose trial functions containing only the small solution (i.e., the root  $p_1$ ). In effect the singularity acts like a regularity condition at the origin, in that it singles out one of the two independent solutions as admissible. Because of this, the interval  $(0, a)$  must be broken into subintervals whose boundaries correspond to the successive zeros of  $F(r) = 0$ . The first and last intervals are bounded by  $r=0$  and  $r=a$ , respectively.

Each subinterval must be tested for stability separately. The analysis given for  $F(r) \neq 0$ ,  $0 < r < a$  can be directly applied to each subinterval. Typical trial functions for the case of one singular surface are illustrated in Fig. 37. The corresponding value of  $\delta W_F$  is given by

$$\frac{\delta W_F}{L} = \pi f \xi_1 \xi'_1 \Big|_{r_s}^{r_0} + \pi f \xi_2 \xi'_2 \Big|_{r_0}^a$$

$$= \pi f(r_0) \xi(r_0) [\xi'_1(r_0) - \xi'_2(r_0)]. \quad (5.104)$$

Note that the requirement that  $\xi_1(r)$  contain only the small solution guarantees that the boundary contribution at  $r=r_s$  vanishes. As before, if  $\xi_1(r)$  has a zero in the subinterval,  $\delta W_F < 0$ . If not,  $\delta W_F > 0$ .

The second part of Newcomb's analysis can be summarized as follows. For values of  $k$  and  $m$  such that  $F(r_s)=0$ ,  $0 < r_s < a$ , the screw pinch is stable if and only if: (1) Suydam's criterion is satisfied at  $r=r_s$ , and (2) the nontrivial solution of the Euler-Lagrange equation containing only the small solution at  $r=r_s$  does not have a zero either for  $r_s > r > 0$  or for  $r_s < r < a$ .

Newcomb's analysis clearly shows how the stability of a given screw-pinch profile is related to the solution for  $\xi$  of the corresponding Euler-Lagrange equation. For any specific application, one can easily solve Eq. (5.100) numerically and then ascertain stability by Newcomb's procedure.

A final practical point worth noting is that in large-aspect-ratio systems where  $k$  can essentially be considered a continuous rather than quantized mode number, the range of  $(m, k)$  parameter space that needs to be tested for stability is significantly reduced from the full range  $-\infty < m < \infty, -\infty < k < \infty$ . This follows from the form of  $f$  and  $g$  given in Eq. (5.85). For  $m \neq 0$  consider  $k'=k/m$  and  $m$  as the two independent mode numbers. Under this transformation,  $f$  is independent of  $m$ , and  $g$  contains only one term with explicit  $m$  dependence given by

$$g(m, k', r) = \hat{g}(r, k') + m^2 r (k' B_z + B_\theta/r)^2. \quad (5.105)$$

Since the  $m$ -dependent term is always stabilizing, the most unstable case corresponds to  $m=1$ . Similarly for  $m=0$ ,  $f$  is independent of  $k$ , and  $g$  contains only one term with explicit  $k$  dependence,

$$g(m=0, k, r) = \hat{g}(r) + r k^2 B_z^2. \quad (5.106)$$

In this case, the most unstable mode corresponds to  $k^2 \rightarrow 0$ .

Consequently, when testing for stability, it is necessary and sufficient to examine only  $m=1, -\infty < k < \infty$  and  $m=0, k^2 \rightarrow 0$ , a significant reduction of the overall parameter space.

#### d. Oscillation theorem

Goedbloed and Sakanaka (1974) have derived an important result concerning the stability of arbitrary screw pinches by showing the existence of an oscillation theorem for the full eigenvalue problem. For fixed  $m$  and  $k$ , the oscillation theorem implies that as the number of radial nodes in a sequence of unstable eigenfunctions monotonically decreases, the corresponding eigenvalue  $\omega^2$  also monotonically decreases (i.e., becomes more unstable). The problem is conceptually similar to that of the classic Sturm-Liouville system, but is significantly more difficult in practice because of the complex manner

in which the eigenvalue enters the equations. A brief outline of the derivation and conclusions of Goedbloed and Sakanaka is given below.

Since the calculation involves the behavior of  $\omega^2$ , the full eigenvalue equation is required and not simply the Euler-Lagrange equation corresponding to  $\delta W$ . The derivation nevertheless is very similar. One writes  $\xi = \xi_r + \eta e_\eta + \xi_{||} e_b$  and substitutes into the full variational form  $\delta \mathcal{L} = \delta W - \omega^2 K$ . Again, because of symmetry, minimization with respect to  $\xi_{||}$  and  $\eta$  is algebraic. After a slightly tedious calculation one obtains the following variational formulation [see Goedbloed (1979) for a detailed derivation of Eq. (5.107)]:

$$\frac{\delta \mathcal{L}}{L} = \pi \int [f(r\xi)'^2 + g(r\xi)^2] dr \quad (5.107a)$$

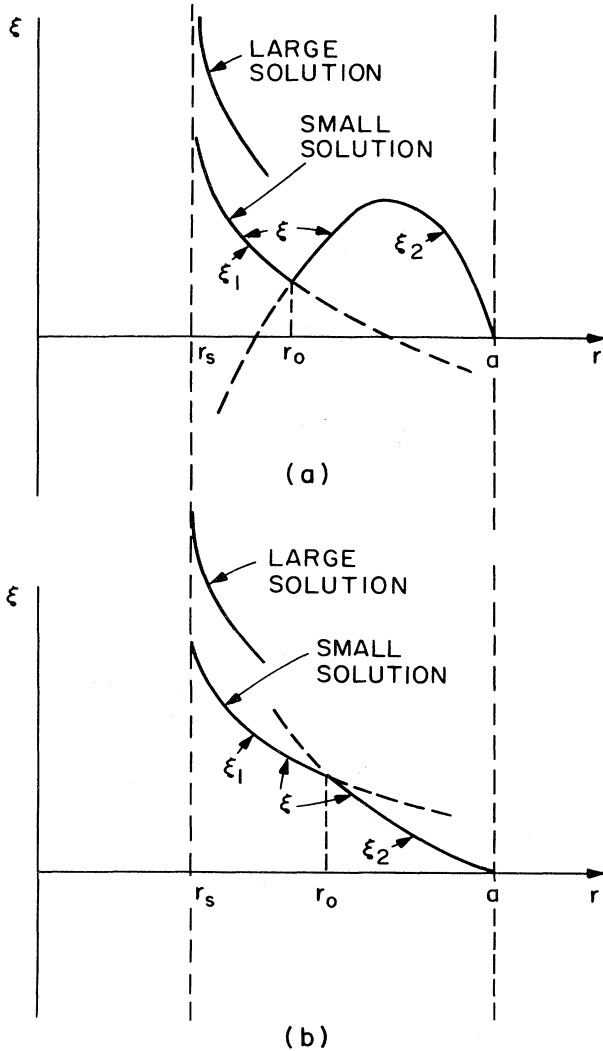


FIG. 37. Trial function showing (a) instability and (b) stability by means of Newcomb's analysis for the case where  $F(r)=0$  at  $r=r_s$ .

or the equivalent Euler-Lagrange equation [first derived by Hain and Lüst (1958)],

$$\frac{d}{dr} \left[ f \frac{d\chi}{dr} (r\xi) \right] - g(r\xi) = 0, \quad (5.107b)$$

where

$$\begin{aligned} f &= \frac{\rho(V_a^2 + V_s^2)}{r} \frac{(\omega^2 - \omega_a^2)(\omega^2 - \omega_h^2)}{(\omega^2 - \omega_f^2)(\omega^2 - \omega_s^2)}, \\ g &= -\frac{\rho}{r} (\omega^2 - \omega_a^2) + \frac{4k^2 B_\theta^2}{r^3} \frac{V_a^2 (\omega^2 - \omega_g^2)}{(\omega^2 - \omega_f^2)(\omega^2 - \omega_s^2)} \\ &\quad + \left[ \frac{B_\theta^2}{r^2} - \frac{2kB_\theta G}{r^2} \frac{(V_a^2 + V_s^2)(\omega^2 - \omega_h^2)}{(\omega^2 - \omega_f^2)(\omega^2 - \omega_s^2)} \right]', \end{aligned} \quad (5.108)$$

and

$$\begin{aligned} G &= mB_z/r - kB_\theta, \quad \omega_a^2 = F^2/\rho, \\ V_a^2 &= B^2/\rho, \quad \omega_h^2 = \omega_a^2 [V_s^2/(V_s^2 + V_a^2)], \\ V_s^2 &= \gamma p/\rho, \quad \omega_g^2 = \omega_a^2 (V_s^2/V_a^2), \\ \omega_{f,s}^2 &= \frac{1}{2} k_0^2 (V_a^2 + V_s^2) [1 \pm (1 - \alpha^2)^{1/2}], \\ \alpha^2 &= 4V_s^2 \omega_a^2 / [k_0^2 (V_a^2 + V_s^2)^2] \geq 0. \end{aligned}$$

The complexity of Eq. (5.107) gives some appreciation of the simplicity of testing stability by means of  $\delta W$  rather than the full eigenvalue formulation.

The oscillation theorem is derived by examining the behavior of  $\xi(a)$  as a function of  $\omega^2$ . Consider two solutions,  $\chi = r\xi_1$  and  $\xi = r\xi_2$ , corresponding to two neighboring values of  $\omega^2$ ,  $\omega_1^2$ , and  $\omega_2^2$ , respectively. Assume each solution is regular at the origin and that  $\omega_2^2 = \omega_1^2 + \delta\omega^2$ ,  $\xi = \chi + \delta\chi$  with  $\delta\omega^2$  and  $\delta\chi$  small. [Note that, for a given  $\omega_1^2$ ,  $\chi$  will not in general satisfy the boundary condition  $\chi(a) = 0$ .] The equations of motion determining  $\chi$  and  $\delta\chi$  are given by

$$\frac{d}{dr} \left[ f \frac{d\chi}{dr} \right] - g\chi = 0, \quad (5.109a)$$

$$\frac{d}{dr} \left[ f \frac{d\delta\chi}{dr} \right] - g\delta\chi = -\delta\omega^2 \left[ \frac{d}{dr} \left( \frac{\partial f}{\partial \omega_1^2} \frac{d\chi}{dr} \right) - \frac{\partial g}{\partial \omega_1^2} \chi \right], \quad (5.109b)$$

where  $f = f(r, \omega_1^2)$ ,  $g = g(r, \omega_1^2)$ .

Assume now that  $\chi(r_1) = 0$ ,  $0 < r_1 \leq a$  (see Fig. 38). The relationship between  $\delta\chi(r_1)$  and  $\delta\omega^2$  is obtained by multiplying Eq. (5.109a) by  $\delta\chi$ , Eq. (5.109b) by  $\chi$ , integrating over the range  $0 \leq r \leq r_1$ , and then subtracting. The result is

$$(f\chi' \delta\chi)_{r_1} = -\delta\omega^2 \int_0^{r_1} \left[ \frac{\partial f}{\partial \omega_1^2} \chi'^2 + \frac{\partial g}{\partial \omega_1^2} \chi^2 \right] dr. \quad (5.110)$$

Although the integral in Eq. (5.110) is straightforward to evaluate in principle, it is difficult in practice because of

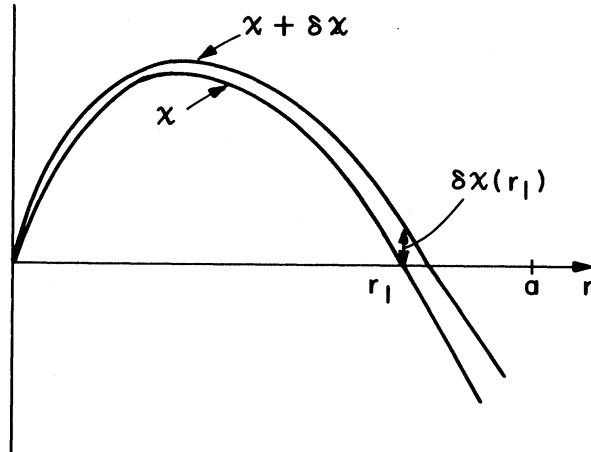


FIG. 38.  $\chi$  solution used in the derivation of the oscillation theorem.

the complexity of  $g$ . Goedbloed and Sakanaka have pointed out a simple method of evaluation by transforming to the original set of dependent variables  $\xi, \eta, \xi_{||}$  as follows:

$$\begin{aligned} I &\equiv \int_0^{r_1} \left[ \frac{\partial f}{\partial \omega_1^2} \chi'^2 + \frac{\partial g}{\partial \omega_1^2} \chi^2 \right] dr \\ &= \left[ \frac{\partial}{\partial \omega^2} \int_0^{r_1} (f\chi'^2 + g\chi^2) dr \right]_{\omega^2=\omega_1^2} \\ &= \left[ \frac{1}{\pi L} \frac{\partial}{\partial \omega^2} (\delta W - \omega^2 K) \right]_{\omega^2=\omega_1^2} \\ &= -\frac{K}{\pi L} = - \int_0^{r_1} r dr (|\xi|^2 + |\eta|^2 + |\xi_{||}|^2) < 0. \end{aligned} \quad (5.111)$$

Equation (5.110) now has the form

$$(f\chi' \delta\chi)_{r_1} = \delta\omega^2 K / \pi L, \quad (5.112)$$

which implies that a given change in  $\delta\omega^2$  causes a corresponding change in  $\delta\chi(r_1)$ , the sign of which is determined by the sign of  $f'(r_1)\chi'(r_1)$ . In the unstable portion of the spectrum,  $\omega^2 < 0$  so that  $f(r) > 0$ ,  $0 < r < a$ . Consequently, if  $\delta\omega^2 < 0$ , the radial node of  $\chi$  at  $r_1$  always moves outward.

Continuous application of this result for a sequence of negative  $\delta\omega^2$ 's leads to the oscillation theorem. If an unstable eigenfunction exists with  $n$  radial nodes and corresponding eigenvalue  $\omega^2 = \omega_n^2 < 0$ , then a continual decrease in  $\omega^2$  (i.e., an increase in instability) eventually gives rise to unstable eigenfunctions with  $n-1, n-2, n-3, \dots, 0$  radial nodes. In all cases, the zero-node mode has the fastest growth rate. Therefore, if Suydam's criterion is violated, the oscillation theorem guarantees the existence of a macroscopic zero-node mode with maximum growth rate (for the given  $m$  and  $k$ ). This points out the importance of satisfying

Suydam's criterion. The oscillation theorem also shows that  $\omega^2=0$  is a point of accumulation from the unstable side of the spectrum when Suydam's criterion is violated. A complete derivation of the oscillation theorem, including its implications on the stable side of the spectrum, can be found in the lecture notes of Goedbloed (1979).

Finally, it is useful to note that as a consequence of the oscillation theorem numerical parameter studies of maximum growth rates are significantly simplified by restricting attention only to the zero-node mode.

#### 4. The reversed field pinch

##### a. Introduction

In this section the general screw-pinch analysis is applied to the reversed-field-pinch configuration. Recall that the appropriate inverse aspect ratio expansion for the RFP requires  $B_z/B_\theta \sim p/B_\theta^2 \sim 1$ . Consequently the toroidal corrections are indeed small, and an essentially complete MHD stability description is obtained from an analysis of the one-dimensional cylindrical model. Furthermore, since the RFP is surrounded by a conducting wall, only internal modes need be considered.

By making use of Suydam's criterion and various trial functions, it is possible to develop an intuition as to why RFP profiles have favorable stability properties with respect to pressure-driven and current-driven modes. Such analyses have been carried out by Robinson (1971) and more recently by Sakanaka and Goedbloed (1974). They have shown that of all reasonable  $B_\theta$  and  $B_z$  profiles containing an isolating, current-free region near the conducting wall, the RFP profile is the one most capable of sustaining complete ideal MHD stability at high values of  $\beta$ . In each case, the intuitive arguments are supported by numerical calculations of the exact equations. As an example, Robinson showed that with a reasonably located conducting wall,  $b/a \sim 2$ , completely stable RFP profiles exist for  $\beta \approx 30\%$ . This optimistic theoretical result and the experimental data from the "quiescent" operating regime of Zeta [see Bodin and Newton (1980) for a review of RFP experiments] provide strong motivation for consideration of the RFP configuration as a fusion concept.

Finally, a brief outline is presented of the recent theory of Taylor (1975) concerning the time evolution of pinch discharges. His theory suggests that, under a wide range of conditions, many configurations will naturally evolve to low- $\beta$  "RFP-like" profiles, including self-reversal of the toroidal field.

##### b. Pressure-driven modes

To determine the influence of pressure-driven modes on the RFP configuration, two stability tests are performed, as originally suggested by Robinson (1971). First, an examination of Suydam's criterion shows that the profiles must possess certain local features for stability.

Second, the use of appropriate trial functions gives reasonable bounds for the overall limit on  $\langle \beta \rangle$ .

Consider first Suydam's criterion. If the toroidal current density on axis,  $J_z(0)$ , is nonzero, then near  $r=0$  Suydam's criterion has the form

$$\left[ \frac{1}{2} B_z(0) \frac{\mu''(0)}{\mu(0)} \right]^2 r^3 + 8p''(0)r > 0. \quad (5.113)$$

Near the axis there is insufficient shear to stabilize the interchange perturbation. To avoid such instabilities it is necessary that  $p''(0) \geq 0$ , implying that for small  $r$  the pressure profile must be hollow or extremely flat.

Suydam's criterion also points out the importance of the reversal in  $B_z$ . To show this, it is convenient to introduce the pitch length  $Q \equiv 1/\mu = rB_z/B_\theta$ . If there is a current-free region near the wall, then  $B_z \sim \text{const}$ ,  $B_\theta \sim 1/r$ , and  $Q \sim r^2$ . In addition, near the axis,  $B_z$  decreases more rapidly than  $J_z$  (to keep the pressure profile hollow), so that  $Q$  is also a decreasing function of  $r$ . Consequently, if  $B_z$  does not reverse, there must be a minimum in  $Q$  near the outside of the plasma as shown in Fig. 39(a). Suydam's criterion indicates that an instability will occur if  $Q'=0$  when  $p' < 0$ . This situation is avoided if  $B_z$  reverses, in which case  $Q$  passes through zero and  $Q' \neq 0$  [see Fig. 39(b)]. Thus, in the RFP configuration, stability to interchange perturbations requires a hollow pressure profile to avoid modes near  $r=0$  and high shear caused by the  $B_z$  reversal to avoid modes on the outside of the profile.

Although Suydam's criterion provides valuable insight into the local properties of the RFP, it does not provide an overall  $\langle \beta \rangle$  limit. Such limits can be estimated by substituting appropriate trial functions into  $\delta W$  for the  $m=1$  and  $m=0$  modes. For the  $m=1$  mode, a trial function likely to cause instability is illustrated in Fig. 40(a). By letting  $\xi$  drop to zero [as it must since  $\xi(b)=0$ ] in a thin layer about  $r_s$ , where  $F(r_s)=0$ , the stabilizing contribution vanishes:  $\int f\xi^2 dr \rightarrow 0$  as  $\epsilon \rightarrow 0$ . Furthermore, the destabilizing region is maximized when  $r_s \rightarrow b$ . Using this trial function, the Energy Principle implies that

$$\frac{\delta W_F}{L} < \pi \xi_0^2 \int_0^b g dr. \quad (5.114)$$

If  $p'$  is eliminated by the pressure balance relation, then  $g$  can be rewritten as

$$g(r) = \left[ k^2 r^2 \left[ \frac{k^2}{k_0^2} B^2 + 2p \right] \right]' - 4k^2 rp - r \frac{k^2}{k_0^2} \left[ kB_z - \frac{B_\theta}{r} \right]^2. \quad (5.115)$$

Since the last term is always negative, a necessary condition for stability is that the remaining contribution be positive. Setting  $k = -B_\theta(b)/bB_z(b)$  and using the RFP definition of  $\langle \beta \rangle$  given by Eq. (4.48), it then follows that

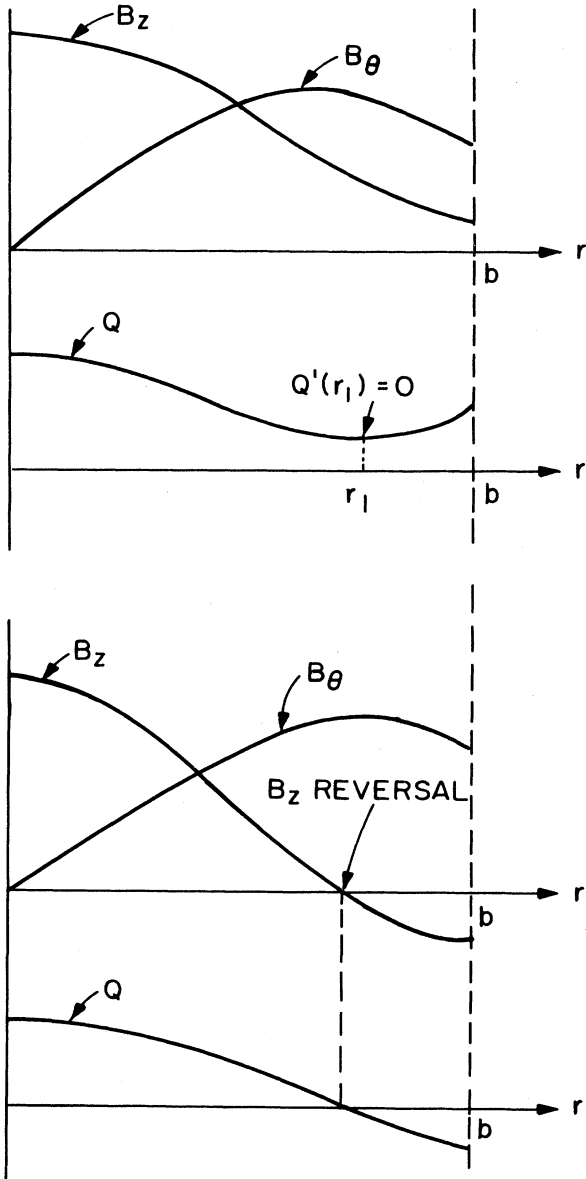


FIG. 39. Avoidance of a pitch minimum in the  $Q$  profile by reversing  $B_z$ . (a) No reversal  $\rightarrow$  instability, (b) reversal  $\rightarrow$  stability.

$$\langle \beta \rangle < 1 . \quad (5.116)$$

Clearly the  $m=1$   $\langle \beta \rangle$  limit is a very weak restriction.

A more stringent condition arises from the  $m=0$  mode. In this case the appropriate trial function is illustrated in Fig. 40(b). Note that the jump in  $\xi$  occurs at  $r=r_0$ , where  $f(r_0) \sim B_z^2(r_0) = 0$ . Hence the potentially large stabilizing contribution from the layer where  $\xi'^2$  is large vanishes as  $\epsilon \rightarrow 0$ . For this trial function,

$$\frac{\delta W_F}{L} < \pi \frac{\xi_0^2}{r_0^2} \int_0^{r_0} (f + r^2 g) dr . \quad (5.117)$$

Upon setting  $m=0$ ,  $k^2 \rightarrow 0$  (the most unstable  $k^2$ ), one

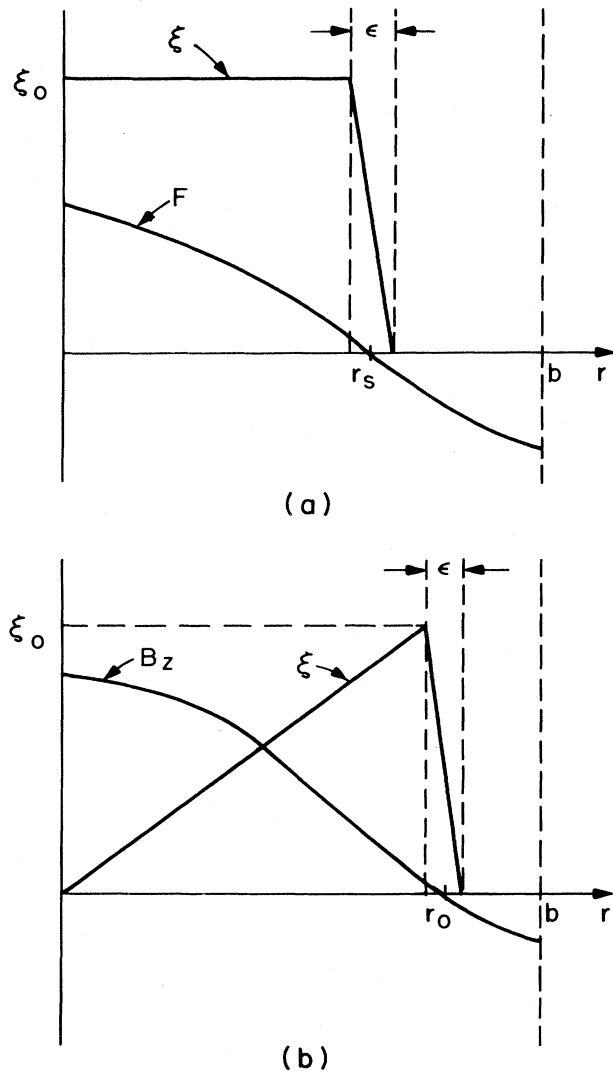


FIG. 40. Trial functions for (a) the  $m=1$  and (b) the  $m=0$  macroscopic pressure-driven modes.

obtains

$$f + r^2 g = 2r^2 p' + 2r B_z^2 . \quad (5.118)$$

Usually the reversal point is relatively close to the current-free region. Thus, to within a small error, substitution of Eq. (5.118) into Eq. (5.117) yields the stability condition

$$\langle \beta \rangle < \frac{1}{2} . \quad (5.119)$$

The  $m=0$  condition is more stringent than for  $m=1$ , but still represents only a weak overall limitation on  $\langle \beta \rangle$ . It reflects the physical fact that near the center of the profile there must be sufficient  $B_z$  field to "stiffen" the plasma against  $m=0$  sausage perturbations.

In summary, a combination of profile shaping and a weak  $\langle \beta \rangle$  limit is required to stabilize the RFP configuration against pressure-driven modes.

### c. Current-driven modes

The influence of internal current-driven modes on the RFP configuration can be determined by means of a procedure first suggested by Robinson (1971). In this procedure a necessary condition for stability is derived by examining the sign of  $g(r)$  vs  $r$  and determining under which circumstances it is negative, consistent with a trial function that makes the  $f\xi^2$  contribution vanish.

To begin, consider  $g(r)$  as given by Eq. (5.85). For low- $\beta$  systems, whose stability is dominated by current-driven modes,  $p'$  can be set to zero and  $g$  can be written as

$$g = \frac{rk^2 B_\theta^2}{k_0^2} (kQ + 1)[(3 + k^2 r^2)kQ - 1 + k^2 r^2], \quad (5.120)$$

where, as before,  $Q = 1/\mu = rB_z/B_\theta$  and  $k_0^2 = k^2 + m^2/r^2$ . Equation (5.120) corresponds to the most unstable situation,  $m=1$ . A useful way to ascertain the sign of  $g(r)$  for a given  $k$  is to plot a diagram of  $k$  vs  $r$  where  $g(r)$  vanishes:

$$\begin{aligned} kQ &= -1, \\ kQ &= (1 - k^2 r^2)/(3 + k^2 r^2). \end{aligned} \quad (5.121)$$

This is illustrated in Fig. 41. In the unshaded region  $g < 0$  (i.e., destabilizing). For the trial function shown in Fig. 40(a),  $\delta W$  satisfies

$$\frac{\delta W}{\pi L} < \xi_0^2 \int_0^{r_s} g(r) dr. \quad (5.122)$$

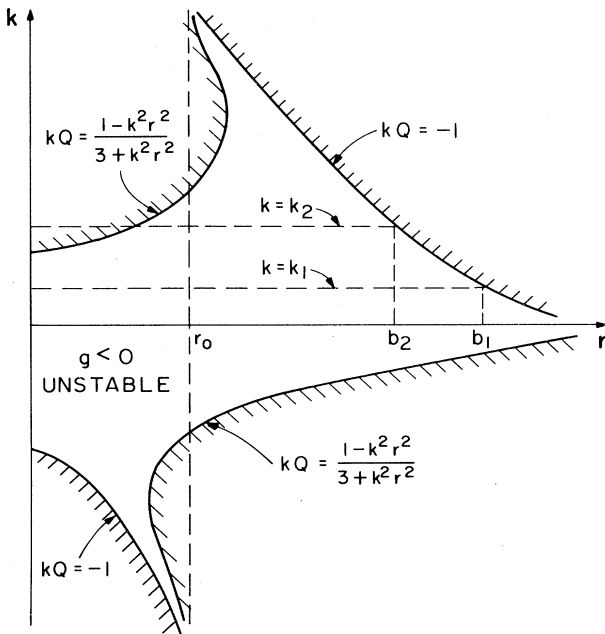


FIG. 41. Plot of  $k$  vs  $r$  where  $g(r)$  vanishes for  $m=1$  current-driven modes.

Note that the trial functions for the  $m=1$  pressure-driven and current-driven modes are identical, having been chosen to minimize the stabilizing line bending magnetic energy. At the singular surface,  $F(r_s)=0$  corresponding to a wave number  $k = -1/Q(r_s)$ . If the conducting wall is sufficiently far out, a value of  $r_s$  (i.e.,  $k$ ) can be chosen so that  $k(0) > k > k(b)$ , where  $k(0) = 1/3Q(0)$  and  $k(b) = -1/Q(b)$  (see the curve  $k = k_1$  in Fig. 41). In this case  $g(r)$  is negative over the whole range  $0 < r < r_s$ , and instability will occur. As the wall is moved closer in, the range of  $k$ 's for which  $g(r)$  is always negative diminishes. Eventually, when  $k(b) > k(0)$ , the most unstable  $k$  becomes  $k = k(b)$ , since  $r_s$  cannot exceed  $b$  for the trial function to satisfy the boundary condition  $\xi(b)=0$ . In this situation a stabilizing contribution develops near the axis, which increases as  $k$  increases (i.e., as the wall moves further in) (see the curve  $k = k_2$  in Fig. 41). It thus follows that a necessary condition for stability is  $k(0) > k(b)$  or

$$k(0) > -\frac{1}{3}Q(b). \quad (5.123)$$

There are two alternative forms in which Eq. (5.123) can be written, which point out the influence of current-driven modes on RFP profiles. First, the radius of the current channel and hence the plasma can be defined as follows:  $a^2 \equiv I/\pi J_z(0)$ . In this case Eq. (5.123) reduces to

$$\frac{b^2}{a^2} < -3 \frac{B_z(0)}{B_z(b)}. \quad (5.124)$$

For a given field reversal, the conducting wall must be sufficiently close to the plasma to prevent current-driven instabilities. The conducting wall essentially prohibits potentially unstable singular surfaces from existing in the plasma.

The second form of Eq. (5.123) is an approximate relation obtained by assuming that  $B_z \approx B_z(0)$  for  $0 < r < a$  and  $B_z \approx B_z(b)$  for  $a < r < b$ . Under this assumption the total toroidal flux is given by  $\Phi = \pi \times [B_z(0)a^2 + B_z(b)(b^2 - a^2)]$ . Equation (5.124) can then be written as  $\Phi > \pi a^2 B_z(0)[2 - 3(a^2/b^2)]$ .

In any realistic RFP experiment it is very difficult to make  $b/a \lesssim 2$  without causing significant plasma-wall interaction. Thus, as a practical matter,  $2 - 3(a^2/b^2) > 0$ , implying that despite the need for a reversed  $B_z$  to stabilize interchanges, the total toroidal flux must still remain positive,

$$\Phi > 0. \quad (5.125)$$

In other words, the region of reversed field cannot be too large.

Finally, consider the situation where  $B_z$  does not reverse and there is a pitch minimum on the outside of the profile. An analysis similar to the one just presented then shows that an  $m=1$  trial function can be constructed which makes  $\delta W < 0$  even if  $p'=0$ ; that is, a pitch minimum can lead to both pressure-driven and current-driven instabilities.

#### d. Summary and numerical results

In the previous sections it has been shown on the basis of various necessary and sufficient conditions that stable high- $\beta$  RFP profiles exist possessing the following properties:

- (1) A hollow or very flat pressure profile to suppress interchange modes near the magnetic axis.
- (2) A  $B_z$  field which reverses on the outside of the plasma. This provides shear to stabilize interchange modes and prevents the formation of  $m=1$  current-driven modes, both of which would occur in the presence of a pitch minimum.
- (3) A value of  $\langle\beta\rangle < \frac{1}{2}$  to suppress  $m=0$  pressure-driven sausage modes.
- (4) A conducting wall sufficiently close to the plasma (corresponding to a net positive toroidal flux) to suppress  $m=1$  current-driven modes.

Since some of the above properties were obtained by the use of trial functions, one cannot guarantee that they are complete or sufficient for stability. However, extensive numerical computations using the exact  $\delta W$  and the full eigenvalue equation indicate that these properties provide a very reliable set of guidelines for obtaining stable configurations. [See, for instance, Robinson (1971) and Sakanaka and Goedbloed (1974).] One early example of physically interesting RFP profiles, completely stable to all internal ideal MHD modes, has been given by Robinson and is illustrated in Fig. 42. All the features of the guidelines are present. Typically, the wall-to-plasma ratio must lie in the range  $2 \leq b/a \leq 3$  to provide both stability and isolation. In addition, the pressure profile corresponds to an  $\langle\beta\rangle = 0.31$ , a very optimistic result.

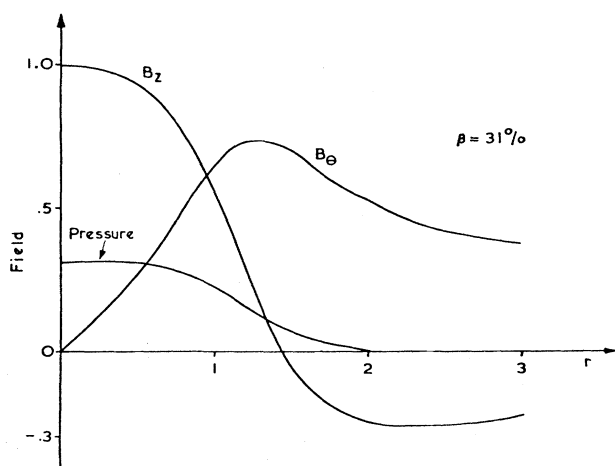


FIG. 42. A set of RFP profiles completely stable to all internal ideal MHD modes for  $\langle\beta\rangle \approx 0.31$  (from Robinson, 1971).

#### e. Taylor's theory

Although stable high- $\beta$  RFP profiles have been shown to exist theoretically, they are difficult to achieve experimentally by direct programming of the toroidal and poloidal circuits. The main reasons are technological, in that very fast rise times, on the order of tens of  $\mu$ secs, are required for full control of the profiles.

A possible solution to this problem is suggested by some of the data from the Zeta experiment. [See, for instance, Bodin and Newton (1980).] Here, after a rather turbulent initial phase, the plasma under certain conditions remarkably evolves to a stable, quiescent state very similar to that of an RFP, including a spontaneous self-reversal of the toroidal field. A theory explaining the evolution to "RFP-like" profiles and the conditions under which self-reversal occurs has been presented recently by Taylor (1974, 1975, and 1976), and these results are summarized here.

The basic idea is as follows. Consider a slightly dissipative plasma surrounded by a perfectly conducting shell which initially is not in a state of stable equilibrium. As the plasma turbulently, perhaps violently, evolves from its initial state, it dissipates energy (through thermal contact with the wall, resistive diffusion, etc.). It will continue to do so until it reaches a state of minimum energy, after which it is incapable of further motion. The properties of the final minimum energy state are determined by the constraints governing the evolution. Clearly, the crucial physics issue is the determination of the appropriate constraints, from which it is then relatively straightforward to obtain the final profiles.

The calculation begins with the following form of the potential energy:

$$W = \frac{1}{2} \int B^2 d\mathbf{r}. \quad (5.126)$$

For simplicity it is assumed that the plasma energy is much smaller than the magnetic energy (i.e.,  $\langle\beta\rangle \ll 1$ ), as is often the case experimentally. The effect of finite  $\langle\beta\rangle$  is discussed later.

To help understand the constraints in a realistic plasma with small but nonzero dissipation, it is useful to investigate the ideal plasma,  $\mathbf{E} + \mathbf{v} \times \mathbf{B} = 0$ , in order to establish a frame of reference. For the ideal case, as the plasma moves, the magnetic field is coupled to the plasma velocity  $\mathbf{v}$  by the relation

$$\frac{\partial \mathbf{B}}{\partial t} = \nabla \times (\mathbf{v} \times \mathbf{B}). \quad (5.127)$$

As shown in Sec. III.D, Eq. (5.127) corresponds to having magnetic lines "frozen into" the plasma so that field line topology is preserved; that is, no coalescing or tearing of field lines is allowed as the plasma moves.

It has been proven by Woltjer (1959) and Taylor (1975) that the restrictions associated with Eq. (5.127), which define the class of allowable magnetic field variations, are equivalent to an infinite set of integral constraints of the form

$$K = \int_V \mathbf{A} \cdot \mathbf{B} d\mathbf{r} = \text{const}, \quad (5.128)$$

where  $\mathbf{A}$  is the vector potential. The quantity  $K$ , sometimes referred to as the helicity, is constant over any volume enclosed by an ergodic flux surface (or flux tube surrounding a closed line). That each of the infinity of  $K$ 's is constant follows from the relation

$$\frac{dK}{dt} = -2 \int_V \mathbf{E} \cdot \mathbf{B} d\mathbf{r} + \int_S \mathbf{n} \cdot \mathbf{A} \times (\mathbf{E} + \mathbf{v} \times \mathbf{B}) dS . \quad (5.129)$$

For ideal MHD,  $\mathbf{E} + \mathbf{v} \times \mathbf{B} = 0$  and  $dK/dt$  is identically zero.

The energy  $W$  can now be minimized, subject to the constraints  $\nabla \cdot \mathbf{B} = 0$  and  $K$  const. The minimizing state must satisfy

$$\begin{aligned} \nabla \times \mathbf{B} &= \lambda(\mathbf{r}) \mathbf{B} , \\ \mathbf{B} \cdot \nabla \lambda &= 0 . \end{aligned} \quad (5.130)$$

Here  $\lambda$  is the Lagrange multiplier which must be determined locally on every flux surface (or closed magnetic line) from the corresponding initial values of  $K$ . Hence the final state depends directly upon the details of the initial conditions. It is also force free, since the plasma energy has been neglected in  $W$ .

The strong correlation between final and initial states is highly artificial and is very unlikely to occur in a realistic plasma with dissipation. It is, in fact, a direct consequence of the perfect conductivity approximation, which prohibits changes in topology. Therefore many nearby states are inaccessible, and there must be a one-to-one correspondence between flux surfaces in the initial and final states.

With the admittedly unrealistic ideal case serving as a reference, consider now the appropriate constraints in a plasma with small but nonzero dissipation. In such systems, field line topology need no longer be preserved as the plasma moves, so that a much wider class of lower-energy states is now accessible. Furthermore, small changes in the magnetic field can often lead to finite changes in the magnetic topology. Consequently, even when the dissipation is small, it is no longer correct to assume that  $K$  is conserved on every flux surface during the evolution, since the continual tearing and coalescing of field lines destroys the identity of most surfaces.

Taylor pointed out that in systems with small but nonzero dissipation over the entire plasma volume, the only flux surface that would preserve its identity during the evolution is the plasma boundary, since it is assumed to be rigid and perfectly conducting. He thus concluded that it was inappropriate to minimize the energy while requiring the infinity of  $K$ 's to remain invariant. Instead, the proper minimization satisfies only the constraint that  $K_b$  remain invariant, where  $K_b$  is the helicity associated with the total volume.

Minimization of  $W$  subject to  $\nabla \cdot \mathbf{B} = 0$  and  $K_b = \text{const}$  leads to a lowest-energy state described by

$$\nabla \times \mathbf{B} = \mu \mathbf{B} , \quad (5.131)$$

where  $\mu$  is now a single-constant Lagrange multiplier

having the same value on all surfaces. Not surprisingly, the final state is force free, since the plasma energy has been neglected in  $W$ . Furthermore, its characterization by only a single constant,  $\mu$ , indicates that the evolved state is almost independent of initial conditions. The energy of this state is lower than that of the corresponding ideal case with similar initial conditions, since all but one of the infinity of  $K$  constraints has been relaxed. The equilibria satisfying Eq. (5.131) are states of minimum potential energy, thus guaranteeing ideal MHD stability (and resistive MHD stability as well).

The quantity  $\mu$  is related to the value of the invariant  $K_b$ . Simple dimensional arguments show that  $K_b/\psi^2 = F(\mu b, \mu R)$ , where  $\psi$  is the total toroidal flux.  $\psi$  is conserved during the evolution because of the conducting shell, and  $F$  is a function determined by solving Eq. (5.131). It can also be shown that  $K_b$  is related to  $\psi$  and  $V_s$ , the volt-seconds stored in the system, by  $K_b = V_s \psi$ . Thus  $V_s/\psi = F(\mu b, \mu R)$ . By specifying the initial toroidal flux, the stored volt-seconds, and the dimensions of the system, one is then able in principle to compute  $\mu$  and  $K_b$ . [It is also worth noting that, in the final state, integration of Eq. (5.131) gives  $\mu b = 2\theta$ , where  $\theta \equiv (\mu_0 I / 2\pi B_i b)$  is the pinch parameter,  $I$  is the final toroidal current, and  $B_i$  is the initial uniform bias  $B_z$  field. This is only true in the final state, since Eq. (5.131) is not satisfied during the evolution.]

Equation (5.131) has been analyzed by Taylor (1975) and more recently by Reiman (1980). Their results show that the solution is not unique. Both cylindrically symmetric and finite-amplitude helical solutions exist. Depending on the ratio  $V_s/\psi$ , the plasma will evolve to that particular force-free configuration corresponding to the absolute minimum energy. In the limit of large aspect ratio (i.e., the straight cylinder) there are only two configurations which can have absolute minimum energy: the  $m=0$  cylindrically symmetric state,

$$\begin{aligned} B_z^{(0)}/B_0 &= J_0(\mu r) , \\ B_\theta^{(0)}/B_0 &= J_1(\mu r) , \end{aligned} \quad (5.132)$$

and the mixed  $m=0, m=1$  helically symmetric state,

$$\begin{aligned} B_z^{(1)}/B_0 &= J_0(\mu r) + c J_1(ar) \cos \chi , \\ B_\theta^{(1)}/B_0 &= J_1(\mu r) - \frac{c}{\alpha} \left[ \mu J'_1(ar) + \frac{k}{ar} J_1(ar) \right] \cos \chi , \\ B_r^{(1)}/B_0 &= -\frac{c}{\alpha} \left[ k J'_1(ar) + \frac{\mu}{ar} J_1(ar) \right] \sin \chi . \end{aligned} \quad (5.133)$$

Here  $\chi = \theta + kz$ ,  $\alpha = (\mu^2 - k^2)^{1/2}$ ,  $c$  is an arbitrary helical amplitude, and  $B_0 \equiv (\psi/\pi b^2) \mu b / 2 J_1(\mu b)$  has been chosen so that each configuration contains the same toroidal flux.

The local minimum energy of any force-free state can be expressed in terms of  $K_b$  as

$$W = \frac{1}{2} \mu \left[ K_b + (R \psi^2 / b) \frac{J_0(\mu b)}{J_1(\mu b)} \right] \quad (5.134)$$

(where for uniqueness it has been assumed that  $\int A_z dS = 0$ ). After a nontrivial analysis, it can be shown that, of the two states of interest, the one corresponding to absolute minimum energy has the lowest value of  $\mu$  for the given  $K_b$  (Reiman, 1980).

For small-to-moderate values of  $V_s/\psi$ , the cylindrically symmetric state has the absolute minimum energy. In this case the boundary condition  $B_r(b)=0$  is satisfied for any  $\mu$ , and  $\mu$  is determined by directly computing  $K_b$  and  $\psi$ . The result is a transcendental equation given by

$$\frac{bV_s}{R\psi} = [x(J_0^2 + J_1^2) - 2J_0J_1]/J_1^2, \quad (5.135)$$

with  $x = \mu b$ ,  $J_0 = J_0(x)$ , and  $J_1 = J_1(x)$ . In general, as  $V_s/\psi$  increases, the value of  $\mu$  also increases.

An important feature of the  $m=0$  solution is that, for  $\mu b > 2.40$  (or  $\theta > 1.20$ ), the  $B_z$  field is predicted to exhibit self-reversal. This is in good agreement with the data from Zeta, which indicates that self-reversal occurs at  $\theta = 1.4$ .

At some point, as  $V_s/\psi$  increases above some critical value, the helically symmetric configuration switches to the absolute minimum energy state. For this system the boundary condition  $B_r(b)=0$  is nontrivial and can only be satisfied for certain  $\mu = \mu(k)$ . A numerical minimization over  $k$  indicates that the lowest value of  $\mu$  occurs for  $kb = 1.2$  and is given by  $\mu b = 3.11$  (or  $\theta = 1.56$ ). This is the transition point between the two configurations and corresponds to  $bV_s/R\psi = 8.21$ . Above this value,  $\mu b$  continues to increase for the  $m=0$  solution. However, once  $bV_s/R\psi$  exceeds the transition value,  $\mu b$  remains constant at 3.11 for the  $m=1$  helical state. Instead, the excess volt-seconds cause the helical amplitude to continually increase, as given by an increasing value of the constant  $c$  in Eq. (5.133).

In summary, Taylor's hypothesis concerning the constancy of  $K_b$  during the evolution of the plasma has been shown to provide a very satisfactory qualitative and semi-quantitative guide to the behavior of reversed field pinches. Within the enormous space of possible equilibrium profiles, most discharges should evolve to an MHD stable, force-free configuration uniquely determined only by the initial toroidal flux, stored volt-seconds, and geometric dimensions. Furthermore, for the final configuration to remain cylindrically symmetric and possess a field reversal (which is important when pressure effects are included), the pinch parameter must lie in the range  $1.20 < \theta < 1.56$  or equivalently  $2.40 < bV_s/R\psi < 8.21$ .

The fact that the final state is force free should not be surprising in view of the fact that plasma energy was neglected in the minimization of  $W$ . However, to the extent that the tearing and reconnecting of field lines allows the pressure to redistribute and equalize itself, the force-free result would apply even for finite- $\beta$  initial states (i.e., the variation of  $\delta p$  would be independent of  $\delta B$  and upon separate minimization would lead to  $\nabla p = 0$ ). This would be a very pessimistic result. In a real plasma, however, the situation is probably somewhere intermediate between the perfect coupling of  $\delta p, \delta B$  to  $\delta v$ , as in ideal MHD, and

the complete decoupling just discussed. The actual pressure profiles will depend upon the details of the plasma turbulence and its effect on the resistivity and thermal conductivity transport coefficients which determine the energy balance. It is likely that the final  $\langle \beta \rangle$ 's will be considerably less than the maximum  $\langle \beta \rangle$ 's which can be theoretically constructed. The determination of the evolved pressure profiles and final  $\langle \beta \rangle$  remains one of the important areas of RFP research.

#### f. Overview of the RFP

By combining the equilibrium and stability results, one can obtain an overview of the RFP, at least with respect to ideal MHD.

The RFP is an axisymmetric toroidal configuration with  $B_\theta^2 \sim B_z^2 \sim p$ , which achieves MHD equilibrium and stability with an optimally efficient use of a minimum of toroidal field. Its radial pressure balance and toroidal force balance are similar to those of a Z pinch. Because of the relatively large  $B_\theta$ , toroidicity is required only to close the field lines, but is not required for MHD stability. Hence the device can have the technological advantage of a large aspect ratio. Another attractive feature is that the toroidal shift of the plasma is very small. Perhaps the main advantage of large  $B_\theta$  is that it is possible in principle to joule heat an RFP to ignition, although such strong heating has yet to be observed experimentally.

Since  $\beta \sim 1$  and  $q \ll 1$ , the stability of the RFP is in general quite sensitive to profiles. For stability at high  $\beta$  the pressure profile must be hollow and the  $B_z$  field reversed on the outside. Equally important, a perfectly conducting shell relatively near the plasma is required, and this is a disadvantage technologically. The rather complicated profiles required for stability are difficult to program externally. However, a recent theory (Taylor, 1976) suggests that over a certain range of the pinch parameter  $\theta$  the system will evolve naturally to an "RFP-like" profile, although very likely with  $\langle \beta \rangle$ 's significantly lower than the theoretically predicted maximum. In addition, once quiescence is reached it is a difficult problem to further increase the joule heating without raising  $\langle \beta \rangle$  or altering the stable profiles, either of which could lead to further relaxations and loss of energy.

Even so, the possibility of producing an MHD stable, high- $\beta$  plasma, capable of being joule heated to ignition, makes the RFP an interesting and important concept to investigate in the magnetic fusion program.

### 5. The "straight" tokamak

#### a. Introduction

The final one-dimensional configuration examined by means of the general screw-pinch analysis is the "straight" tokamak, a circular cylinder of plasma of length  $2\pi R$ , in which the fields satisfy the tokamak inverse aspect ratio expansion  $B_\theta/B_z \sim \epsilon, q \sim 1, p/B_z^2 \sim \epsilon^2$

(conventional tokamak) or  $p/B_z^2 \sim \epsilon$  (high- $\beta$  tokamak). Although a reasonably complete stability picture is obtained from this model, the results can be unreliable because the geometric effects of toroidicity are of the same order as the field ratio. Thus toroidicity sometimes gives rise to contributions in  $\delta W$  which are of the same order as those of the straight tokamak. Despite these uncertainties the model provides a very useful frame of reference for the understanding of tokamak stability.

It is shown that the most dangerous instabilities in a straight tokamak are current-driven modes, both internal and external. In the straight tokamak case, unlike that of the RFP, external modes play a major role because: (1) in current experiments, time scales are sufficiently long compared to the penetration time that the first wall does not behave like a perfect conductor, and (2) in future tokamak extrapolations, particularly those with divertors, the first wall is located a significant distance from the plasma surface. The pressure-driven modes do not have a dominant role because of the combination of finite shear and low  $\beta$ .

The straight tokamak is predicted to have good MHD stability properties if the total toroidal current is limited and the current profile is peaked. This result is qualitatively and often quantitatively valid for the fully toroidal case. The stability of the straight tokamak imposes no important restrictions on  $\langle \beta \rangle$  or the pressure profile, and in this is qualitatively different from the torus. Toroidal modifications to tokamak stability are discussed in Sec. V.D.1.

As in the case of the RFP, much of the intuition concerning stability is derived from the use of trial functions and from the exploitation of the tokamak expansion in  $\delta W$ . This intuition is supported by a large number of numerical calculations carried out in recent years.

Finally, it should be noted that the discussion here is limited in scope in that it is concerned primarily with the basic physics issues of ideal MHD stability in tokamaks. Much more complete and extensive reviews of ideal and resistive MHD tokamak stability have been given by Mukhovatov and Shafranov (1971), Wesson (1978), and Bateman (1978).

### b. Internal modes (localized)

Stability against localized interchange modes can be determined by substituting the tokamak expansion into Suydam's criterion, which is valid for arbitrary profiles. Using the relationship for the safety factor,  $q = 1/\mu R = Q/R$ , and the definition  $\beta(r) \equiv 2p(r)/B_0^2$ , Suydam's criterion has the form

$$(rq'/q)^2 + 4r\beta' > 0. \quad (5.136)$$

Since  $\beta$  is either of order  $\epsilon^2$  or  $\epsilon$ , and  $q$  is a monotonically increasing function of radius with  $rq'/q \sim 1$ , (i.e., finite nonzero shear), Suydam's criterion is easily satisfied over almost the entire profile. The only exception is very near the axis, where the shear is small, a situation similar to that in the RFP [see Eq. (5.113)]. Within the model of

the straight tokamak, these modes can be stabilized by keeping the pressure flat over a region  $\Delta r/a \sim \beta^{1/2} \ll 1$ , which represents only a minor restriction on the profile.

Furthermore, as shown in Sec. V.D.1, there are important toroidal modifications to Suydam's criterion when  $q \sim 1$ . These are unimportant for the RFP, since  $q \sim \epsilon$ . However, for the tokamak they imply that, under reasonable conditions, even the small flattening of the pressure profile is no longer required for stability.

In summary, the combination of low  $\beta$  and increasing  $q$  profile implies that localized interchange perturbations are not very dangerous in a straight tokamak.

### c. Internal modes (general)

The stability of general nonlocalized internal modes can be ascertained by substituting the tokamak expansion into  $\delta W_F$  as given by Eq. (5.84). This gives rise to an asymptotic expansion of the form  $\delta W_F = \delta W_0 + \epsilon^2 \delta W_2 + \epsilon^4 \delta W_4 \dots$ . The calculation is straightforward, although one must include the toroidal periodicity constraint by setting

$$k = -n/R, \quad (5.137)$$

with  $n$  an integer representing the toroidal mode number. Toroidal periodicity is important in tokamaks because the unstable modes correspond to long wavelengths, typically  $n \sim 1$ . (This is not important in an RFP, where the instabilities occur for  $ka \sim 1$  or  $n \sim 1/\epsilon$ ; hence  $n$  can effectively be considered continuous.)

The first contribution to  $\delta W_F$  which does not trivially vanish is of second order and is given by (Shafranov, 1970)

$$\frac{\epsilon^2 \delta W_2}{2\pi R} = \frac{\pi B_0^2}{R^2} \int_0^a \left[ \frac{n}{m} - \frac{1}{q} \right]^2 [r^2 \xi'^2 + (m^2 - 1)\xi^2] r dr. \quad (5.138)$$

Since  $\delta W_2 > 0$  for  $m \geq 2$  and  $n$  arbitrary, these modes are stable. Similarly, the  $m=1$  mode in systems with increasing  $q$  profiles is stable if  $nq(0) > q(0) > 1$ .

However, if a  $q=1$  surface exists in the plasma [i.e.,  $q(0) < 1 < q(a)$ ], a trial function can be constructed as shown in Fig. 43, which in the limit  $\delta \rightarrow 0$  causes  $\delta W_2 \rightarrow 0$ . For this case, stability is determined by the high-order corrections to  $\delta W_F$ . The next contribution is of order  $\epsilon^4$  and for  $n=1$  can be written as (Rosenbluth et al., 1973)

$$\frac{\epsilon^4 \delta W_4}{2\pi R} = \frac{\pi B_0^2}{R^2} \xi_0^2 \int_0^{r_s} \left[ r\beta' + \frac{r^2}{R^2} \left[ 1 - \frac{1}{q} \right] \right] \left[ 3 + \frac{1}{q} \right] r dr, \quad (5.139)$$

where  $r_s$  is the location of the  $q(r_s)=1$  surface. In Eq. (5.139) the contributions from both the pressure and parallel current are destabilizing, and thus the system is unstable.

This instability is often referred to as the  $m=1$  internal kink mode, a slightly misleading nomenclature since the

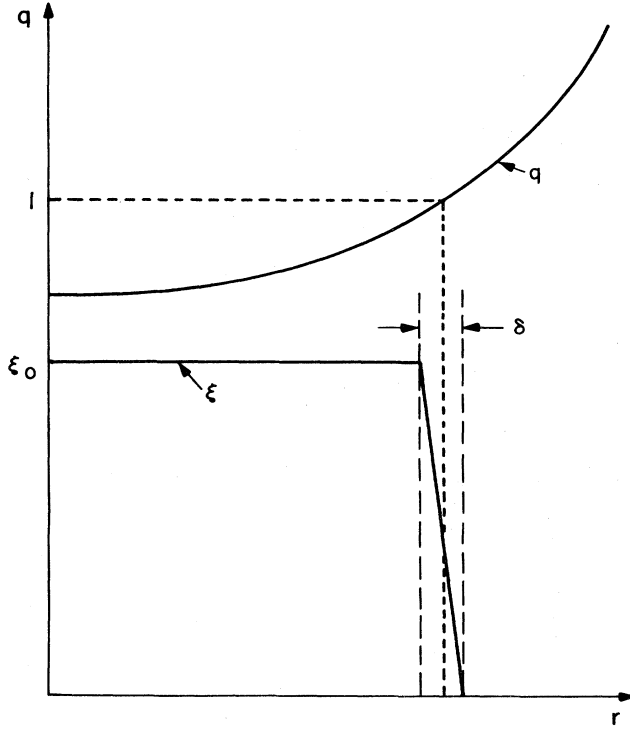


FIG. 43. Trial function for an  $m=1$  internal kink mode in a straight tokamak.

mode can be driven by pressure, particularly in the high- $\beta$  tokamak regime. Many of the qualitative features of the mode persist in the toroidal case, although there are important corrections to the  $n=1$  driving term. These are discussed in Sec. V.D.1. It is also worth noting that the nonlinear evolution of the resistive counterpart of the  $m=1$  internal kink mode is believed to play an important role in the "sawtooth" oscillations observed in many tokamak experiments. [For a theoretical discussion of sawtooth oscillations, see Kadomtsev (1975), Sykes and Wesson (1976), Jahns *et al.* (1978), and Bateman (1978).]

To summarize, in a straight tokamak  $m \geq 2$  internal modes are stable for both the conventional and high- $\beta$  ordering. The  $m=1$  internal mode exhibits a weak instability (i.e.,  $\delta W \sim \epsilon^4$ ) which can be prevented if

$$q(0) > 1 \quad (5.140)$$

The mode does play an important role in tokamak operation in that it limits the value of the toroidal current density on axis. Nevertheless, even when the mode becomes unstable, as it presumably does during the sawtooth oscillations, it is not catastrophic, since its activity mainly consists of a redistribution of plasma energy within the relatively small region internal to the  $q=1$  surface. In effect, the oscillations anchor the average value of the safety factor on axis to its threshold value,  $q(0)=1$ .

#### d. External modes ( $m=1$ Kruskal-Shafranov limit)

The most dangerous ideal MHD instabilities in a straight tokamak are the external kink modes. These are

current-driven modes in which the  $\mathbf{k} \cdot \mathbf{B}=0$  singular surface lies in the vacuum region. External kinks are more dangerous than internal modes in that their stability is determined solely by the second-order contribution to  $\delta W$ . One consequence of this fact is that the stability boundaries are unaffected by the pressure (in the straight model).

Much of the basic insight concerning external kinks is due to Shafranov (1970) and has recently been summarized by Wesson (1978). The essence can be obtained by examining the first nonvanishing contribution to  $\delta W$ , which is of order  $\epsilon^2$ . From Eq. (5.90) it follows that, in the limit where the conducting shell moves to infinity (i.e.,  $b/a \rightarrow \infty$ ),  $\delta W$  for either the conventional or the high- $\beta$  expansion can be written as

$$\begin{aligned} \frac{\delta W}{2\pi R} \approx \frac{\pi B_0^2}{R^2} & \left\{ \int_0^a \left[ \frac{n}{m} - \frac{1}{q} \right]^2 [r^2 \xi'^2 + (m^2 - 1)\xi^2] r dr \right. \\ & + a^2 \xi^2(a) \left[ (1+m) \left[ \frac{n}{m} - \frac{1}{q_a} \right]^2 \right. \\ & \left. \left. + \frac{2}{q_a} \left[ \frac{n}{m} - \frac{1}{q_a} \right] \right] \right\}, \end{aligned} \quad (5.141)$$

where  $q_a \equiv q(a)$ .

Consider first the  $m=1$  mode. For this case the minimizing eigenfunction in the plasma is given by  $\xi(r) = \xi_a = \text{const}$  and causes the integral contribution to vanish. Note that such an eigenfunction can only be chosen for external modes, since the internal mode boundary condition  $\xi(a)=0$  is no longer required. Furthermore, the minimizing function  $\xi = \text{const}$  is independent of  $q$  profile. This leads to the important conclusion that the  $m=1$  stability boundary is a function only of  $q(a)$  (i.e., it depends only on the total current, and not on the current profile).

Under these conditions  $\delta W$  reduces to

$$\frac{\delta W}{2\pi R} = 2\pi \epsilon^2 B_0^2 \xi^2(a) \left[ n \left[ n - \frac{1}{q_a} \right] \right]. \quad (5.142)$$

From Eq. (5.142) it follows that the stability condition for the  $m=1$  external kink mode for the worst case,  $n=1$ , is given by

$$q(a) > 1. \quad (5.143)$$

This criterion is known as the Kruskal-Shafranov condition (Kruskal and Schwarzschild, 1954; Shafranov, 1956). It imposes an important constraint on tokamak operation in that it limits the total toroidal current that can flow to  $I < I_{KS}$ , where (in full mks units)

$$I_{KS} \equiv 2\pi a^2 B_0 / \mu_0 R. \quad (5.144)$$

In certain ways the driving term for the instability is similar to that for the  $m=1$  mode in a pure  $Z$  pinch. However, because of the presence of the strong  $B_z$  field, the instability is restricted to long wavelengths [rather

than  $k \rightarrow \infty$ ; see Eqs. (5.73) and (5.74)] in order to prevent a strong stabilizing contribution from line bending. In fact, the criterion  $q(a) > 1$  can be viewed as a condition on the geometry (i.e., the inverse aspect ratio) for prohibiting the formation of potentially unstable long-wavelength modes because of toroidal periodicity requirements.

Finally, it is worth noting that the  $m=1$  external kink is difficult to observe experimentally because higher- $m$  modes, usually resistive, impose even stronger requirements on  $q(a)$ . These modes, although more sensitive to profile and slower growing, can terminate the discharge by means of a "major disruption" before the current can be increased above the Kruskal-Shafranov limit. [For a theoretical discussion of major disruptions, see Waddell *et al.* (1978, 1979), Bateman (1978), and Hicks *et al.* (1980).]

#### e. External modes ( $m \geq 2$ kinks)

In general the  $m \geq 2$  external kinks impose more stringent conditions on  $q(a)$  and the current profile than those corresponding to the  $m=1$  mode.

The  $m \geq 2$  stability boundaries also follow from an analysis of Eq. (5.141). Clearly, a sufficient condition for stability to a given  $(m,n)$  mode is  $q(a) > m/n$ . This is not a very useful criterion because it imposes unnecessarily low limits on the toroidal current for high- $m$ , low- $n$  modes.

A slightly improved stability estimate can be obtained by noting that for monotonically increasing  $q$  profiles, a lower bound for  $\delta W$  is obtained by setting  $q(r)=q(a)$  in the integral contribution (since by definition  $q_a < m/n$  for an external mode). The factor  $(n/m - 1/q_a)^2$  can then be removed from the integrand and the remaining integral minimized by choosing  $\xi(r)=\xi(a)(r/a)^{m-1}$ . The resulting form of  $\delta W$  is given by

$$\frac{\delta W}{W_0} \geq \left[ 1 - \frac{m}{nq_a} \right] \left[ 1 - \frac{m-1}{nq_a} \right], \quad (5.145)$$

where  $W_0 = [2\pi e B_0(n/m)\xi_a]^2 R$ . Consequently, for a given  $n$  and  $m$ , the regions of instability are bounded by (Shafranov, 1970)

$$\frac{m-1}{n} \leq q(a) \leq \frac{m}{n} \quad (5.146)$$

Equation (5.146) is usually not a very useful estimate because a continual incrementing of  $m$  by one indicates that the entire range of  $q_a$ ,  $0 < q_a < \infty$  could be potentially unstable. However, for the special case  $B_z = \text{const}$ ,  $B_\theta \propto r$ , the  $J_z$  profile is constant for  $0 < r < a$  and jumps to zero just outside the plasma surface. This corresponds to a shearless  $q$  profile,  $q(r)=q(a)=\text{const}$ , and implies that the inequality in Eq. (5.145) becomes equality so that the entire range of  $q_a$  is indeed unstable.

Shafranov (1970) first pointed out that this pessimistic result is strongly dependent upon the shape of the current profile. He showed both analytically and numerically that for more realistic profiles, where the current goes smoothly to zero at the plasma surface, the stability prop-

erties are far more optimistic. In essence, for  $m \geq 2$  external kinks the main force driving the instability is proportional to the current gradient at the surface rather than to the total current itself. In this connection, Wesson (1978) has given a physical picture which demonstrates how the current gradient produces a destabilizing torque on the plasma. A convenient way to obtain a quantitative analytic theory which describes these results has been given by Laval and Pellat (1973) and Laval, Pellat, and Soule (1974). They considered the external kink mode in the limit of large  $m$ , including the effects of noncircularity. For the present purposes, it suffices to summarize their theory for the circular case.

The key feature in the analysis is the realization that, for large  $m$ , instability can only occur if the resonant surface lies slightly outside the plasma. This gives rise to a plasma displacement which is highly localized just inside the plasma surface. By calculating the large- $m$  asymptotic solution to the Euler-Lagrange equation one can obtain a good estimate of the integral contribution to  $\delta W$ , from which it is then straightforward to determine the stability boundaries.

If one sets  $\xi(r)=b(r)/[r^{3/2}\Delta(r)]$ ,  $r=a(1-z/2m)$ , then near the plasma surface  $0 \leq z \lesssim 1$  the Euler-Lagrange equation for  $b$  in the limit of large  $m$  is given by

$$\frac{d^2b}{dz^2} - \left[ \frac{1}{4} - \frac{\lambda}{z+z_0} \right] b = 0, \quad (5.147)$$

where  $\Delta(r)=[m/nq(r)]-1$ ,  $\Delta_a=\Delta(a)$ ,  $\langle J \rangle=I/\pi a^2$ ,

$$z_0=m\Delta_a \left[ \frac{m}{nq_a} \right] \left[ 1 - \frac{J(a)}{\langle J \rangle} \right]^{-1},$$

and

$$\lambda = - \left[ \frac{1}{2m} \right] \left[ \frac{aJ'(a)}{\langle J \rangle} \right] \left[ 1 - \frac{J(a)}{\langle J \rangle} \right]^{-1}.$$

Note that, for large  $m$ ,  $0 < \Delta_a \ll 1$  (i.e., the resonant surface is just outside the plasma) and, for monotonically decreasing  $J$  profiles,  $0 < \lambda \ll 1$ . Also, since  $z_0 > 0$ , Eq. (5.147) is nonsingular in the regime of interest  $z > 0$ .

The solution for  $b$  which is regular as  $z \rightarrow \infty$  and satisfies  $b(0)=a^{3/2}\Delta_a\xi_a$  is given by

$$b(z)=a^{3/2}\Delta_a\xi_a(1+z/z_0)e^{-z/2} \left[ \frac{\Psi(1-\lambda, 2; z+z_0)}{\Psi(1-\lambda, 2; z_0)} \right], \quad (5.148)$$

where  $\Psi(a, c; x)$  is the confluent hypergeometric function containing the logarithmic singularity as  $x \rightarrow 0$  (Erdelyi, 1953). Substituting Eq. (5.148) into Eq. (5.141) yields the following expression for  $\delta W$ :

$$\frac{\delta W}{W_0} \approx \frac{1}{m} \left[ \left[ 1 - \frac{\Psi'(z_0)}{\Psi(z_0)} - \frac{1}{z_0} \right] (m\Delta_a)^2 - \frac{J(a)}{\langle J \rangle} (m\Delta_a) \right]. \quad (5.149)$$

There are two regimes of interest to consider. First, assume the current profile is a decreasing function of  $r$

which remains finite at  $r=a$  [i.e.,  $J(a) \neq 0$ ]. In this case the  $(\Psi'/\Psi + 1/z_0)$  term can be neglected and the stability boundaries are given by  $0 \leq m\Delta_a \leq J(a)/\langle J \rangle$  or

$$\frac{1}{n} \left[ m - \frac{J(a)}{\langle J \rangle} \right] \leq q(a) \leq \frac{m}{n}, \quad (5.150)$$

Equation (5.150) shows that any profile with a current jump at the surface is unstable to high- $m$  external kinks over bands of  $q_a$  values. The most unstable case occurs for uniform current,  $J(a)/\langle J \rangle = 1$ , in which neighboring bands touch and all  $q_a$  values are unstable. As the current at the boundary decreases, the unstable bands become narrower, forming windows of stability.

In fact, Eq. (5.150) implies that when the current on the boundary vanishes,  $J(a)=0$ , the system becomes stable. This is not quite the situation because the  $(\Psi'/\Psi + 1/z_0)$  term then becomes important. The most unstable regime corresponds to  $z_0 \ll 1$ , and in this limit  $\Psi'(z_0)/\Psi(z_0) + 1/z_0 \approx -\lambda \ln z_0$ . Instability occurs only over exponentially narrow bands of  $q_a$  given by  $1 + \lambda \ln z_0 < 0$  or

$$\frac{1}{n} \left[ m - \exp \left[ 2m \frac{\langle J \rangle}{aJ'(a)} \right] \right] \leq q(a) \leq \frac{m}{n}. \quad (5.151)$$

Thus, if the current vanishes at  $r=a$ , the range of unstable  $q_a$  values is greatly reduced. If in addition the current gradient vanishes, the high- $m$  external kinks can be completely stabilized. Exactly how fast the current gradient must vanish [i.e., if  $J \propto (a-r)^\nu$  for  $r$  near  $a$ , determine the critical  $\nu$ ] is difficult to calculate, particularly for the low- $m$  modes where the eigenfunctions are not highly localized.

This question has been addressed numerically by Wesson (1978), who studied the family of profiles  $J=J_0(1-r^2/a^2)^\nu$  or equivalently  $q=q(a)u \times [1-(1-u)^{\nu+1}]^{-1}$  with  $\nu+1=q(a)/q(0)$  and  $u=r^2/a^2$ . Note that the parameter  $q(a)/q(0)$  is a measure of the steepness of the current profile. The results of Wesson's calculations are illustrated in Fig. 44 as marginal stability curves of  $q(a)/q(0)$  vs  $q(a)$ . Also superimposed is the stability boundary for ideal internal kink modes,  $q(0) \geq 1$ .

Observe that the unshaded region is stable to both internal and external ideal MHD modes. Most existing tokamaks operate in this regime. With regard to external kinks, Wesson finds that for  $\nu > 2.5$  or  $q(a)/q(0) \gtrsim 3.5$ , all  $m \geq 2$  modes are stable for any  $q_a$ . Windows of stability in  $q_a$  also exist for  $1 < \nu < 2.5$ . Complete stability is achieved by the additional requirement  $q_a > 1$  to stabilize the  $m=1$  mode. In fact, if it were not for the internal mode criterion, tokamaks could operate at significantly higher currents (i.e., lower  $q_a$ ) than they normally do; for instance,  $q(a)=1$ ,  $q(0)=1/4$  satisfies the external kink conditions.

To summarize, it has been shown that the  $m \geq 2$  external kink mode is driven by the toroidal current gradient and is consequently sensitive to the features of the profile. A combination of rapidly vanishing current gradient and a limit on the total current is sufficient to completely sta-

bilize all high- $m$  and low- $m$  modes, respectively. The dual requirements of  $q(0) > 1$  for internal mode stability and peaked current profiles for high- $m$  external kink stability can only be simultaneously satisfied if  $q(a) \gtrsim 3$ . It is for this reason that  $m \geq 2$  kinds impose stronger constraints on  $q(a)$  than the  $m=1$  Kruskal-Shafranov mode.

#### f. Summary

The one-dimensional "straight" tokamak provides a useful, if sometimes unreliable, guide to the stability of the tokamak configuration. The model predicts that the most dangerous ideal MHD instabilities are the current-driven, external kink modes. The  $m=1$  mode becomes unstable if the total toroidal current exceeds the Kruskal-Shafranov limit; that is, independent of profile,  $q(a) < 1$  leads to instability. High- $m$  external kinks are driven unstable if a significant current gradient exists at the edge of the plasma. These modes require a peaked current profile,  $q(a)/q(0) \sim 3$  [i.e.,  $J'(a) \rightarrow 0$ ] in order to be stabilized.

Of the internal modes, only  $m=1$  can be unstable in a straight tokamak. This is a weaker instability than the external kink, but can be driven by either the parallel current or the pressure gradient. The stability condition for the  $m=1$  mode is  $q(0) > 1$ . In practice most experimental tokamaks exhibit a form of relaxation oscillation near the magnetic axis as a result of the competition between the  $m=1$  internal mode (and its nonlinear resistive evolution) and a thermal instability resulting from the temperature dependence of the resistivity, which causes the current to peak. The net effect of these "sawtooth" oscillations is to maintain  $q(0)$  at unity during most of the duration of the experiment.

In general the straight tokamak provides an unreliable description of the influence of  $\beta$  on ideal MHD stability. Specifically, most of the stability results are only weakly dependent on  $\beta$ . Consequently, even in the regime of the high- $\beta$  tokamak, no  $\beta$  limits arise within the context of the model. This is perhaps the main deficiency of the straight tokamak, since there are important  $\beta$  limits when one considers the full toroidal geometry. These are discussed in the next section.

In summary, the combination of peaked profile  $q(a)/q(0) \gtrsim 3$  and limited current density on axis  $q(0) \geq 1$  is sufficient to stabilize the straight tokamak to ideal MHD instabilities. It should be noted, however, that there are important resistive MHD modes (i.e., tearing modes) which can also occur. [See, for instance, Furth, Killeen, and Rosenbluth (1963), and Greene (1976).] These modes further decrease the stable region of parameter space illustrated in Fig. 44. Most tokamaks, in fact, actually operate in a regime that is resistively unstable. Such operation is possible because resistive modes are inherently much weaker instabilities than those of ideal MHD. Their nonlinear evolution often produces only minor turbulence while permitting operation at much higher currents than those allowed by "completely stable" operation. This subject has been reviewed by Bateman (1978).

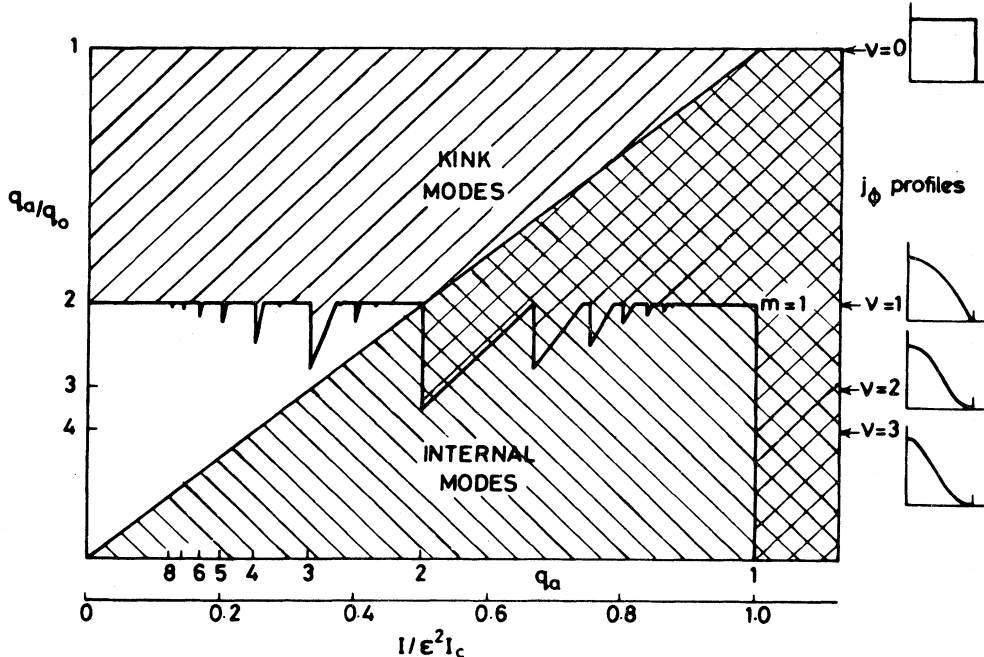


FIG. 44. Marginal stability diagrams for external kinks in a straight tokamak for the current profile  $J(r)=J_0(1-r^2/a^2)^v$ . The stable region is unshaded (from Wesson, 1978).

#### D. Application to 2D configurations

This section describes the effects of multidimensionality on ideal MHD stability. The main application concerns the influence of toroidicity on tokamaks. In addition, wherever applicable, a brief description of the effects of cross-section shaping is presented as well. A second application discusses the stability of an “infinitely long” two-dimensional Elmo bumpy torus.

As a general comment it should be noted that 2D configurations are considerably more difficult to analyze than their 1D counterparts. Consequently, most of the analysis involves studies of special classes of modes, usually those highly localized in the vicinity of a flux surface. To obtain more complete stability results one must make use of rather sophisticated numerical codes which have been developed in recent years (Sykes and Wesson, 1974; Bateman *et al.*, 1974; Grimm *et al.*, 1976; and Berger *et al.*, 1977a).

##### 1. Tokamak

###### a. Introduction

It is shown here that toroidicity plays a very important role in determining the stability of tokamaks, particularly the high- $\beta$  tokamak. Toroidicity often leads to quantitative changes in the stability of current-driven modes. More important, it leads to qualitative changes for pressure-driven modes. For these perturbations its main effect is to determine an upper limit on the value of  $\langle\beta\rangle$  that can be stably confined.

The first instabilities discussed are those involving localized interchange perturbations. These give rise to the Mercier criterion, a 2D generalization of Suydam's criterion. This is an exact analytic criterion, necessary but not sufficient for stability, which makes important modifications to the 1D criterion in the vicinity of the magnetic axis.

A second class of modes discussed represents a generalization of the interchange perturbation and allows the plasma displacement to “balloon” in the regions of unfavorable curvature. The corresponding ballooning mode formalism leads to a one-dimensional *ordinary* differential equation that can be solved on one flux surface at a time, a significant simplification over the full 2D problem.

Although some analytic work has been performed on global, low- $m$  internal modes, much of the recent progress has resulted from numerical studies. The situation is somewhat similar with respect to external modes. However, in this case there exists a relatively simple model, known as the surface current model, which makes surprisingly reliable predictions of external kink mode stability limits. The current status of this research is briefly summarized.

Finally, a short discussion is given of the axisymmetric,  $n=0$  mode, the most unstable perturbation usually corresponding to a nearly rigid vertical shift. In the straight tokamak with circular cross section, such modes (by symmetry) are neutrally stable. In a torus, however, if the vertical field is not properly designed, the plasma, particularly if it is elongated, has a tendency to drift upward. Stabilization of the  $n=0$  mode is discussed at the end of this section.

*b. Internal modes (localized: Mercier criterion)*

One of the simplest and most widely used tests for tokamak stability is the Mercier criterion for localized interchanges (Mercier, 1960; Greene and Johnson, 1962; Solov'ev, 1968). This is a necessary but not sufficient condition, which is valid for arbitrary  $\beta$ , and arbitrary aspect ratio. The derivation, outlined below, requires two steps. First, a general form of  $\delta W$  is derived for the most dangerous modes in the limit  $n \rightarrow \infty$ . This form, which is valid for both interchange and ballooning modes, is an explicit function only of the single scalar  $\mathbf{n} \cdot \xi$ .

Second, by substituting a special trial function for  $\mathbf{n} \cdot \xi$  corresponding to the interchange perturbation, it is possible to evaluate  $\delta W$  and derive the Mercier criterion. A

$$\delta W = \frac{1}{2} \int J d\psi d\chi d\phi \left[ \frac{B^2}{R^2 B_p^2} |k_{||} X|^2 + \frac{R^2}{J^2} \left| \frac{\partial U}{\partial \chi} - F \frac{\partial}{\partial \psi} \left( \frac{JX}{R^2} \right) \right|^2 + B_p^2 \left| inU + \frac{\partial X}{\partial \psi} + \frac{J_\phi}{RB_p^2} X \right|^2 - 2K |X|^2 \right]. \quad (5.152)$$

In this expression  $X = RB_p \mathbf{n} \cdot \xi_\perp$  and  $U = \mathbf{n} \cdot (\mathbf{B} \times \xi_\perp) / RB_p$  are proportional to the two components of  $\xi_\perp$ ,  $J$  represents the Jacobian of the transformation (i.e.,  $rR dr d\theta d\phi \equiv J d\psi d\chi d\phi$ ),  $k_{||}$  represents the derivative along the field line

$$ik_{||} = \frac{1}{JB} \left( \frac{\partial}{\partial \chi} + in\nu \right), \quad (5.153)$$

$$\nu(\psi, \chi) = FJ/R^2,$$

and the quantity  $K$  is given by

$$K = \frac{FF'}{R^2} \frac{\partial}{\partial \psi} (\ln R) - \frac{J_\phi}{R} \frac{\partial}{\partial \psi} (\ln JB_p), \quad (5.154)$$

$$J_\phi = Rp' + \frac{FF'}{R} = -\frac{R}{J} \frac{\partial}{\partial \psi} (JB_p^2).$$

Also,  $B_p = R |\nabla \psi|$  and  $p(\psi), F(\psi)$  are the free functions appearing in the Grad-Shafranov equation [Eq. (4.35)].

$$\delta W = \pi \int J d\psi d\chi \left[ \frac{B^2}{R^2 B_p^2} |k_{||} X|^2 + R^2 B_p^2 \left| \frac{1}{n} \frac{\partial}{\partial \psi} k_{||} X \right|^2 - 2p' \left[ \frac{\kappa_n}{RB_p} |X|^2 - i \frac{FB_p \kappa_s}{B^2} \frac{X}{n} \frac{\partial X^*}{\partial \psi} \right] \right]. \quad (5.155)$$

Here  $\kappa_n$  and  $\kappa_s$  are the normal and geodesic curvatures, respectively,

$$\kappa_n = \frac{RB_p}{B^2} \frac{\partial}{\partial \psi} \left[ p + \frac{B^2}{2} \right], \quad (5.156)$$

$$\kappa_s = -\frac{1}{JB_p B^2} \frac{\partial}{\partial \chi} \left[ \frac{B^2}{2} \right].$$

Equation (5.155) indicates that the only destabilizing term is driven by the pressure gradient. The current-driven term is negligible in the limit  $n \rightarrow \infty$ .

more general choice of  $\mathbf{n} \cdot \xi$  leads to the ballooning mode equation, and this is discussed in the next section. [Other localized stability criteria have been derived by Lortz (1973), Mercier (1973), and Mikhailovskii (1973).]

The first step in the calculation is to express the exact  $\delta W$  for an axisymmetric torus in terms of a more convenient set of "flux coordinates." In the new system the transverse variables  $(r, \theta)$  are replaced by the coordinates  $(\psi, \chi)$ , where  $\psi(r, \theta)$ , the poloidal flux function, plays the role of a radial variable and  $\chi(r, \theta)$  is an anglelike variable orthogonal to  $\psi$  (i.e.,  $\nabla \psi \cdot \nabla \chi = 0$ ), normalized so that  $\chi = 2\pi$  is the natural period. After a straightforward calculation,  $\delta W$  can be expressed as [see, for instance, Connor, Hastie, and Taylor (1979).]

Note that  $\oint \nu d\chi = 2\pi q(\psi)$  and that the plasma compressibility term has been eliminated by a proper choice of  $\xi_{||}$ .

Consider now the limit  $n \rightarrow \infty$ . Equation (5.152) implies that unless  $k_{||} \sim O(1)$ ,  $\delta W$  will be large and positive because of the line bending terms; that is, instabilities can only occur for perturbations which are nearly constant along a field line. Similarly, unless there is rapid variation perpendicular to the field (i.e.,  $\partial X / \partial \psi \sim inU$ ), there is a large stabilizing contribution from the magnetic compression terms. These properties imply that the minimizing  $U$  can be represented as an asymptotic expansion in  $1/n$  as follows:  $U = U_0 + U_1/n + U_2/n^2 + \dots$  The value of  $\partial U_1 / \partial \chi$  can then be determined by a straightforward iteration of Eq. (5.153):  $\partial U_1 / \partial \chi = -inU_1 + iJBk_{||}U_{l-1}$ . This feature allows for an order-by-order algebraic minimization of  $\delta W$  with respect to the  $U_l$ , since  $\partial U / \partial \chi$  does not explicitly appear.

Carrying out this procedure yields an expression for the leading-order  $\delta W$  which is a function only of  $X$  and which is valid for interchange and ballooning modes:

$$X(\psi, \chi, \phi) = f(\psi, \chi) \exp \left[ in\phi - in \int_0^\chi \nu(\psi_0, \chi') d\chi' \right]. \quad (5.157)$$

For the Mercier criterion, the next and perhaps key step in the derivation is to devise an accurate representation of the interchange trial function for substitution into  $\delta W$ . In analogy with Suydam's criterion, the perturbation is assumed to be almost exactly constant along a field line [i.e.,  $ik_{||} X(\psi_0, \chi, \phi) \approx 0$ ],

$$X(\psi, \chi, \phi) = f(\psi, \chi) \exp \left[ in\phi - in \int_0^\chi \nu(\psi_0, \chi') d\chi' \right]. \quad (5.157)$$

The surface  $\psi = \psi_0$  is assumed to be rational, so that  $nq(\psi_0) = m$ , thus guaranteeing that the rapidly varying

exponential part of the perturbation is periodic in  $\chi$ . The function  $f(\psi, \chi)$  is slowly varying and also periodic in  $\chi$ , but very rapidly varying in  $\psi$ . It is convenient to distinguish between the two widely disparate radial length scales appearing in the analysis by introducing a new radial variable  $x = n^2(\psi - \psi_0)$ . Hence equilibrium quantities are functions of  $\psi \approx \psi_0$ , while perturbation quantities are functions of  $x$ . This implies that the geodesic curvature term is large in magnitude but oscillatory in  $\chi$  and leads to an appropriate representation for  $f(\psi, \chi)$  given by

$$f(\psi, \chi) = f_0(x) + \frac{i}{n} f_1(x, \chi) \dots \quad (5.158)$$

In the 1D case  $f_1 = 0$ , since  $\kappa_s = 0$ . In the 2D case  $f_1$  represents a very slight ballooning of the perturbation which emphasizes the regions of local unfavorable geodesic curvature. The constraints of periodicity in  $\chi$  and strong localization in  $\psi$  imply that with the form of  $X$  given by Eq. (5.157) only a small ballooning effect is allowed (i.e.,  $f_1/n \ll f_0$ ). Even so, since the geodesic cur-

vature contribution is large, the small ballooning effect makes a contribution to  $\delta W$  comparable to that of the normal curvature.

Substitution of Eqs. (5.157) and (5.158) into Eq. (5.155) leads to an expression which can be algebraically minimized with respect to  $\partial^2 f_1 / \partial x \partial \chi$ . Taking into account the constraint that  $f_1$  must be periodic in  $\chi$ , one finds

$$\frac{\partial}{\partial \chi} \left[ \frac{\partial f_1}{\partial x} \right] = - \frac{\partial \nu}{\partial \psi_0} \frac{d}{dx} (x f_0) + \frac{\nu}{B_p^2} \left[ \frac{dp}{d\psi_0} + \frac{B^2}{F} \lambda \right], \quad (5.159)$$

with  $\lambda(\psi_0)$  the Lagrange multiplier given by

$$\begin{aligned} \lambda(\psi_0) = & \left[ \oint \frac{\nu B^2}{B_p^2} d\chi \right]^{-1} \left[ 2\pi F \frac{dq}{d\psi_0} \frac{d}{dx} (x f_0) \right. \\ & \left. + f_0 F \frac{dp}{d\psi_0} \oint \frac{\nu}{B_p^2} d\chi \right]. \end{aligned} \quad (5.160)$$

---

Here the integrals are performed over the surface  $\psi = \psi_0$ .

When Eq. (5.159) is substituted into  $\delta W$ , an expression is obtained which is identical in form to that arising in the derivation of Suydam's criterion [Eq. (5.92)]:

$$\begin{aligned} \delta W = & \frac{\pi}{n^2} W_0 \int dx \left[ x^2 \left[ \frac{df_0}{dx} \right]^2 + \alpha f_0^2 \right], \\ W_0 = & \left[ \pi \frac{dq}{d\psi_0} \right]^2 F \left[ \oint \frac{\nu B^2}{B_p^2} d\chi \right]^{-1}, \\ \alpha(\psi_0) = & \frac{dp/d\psi_0}{F(2\pi dq/d\psi_0)^2} \left[ \left[ \oint \frac{\partial J}{\partial \psi_0} d\chi - \frac{dp}{d\psi_0} \oint \frac{J}{B_p^2} d\chi \right] \left[ \oint \frac{\nu B^2}{B_p^2} d\chi \right] + \left[ F \frac{dp}{d\psi_0} \oint \frac{\nu d\chi}{B_p^2} - 2\pi \frac{dq}{d\psi_0} F \right] \left[ \oint \frac{\nu}{B_p^2} d\chi \right] \right]. \end{aligned} \quad (5.161)$$

---

Note that the specific form for  $f$  given by Eq. (5.158) has resulted in a one-dimensional integral independent of  $\chi$ . The original  $\chi$  dependence of  $\delta W$  appears only as equilibrium averages in the coefficient  $\alpha$ .

In exact analogy with Suydam's criterion, an analysis of Eq. (5.161) indicates that, for sufficiently negative  $\alpha$ , the behavior of  $f_0$  becomes oscillatory, implying instability. The transition from oscillatory to exponential behavior is known as Mercier's criterion and is given by (Mercier, 1960)

$$\alpha + \frac{1}{4} > 0. \quad (5.162)$$

The criterion, which must be tested on every flux surface, is necessary but not sufficient for stability, since the special interchange perturbation has been substituted for  $X$ .

Mercier's criterion is perhaps the simplest test of tokamak stability, although it still in general requires a numerical solution to the equilibrium Grad-Shafranov equation. One of the better known limits (Ware and Haas, 1966; Shafranov and Yurchenko, 1968) corresponds to the case of circular cross section, large aspect ratio, and

$\beta_p \sim 1$ , and is given by

$$(rq'/q)^2 + 4r\beta'(1-q^2) > 0. \quad (5.163)$$

Note that this expression is very similar to Suydam's criterion for the straight tokamak [Eq. (5.136)] except for the factor  $(1-q^2)$ . This modification predicts that configurations with a negative pressure gradient, even near the axis, can be stabilized if  $q > 1$ . In contrast, the straight tokamak always predicts a small region of instability under similar circumstances.

The additional stability found in the torus is associated with the existence of a "magnetic well." It corresponds to the fact that in a torus the average curvature of a field line, which is precisely what the interchange perturbation samples, can be favorable; that is, on the inside of the torus ( $\theta = \pi$ ) the toroidal field bends away from the plasma, producing favorable curvature. The opposite is true on the outside ( $\theta = 0$ ). A careful averaging indicates that there is a net favorable effect. If the poloidal field, which has unfavorable curvature everywhere, is sufficiently small,  $q > 1$ , the overall effect of both fields remains favorable, and the system is stabilized.

The full Mercier criterion essentially sets a limit on the minimum  $q(0)$ . In addition, once  $p(\psi), F(\psi)$  are specified and the Grad-Shafranov equation solved, a  $\langle\beta\rangle$  limit is implied for sufficiently large  $\beta_p \sim 1/\epsilon$  where Eq. (5.163) is no longer valid; (that is, at high  $\beta_p$  the plasma diamagnetic currents significantly alter the toroidal field, destroying the magnetic well).

Perhaps a more important question concerning the Mercier criterion is the effect of noncircularity. This problem has been investigated by a number of authors, who examined the behavior of the Mercier criterion near the magnetic axis [see, for instance, Solov'ev *et al.* (1969), Laval *et al.* (1971), Lortz and Nuhrenberg (1973), Mikhailovskii and Shafranov (1974), Mikhailovskii (1974), and the reviews by Solov'ev (1976), Wesson (1978), and Bateman (1978)]. Their results can be summarized as follows. For  $\beta_p \sim 1$ , ellipticity by itself tends to be destabilizing [i.e., the allowable value of  $(RJ_\phi/B_\phi)$  on the magnetic axis is reduced]. However, a combination of ellipticity and triangularity is favorable for an elongated outward-pointing triangle or a flattened inward-pointing triangle. For higher  $\beta_p$  (but still  $\beta_p \sim 1$ ) the ballooning nature of the perturbation, which is destabilizing, becomes more apparent, while the larger toroidal shift increases the magnetic well effect, which is stabilizing. The overall picture is slightly complicated. For relatively large ellipticities, the ballooning effect dominates, and higher  $\beta_p$  is destabilizing. For nearly circular cross sections, the increased magnetic well dominates, and higher  $\beta_p$  is stabilizing.

In summary, the Mercier criterion basically limits the value of  $J_\phi \sim 1/q$  on axis in a toroidal tokamak. For sufficiently high  $q(0)$  the average curvature of a field line becomes favorable, and a negative pressure gradient on axis, which is always unstable in the straight tokamak, is stabilized. As with the Suydam criterion, a Mercier interchange perturbation by itself is unlikely to be important in a real experiment. However, the presence of such instabilities implies that dangerous large-scale modes are also very likely to exist.

### c. Internal modes (localized: ballooning modes)

One of the most important physics questions in the tokamak program is the determination of the  $\langle\beta\rangle$  limits resulting from ideal MHD instabilities. Such limits can result from both internal and external modes. In this section a summary is given of the ballooning mode analysis, which determines the critical  $\langle\beta\rangle$  for stability against  $n \rightarrow \infty$  internal modes. [The ballooning mode formalism has been investigated by a number of authors, including Laval *et al.* (1970), Coppi (1977), Dobrott *et al.* (1977), and Connor *et al.* (1978). A complete theory has been given by Conner *et al.* (1979).]

The end result of the analysis is an ordinary differential equation describing the angular dependence of  $n \cdot \xi$  on each surface. It can be solved on one flux surface at a time, providing a substantial saving over the full 2D problem. The analysis, which is valid for arbitrary  $\beta$  and arbitrary

aspect ratio, determines the true minimizing perturbation for  $n \rightarrow \infty$  modes. Thus the resulting  $\langle\beta\rangle$  limits are both necessary and sufficient for these modes. The corresponding eigenfunctions have a strong tendency to concentrate in the regions of unfavorable curvature.

As stated previously, the derivation begins with Eq. (5.155). However, in contrast to the special interchange trial function, a more general, maximally ordered (with respect to  $n$ ) perturbation is allowed. Its form can be ascertained by noting that, as for any instability  $n \cdot \xi$  must be nearly constant along a field line (i.e.,  $ik_{||}X \approx 0$ ) or else  $\delta W$  is dominated by large stabilizing line bending contributions. Consequently, to leading order it is appropriate to write

$$X(\psi, \chi, \phi) = f(\psi, \chi) \exp \left[ in\phi - in \int_0^\chi v(\psi_0, \chi') d\chi' \right], \quad (5.164)$$

where  $\psi_0$  is any rational surface. The function  $f$  is slowly varying in  $\chi$ , but rapidly varying in  $\psi$ .

In analogy with the Mercier criterion, a new "radial" variable can be introduced to distinguish the slow  $\psi$  variation of the equilibrium quantities from the rapid  $\psi$  dependence of the perturbation. For the maximally ordered ballooning mode the appropriate "length" scale is  $x = n(\psi - \psi_0)$  [as opposed to  $x = n^2(\psi - \psi_0)$  for Mercier interchanges]. Consequently, while ballooning modes are still localized radially, they are not so localized as interchange perturbations. This has the following physical effect. Even though  $n \rightarrow \infty$  implies rapid oscillations, Mercier interchanges are so localized that the deviation from  $ik_{||}X = 0$  on nearby flux surfaces ( $\Delta\psi \sim 1/n^2$ ) involved in the perturbation remains small [i.e., on the surface  $\psi \approx \psi_0(1 + 1/n^2)$ ,  $|Rk_{||}X(\psi, \chi, \phi)| / |X| \sim 1/n \ll 1$ ]. As a result only small modulations in  $\chi$  are allowed, in order to prevent large stabilizing line bending contributions from dominating. In contrast, the ballooning perturbation extends sufficiently further out that the deviation from  $ik_{||}X = 0$  is of order unity [i.e., on the surface  $\psi \approx \psi_0(1 + 1/n)$ ,  $|Rk_{||}X(\psi, \chi, \phi)| / |X| \sim 1$ ]. Thus the maximal expansion creates a situation where the effects of line bending and ballooning are both finite and competitive in the same order.

Introduction of the ballooning mode scaling into Eq. (5.155) leads to a form of  $\delta W$  independent of  $n$ , given by

$$\begin{aligned} \delta W = \pi \int d\psi d\chi & \left[ \frac{1}{JR^2B_p^2} |Lf|^2 + \frac{R^2B_p^2}{JB^2} \left| \frac{\partial}{\partial x}(Lf) \right|^2 \right. \\ & \left. - 2Jp' \left[ \frac{\kappa_n}{RB_p} |f|^2 - \frac{iFB_p\kappa_s}{B^2} f \frac{\partial f^*}{\partial x} \right] \right], \\ iLf & \equiv \frac{\partial f}{\partial \chi} + ix \frac{\partial v}{\partial \psi_0} f. \end{aligned} \quad (5.165)$$

Since the modulations are finite, the  $\chi$  dependence can no longer be eliminated by expanding  $f(x, \chi) = f_0(x) + if_1(x, \chi)/n$ . Instead, the full two-dimensional system must be solved self-consistently. If the requirement of periodicity in  $\chi$  is temporarily relaxed, a convenient way to solve the Euler-Lagrange equation resulting from Eq.

(5.165) is by Fourier analysis in  $x$ :

$$\begin{aligned} f(x, \chi; \psi_0) &= g(k, \chi; \psi_0) \exp(i\hat{k}x), \\ \hat{k}(\chi, \psi_0) &= k - \int_0^\chi \frac{\partial}{\partial \psi_0} v(\psi_0, \chi') d\chi'. \end{aligned} \quad (5.166)$$

Here  $k$  is the transform variable. In this case,  $\delta W$  reduces to a one-dimensional quadratic form with  $k$  and  $\psi_0$  appearing as parameters,

$$\begin{aligned} \delta W = \frac{\pi}{n} \int dx d\chi \left\{ \frac{1}{JR^2 B_p^2} \left[ 1 + \left( \frac{R^2 B_p^2 \hat{k}}{B} \right)^2 \right] \left| \frac{\partial g}{\partial \chi} \right|^2 \right. \\ \left. - 2p' J \left( \frac{\kappa_n}{RB_p} - \frac{FB_p \kappa_s \hat{k}}{B^2} \right) |g|^2 \right\}. \end{aligned} \quad (5.167)$$

As convenient as this form is, it has the difficulty that unless  $g$  smoothly approaches zero at each end of the interval  $0 \leq \chi \leq 2\pi$ , the function  $f$  will not in general be periodic on all nearby surfaces away from the resonant surface,  $x = 0$ . The basic incompatibility between periodicity in  $\chi$  and local Fourier analysis in  $x$  (i.e., use of an eikonal representation) was resolved by Connor *et al.* (1979). They pointed out that, starting with a nonperiodic function such as that given by Eq. (5.166), one can generate a periodic function by extending the domain of validity from  $0 \leq \chi \leq 2\pi$  to  $-\infty < \chi < \infty$  and assuming suitable convergence properties at  $\chi = \pm\infty$ . This procedure leads to the quasimode representation of  $f$ ,

$$f(x, \chi; \psi_0) = \sum_m \hat{f}(x, \chi + 2m\pi; \psi_0). \quad (5.168)$$

Since  $f$  by definition is periodic, it can be expanded in a Fourier series,

$$f(x, \chi; \psi_0) = \sum_m A_m(x; \psi_0) \exp(im\chi), \quad (5.169)$$

where it can be shown by direct calculation that the coefficients  $A_m$  are related to  $\hat{f}$  as follows:

$$A_m(x; \psi_0) = \frac{1}{2\pi} \int_{-\infty}^{\infty} d\chi \hat{f}(x, \chi; \psi_0) \exp(-im\chi). \quad (5.170)$$

If one now Fourier analyses  $\hat{f}(x, \chi; \psi_0) = \hat{g}(k, \chi; \psi_0) \exp(i\hat{k}x)$  and substitutes into the Euler-Lagrange equation resulting from Eq. (5.165), there results a single ordinary differential equation for  $\hat{g}$  given by [see, for instance, Connor *et al.* (1979)]

$$\begin{aligned} \frac{\partial}{\partial \chi} \left\{ \frac{1}{JB^2 B_p^2} \left[ 1 + \left( \frac{R^2 B_p^2}{B} \right)^2 \hat{k}^2 \right] \frac{\partial \hat{g}}{\partial \chi} \right\} \\ + \frac{2p' J}{RB_p} \left[ \kappa_n - \frac{FRB_p^2}{B^2} \hat{k} \kappa_s \right] \hat{g} = 0. \end{aligned} \quad (5.171)$$

This equation is identical to the Euler-Lagrange equation resulting from the “nonperiodic”  $\delta W$  [i.e., Eq. (5.167)]. However, the boundary conditions require only that  $\hat{g}$  vanish sufficiently rapidly at  $\chi = \pm\infty$ . Furthermore, because of the quasimode representation, the full solution for  $f$  is periodic even though  $\hat{g}$  itself is not.

Equation (5.171) is the ballooning mode differential equation. It is an ordinary differential equation that can be solved separately on each flux surface  $\psi_0$  for any given  $k$  once an equilibrium is specified. Stability can be ascertained in either of two ways. First, Newcomb's analysis can be applied. Thus, if on any flux surface a value of  $k$  is found such that the solution to Eq. (5.171), which is regular at  $\chi \rightarrow -\infty$  and has a zero crossing for  $\chi < +\infty$ , the system is unstable. A second approach is to introduce a convenient normalization and then compute the corresponding eigenvalue (as a function of  $k$ ) as a two-point boundary value problem. Stability is determined by the sign of the eigenvalue.

Recently an analytic solution for the large-aspect-ratio, circular-cross-section configuration has been given by Pogutse and Yurchenko (1978). They find a local criterion for the maximum allowable value of  $\beta'(r)$ , which is given by

$$\begin{aligned} S^2 + 2r\beta' \left\{ 1 - q^2 \left[ 1 - \frac{7}{4} \frac{R}{r} \left[ 1 - \frac{5}{7} S^2 \right] \exp \left[ -1/|S| \right] \right] \right\} \\ - \frac{3}{2} S(r\beta')^2 \frac{q^4 R^2}{r^2} > 0, \end{aligned} \quad (5.172)$$

where the shear  $S \equiv rq'/q$ .

Note that near the magnetic axis  $S \sim r^2$ , and the ballooning mode criterion requires a magnetic well  $q(0) > 1$  for stability. However, unlike the Mercier criterion, a well does not imply stability away from the axis. In fact, a simple estimate obtained by neglecting the middle term of Eq. (5.172) shows that, for stability,

$$-r\beta' < \left[ \frac{2}{3} S \right]^{1/2} \left[ \frac{r}{Rq^2} \right]. \quad (5.173)$$

For the simple model,  $q = q(0)(1+r^2/r_0^2)$ , integration of Eq. (5.173) over the plasma cross section yields

$$\langle \beta \rangle < \frac{2}{3\sqrt{3}} \frac{\epsilon}{q_0^2} \left[ 1 - \frac{1}{2} \left[ \frac{q_0}{q_a} \right]^{1/2} \left[ 3 - \frac{q_0}{q_a} \right] \right], \quad (5.174)$$

where  $q_0 = q(0)$  and  $q_a = q(a) = q_0(1+a^2/r_0^2)$ . Equations (5.173) and (5.174) indicate that the critical  $\langle \beta \rangle$  scales as that of a high- $\beta$  tokamak and that large shear is favorable for stability against ballooning modes.

Because of the relative simplicity of Eq. (5.171), a number of numerical codes have been developed for testing ballooning mode stability (Dobrott *et al.*, 1979; Miller and Moore, 1979; Charlton *et al.*, 1979; Todd *et al.*, 1979; Bernard *et al.*, 1980). Such studies show that by optimizing profiles and cross sections, one can obtain critical  $\langle \beta \rangle$ 's on the order of 5–10%. This optimistic result should, however, be viewed cautiously. The most stable

configurations almost always have broad pressure profiles with relatively sharp gradients near the plasma surface where the shear is high. Thus the optimistic stability results are to a certain extent a consequence of the "wall stabilization" associated with the boundary condition  $\mathbf{n} \cdot \boldsymbol{\xi} = 0$  for internal modes. As indicated before, sharp gradients near the plasma surface are likely to drive higher- $m$  external modes unstable. Since there are opposing constraints for ballooning mode and external kink stability, the optimum profile represents some compromise between those two effects.

Finally, it should be noted that both analytical (Connor *et al.*, 1979) and numerical (e.g., Charlton *et al.*, 1979; Todd *et al.*, 1979), studies have shown that the  $\langle \beta \rangle$  limits for arbitrary *internal* modes are most stringent for the  $n \rightarrow \infty$  ballooning modes. However, modes with such a fine-scale structure are likely to be affected by other physics (e.g., by finite gyroradius). Consequently, in a real experiment, the most unstable modes will probably correspond to lower- $n$  values, with somewhat higher  $\langle \beta \rangle$  limits than for  $n \rightarrow \infty$ . The nonlinear evolution of such modes, including resistivity, is an important area of current theoretical tokamak research.

In summary, ballooning modes are pressure-driven instabilities localized in the region of unfavorable curvature on the outside of the torus. These modes set an upper limit on the value of  $\langle \beta \rangle \sim \epsilon/q^2(0)$  that can be stably confined in a tokamak. High shear is in general favorable for stability. However, near the magnetic axis where the shear is small, a magnetic well is required [ $q(0) \geq 1$ ], as in the Mercier criterion. This corresponds to a limit on the current density on axis. The current-density limit is not too restrictive in that, even if it is violated, a small localized flattening of the central pressure profile restores stability. Numerical calculations have shown that reasonable current and pressure profiles can be stable to ballooning modes, as well as to all other internal modes, for  $\langle \beta \rangle \sim 5-10\%$ .

#### d. Internal modes (general)

Although the high- $n$  ballooning modes lead to the lowest critical  $\langle \beta \rangle$ 's for internal instabilities, it is still of interest to examine more general lower- $n$  modes. The reason is that such modes set an upper limit on the toroidal current density on axis. Recall that in a straight tokamak  $q(0) > 1$  is required for  $n=1, m=1$  stability. Note also that  $q(0) > 1$  is required in a torus for a magnetic well, but this is a weak condition because a small flattening of the pressure profile eliminates the high- $n$  interchanges near the axis.

Since low- $n$  modes have large-scale radial structure, the stability boundaries can often only be determined by numerical computation. However, an interesting analytic calculation has been carried out in the limit of a large-aspect-ratio, circular-cross-section tokamak by Bussac *et al.* (1975), which sheds considerable light on this problem. By applying the conventional tokamak expansion,  $\beta \sim \epsilon^2, \beta_p \sim 1$ , they derive an expression for  $\delta W$  as a func-

tion of  $n$  for the toroidal case. Since  $\beta$  is not assumed to be large (i.e., not the high- $\beta$  tokamak ordering), their calculation can be viewed as a determination of the effects of toroidicity on the current-density limit of low- $n$  internal kinks.

After a rather involved calculation, Bussac *et al.* derive an expression for  $\delta W$  which can be written as

$$\frac{\delta W}{2\pi R} = \frac{\pi B_0^2 \epsilon^2}{R^2} \left[ \left( 1 - \frac{1}{n^2} \right) \delta W_c + \frac{1}{n^2} \delta W_T \right]. \quad (5.175)$$

Here

$$\delta W_c = \int_0^{r_s} \left[ r \beta' + \frac{n^2 r^2}{R^2} \left( 1 - \frac{1}{nq} \right) \left( 3 + \frac{1}{nq} \right) \right] r dr \quad (5.176)$$

is the contribution due to a straight tokamak using the standard  $m=1$  internal mode eigenfunction [see Eq. (5.139) and Fig. 43] with  $r_s$  the singular surface defined by  $nq(r_s) = 1$ . The toroidal contribution  $\delta W_T$  is in general quite complicated. However, in the limit of  $|q(0)-1| \ll 1, q(0) < 1$ , and with a parabolic current profile, a simple expression is obtained,

$$\delta W_T \approx \frac{3n^2 r_s^4}{R^2} [1-q(0)] \left[ \frac{13}{144} - \beta_p^2 \right],$$

$$\beta_p = -\frac{R^2}{n^2 r_s^2} \int_0^{r_s} r^2 \beta' dr. \quad (5.177)$$

Note that, for  $n \gg 1$ ,  $\delta W \approx (\pi B_0^2 / R^2) \delta W_c$  and stability is identical to that in the straight tokamak, requiring  $nq(0) > 1$ . For the most severe case,  $n=1$ , the cylindrical contribution vanishes and  $\delta W = (\pi B_0^2 / R^2) \delta W_T$ . Here, in contrast to the cylindrical result, the internal kink mode is stable in the limit  $\beta_p \rightarrow 0$  if  $q(0) < 1$ . However, in both cases, increasing  $\beta_p$  is destabilizing and the toroidal calculation predicts instability for  $\beta_p > \sqrt{13/12} \approx 0.3$  unless  $q(0) > 1$ .

Similar results have been found numerically (Sykes and Wesson, 1974; Kerner, 1976; Berger *et al.*, 1977). These calculations show that for small  $\beta_p$  there still exists a current-density limit, but that it is associated with the  $n=2, m=1$  mode,  $q(0) \geq 0.5$ . Consistent with the analytic calculation of Bussac *et al.*, the  $n=1$  mode is stabilized by toroidicity at low  $\beta_p$ . However, as  $\beta_p$  increases the  $n=1, m=1$  mode is excited. The numerical results show that this instability is stabilized for  $q(0) \geq 1$ .

In summary, toroidicity has a number of important effects on the stability of internal ideal MHD modes:

(a) Toroidicity has a stabilizing effect on pressure-driven interchanges to the extent that a magnetic well can be created.

(b) Toroidicity has a destabilizing effect on more general pressure-driven modes. In particular, ballooning instabilities, which have no simple analog in the straight tokamak, can be excited, even if  $q(0) > 1$ . These modes set an upper limit on the value of  $\langle \beta \rangle / \epsilon$ .

(c) Toroidicity has a slight stabilizing effect on the limiting current density on axis, due to the internal  $m=1, n=1$  kink mode at low  $\beta_p$ . However, for  $\beta_p \gtrsim \frac{1}{2}$ , stability still requires  $q(0) \gtrsim 1$ .

Thus, in order to stabilize a tokamak to internal modes, the current density on axis must be limited to  $q(0) \gtrsim 1$  and the pressure must be sufficiently low so that  $\langle\beta\rangle \lesssim 0.1$ . In general profiles with high shear have higher  $\langle\beta\rangle$  ballooning limits. The alternative approach to ballooning mode stability, very low shear plus a magnetic well, is not likely to be satisfactory when one includes the low current gradient requirements of external kinks. Noncircularity, if properly chosen, can also improve internal mode stability. A combination of elongation and outward-pointing triangularity can lead to substantial increases in the  $\langle\beta\rangle/\epsilon$  limit, as well as the on-axis current density. These increases appear to saturate for elongations greater than about 2:1.

#### e. External modes

As in the straight tokamak, the external modes set the most severe limits on ideal MHD stability. Recall that in a straight tokamak stability is achieved by requiring  $q(a) \geq 1$  for the  $m=1$  mode and requiring a peaked current profile for the higher- $m$  modes. In a torus, there is a further limitation which sets a maximum value for  $\langle\beta\rangle$ . This limit is in general more severe than that due to  $n \rightarrow \infty$  internal ballooning modes.

In the regime of the conventional tokamak,  $\langle\beta\rangle \sim \epsilon^2$ , ballooning effects are unimportant. Stability is determined by external kink modes, and the results are similar to those in the straight tokamak. The new stability limits appear in the high- $\langle\beta\rangle$  regime ( $\langle\beta\rangle \sim \epsilon$ ) and are associated with toroidal ballooning effects. In fact, for the most unstable modes, the eigenfunction corresponds to a combination of ballooning and kinking. Thus, in contrast to  $n \rightarrow \infty$  internal ballooning modes, which are driven solely by the pressure gradient, external modes are driven by a combination of the pressure gradient and the parallel current.

Since these are low- $m$  modes with gross radial structure, many of the stability results have been obtained from numerical computations (Wesson and Sykes, 1974; Schneider and Bateman, 1974; Todd *et al.*, 1977, 1979; Berger *et al.*, 1977; Dory *et al.*, 1977; Charlton *et al.*, 1979; and Bernard *et al.*, 1980). There is, however, one simple equilibrium model which gives unexpectedly reliable information about the  $\langle\beta\rangle$  limits. This model is known as the surface current model, and its equilibrium and stability properties are summarized below (Freidberg and Haas, 1973; D'Ippolito *et al.*, 1978).

In the model, the shape of the plasma surface is prescribed and all currents are assumed to flow only in this surface. Within the plasma  $\mathbf{J}=0$  and  $p=\text{const}$ . Outside, the plasma is surrounded by a vacuum. The only requirements for equilibrium are  $[\mathbf{n} \cdot \mathbf{B}] = 0$  and  $[p + B^2/2] = 0$  across the surface. Because of its simplicity,

the model can be solved exactly or in the context of either the conventional or high- $\beta$  expansion. For present purposes it is useful to focus attention on the high- $\beta$  expansion. In this case it has been shown that for a circular cross section the poloidal field just outside the plasma is given by (Freidberg and Haas, 1973)

$$\frac{B_\theta(a, \theta)}{\epsilon B_0} = \frac{1}{q^*} \left[ \frac{\pi}{2E(k)} \right] [1 - k^2 \sin^2(\theta/2)]^{1/2}, \quad (5.178)$$

where (in mks units)  $q^* = 2\pi a^2 B_0 / \mu_0 I R_0$ ,  $E(k)$  is the complete elliptic integral of the second kind, and  $k \sim 1$  is a parameter related to  $\langle\beta\rangle \equiv 2p/B_0^2$  by

$$\langle\beta\rangle q^{*2}/\epsilon = [\pi k / 4E(k)]^2.$$

As  $\langle\beta\rangle$  varies, the shape of the cross section is held fixed. If the current  $I$  (i.e.,  $q^*$ ), is also held fixed, there is an equilibrium limit corresponding to  $k \rightarrow 1$ , given by

$$\begin{aligned} \langle\beta\rangle/\epsilon &\leq \pi^2/16q^{*2}, \\ \epsilon \langle\beta_p\rangle &\leq \pi^2/16. \end{aligned} \quad (5.179)$$

In analogy with the uniform current equilibrium (see Sec. IV.C.6), a crude approximation to flux conservation can be made by requiring  $q(a)$  to be held fixed, rather than  $q^*$ , as  $\langle\beta\rangle$  is varied. In this case there is no equilibrium limit, and, as  $\langle\beta\rangle/\epsilon \rightarrow \infty$ ,

$$\begin{aligned} 1/q^* &\rightarrow (4/\pi)(\langle\beta\rangle/\epsilon)^{1/2}, \\ \epsilon \langle\beta_p\rangle &\rightarrow \pi^2/16. \end{aligned} \quad (5.180)$$

Thus, despite its simplicity, the surface current equilibrium has many features in common with more complicated diffuse high- $\beta$  equilibria.

The stability of the system is determined by an analysis of the extended Energy Principle,  $\delta W = \delta W_F + \delta W_S + \delta W_V$  (see Sec. V.B.4.c). An advantage of the surface current model is that, after Fourier analysis with respect to  $\phi$  the stability problem is reduced to a minimization with respect to a single, one-dimensional, scalar quantity  $\xi(\theta) \equiv \mathbf{n} \cdot \xi[r_p(\theta), \theta]$ , evaluated on the plasma surface  $r = r_p(\theta)$ . The procedure can be carried out for arbitrarily shaped cross sections and represents a substantial saving over the general diffuse case, where the unknown perturbations are two-dimensional functions of  $r$  and  $\theta$ .

Some insight into the nature of the high- $\langle\beta\rangle$  instabilities can be gained by examining  $\delta W_S$ , the only source of instability in the surface current model. For the circular-cross-section case,

$$\begin{aligned} \frac{\delta W_S}{2\pi R_0} &= -\epsilon^2 B_0^2 \\ &\times \int_0^{2\pi} |\xi(\theta)|^2 \left[ \left( \frac{B_\theta(a, \theta)}{\epsilon B_0} \right)^2 + \frac{\langle\beta\rangle}{\epsilon} \cos\theta \right] d\theta. \end{aligned} \quad (5.181)$$

Note that there are two contributions to instability. The first, proportional to  $B_\theta^2$ , is the usual destabilizing effect of the parallel currents (i.e., the kink term). The second

contribution is the effect of the toroidal field curvature (i.e., the pressure-driven term). The  $\cos\theta$  dependence reflects the fact that the toroidal curvature is unfavorable on the outside of the torus but favorable on the inside. Indeed, it is just this effect which causes the eigenfunction to balloon. Observe, also, that for the conventional ordering  $\langle\beta\rangle \sim \epsilon^2$  the ballooning contribution is negligible.

The stability analysis is carried out by first Fourier analyzing the normal component of plasma displacement,

$$\xi(\theta) = \exp(-in\phi) \sum_m' \xi_m \exp(im\theta),$$

and then minimizing over the coefficients  $\xi_m$ . Both the plasma and vacuum contributions can be converted to surface integrals. These are then expressed in terms of the  $\xi_m$  through the solution to Laplace's equations for the perturbed scalar magnetic potentials and application of the boundary conditions given by Eq. (5.45).

After a lengthy calculation, an expression for  $\delta W$  is obtained which can be written as (Freidberg and Haas, 1973)

$$\frac{\delta W}{2\pi R_0} = \pi\epsilon^2 B_0^2 \sum_m' \xi_m W_{mp} \xi_p^*, \quad (5.182)$$

where the matrix elements  $W_{mp}$  for the circular-cross-section case are given by

$$W_{mp} = W_{pm} = -H_{mp} + \sum_l' (G_{lm} G_{lp} + \hat{G}_{lm} \hat{G}_{lp}) / |l|, \\ H_{mp} = \frac{\langle\beta\rangle}{2\epsilon} \left[ 4 \left( \frac{2-k^2}{k^2} \right) \delta_{m-p} + 3(\delta_{m-p-1} + \delta_{p-m-1}) \right], \\ G_{lm} = -n \delta_{l-m}, \\ \hat{G}_{lm} = -n \delta_{l-m} + \frac{l}{\pi} \int_0^\pi \left( \frac{B_\theta}{\epsilon B_0} \right) \cos[(l-m)\theta] d\theta. \quad (5.183)$$

The marginal stability boundary is determined by varying  $\langle\beta\rangle$  until the lowest eigenvalue of  $\tilde{W}$  crosses zero. This is a simple numerical procedure.

The stability curve for the circular-cross-section, high- $\beta$  tokamak is shown in Fig. 45. Plotted here is the critical  $\langle\beta\rangle/\epsilon$  vs  $q^* \sim 1/I$ . Also illustrated is the equilibrium limit  $\langle\beta\rangle q^{*2}/\epsilon = \pi^2/16$ . Observe that for low- $q^*$  ( $< 1$ ) the plasma is unstable for any  $\langle\beta\rangle$ . When  $q^* > 1$ , the plasma becomes stable and the critical  $\langle\beta\rangle$  increases from zero. At  $q^* \approx 1.7$  the stability curve intersects the equilibrium curve, predicting a maximum critical  $\langle\beta\rangle/\epsilon \approx 0.21$ . At higher values of  $q^*$  the plasma is always stable, but these lower currents support increasingly smaller  $\langle\beta\rangle$ 's in toroidal equilibrium.

Thus the surface current model demonstrates that external modes in a toroidal tokamak require both a current limit  $q^* > 1$  and a pressure limit  $\langle\beta\rangle/\epsilon = 0.21$  for stability. The  $\langle\beta\rangle$  limit, which is not very high for the circular case, has also been investigated for a number of noncircular cross sections (Freidberg and Haas, 1974; D'Ippolito *et al.*, 1978). For the ellipse, which is relatively pointed at the ends, the critical  $\langle\beta\rangle$  increases with elongation,  $b/a$ , up until an optimum value  $b/a \approx 2.2$ , after which it decreases. The optimum critical  $\langle\beta\rangle$  at  $b/a = 2.2$  is equal to  $\langle\beta\rangle/\epsilon = 0.37$ . For more rounded,

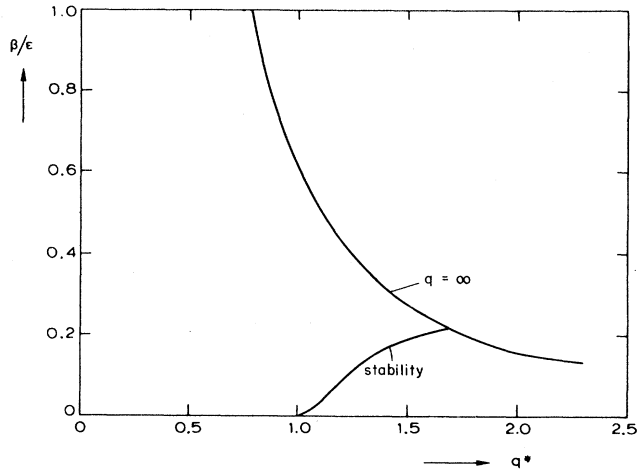


FIG. 45. Stability boundary for external modes in a high- $\beta$  tokamak described by the surface current model (from D'Ippolito *et al.*, 1978).

"race-tracklike" cross sections, the critical  $\langle\beta\rangle$  appears to increase with elongation and then saturate, rather than decrease at large  $b/a$ . The saturated critical  $\langle\beta\rangle$  is approximately  $\langle\beta\rangle/\epsilon \approx 0.5$ . It has also been shown that the presence of force-free currents on the outside of the plasma can lead to substantial further increases in the critical  $\langle\beta\rangle$ .

Recently, more realistic numerical studies of external kink stability have been carried out. [See, for instance, Todd *et al.* (1979), Charlton *et al.* (1979), and Bernard *et al.* 1980.] These calculations are based on an exact formulation of the Energy Principle in which no expansions are made with respect to  $\langle\beta\rangle$  or the inverse aspect ratio. The numerical results and the surface current results agree surprisingly well, despite the simplicity of the latter model. One possible reason may be that, as indicated by the straight tokamak, the stability of  $m=1$  external kinks is independent of current profile.

At present, there is no unique optimum value of critical  $\langle\beta\rangle$  for a tokamak, since the results depend somewhat upon profiles and cross sections. However, the numerical results indicate that external modes give rise to the most severe limits on critical  $\langle\beta\rangle$ , which typically lie in the range of 1–5%. The higher values are obtained with elongated cross sections,  $b/a \sim 2$ , sometimes modified by a small outward-pointing triangularity. To achieve much higher  $\langle\beta\rangle$ 's a conducting shell quite close to the plasma is required,  $a_{\text{wall}}/a_{\text{plas}} \approx 1.2$ . As in the straight tokamak, sharp gradients near the plasma surface lead to high- $m$  instabilities unless the conducting shell is very close.

In summary, external modes appear to be the most dangerous ideal MHD instabilities from the theoretical point of view. However, their behavior is strongly dependent on external conditions, so that the presence of a metal limiter or quasicomducting vacuum chamber near the plasma could have a substantial effect on the actual critical  $\langle\beta\rangle$  achievable in any experiment. These problems require further investigation, particularly an understanding of their nonlinear consequences.

### f. Axisymmetric modes

The final class of toroidal instabilities to be considered is the axisymmetric mode. This perturbation corresponds to an  $n=0$  external mode which at marginal stability can be viewed equivalently as a neighboring equilibrium state. The most unstable perturbation usually corresponds to a nearly rigid vertical shift of the plasma (i.e., there is a large  $m=1$  component to the eigenfunction). It is important to stabilize these modes, since they represent a macroscopic motion of the plasma towards the wall of the discharge chamber.

The stability of axisymmetric modes is directly coupled to toroidicity and noncircularity. This can be seen by examining  $\delta W$  for the  $m=1, n=0$  external mode in a straight circular tokamak [see Eq. (5.142)]. As might be expected because of symmetry, one finds  $\delta W=0$ , indicating neutral stability. Toroidicity and noncircularity in general require relatively complicated two-dimensional calculations. There is, however, one simple model that can be analyzed, illustrating the basic nature of the axisymmetric instability. This model, first investigated by Osovets (1959) and later by Yoshikawa (1964) and Mukhovatov and Shafranov (1971), is discussed below. It has also been recently summarized by Wesson (1978) and Bateman (1978).

The calculation treats the plasma as a thin ( $a/R_0 \ll 1$ ) current-carrying loop of wire embedded in an externally applied vertical field. For simplicity the effects of plasma pressure and internal magnetic flux are neglected. The object of the calculation is to determine the appropriate constraints on the shape of the vertical field to provide stability against rigid vertical and horizontal displacements. Clearly, a pure uniform vertical field  $\mathbf{B}_v = B_v \mathbf{e}_z$ ,  $B_v = \text{const}$  would not be adequate, since by symmetry the system would be only neutrally stable to vertical displacements.

The calculation proceeds by introducing a potential,  $\Phi(R, Z)$ , such that the equilibrium forces acting on the plasma are given by  $\mathbf{F}(R, Z) = -\nabla\Phi$ . Equilibrium occurs at the point  $R_0, Z_0$  where  $F_R(R_0, Z_0) = F_Z(R_0, Z_0) = 0$ . The condition that the plasma then remain stable to a rigid shift in either the vertical or horizontal direction is that  $\partial F_Z(R_0, Z_0)/\partial Z_0 < 0$  and  $\partial F_R(R_0, Z_0)/\partial R_0 < 0$ , respectively; that is, stability occurs when the restoring force is in the opposite direction from the displacement. Note that because the plasma is a perfect conductor the calculation must be carried out under the constraint that the poloidal flux contained within the current loop be conserved under either plasma displacement.

For the simple model under consideration, the appropriate equilibrium potential and the poloidal flux contained within the current loop are given by (see Fig. 46)

$$\Phi(R, Z) = \frac{1}{2} L I^2, \quad (5.184)$$

$$\psi_p(R, Z) = L I - 2\pi \int_0^R B_Z(R', Z) R' dR'.$$

Here  $L(R) = \mu_0 R [\ln(8R/a) - 2]$  is the external induc-

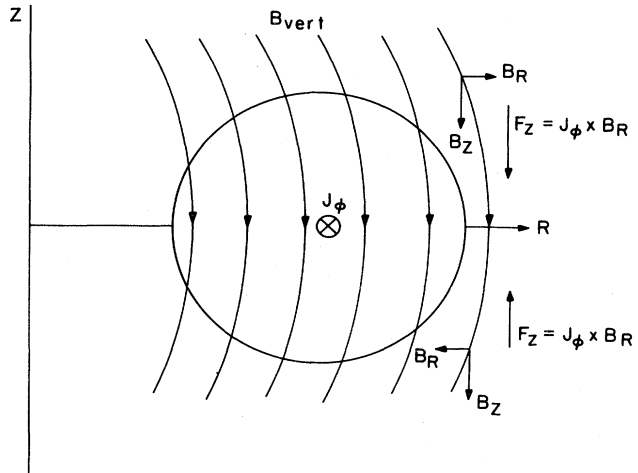


FIG. 46. Geometry for calculating  $n=0$ , axisymmetric mode stability.

tance associated with the toroidal current  $I$ , and  $B_Z$  and  $B_R$  are the components of the externally applied vertical field.

The equilibrium forces, calculated from  $\Phi$ , can be written as

$$F_Z = -LI \frac{\partial I}{\partial Z}, \quad (5.185)$$

$$F_R = -LI \frac{\partial I}{\partial R} - \frac{I^2}{2} \frac{dL}{dR}.$$

From  $\psi_p = \text{const}$  it then follows that the equilibrium relation  $\mathbf{F}(R_0, Z_0) = 0$  reduces to

$$B_R(R_0, Z_0) = 0, \quad (5.186a)$$

$$B_Z(R_0, Z_0) = \frac{I}{4\pi R_0} \frac{dL}{dR_0}. \quad (5.186b)$$

Note that Eq. (5.186b) is identical to those terms in the Shafranov shift associated with the external poloidal flux [see Eq. (4.67)].

Consider now the stability of the plasma to a rigid vertical shift. Using the fact that  $\nabla \times \mathbf{B} = 0$  for the externally applied vertical field, one can easily calculate  $\partial F_Z(R_0, Z_0)/\partial Z_0$ . One finds

$$\frac{\partial F_z}{\partial Z_0} = -\frac{I^2}{2R_0} \frac{dL}{dR_0} n, \quad (5.187)$$

where

$$n(R_0, Z_0) \equiv - \left[ \frac{R_0}{B_Z} \frac{\partial B_Z}{\partial R_0} \right]_{R_0, Z_0}$$

is known as the decay index. The condition for vertical stability is thus given by

$$n > 0. \quad (5.188)$$

This condition can easily be understood from Fig. 46. If the directions of the vertical field and toroidal current are as shown, then: (1) the vertical field produces an in-

ward force for toroidal equilibrium, and (2) a small upward shift of the plasma gives rise to a downward  $\mathbf{J} \times \mathbf{B}$  force, of magnitude  $2\pi RIB_R$ , which is in the direction to restore equilibrium. Thus the curvature of the vertical field shown in Fig. 46 is the appropriate one for stability, and corresponds to the condition  $n > 0$ .

A more exact theorem concerning vertical stability, similar to Earnshaw's theorem in electrostatics, has been derived by Haas and Papaloizou (1977). They considered an arbitrary-cross-section, arbitrary-aspect-ratio, axisymmetric torus subject to antisymmetric perturbations about the  $Z=0$  plane. By allowing a more general trial function than the simple rigid shift displacement, they were able to prove the following theorem. "Any axisymmetric toroidal plasma with toroidal current decreasing monotonically towards the boundary, and maintained in equilibrium by external fields such that the decay index is negative throughout the region occupied by the plasma, is unstable in the absence of active or passive feedback."

Consider now horizontal stability which is only slightly more complicated. In this case, a straightforward calculation yields the following expression:

$$\frac{\partial F_R(R_0, Z_0)}{\partial R_0} = \frac{I^2}{2R_0} \frac{dL}{dR_0} \left[ n - 1 - \frac{1}{2} \frac{d \ln L}{d \ln R_0} + \frac{1}{2} \frac{d \ln(dL/dR_0)}{d \ln R_0} \right]. \quad (5.189)$$

In the simple limit  $\ln(8R_0/a) \gg 1$  horizontal stability is achieved when

$$n < 3/2. \quad (5.190)$$

This situation can be understood as follows. Assume the plasma is given a small outward shift. At constant flux, the outward hoop force on the plasma decreases because of the smaller current at the larger major radius. However, because of the larger radius of curvature of the vertical field, the toroidal restoring force also decreases at the larger major radius. The stability condition given by Eq. (5.190) requires that the curvature of the vertical field be sufficiently weak that toroidal restoring force decay at a slower rate than that of the hoop force, thus providing a net inward stabilizing force.

The results of this simple model are in good agreement with more exact numerical calculations (Wesson and Sykes, 1974; Johnson *et al.*, 1977). In general, for circular-cross-section plasmas, axisymmetric stability is relatively easy to achieve, requiring only a modest shaping of the vertical fields. The situation is more serious for elongated tokamaks. In such configurations there is a strong tendency for the plasma to be unstable to vertical shifts as the elongation increases. A number of calculations which derive a more accurate form of the vertical stability condition and relate the elongation  $b/a$  to  $n$  indicate that only rather small elongations,  $b/a \lesssim 1.25$ , can be stable to vertical shifts when no conducting wall is present (Laval *et al.*, 1974; Laval and Pellat, 1973;

Rebhan, 1975; Haas, 1975). Also, with no wall, the critical elongation does not depend very strongly on  $\langle \beta_p \rangle$  or the current profile. If a conducting wall is allowed even a moderate distance away,  $a_{\text{wall}}/a_{\text{plas}} \sim 1.5 - 2.0$ , there is a substantial improvement in vertical stability. However, the need for such a wall in a reactor is a disadvantage. Even more important, such a wall would certainly be resistive on the reactor time scale, necessitating a feedback system for vertical positioning. This would be in addition to the horizontal feedback system, which is responsible for centering the plasma column along the major radius.

A further point concerning the stability of elongated plasmas has been made by Thyagaraja and Haas (1979). They showed that, even when the  $m=1$  vertical shift mode is assumed to be feedback stabilized, higher- $m$  instabilities can be excited if more realistic boundary conditions are applied. Specifically, the usual assumption which treats the whole system (including the vacuum region) as being surrounded by a closed conducting shell is relaxed. Instead, it is assumed that the plasma is held in equilibrium by a set of fixed external currents. The resulting  $m \geq 2$ , so-called secular instabilities are difficult to feedback stabilize and lead to further strong limitations on the allowable elongations.

In summary,  $n=0$  axisymmetric modes can lead to potentially serious instabilities in a tokamak. For circular cross sections, a moderate shaping of the vertical field should provide stability. For noncircular tokamaks, vertical instabilities produce important limitations on the maximum achievable elongations. Even moderate elongations require a conducting wall or a feedback system for vertical stability.

#### *g. Overview of the tokamak*

By combining the equilibrium and stability results one obtains the following overview of the tokamak concept with respect to ideal MHD behavior.

The tokamak is a relatively low- $\beta$  axisymmetric toroidal configuration. It has a large component of toroidal magnetic field which is required for stability. In the "high- $\beta$ " regime,  $\beta \sim \epsilon$ , the toroidal field also supports the plasma in radial pressure balance (as in a  $\theta$  pinch). The poloidal field provides radial pressure balance in the conventional regime,  $\beta \sim \epsilon^2$  (as in a  $Z$  pinch). In both cases toroidal force balance is provided by a small toroidal current  $B_\theta/B_\phi \sim \epsilon$  interacting with an externally applied vertical field. Since the highest values of  $\beta$  and toroidal current scale with  $\epsilon$  for a fixed toroidal field, tokamaks are inherently low-aspect-ratio devices, somewhat of a technological disadvantage for reactor use.

There are two classes of ideal MHD instabilities which define important boundaries for tokamak operation. These involve a current limit which is found in both straight and toroidal systems and a  $\beta$  limit which is predominantly a toroidal effect.

The best known current limit arises from the  $m=1$

external kink mode. This leads to the Kruskal-Shafranov condition  $q(a) > 1$ . Also,  $m=1$  internal kinks and their nonlinear resistive evolution are responsible for the sawtooth oscillations observed in most tokamaks. The net effect of the internal modes is to cause tokamaks to operate on the borderline of MHD stability,  $q(0) \approx 1$ . In practice, even with  $q(0) \approx 1$ , tokamaks cannot reach the  $q(a) \approx 1$  limit but instead operate with  $q(a) \approx 2-3$ . This is not inconsistent with the requirements of higher- $m$  external kink mode stability. But it is almost certainly more related to the presence of resistive tearing modes, which can cause major disruptions and terminate the discharge if the current becomes too large. Thus, with regard to current-driven instabilities, most tokamaks operate in a regime which is stable, or at least marginally stable to ideal modes, but with some finite level of resistive MHD turbulence. Although there are regions of parameter space where even resistive modes can be stabilized, these are not very attractive because they correspond to low values of the current limit; that is, the benefits of higher current outweigh the enhanced transport due to weak resistive modes at the optimum operating conditions.

The second class of instabilities is responsible for setting limits on the maximum achievable  $\langle\beta\rangle$ . These limits, which occur for both internal and external modes, are associated with the tendency of unstable perturbations to balloon in regions of locally unfavorable curvature. In general the low- $n$  external ballooning kink modes predict more severe  $\langle\beta\rangle$  limits (1–5%) than those of the  $n \rightarrow \infty$ , internal ballooning modes (3–10%). However, the seriousness of either of these modes has not as yet been established experimentally, since most tokamaks operate well below the maximum limits. One exception is the ISX experiment at Oak Ridge, which has recently achieved  $\langle\beta\rangle$  values on the order of 3%. This is just the regime where ballooning effects should become important, and future experimental investigations should shed considerable light on the important issue of  $\langle\beta\rangle$  limits.

There is one further, indirect constraint on tokamak operation, resulting from MHD requirements, which should be noted. The combination of the stability requirement  $q \gtrsim 1$  and the technological constraints limiting the maximum  $B_\phi$  sets an upper limit on the toroidal current. There is theoretical and experimental evidence that this current can, at most, joule heat a plasma to several keV, still significantly below the ignition temperature. As a result, the standard operation of both current experiments and future reactor tokamaks requires some form of auxiliary heating, such as neutral beams or rf power.

In summary, ideal MHD equilibrium and stability requirements impose significant constraints on the operation of a tokamak. Nevertheless, the available stable operating space is sufficiently broad and flexible that tokamaks are currently the most successful experimental configuration and the most promising concept on the path to a fusion reactor.

## 2. Closed-line configurations

### a. Interchanges, ballooning modes, and the “magnetic well”

Significant simplifications occur in the stability analysis of multidimensional closed-line configurations, in particular of the EBT. Such systems have either zero or small zero-averaged parallel currents, so that pressure-driven modes are the dominant source of instability. Of these, the localized  $k_\perp \rightarrow \infty$  modes usually lead to the most severe  $\beta$  limitations in the context of the ideal model. The simplifications associated with closed-line symmetry allow a more general and complete derivation than that presented for the tokamak.

This simplification is realized by reducing  $\delta W$  from its original three-dimensional form, involving the three components of  $\xi$ , into a more tractable one-dimensional form, involving only the normal component of  $\xi$ . Stability can then be tested separately on each magnetic line, representing an enormous savings in effort. The key feature in this reduction is the restriction of the class of modes under consideration to those with  $k_\perp \rightarrow \infty$ . These, in fact, are often the most unstable, and take the form of interchanges and ballooning modes.

The analysis proceeds as follows. Consider the “intuitive” form of  $\delta W_F$  [i.e., Eq. (5.48)], repeated here for convenience:

$$\delta W_F = \frac{1}{2} \int d\mathbf{r} \left[ |\mathbf{Q}_\perp|^2 + B^2 |\nabla \cdot \xi_\perp + 2\xi_\perp \cdot \kappa|^2 + \gamma p |\nabla \cdot \xi|^2 - 2(\xi_\perp \cdot \nabla p)(\xi_\perp^* \cdot \kappa) - \frac{\mathbf{J} \cdot \mathbf{B}}{B^2} (\xi_\perp^* \times \mathbf{B}) \cdot \mathbf{Q}_\perp \right]. \quad (5.191)$$

The calculation is carried out in flux coordinates  $(\psi, \chi, l)$ , where  $\psi$  and  $\chi$  are poloidal variables representing “radius” and “angle,” respectively, and  $l$  is arc length along the magnetic field. Without loss in generality  $\psi$  can be chosen so that: (1)  $p = p(\psi)$ ; (2)  $\psi$ ,  $\chi$ , and  $l$  are locally orthogonal; and (3)  $\mathbf{B} = \nabla\psi \times \nabla\chi$ .

In order to exploit the  $k_\perp \rightarrow \infty$  limit, an eikonal representation is used for  $\xi_\perp$ :

$$\xi_\perp = \eta_\perp(\psi, \chi, l) \exp[iS(\psi, \chi)], \quad (5.192)$$

where  $\mathbf{k}_\perp$  is defined as

$$\begin{aligned} \mathbf{k}_\perp &= \nabla S(\psi, \chi), \\ \mathbf{B} \cdot \nabla S &= 0. \end{aligned} \quad (5.193)$$

The quantity  $\eta_\perp(\psi, \chi, l)$  is assumed to vary “slowly” with  $(\psi, \chi, l)$  on the equilibrium length scale. In contrast, the assumption  $k_\perp \rightarrow \infty$  implies that the  $(\psi, \chi)$  dependence of  $S$  is “rapid.”

The mathematical motivation for introducing separate length scales can be understood by substituting Eq. (5.192) into Eq. (5.191) without approximation. The result is

$$\delta W_F = \frac{1}{2} \int d\mathbf{r} \left[ |\nabla \times (\boldsymbol{\eta}_\perp \times \mathbf{B})_\perp|^2 + B^2 |i\mathbf{k}_\perp \cdot \boldsymbol{\eta}_\perp + \nabla \cdot \boldsymbol{\eta}_\perp + 2\kappa \cdot \boldsymbol{\eta}_\perp|^2 - 2(\boldsymbol{\eta}_\perp \cdot \nabla p)(\boldsymbol{\eta}_\perp^* \cdot \boldsymbol{\kappa}) - \frac{\mathbf{J} \cdot \mathbf{B}}{B^2} (\boldsymbol{\eta}_\perp^* \times \mathbf{B}) \cdot \nabla \times (\boldsymbol{\eta}_\perp \times \mathbf{B})_\perp \right]. \quad (5.194)$$

Note that the plasma compressibility term is not included in Eq. (5.194). Strictly speaking, the analysis presented in Sec. V.B.5 indicates that the stabilizing effect of compressibility must be included for closed-line systems. Nevertheless, it is neglected here: (1) for reasons of mathematical simplicity, (2) because of the unreliability of the energy equation, (3) because the specific application considered, the EBT, is quantitatively but not qualitatively affected by compressibility, and (4) because by so doing one is led to a conservative estimate of  $\delta W_F$ .

An examination of Eq. (5.194) indicates that the only explicit appearance of  $S$  (i.e.,  $\mathbf{k}_\perp$ ) occurs in the magnetic compression term. If one now considers the limit  $k_\perp \rightarrow \infty$ ,  $\delta W$  can be systematically minimized by expanding  $\boldsymbol{\eta}_\perp$ ,

$$\boldsymbol{\eta}_\perp = \boldsymbol{\eta}_{10} + \boldsymbol{\eta}_{11} \dots, \quad (5.195)$$

with  $|\boldsymbol{\eta}_{11}| / |\boldsymbol{\eta}_{10}| \sim 1/k_\perp$ .

The zeroth-order contribution to  $\delta W_F$  reduces to

$$\delta W_0 = \frac{1}{2} \int d\mathbf{r} |\mathbf{k}_\perp \cdot \boldsymbol{\eta}_{10}|^2. \quad (5.196)$$

Clearly, the minimizing perturbation satisfies  $\mathbf{k}_\perp \cdot \boldsymbol{\eta}_{10} = 0$ , implying that  $\boldsymbol{\eta}_{10}$  can be written as

$$\boldsymbol{\eta}_{10} = Y(\psi, \chi, l) \mathbf{e}_b \times \mathbf{k}_\perp. \quad (5.197)$$

Here  $Y$  is a scalar quantity, varying on the "slow" equilibrium length scale.

The first nonvanishing contribution to  $\delta W_F$  occurs in second order. In this expression the only appearance of the quantity  $\boldsymbol{\eta}_{11}$  is in the magnetic compression term,

$$\delta W_2(\text{comp}) = \frac{1}{2} \int d\mathbf{r} B^2 |i\mathbf{k}_\perp \cdot \boldsymbol{\eta}_{11} + \nabla \cdot \boldsymbol{\eta}_{10} + 2\kappa \cdot \boldsymbol{\eta}_{10}|^2. \quad (5.198)$$

Clearly  $\delta W_2$  is minimized by choosing  $i\mathbf{k}_\perp \cdot \boldsymbol{\eta}_{11} = -\nabla \cdot \boldsymbol{\eta}_{10} - 2\kappa \cdot \boldsymbol{\eta}_{10}$ . Thus the most unstable modes for  $k_\perp \rightarrow \infty$  do not involve any compression of the magnetic field.

In the evaluation of  $\delta W_2$  it is useful to note that the quantity  $\nabla \times (\boldsymbol{\eta}_{10} \times \mathbf{B})_\perp$  can be expressed as

$$\nabla \times (\boldsymbol{\eta}_{10} \times \mathbf{B})_\perp = \frac{\partial X}{\partial l} \mathbf{e}_b \times \mathbf{k}_\perp, \quad (5.199)$$

where  $X(\psi, \chi, l) \equiv BY$  and  $\partial/\partial l \equiv \mathbf{e}_b \cdot \nabla$ . A simple calculation then shows that the quantity  $(\boldsymbol{\eta}_{10} \times \mathbf{B}) \cdot \nabla \times (\boldsymbol{\eta}_{10} \times \mathbf{B}) = 0$ . Thus, in the limit  $k_\perp \rightarrow \infty$ , the kink term makes no contribution to stability.

The remaining contributions to  $\delta W_2$  describe a competition between the stabilizing effects of line bending and the destabilizing effects of unfavorable curvature:

$$\delta W_2 = \frac{1}{2} \int d\mathbf{r} \left[ k_\perp^2 \left| \frac{\partial X}{\partial l} \right|^2 - 2 \frac{|X|^2}{B^2} (\mathbf{e}_b \times \mathbf{k}_\perp \cdot \nabla p)(\mathbf{e}_b \times \mathbf{k}_\perp \cdot \boldsymbol{\kappa}) \right]. \quad (5.200)$$

Upon explicitly introducing flux coordinates, one can rewrite  $\delta W_2$  in a form in which stability can be tested individually on each magnetic line. This form is given by

$$\begin{aligned} \delta W_2 &= \frac{1}{2} \int d\psi d\chi W(\psi, \chi), \\ W(\psi, \chi) &= \oint \frac{dl}{B} \left[ k_\perp^2 \left| \frac{\partial X}{\partial l} \right|^2 \right. \\ &\quad \left. - 2 |X|^2 \left[ \frac{|\nabla \psi|}{B^2} \frac{dp}{d\psi} k_s^2 \kappa_n \right. \right. \\ &\quad \left. \left. - k_s k_n \frac{\partial J_{||}}{\partial l} \frac{B}{B} \right] \right]. \end{aligned} \quad (5.201)$$

In the above expression, the curvature and wave vector have been decomposed into normal and geodesic components,  $\boldsymbol{\kappa} = \kappa_n \mathbf{e}_n + \kappa_s \mathbf{e}_s$ ,  $\mathbf{k}_\perp = k_n \mathbf{e}_n + k_s \mathbf{e}_s$ , with  $\mathbf{e}_n = \nabla \psi / |\nabla \psi|$  and  $\mathbf{e}_s = \mathbf{e}_b \times \mathbf{e}_n$ . Here

$$\begin{aligned} k_n &= |\nabla \psi| \frac{\partial S}{\partial \psi}, \\ k_s &= |\nabla \chi| \frac{\partial S}{\partial \chi}, \\ \kappa_n &= \frac{|\nabla \psi|}{B^2} \frac{\partial}{\partial \psi} \left( p + \frac{B^2}{2} \right), \\ \kappa_s &= \frac{|\nabla \chi|}{B} \frac{\partial B}{\partial \chi}. \end{aligned} \quad (5.202)$$

Also, in deriving Eq. (5.201), use has been made of the general parallel current relationship [i.e., Eq. (4.144)] to obtain the identity

$$\frac{\partial J_{||}}{\partial l} \frac{B}{B} = \frac{|\nabla \psi|}{B^2} \frac{dp}{d\psi} \kappa_s. \quad (5.203)$$

Equation (5.201) implies that a configuration will be stable to  $k_\perp \rightarrow \infty$  modes if and only if the quantity  $W(\psi, \chi)$  is positive on each magnetic line (i.e., for every value of  $\psi$  and  $\chi$ ). Furthermore, when minimizing  $W$ , the angle  $\gamma \equiv \tan^{-1}(k_s/k_n)$  representing the orientation of  $\mathbf{k}_\perp$  must be varied, as well as the eigenfunction  $X$ .

The first useful stability information from Eq. (5.201) follows from employing the special trial function  $X = 1$ ,

thus setting the line bending magnetic energy to zero and causing the contribution of the geodesic curvature to average to zero. This corresponds to the “interchange” perturbation. The resulting stability condition has the form

$$\frac{dp}{d\psi} \oint \frac{dl}{B^3} \frac{\partial}{\partial \psi} \left[ p + \frac{B^2}{2} \right] < 0. \quad (5.204)$$

A more familiar form, valid for  $\beta \ll 1$ , is obtained by neglecting the  $p$  term in the integrand of Eq. (5.204) and setting  $B = \hat{B}$ , the vacuum field. One finds

$$\frac{dp}{d\psi} \frac{\partial}{\partial \psi} \oint \frac{dl}{\hat{B}} > 0. \quad (5.205)$$

When Eq. (5.205) is satisfied, the configuration is said to possess a “magnetic well.” Since the interchange perturbation samples the average curvature of the field (i.e., ballooning effects are not included), it is perhaps more appropriate to describe such systems as having “average favorable curvature.”

Because of its simplicity, and the fact that only a knowledge of the vacuum fields is required, Eq. (5.205) is widely used in the evaluation of different magnetic geometries, including both closed-line and ergodic systems. Strictly speaking, Eq. (5.205) is a necessary criterion for stability only for low- $\beta$  closed-line systems. At higher  $\beta$ , the self-consistent diamagnetic fields must be included, as in Eq. (5.204). For ergodic systems, the surface-averaged generalizations of the conditions are neither necessary (since the effects of shear are not included) nor sufficient (since  $X=1$  is not the minimizing eigenfunction, even for  $k_\perp \rightarrow \infty$ ). Hence caution should be used in applying these criteria to such configurations. Even so, the property of average favorable curvature often does provide a reliable general guideline to the evaluation of different magnetic geometries.

Consider now the general minimization of  $W(\psi, \chi)$ . On each magnetic line this requires the solution of a one-dimensional (in  $l$ ) Euler-Lagrange equation for  $X$ . Stability can be determined by introducing an appropriate normalization and then calculating the value of the corresponding Lagrange multiplier (i.e., eigenvalue) so that  $X$  is periodic over the length of the line,  $L$ . The sign of the eigenvalue then determines stability or instability.

In applying Eq. (5.201) to general three-dimensional, closed-line systems, one must vary  $k_s/k_n$  separately on each magnetic line to minimize  $W$ . A considerable simplification occurs in an axisymmetric geometry, such as would characterize a “straight EBT” configuration. For such systems the symmetry implies that  $\chi = \theta$ ,  $\partial(\text{equil. quant.})/\partial\theta = 0$ , and  $k_s = 0$ . It then follows that the most unstable orientation of  $\mathbf{k}_\perp$  is such that  $k_n = 0$ ; that is,  $S = S(\chi)$ . To within a positive multiplicative factor,  $W$  reduces to

$$W = \oint \frac{dl}{r^2 B} \left( \left| \frac{\partial X}{\partial l} \right|^2 - 2 \frac{r}{B} \frac{dp}{d\psi} k_n |X|^2 \right), \quad (5.206)$$

where  $r = r(\psi, l)$  is the radial equilibrium position of the magnetic line under consideration.

For the EBT geometry,  $k_n$  oscillates between regions of favorable and unfavorable curvature. The minimizing perturbation then has the structure of a ballooning mode, concentrating in the unfavorable regions. It does this in such a way that the increase in the destabilizing term more than compensates for the increase in stability from the line-bending energy. Perhaps the most important consequence of ballooning mode analysis is that the resulting stability criterion sets a maximum  $\langle \beta \rangle$  limit for  $k_\perp \rightarrow \infty$  modes, which is usually the most severe limit for internal modes.

In summary, by considering the  $k_\perp \rightarrow \infty$  limit, one can reduce the stability of multidimensional closed-line systems to a one-dimensional Energy Principle whose behavior can be examined one magnetic line at a time. In this limit there are two competing effects determining stability: the stabilizing effect of line bending and the destabilizing effect of unfavorable curvature. The interchange perturbation represents a special trial function which causes the line bending to vanish. The resulting necessary condition for stability, is that systems have “average favorable curvature” or possess a “magnetic well.” The ballooning mode represents the true minimizing eigenfunction and in general sets a limit on the maximum stable  $\langle \beta \rangle$ . These criteria will now be used to investigate the stability of the EBT configuration.

### b. Application to the Elmo bumpy torus

In Sec. IV.D.2 it was shown that the EBT can be viewed as a closed-line toroidal configuration consisting of a series of linked mirror cells. In the bulge region of each mirror there is an ECRH (electron cyclotron resonance heated) electron ring. The combined effects of toroidicity and mirror bumpiness imply that the EBT is a three-dimensional configuration. However, because of the large aspect ratio, toroidicity does not play an essential role in EBT stability, and in this respect it is sufficient to treat the system as a straight, infinitely long, two-dimensional series of linked mirrors. The MHD stability of such systems has been investigated extensively at Oak Ridge [see, for instance, Nelson and Spies (1974), Nelson and Hedrick (1979)] and this section presents a summary of these results.

The most dangerous MHD instabilities in the EBT are  $k_\perp \rightarrow \infty$ , internal pressure-driven ballooning modes. This follows because  $J_{||} = 0$ , so that current-driven kinks cannot exist. Furthermore, since the most severe stability limits arising from pressure-driven modes occur for  $k_\perp \rightarrow \infty$ , the corresponding eigenfunctions are highly localized in radius. Consequently the vacuum region is decoupled, and only internal modes need be considered.

The basic instability mechanism of the EBT is associated with the alternating regions of favorable and unfavorable curvature in the configuration. A detailed analysis shows that without the hot-electron rings, the low field, unfavorable regions are more heavily weighted,

so that both interchange and ballooning modes can be driven unstable.

The analysis of EBT internal modes is very similar to that of the  $n \rightarrow \infty$  ballooning modes in tokamaks. There are, however, three distinctions which must be made. First, in the analysis the hot-electron rings are assumed to remain rigid during the MHD perturbation of the main plasma core. The physical reason for this is the normal EBT operating condition  $T_{\text{ring}}/T_{\text{plas}} \sim 10^3$ , which implies that the characteristic diamagnetic drift velocity  $V_D \sim T_{\text{ring}}/erB$  is much greater than the ion thermal velocity  $V_{Ti} \sim (T_i/m_i)^{1/2}$  (Nelson, 1980). If the rings were allowed to move as part of the plasma, the system would be very unstable (Nelson and Spies, 1979). The effect of holding the electron rings rigid is to modify the Energy Principle as follows (Johnson *et al.*, 1969):

$$\delta W = \frac{1}{2} \int d\mathbf{r} [ |\mathbf{Q}|^2 + (\nabla \times \mathbf{B} - \mathbf{J}_e) \times \xi_1^* \cdot \mathbf{Q} + (\xi_1 \cdot \nabla p)(\nabla \cdot \xi_1^*) - \gamma p |\nabla \cdot \xi|^2 ], \quad (5.207)$$

where  $\mathbf{J}_e$  is the hot-electron current and  $p$  is the pressure of the plasma core.

The second distinction is associated with compressibility. Since the EBT has closed field lines, one cannot set  $\nabla \cdot \xi = 0$  because of periodicity requirements. Nelson and Hedrick (1979) have taken this into account and have shown that there is an additional stabilizing contribution in  $\delta W$  (i.e., from the  $\gamma p |\nabla \cdot \xi|^2$  term), which makes a quantitative but not qualitative change in the stability. Nevertheless there is still uncertainty with respect to the compressibility because of the unreliability of the equation of state. For these reasons, and for the sake of simplicity, the compressibility contribution is neglected, thus leading to a more conservative form of  $\delta W$ .

The third distinction has to do with shear and periodicity. Recall that in the tokamak geometry it was necessary to introduce the quasimode representation for the eigenfunction to insure periodicity [Eq. (5.168)]. Since there is no shear in an EBT, this problem does not arise, and one can Fourier analyze the perturbation  $X(r, \theta, z)$  as

$$X(r, \theta, z) = X(r, z) \exp(im\theta), \quad (5.208)$$

where  $X(r, z) = X(r, z + L)$ ,  $L$  is period of the mirror cells, and the  $z$  variation of  $X$  is "slow" (i.e., on the equilibrium scale).

With these considerations in mind, the appropriate  $\delta W$  for the EBT can be derived in a manner very similar to that used for the ballooning mode for tokamaks, or equivalently to the general analysis of closed-line systems given in Sec. V.D.2.a. The EBT  $\delta W$  is given by

$$\begin{aligned} \delta W = & \frac{\pi}{n} \int \frac{dx dl}{r^2 B} \left[ \left| \frac{\partial X}{\partial l} \right|^2 \right. \\ & \left. - \frac{1}{rB} \frac{dp}{d\psi} \left( 2\kappa_n - \frac{J_e}{B} \right) |X|^2 \right], \\ \kappa_n = & \frac{r}{B} \frac{\partial}{\partial \psi} \left( p + \frac{B^2}{2} \right). \end{aligned} \quad (5.209)$$

With the exception of the  $J_e$  term, Eq. (5.209) is identical to Eq. (5.201), or can be obtained by making the identification  $R \rightarrow r$ ,  $Z \rightarrow z$ ,  $\phi \rightarrow \theta$ ,  $x \rightarrow n(\psi - \psi_0)$ ,  $n \rightarrow m$ ,  $B_p \rightarrow B$ ,  $Jd\chi = dl/B$ , and setting  $v(\psi) = F(\psi) = 0$  in Eq. (5.171). Note that  $dl$  corresponds to arc length along the magnetic field and that the most unstable  $k$  value in Eq. (5.171) corresponds to  $k = \hat{k} = 0$  when  $F = 0$ .

Equation (5.209) has been analyzed and solved numerically by Nelson and Hedrick (1979) for realistic experimental situations, including the effects of anisotropic hot-electron rings, finite mirror ratio in each cell, and finite  $\beta$ 's in the plasma core and hot-electron rings.

The key physical results of their investigation can be obtained analytically by introducing the appropriate small-mirror-ratio asymptotic expansion. The basic ordering, which is somewhat different from that introduced for the three-dimensional EBT equilibria [Sec. IV.D.2, Eq. (4.108)], is given by

$$\begin{aligned} \beta_c &\equiv \frac{2p}{B_0^2} \sim 1, \quad \beta_e \equiv \frac{2p_e}{B_0^2} \sim \delta^2, \\ ha &\sim 1, \quad \delta \equiv \frac{B_{z\max} - B_{z\min}}{B_{z\max} + B_{z\min}} \ll 1. \end{aligned} \quad (5.210)$$

Here  $\beta_c$  and  $\beta_e$  are the beta values of the plasma core and hot-electron rings, respectively,  $h = 2\pi/L$  is the pitch number of the mirror fields,  $B_0$  is the average amplitude of the vacuum mirror field, and  $\delta$  represents the bumpiness of the mirror field. As in Sec. IV.D.2, the expansion parameter is  $\delta \ll 1$ , and for simplicity the hot-electron rings are assumed to be isotropic. The main difference in the expansions is that in the present stability analysis  $\beta_c \sim 1$ , whereas in the toroidal equilibrium calculation  $\beta_c \sim \delta^2$  for purposes of analytical simplicity. Since only a two-dimensional equilibrium is required for the stability analysis, it is possible to analytically treat the case  $\beta_c \sim 1$ , which corresponds to the maximal ordering; that is, the small destabilizing effect of the mirror field, of order  $\delta^2$ , is stabilized by the small magnetic well created by the low- $\beta_e \sim \delta^2$  hot-electron rings, thus providing a configuration which can stably confine a high- $\beta_c \sim 1$  plasma core against all ideal MHD modes.

Under these assumptions it is straightforward to calculate an expanded equilibrium. The magnetic field is written as  $\mathbf{B}(r, z) = (1/r)\nabla \psi \times \mathbf{e}_\theta$ , where the flux function  $\psi(r, z) = \psi_0(r) + \psi_1(r)\cos(hz)$ , ( $\psi_1/\psi_0 \sim \delta$ ) satisfies the Grad-Shafranov equation with  $F = 0$ . In zeroth order one finds

$$\begin{aligned} p(r) + \frac{1}{2} B_{z0}^2(r) &= \frac{B_0^2}{2}, \\ B_{z0} &= \frac{1}{r} \frac{d\psi_0}{dr}. \end{aligned} \quad (5.211)$$

In first order,  $\psi_1$  satisfies

$$\begin{aligned} \frac{d}{dr} \left[ \frac{B_{z0}^2}{r} \frac{d}{dr} \left( \frac{\psi_1}{B_{z0}} \right) \right] - \frac{h^2 B_{z0}^2}{r} \left( \frac{\psi_1}{B_{z0}} \right) &= 0, \\ \psi_1(0) = 0; \quad \psi_1'(b) &= \delta b B_0. \end{aligned} \quad (5.212)$$

Here it has been assumed that far from the plasma,  $b/a \gg 1$ , the applied magnetic field has the form  $B_z(b,z) = B_0[1 + \delta \cos(hz)]$ .

Assuming that,  $\psi_1$  and hence  $\mathbf{B}_1$ ,  $p_1$ , and  $\kappa_n$  are known, this equilibrium is substituted into  $\delta W$  [Eq. (5.209)]. The eigenfunction  $X$  must also be expanded. On each magnetic line,  $X$  has the form  $X = X_0 + X_1 \cos(hz)$ , where  $X_0(r)$  and  $X_1(r)$  are constants on the rapid  $x$  scale and represent the interchange and ballooning contributions, respectively. After a straightforward calculation,  $\delta W$  can be written as

$$\begin{aligned} \frac{\delta W}{L} &= \frac{\pi}{n} \int dx \delta \hat{W} \\ \delta \hat{W} &= \frac{1}{2r^2 B_{z0}} \left\{ \frac{\beta'_c}{(1-\beta_c)^2} \left[ \frac{1}{2} \beta_e + \frac{(1-\beta_c)}{r} \left( \frac{U^2}{r} \right)' \right] X_0^2 \right. \\ &\quad \left. + Y_1^2 - 2 \left( \frac{\beta'_c U}{r(1-\beta_c)} \right) Y_1 X_0 \right\}, \end{aligned} \quad (5.213)$$

where  $Y_1 = hX_1$  and  $U(r) = h\psi_1(r)/B_{z0}(r)$ .

There are two stability conditions of interest resulting from Eq. (5.213). First, the special interchange perturbation  $Y_1 = 0$  gives rise to the necessary, but not sufficient, stability condition

$$\beta'_c \left[ \frac{1}{2} \beta'_e + \left( \frac{1-\beta_c}{r} \right) \left( \frac{U^2}{r} \right)' \right] > 0. \quad (5.214)$$

Necessary and sufficient conditions follow from the full ballooning mode perturbation, obtained by algebraically minimizing over the coefficient  $Y_1$ . The result is

$$\beta'_c \left[ \frac{1}{2} \beta'_e + \left( \frac{(1-\beta_p)U^2}{r^2} \right)' \right] > 0. \quad (5.215)$$

From these two conditions emerges the following relatively simple picture of EBT stability. Consider first the interchange condition and assume  $\beta'_c < 0$  for confinement. The term in the bracket of Eq. (5.214), which represents the total magnetic well, is positive (i.e., destabilizing) if  $\beta'_e > 0$ , since  $U$  is in general an increasing function of radius. The well contribution can be negative only if  $\beta'_e$  is sufficiently negative. Since the hot-electron ring pressure is peaked off axis, the region from the axis  $r=0$  to the maximum ring pressure is potentially unstable because of the average unfavorable curvature of the mirror field. To avoid such instabilities, the EBT pressure profile must be flat (i.e.,  $\beta'_c = 0$ ) out to a radius somewhat past the peak of the ring pressure, where the well first forms. The entire pressure gradient of the plasma core must occur over the relatively narrow region of space where  $\beta'_e$  is sufficiently negative to create a well. Typical stable profiles are illustrated in Fig. 47.

A simple criterion for the minimum properties required to create a well can be obtained as follows. First, assume that the hot-electron ring profile is parabolic:  $\beta_e = \beta_{e0}[1 - (r - a)^2/d^2]$ , where  $\beta_{e0}$  is the peak beta,  $a$  is the radius where the ring is located, and  $d$  is the half-width of the ring. Second, consider the "slow  $z$ " approx-

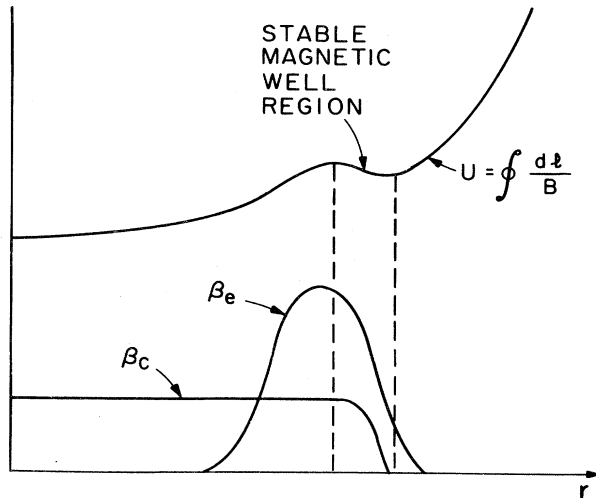


FIG. 47. Stabilized EBT plasma pressure profiles due to the magnetic well of the hot-electron rings.

imation,  $ha \ll 1$ , and the limit of a thin ring,  $d/a \ll 1$ . Under these conditions, in the region of interest the function  $U$  is given by  $U \approx h\delta r^2/[2(1-\beta_{c0})]$ , where  $\beta_{c0}$  is the peak beta value of the plasma core. Substituting into Eq. (5.214) then yields the following condition for creating a magnetic well:

$$\beta_{e0} > \frac{3}{4} \left( \frac{h^2 \delta^2}{1-\beta_{c0}} \right) ad. \quad (5.216)$$

The next question that arises is to determine the maximum  $\beta_c$  that can be stably confined in the magnetic well. The  $\beta_c$  limit is a consequence of ballooning modes and can be estimated from the necessary and sufficient conditions given by Eq. (5.215). Using the same assumptions made above, and ordering  $\beta_{c0} \sim d/a \ll 1$ , it follows that

$$-a \frac{d\beta_c}{dx} \leq 3 \left( \frac{\beta_{e0}}{\beta_c} \frac{x}{d} - 1 \right), \quad (5.217)$$

where  $\beta_{ec} = (\frac{3}{4})h^2 \delta^2 ad$ ,  $x = r - a$ ,  $x_1 \leq x \leq d$ , with  $x_1 = d(\beta_{ec}/\beta_{e0})$ . Note that for a magnetic well  $\beta_{e0} > \beta_{ec}$ . The maximum stable  $\langle \beta_c \rangle$  can be calculated by assuming equality in Eq. (5.217) and then integrating across the magnetic well region. Using the relation  $\langle \beta_c \rangle \approx \beta_{c0}$  for a thin ring, one finds

$$\langle \beta_c \rangle \leq \frac{3}{2} \left( \frac{d}{a} \right) \frac{(\beta_{e0} - \beta_{ec})^2}{\beta_{e0} \beta_{ec}}. \quad (5.218)$$

This result is in good agreement with the numerical studies carried out by Nelson and Hedrick (1979). They found that for realistic configurations, including finite mirror ratio, finite  $\beta$ , anisotropic hot-electron rings, and plasma compressibility, the threshold value of  $\beta_{e0}$  occurs between 0.1 and 0.15. Above this threshold the marginal value of  $\langle \beta_c \rangle$  increases rapidly, and in the case of long

electron rings a value of  $\beta_{e0}=0.2$  stabilizes the plasma core up to values of  $\langle\beta_c\rangle\approx 0.3$ .

In summary, high- $\langle\beta_c\rangle$  EBT profiles exist which are stable to all ideal MHD modes, in particular to interchange and ballooning modes. The stability is sensitively dependent upon the assumption that the hot-electron rings are rigid with respect to MHD perturbations. Without this assumption, the system would be very unstable. An interesting feature of the results is that finite values of  $\langle\beta_c\rangle$  can be stabilized by relatively low values of  $\beta_{e0}$  if the mirror ratio (i.e.,  $\beta_{ec}$ ) is also small. (This optimistic result does not hold when the hot electron rings are treated with a self-consistent kinetic model. In this case typically  $\langle\beta_c\rangle\lesssim\beta_{ec}$ .) One characteristic feature of the stable profiles is that plasma pressure must be flat, out to the magnetic well region, in order to avoid instabilities. In a certain sense this requirement corresponds to "infinite" transport in this region, since no gradients are allowed. Consequently the overall transport is determined by the properties of the well region and may give rise to an energy confinement scaling law  $\tau_E\sim ad$  rather than  $a^2$  as in the tokamak or RFP. The question of transport, as well as a more realistic treatment of the hot-electron rings in the MHD stability analysis, are important areas in EBT research.

## VI. CONCLUSIONS

It has been shown that ideal MHD is a single-fluid model which describes the macroscopic equilibrium and stability properties of toroidal magnetic fusion configurations.

With regard to equilibrium, the model explains how forces are developed which hold the plasma in both radial pressure balance and toroidal force balance. In particular, two basic methods of radial pressure balance are identified, the  $\theta$  pinch and the  $Z$  pinch. Similarly, three basic methods of toroidal force balance are also identified: equilibria by net toroidal current (e.g.,  $Z$  pinch, RFP, tokamak); equilibria by the helical sideband force (e.g., EBT, high- $\beta$  stellarator); and equilibria by the Pfirsch-Schluter-current average helical field force (e.g., conventional stellarator).

It was pointed out that there is a fundamental incompatibility between toroidal equilibrium and stability; that is, the pure  $Z$  pinch can easily be bent into a toroidal configuration but has very poor stability properties. On the other hand, the straight  $\theta$  pinch has inherently good stability properties but no toroidal equilibria exist. In order to resolve this incompatibility, researchers have evolved a number of different configurations, each containing various combinations of the basic fields, with the aim of simultaneously optimizing equilibrium and stability behavior.

Once toroidal equilibrium is achieved, a configuration can in general become unstable from two different sources: current-driven modes and pressure-driven modes. In current-free devices such as the EBT and the stellarator, the most dangerous modes are  $k_\perp\rightarrow\infty$  inter-

change and ballooning instabilities. If the average field line curvature is unfavorable, interchanges are likely to occur for any negative pressure gradient. If the system has average favorable curvature, there is a maximum  $\beta$  limit set by ballooning modes.

For configurations with nonzero parallel current, low  $k_\perp$  current-driven kink instabilities can be excited. These modes can be stabilized by keeping the total current sufficiently low and somewhat peaked (tokamak) or by having a conducting wall very close to the plasma (RFP). In systems with  $J_{||}\neq 0$ , the resultant shear can also help stabilize pressure-driven modes, even if the average curvature is unfavorable.

Ideal MHD theory has received wide application in the experimental fusion program. To appreciate its usefulness in this connection, it is worthwhile pointing out that each of the currently successful fusion concepts is designed to operate on or near certain critical boundaries of equilibrium and/or stability set by ideal MHD.

However, it should also be noted that ideal MHD equilibrium and stability are not sufficient to guarantee a macroscopically well-behaved system. In many cases there exist a variety of resistive instabilities which, although growing more slowly, allow the magnetic field topology to change on a time scale shorter than typical experimental lifetimes. This can have important consequences, particularly in configurations with  $J_{||}\neq 0$ . These modes lie outside the scope of the present review.

In summary, despite its apparent simplicity, the ideal MHD model provides a very reliable guide to the understanding and evaluation of the macroscopic equilibrium and stability properties of toroidal magnetic geometries.

## ACKNOWLEDGMENTS

The author would like to thank G. Berge, J. P. Goedbloed, H. Grad, J. L. Johnson, K. Molvig, P. A. Politzer, D. J. Sigmar, H. Weitzner, and J. A. Wesson for numerous helpful discussions, not only during the writing of the manuscript, but in prior years as well, which significantly contributed to his overall understanding of the MHD model. The author would also like to thank Ms. C. Lydon for preparing this rather long manuscript and for her patience in the face of an apparently endless series of rewritten sections. This work was partially supported by the U. S. Department of Energy.

## REFERENCES

- Baldwin, D. E., 1977, Rev. Mod. Phys. **49**, 317.
- Baldwin, D. E., and B. G. Logan, 1979, Phys. Rev. Lett. **43**, 1318.
- Barnes, D. C., and J. U. Brackbill, 1977, Nucl. Sci. Eng. **64**, 18.
- Bartlett, D. V., et al., 1980, Nucl. Fusion **20**, 1093.
- Bartsch, R. R., E. L. Cantrell, R. F. Gribble, K. A. Klare, K. A. Kutac, G. Miller, and R. E. Siemon, 1978, Phys. Fluids **21**, 2287.

- Bateman, G., 1978, *MHD Instabilities* (MIT, Cambridge, Mass.).
- Bateman, G., W. Schneider, and W. Grossmann, 1974, Nucl. Fusion **14**, 669.
- Bateman, G., and D. J. Sigmar, 1982, Nucl. Fusion (to be published).
- Bennett, W. H., 1934, Phys. Rev. **45**, 980.
- Berge, G., and J. P. Freidberg, 1975, Phys. Fluids **18**, 1362.
- Berger, D., L. C. Bernard, R. Gruber, and F. Troyon, 1977a, in *Plasma Physics and Controlled Nuclear Fusion Research 1976* (IAEA, Vienna), Vol. II, p. 411.
- Berger, D., R. Gruber, and F. Troyon, 1977b, in *Controlled Fusion and Plasma Physics*, Proceedings of the Eighth European Conference, Prague, Vol. I, p. 51.
- Bernard, L. C., D. Dobrott, F. J. Helton, and R. W. Moore, 1980, Nucl. Fusion **20**, 1199.
- Bernstein, I. B., E. A. Frieman, M. D. Kruskal, and R. M. Kulsrud, 1958, Proc. R. Soc. London, Ser. A **244**, 17.
- Betancourt, O., and P. Garabedian, 1976, Proc. Natl. Acad. Sci. U.S.A. **73**, 984.
- Blank, A. A., H. Grad, and H. Weitzner, 1969, in *Plasma Physics and Controlled Nuclear Fusion Research 1968* (IAEA, Vienna), Vol. II, p. 607.
- Bodin, H. A. B., and A. A. Newton, 1980, Nucl. Fusion **20**, 1255.
- Bowers, E. C., and M. G. Haines, 1971, Phys. Fluids **14**, 165.
- Boyd, T. J. M., and J. J. Sanderson, 1969, *Plasma Dynamics* (Barnes & Noble, New York).
- Brackbill, J. U., and W. E. Pracht, 1973, J. Comp. Phys. **13**, 455.
- Braginskii, S. I., 1965, in *Reviews of Plasma Physics*, edited by M. A. Leontovich (Consultants Bureau, New York), Vol. I.
- Bussac, M. N., R. Pellat, D. Edery, and J. L. Soule, 1975, Phys. Rev. Lett. **35**, 1638.
- Butt, E. P., R. Curruthers, J. T. D. Mitchell, R. S. Pease, P. C. Thonemann, M. A. Bird, J. Blears, and E. R. Hartill, 1958, in *Proceedings of the Second United Nations International Conference on the Peaceful Uses of Atomic Energy* (United Nations, Geneva), Vol. 32, p. 42.
- Callan, J. D., and R. A. Dory, 1972, Phys. Fluids **15**, 1523.
- Chandraseker, S., 1961, *Hydrodynamic and Hydromagnetic Stability* (Clarendon, Oxford).
- Charlton, L. A., R. A. Dory, Y.-K. M. Peng, D. J. Stricker, S. J. Lynch, D. K. Lee, R. Gruber, and F. Troyon, 1979, Phys. Rev. Lett. **43**, 1395.
- Chen, F. F., 1974, *Introduction to Plasma Physics* (Plenum, New York).
- Chew, G., M. Goldberger, and F. Low, 1956, Proc. R. Soc. London, Ser. A **236**, 112.
- Clarke, J. F., and D. J. Sigmar, 1977, Phys. Rev. Lett. **38**, 70.
- Connor, J. W., R. J. Hastie, and J. B. Taylor, 1978, Phys. Rev. Lett. **40**, 396.
- Connor, J. W., R. J. Hastie, and J. B. Taylor, 1979, Proc. R. Soc. London, Ser. A **365**, 1.
- Coppi, B., 1977, Phys. Rev. Lett. **39**, 939.
- Davidson, R. C., and J. P. Freidberg, 1976, in *Pulsed High Beta Plasmas*, edited by D. E. Evans (Pergamon, New York), p. 13.
- Dimov, G. I., V. V. Zakaïdakov, and M. E. Kishinevsky, 1976, Fiz. Plazmy **2**, 597.
- D'Ippolito, D. A., J. P. Freidberg, J. P. Goedbloed, and J. Rem, 1977, in *Plasma Physics and Controlled Nuclear Fusion Research 1976* (IAEA, Vienna), Vol. I, p. 523.
- D'Ippolito, D. A., J. P. Freidberg, J. P. Goedbloed, and J. Rem, 1978, Phys. Fluids **21**, 1600.
- Dobrott, D., J. F. Helton, R. W. Moore, L. C. Bernard *et al.*, 1979, in *Plasma Physics and Controlled Nuclear Fusion Research 1978* (IAEA, Vienna), Vol. I, p. 717.
- Dobrott, D., D. B. Nelson, J. M. Greene, A. H. Glasser, M. S. Chance, and E. A. Frieman, 1977, Phys. Rev. Lett. **39**, 943.
- Dory, R. A., D. B. Nelson, Y.-K. M. Peng, D. Berger *et al.*, 1977, in *Controlled Fusion and Plasma Physics*, Proceedings of the Eighth European Conference, Prague, Vol. I, p. 69.
- Dory, R. A., and Y.-K. M. Peng, 1977, Nucl. Fusion **17**, 21.
- Ellis, W. R., F. C. Jahoda, R. Kristal, W. E. Quinn, F. L. Ribe, G. A. Sawyer, and R. E. Siemon, 1974, Nucl. Fusion **14**, 841.
- Erdelyi, A., 1953, *Higher Transcendental Functions*, Bateman Manuscript Project (McGraw-Hill, New York), Vol. II.
- Eubank, H. *et al.*, 1979, in *Plasma Physics and Controlled Nuclear Fusion Research 1978* (IAEA, Vienna), Vol. I, p. 167.
- Fisch, N. J., 1978, Phys. Rev. Lett. **41**, 873.
- Fisch, N. J., and A. Bers, 1978, in *RF Plasma Heating*, Proceedings of the Third Topical Conference, Pasadena, Papers E5 and 6.
- Fowler, T. K., and B. G. Logan, 1977, Comments Plasma Phys. Controlled Fusion **2**, 167.
- Freidberg, J. P., 1980, Nucl. Fusion **20**, 673.
- Freidberg, J. P., R. Y. Dagazian, and D. C. Barnes, 1979, Phys. Fluids **22**, 926.
- Freidberg, J. P., and F. A. Haas, 1973, Phys. Fluids **16**, 1909.
- Freidberg, J. P., and F. A. Haas, 1974, Phys. Fluids **17**, 440.
- Freidberg, J. P., and D. W. Hewett, 1977, Phys. Fluids **20**, 2128.
- Freidberg, J. P., and B. M. Marder, 1973, Phys. Fluids **16**, 247.
- Freidberg, J. P., and L. D. Pearlstein, 1978, Phys. Fluids **21**, 1207.
- Freidberg, J. P., and J. A. Wesson, 1970, Phys. Fluids **13**, 1117.
- Funfer, E., M. Kaufmann, W. Lotz, J. Neuhauser, G. Schramm, and U. Seidel, 1975, Nucl. Fusion **15**, 133.
- Furth, H. P., 1975, Nucl. Fusion **15**, 487.
- Furth, H. P., J. Killeen, M. N. Rosenbluth, and B. Coppi, 1965, in *Plasma Physics and Controlled Nuclear Fusion Research 1964* (IAEA, Vienna), Vol. I, p. 103.
- Furth, H. P., J. Killeen, and M. N. Rosenbluth, 1963, Phys. Fluids **6**, 459.
- Goedbloed, J. P., 1975, Phys. Fluids **18**, 1258.
- Goedbloed, J. P., 1979, *Lecture Notes on Ideal Magnetohydrodynamics* (Fom-Instituut voor Plasmaphysica, Nieuwegein, Netherlands).
- Goedbloed, J. P., and P. H. Sakanaka, 1974, Phys. Fluids **17**, 908.
- Gondhalekar, A. *et al.*, 1979, in *Plasma Physics and Controlled Nuclear Fusion Research 1978* (IAEA, Vienna), Vol. I, p. 199.
- Grad, H., 1962, in *Electromagnetics and Fluid Dynamics of Gaseous Plasma* (Polytechnic, Brooklyn), Vol. XI, p. 37.
- Grad, H., 1967a, Phys. Fluids **10**, 137.
- Grad, H., 1967b, in *Magneto-Fluid and Plasma Dynamics*, edited by H. Grad (American Mathematical Society, Providence), Vol. 18, p. 162.
- Grad, H., 1971, in *Plasma Physics and Controlled Nuclear Fusion Research 1970* (IAEA, Vienna), Vol. II, p. 229.
- Grad, H., 1973, Proc. Natl. Acad. Sci. U.S.A. **70**, 3277.
- Grad, H., and H. Rubin, 1958, in *Proceedings of the Second United Nations International Conference on the Peaceful Uses of Atomic Energy* (United Nations, Geneva), Vol. 31, p. 190.
- Greene, J. M., 1976, "Introduction to resistive instabilities"

- (Ecole Polytechnique Federale de Lausanne), Report LRP 114/76, CRPP (unpublished).
- Greene, J. M., and J. L. Johnson, 1961, Phys. Fluids 4, 875.
- Greene, J. M., and J. L. Johnson, 1962, Phys. Fluids 5, 510.
- Greene, J. M., and J. L. Johnson, 1968, Plasma Phys. 10, 729.
- Grimm, R. C., J. M. Greene, and J. L. Johnson, 1976, in *Methods in Computational Physics* (Academic, New York), Vol. 16, p. 253.
- Haas, F. A., 1972, Phys. Fluids 15, 141.
- Haas, F. A., 1975, Nucl. Fusion 15, 407.
- Haas, F. A., and J. C. B. Papaloizou, 1977, Nucl. Fusion 17, 721.
- Hain, K., and R. Lüst, 1958, Z. Naturforsch. Teil A 13, 936.
- Hameiri, E., 1979, Phys. Fluids 22, 89.
- Hameiri, E., 1981, submitted to J. Math. Phys.
- Hedrick, C. L., 1979, private communication.
- Hedrick, C. L., R. A. Dandl, J. A. Cobble, R. A. Dory, H. O. Eason et al., 1977, in *Plasma Physics and Controlled Nuclear Fusion Research 1976* (IAEA, Vienna), Vol. II, p. 145.
- Helton, F. J., and T. S. Wang, 1978, Nucl. Fusion 18, 1523.
- Hicks, H. R., J. A. Holmes, B. A. Carreras, D. J. Tetreault et al., 1980, in *Plasma Physics and Controlled Nuclear Fusion Research* (Brussels IAEA Meeting), Paper IAEA-CN-38/J-3.
- Hinton, F. L., and R. D. Hazeltine, 1976, Rev. Mod. Phys. 48, 239.
- IAEA, 1976, in *World Survey of Major Facilities in Controlled Fusion Research* (IAEA, Vienna).
- Jahns, G. L., M. Soler, B. V. Waddell, J. D. Callan, and H. R. Hicks, 1978, Nucl. Fusion 18, 609.
- Johnson, J. L., M. S. Chance, J. M. Greene, R. C. Grimm et al., 1977, in *Plasma Physics and Controlled Nuclear Fusion Research 1976* (IAEA, Vienna), Vol. II, 395.
- Johnson, J. L., H. E. Dahled, J. M. Greene, R. C. Grimm, Y. Y. Hsieh, S. C. Jardin, J. Manickam, M. Okabayashi, R. G. Storer, A. M. M. Todd, D. E. Voss, and K. E. Weimer, 1979, J. Comput. Phys. 32, 212.
- Johnson, J. L., R. M. Kulsrud, and K. E. Weimer, 1969, Plasma Phys. 11, 463.
- Kadomtsev, B. B., 1960, in *Plasma Physics and the Problems of Controlled Thermonuclear Reactions*, edited by M. A. Leontovich and J. Turkevich (Pergamon, New York).
- Kadomtsev, B. B., 1966, in *Reviews of Plasma Physics*, edited by M. A. Leontovich (Consultants Bureau, New York), Vol. II.
- Kadomtsev, B. B., 1975, Sov. J. Plasma Phys. 1, 389.
- Kerner, W., 1976, Princeton University, PPL Report MATT-1229.
- Krall, N. A., and A. W. Trivelpiece, 1973, *Principles of Plasma Physics* (McGraw-Hill, New York).
- Kruskal, M. D., and M. Schwarzschild, 1954, Proc. R. Soc. London, Ser. A 223, 348.
- Laval, G., H. Luc, E. K. Maschke, C. Mercier, and R. Pellat, 1971, in *Plasma Physics and Controlled Nuclear Fusion Research 1970* (IAEA, Vienna), Vol. II, p. 507.
- Laval, G., E. K. Maschke, and R. Pellat, 1970a, Phys. Rev. Lett. 24, 1229.
- Laval, G., E. K. Maschke, R. Pellat, and M. N. Rosenbluth, 1970b, International Center for Theoretical Physics, Report IC/70/35 (unpublished).
- Laval, G., C. Mercier, and R. M. Pellat, 1965, Nucl. Fusion 5, 156.
- Laval, G., and R. Pellat, 1973, in *Controlled Fusion and Plasma Physics*, Proceedings of the Sixth European Conference, Moscow, Vol. II, p. 640.
- Laval, G., R. Pellat, and J. L. Soule, 1972, in *Controlled Fusion and Plasma Physics*, Proceedings of the Fifth European Conference (Euratom CEA, Grenoble), Vol. I, p. 25.
- Laval, G., R. Pellat, and J. L. Soule, 1974, Phys. Fluids 17, 835.
- Lawson, J. D., 1957, Proc. Phys. Soc. London, Sect. B 70, 6.
- Longmire, C. L., 1963, *Elementary Plasma Physics* (Wiley-Interscience, New York).
- Lortz, D., 1970, Z. Angew. Math. Phys. 21, 196.
- Lortz, D., 1973, Nucl. Fusion 13, 817.
- Lortz, D., and J. Nührenberg, 1973, Nucl. Fusion 13, 821.
- Lortz, D., and J. Nührenberg, in *Plasma Physics and Controlled Nuclear Fission Research*, 1978 (IAEA, Vienna), Vol. II.
- McAales, D. G., N. Uckan, L. M. Lidsky et al., 1976, Oak Ridge National Laboratory Report ORNL/TM-5669 (unpublished).
- McKenna, K. F., R. R. Bartsch, R. J. Commisso, C. Ekdahl, W. E. Quinn, and R. E. Siemon, 1979, Phys. Fluids 23, 1443.
- Mercier, C., 1960, Nucl. Fusion 1, 47.
- Mercier, C., 1973, in *Controlled Fusion and Plasma Physics*, Proceedings of the Fifth European Conference, Moscow, Vol. I, p. 381.
- Mikhailovskii, A. B., 1967, in *Reviews of Plasma Physics*, edited by M. A. Leontovich (Consultants Bureau, New York), Vol. III, p. xx.
- Mikhailovskii, A. B., 1973, Sov. Phys.—JETP 37, 274.
- Mikhailovskii, A. B., 1974, Nucl. Fusion 14, 483.
- Mikhailovskii, A. B., and V. D. Shafranov, 1974, Sov. Phys.—JETP 39, 88.
- Miller, G., 1977, Phys. Fluids 20, 928.
- Miller, R. L., and R. W. Moore, 1979, Phys. Rev. Lett. 43, 765.
- Mills, R. G., 1970, Princeton University, PPL Report MATT-800 (unpublished).
- Miyamoto, K., 1978, Nucl. Fusion 18, 243.
- Molvig, K., S. P. Hirshman, and J. C. Whitson, 1979, Phys. Rev. Lett. 43, 582.
- Montgomery, D. C., and D. A. Tidman, 1964, *Plasma Kinetic Theory* (McGraw-Hill, New York).
- Morozov, A. I., and L. S. Solov'ev, 1966, in *Review of Plasma Physics*, edited by M. A. Leontovich (Consultants Bureau, New York), Vol. II.
- Mukhovatov, V. S., and V. D. Shafranov, 1971, Nucl. Fusion 11, 605.
- Nelson, D. B., 1980, Phys. Fluids 23, 1850.
- Nelson, D. B., and C. L. Hedrick, 1979, Nucl. Fusion 19, 283.
- Nelson, D. B., and G. O. Spies, 1974, Phys. Fluids 17, 2133.
- Nelson D. B., and G. O. Spies, 1979, Phys. Fluids 22, 1182.
- Newcomb, W. A., 1958, Ann. Phys. (N.Y.) 3, 347.
- Newcomb, W. A., 1960, Ann. Phys. (N.Y.) 10, 232.
- Osovska, S. M., 1959, in *Plasma Physics and the Problems of Controlled Thermonuclear Reactions* (Pergamon, Oxford), Vol. 2, p. 322.
- Pearlstein, L. D., and J. P. Freidberg, 1978, Phys. Fluids 21, 1218.
- Pogutse, O. P., and E. I. Yurchenko, 1978, JETP Lett. 28, 318.
- Rebhan, E., 1975, Nucl. Fusion 15, 277.
- Reiman, A., 1980, Phys. Fluids 23, 230.
- Ribe, F. L., 1969, Los Alamos Scientific Laboratory Report LA-4098 (unpublished).
- Ribe, F. L., 1975, Rev. Mod. Phys. 47, 7.
- Ribe, F. L., and M. N. Rosenbluth, 1970, Phys. Fluids 13, 2572.
- Robinson, D. C., 1971, Plasma Phys. 13, 439.
- Rose, D. J., and M. Clark, 1961, *Plasma and Controlled*

- Fusion* (MIT, Cambridge, Mass.).
- Rosenbluth, M. N., R. Y. Dagazian, and P. H. Rutherford, 1973, *Phys. Fluids* **11**, 1894.
- Rosenbluth, M. N., J. L. Johnson, J. M. Greene, and K. E. Weimer, 1969, *Phys. Fluids* **12**, 726.
- Rosenbluth, M. N., N. A. Krall, and N. Rostoker, 1962, *Nucl. Fusion Suppl.*, Part I, 143.
- Rosenbluth, M. N., and C. L. Longmire, 1957, *Ann. Phys. (N.Y.)* **1**, 120.
- Sakanaka, P. H., and J. P. Goedbloed, 1974, *Phys. Fluids* **17**, 918.
- Schneider, W., and G. Bateman, 1974, in *Plasma Physics and Controlled Nuclear Fusion Research 1974* (IAEA, Vienna), Vol. I, p. 429.
- Shafranov, V. D., 1956, *At. Energy* **5**, 38.
- Shafranov, V. D., 1960, *Sov. Phys.—JETP* **26**, 682.
- Shafranov, V. D., 1966, in *Review of Plasma Physics*, edited by M. A. Leontovich (Consultants Bureau, New York), Vol. III.
- Shafranov, V. D., 1970, *Sov. Phys.—Tech. Phys.* **15**, 175.
- Shafranov, V. D., 1971, *Plasma Phys.* **13**, 757.
- Shafranov, V. D., and E. I. Yurchenko, 1968, *Sov. Phys.—JETP* **26**, 682.
- Solov'ev, L. S., 1967, in *Reviews of Plasma Physics*, edited by M. A. Leontovich (Consultants Bureau, New York), Vol. III.
- Solov'ev, L. S., 1968, *Sov. Phys.—JETP* **26**, 400.
- Solov'ev, L. S., 1976, in *Reviews of Plasma Physics*, edited by M. A. Leontovich (Consultants Bureau, New York), Vol. VI.
- Solov'ev, L. S., V. D. Shafranov, and E. I. Yurchenko, 1969, in *Plasma Physics and Controlled Nuclear Fusion Research 1968* (IAEA, Vienna), Vol. I, p. 173.
- Spies, G. O., 1978a, *Nucl. Fusion* **18**, 1671.
- Spies, G. O., 1978b, *Phys. Fluids* **21**, 580.
- Spies, G. O., 1979, *Nucl. Fusion* **19**, 1531.
- Spies, G. O., 1980, *Phys. Fluids* **23**, 2017.
- Spitzer, L., 1956, *Physics of Fully Ionized Gases* (Interscience, New York).
- Spitzer, L., Jr., 1958, *Phys. Fluids* **1**, 253.
- Stratton, J. A., 1941, *Electromagnetic Theory* (McGraw-Hill, New York).
- Strauss, H. R., 1971, *Phys. Rev. Lett.* **26**, 616.
- Strauss, H. R., 1979, University of Texas, Austin, Fusion Research Center Report FRC-198 (unpublished).
- Suydam, B. R., 1958, in *Proceedings of the Second United Nations International Conference on the Peaceful Uses of Atomic Energy* (United Nations, Geneva), Vol. 31, p. 157.
- Sykes, A., and J. A. Wesson, 1974, *Nucl. Fusion* **14**, 645.
- Sykes, A., and J. A. Wesson, 1976, *Phys. Rev. Lett.* **38**, 491.
- Sykes, A., and J. A. Wesson, and S. J. Cox, 1977, *Phys. Rev. Lett.* **39**, 757.
- Tataronis, J. A., and W. Grossmann, 1977, Courant Institute of Mathematical Sciences Report C00-3077-102, MF-84 (unpublished).
- Tataronis, J. A., and A. Salat, 1981, Courant Institute of Mathematical Sciences Report No. DOE/ER/03077-171, MF-98.
- Taylor, J. B., 1962, *J. Nucl. Energy, Part C* **4**, 406.
- Taylor, J. B., 1974, *Phys. Rev. Lett.* **33**, 139.
- Taylor, J. B., 1975, in *Plasma Physics and Controlled Nuclear Fusion Research* (IAEA, Vienna), Vol. I, p. 161.
- Taylor, J. B., 1976, in *Pulsed High Beta Plasmas*, edited by D. E. Evans (Pergamon, Oxford), p. 59.
- Thyagaraja, A., and F. A. Haas, 1979, *Nucl. Fusion* **19**, 1392.
- Todd, A. A., M. S. Chance, J. M. Greene, R. C. Grimm, J. L. Johnson, and J. Manickam, 1977, *Phys. Rev. Lett.* **38**, 826.
- Todd, A. A., J. Manickam, M. Okabayashi, M. S. Chance, R. C. Grimm, J. M. Greene, and J. L. Johnson, 1979, *Nucl. Fusion* **19**, 743.
- W. VII-A Team—see Bartlett *et al.*, 1980.
- Waddell, B. V., B. Carreras, H. R. Hicks, J. A. Holmes, and D. K. Lee, 1978, *Phys. Rev. Lett.* **41**, 1386.
- Waddell, B. V., B. Carreras, H. R. Hicks, and J. A. Holmes, 1979, *Phys. Fluids* **22**, 896.
- Ware, A. A., and F. A. Haas, 1966, *Phys. Fluids* **9**, 956.
- Wesson, J. A., 1978, *Nucl. Fusion* **18**, 87.
- Wesson, J. A., and A. Sykes, 1974, in *Plasma Physics and Controlled Nuclear Fusion Research 1974* (IAEA, Vienna), Vol. I, p. 449.
- Woltjer, L., 1959, *Proc. Natl. Acad. Sci. U.S.A.* **45**, 769.
- Yoshikawa, S., 1964, *Phys. Fluids* **7**, 278.

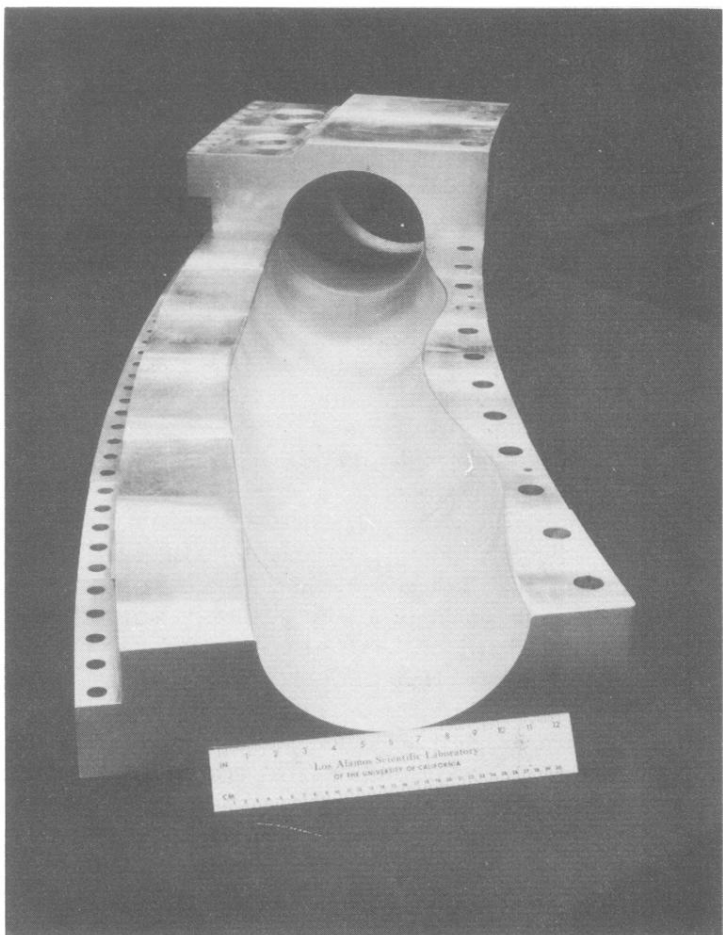


FIG. 26. Shaped conducting wall for producing an  $l=1,0$  high- $\beta$  stellarator configuration in the Scyllac experiment (courtesy K. F. McKenna, Los Alamos Scientific Laboratory, 1981).